Faculdade de Medicina de São José do Rio Preto
Programa de Pós-Graduação em Ciências da Saúde

Luciana Volpon Soares Souza Marin

Associação entre sinal da veia pulmonar e diagnóstico de tromboembolismo pulmonar agudo

São José do Rio Preto
2024

Luciana Volpon Soares Souza Marin

Associação entre sinal da veia pulmonar e diagnóstico de tromboembolismo pulmonar agudo

Tese apresentada à Faculdade de Medicina de São José do Rio Preto para obtenção do título de Doutor no Curso de Pós-Graduação em Ciências da Saúde.

Eixo Temático: Medicina Interna

Orientador: Prof. Dr. Arthur Soares Souza Júnior

São José do Rio Preto

2024

Ficha Catalográfica

Souza-Marin, Luciana Volpon Soares
Associação entre sinal da veia pulmonar e diagnóstico de tromboembolismo pulmonar agudo / Luciana Volpon Soares Souza Marin
São José do Rio Preto, 2024,
108 p.

Tese (Doutorado) − Faculdade de Medicina de São José do Rio Preto − FAMERP
Eixo Temático: Medicina Interna.

Orientador: Prof. Dr. Arthur Soares Souza Júnior

1. Tromboembolismo; 2. Tomografia; 3. Diagnóstico.

Luciana Volpon Soares Souza Marin

Associação entre sinal da veia pulmonar e diagnóstico de tromboembolismo pulmonar agudo

BANCA EXAMINADORA

TESE PARA OBTENÇÃO DO GRAU DE DOUTOR

Presidente e Orientador: Prof. Dr. Arthur Soares Souza Júnior

2º Examinador: Prof. Dr. Edson Marchiori

3º Examinador: Prof. Dr. Marcos Pontes Muniz

4º Examinador: Prof. Dr. Bruno Hochhegger

5º Examinador: Prof. Dr. Airton Moscardini

Suplentes: Profa. Dra. Lilian Beani

Profa. Dra. Luciana Vargas

São José do Rio Preto, 06 /12 / 2024.

SUMÁRIO

Ao meu marido Marcelo, por me estimular a finalizar esse projeto, sempre me apoiar com muita admiração na busca e concretização de projetos científicos.

Aos meus pais Arthur e Lucília, que são meus maiores exemplos de vida, e aos meus filhos Mariana e Pedro os quais desde pequenos compreenderam a minha profissão e ausência pelo trabalho em alguns momentos.

Aos meus enteados, Maria Victória e João Marcello pelo convívio e carinho diário.

Ao meu irmão Tuike e à Susanna e Aina que me acompanham sempre com muito amor, mesmo à distância.

AGRADECIMENTOS

Ao Prof. Dr. Arthur Soares Souza Junior, pela orientação e por ser meu maior exemplo e estimulador desse projeto e da minha jornada científica. Te admiro muito e é uma enorme satisfação poder aprender contigo, diariamente.

Aos Profs. Drs. Arthur Soares Souza Júnior, Dorotéia Rossi Silva Souza, Marcos Pontes Muniz, Luciana Vargas Cardoso e Lilian Beani, pelas críticas durante o exame geral de qualificação.

A todos os docentes do Programa de Pós-Graduação em Ciências da Saúde da Faculdade de Medicina de São José do Rio Preto (FAMERP), pela contribuição para minha formação durante o doutorado.

A todos os funcionários da Seção de Pós-Graduação da FAMERP pelo auxílio desde o início desta jornada.

Ao Prof. Dr. Renato Braz de Araujo da Fundação Faculdade Regional de Medicina de São José do Rio Preto (FUNFARME), pela amizade e entusiasmo, fornecendo embasamento científico e apoio afetivo para sua realização.

Ao Instituto de Radiodiagnóstico Rio Preto (Ultra-X) pelo suporte e infra-estrutura, fundamentais para o desenvolvimento desta pesquisa, em especial ao Dr. Fernando Paiva e Dr. Antônio Soares Souza.

Aos funcionários do Ultra-X, especialmente, Alberto e Edna, pela disponibilidade; excelente qualidade dos exames tomográficos e apoio na organização de toda a documentação referente à pesquisa de doutorado.

Ao Dr. Bruno Hochhegger da Universidade Federal de Ciências da Saúde de Porto Alegre (UFCSPA), pela importante contribuição e consolidação na descoberta do sinal da veia pulmonar em pacientes com tromboembolismo pulmonar agudo.

Ao Prof. Dr. Edson Marchiori da Universidade Federal do Rio de Janeiro (UFRJ), pelo estímulo constante na busca pela formação científica e grande estimulador deste projeto.

Ao Dr. Matheus Zanon, da Universidade Federal de Ciências da Saúde de Porto Alegre (UFCSPA), pela grande ajuda e contribuição para essa pesquisa.

À minha família por estar presente em todos momentos da minha vida e me apoiar de forma tão especial.

EPÍGRAFE

"O mistério gera curiosidade e a curiosidade é a base do desejo humano para compreender."

Neil Armstrong

LISTA DE TABELAS

LISTA DE FIGURAS

LISTA DE ABREVIATURAS E SÍMBOLOS

Angio-TC	Angiotomografia
CTPA	Computed Tomography Pulmonary Angiography
FAMERP	Faculdade de Medicina de São José do Rio Preto
HB	Hospital de Base
MIP	Projeção de Intensidade Máxima
PE	Pulmonary Thromboembolism
SVP	Sinal da Veia Pulmonar
TC	Tomografia Computadorizada
TEP	Tromboembolia pulmonar
TVP	Trombose Venosa Profunda
UH	Unidade de Hounsfield
%	Porcentagem
>	Maior
<	Menor
≤	Menor ou Igual
≥	Maior ou Igual

RESUMO

Introdução: Tromboembolismo Pulmonar (TEP) é a terceira causa de mortalidade entre as doenças cardiovasculares agudas, após infarto miocárdico e acidente vascular cerebral. A angiotomografia das artérias pulmonares (angio-TC) é o padrão ouro no diagnóstico de TEP, possibilitando a identificação de defeitos de enchimento nas veias pulmonares em áreas adjacentes ao TEP. **Objetivo:** Considerando que a obstrução arterial pulmonar diminui o fluxo venoso; levantamos a hipótese de que defeitos de enchimento nas veias pulmonares podem ser identificados em áreas adjacentes à embolia pulmonar (TEP), cujo sinal foi denominado "sinal da veia pulmonar" (SVP) avaliamos a sua prevalência e desempenho no diagnóstico de TEP na angio-TC. **Casuística e Método:** Este estudo retrospectivo incluiu pacientes consecutivos com suspeita clínica de TEP que foram submetidos à angio-TC. O SVP foi definido pelos seguintes critérios: (a) presença de um defeito de enchimento homogêneo de pelo menos 2 cm em uma veia pulmonar; (b) atenuação do átrio esquerdo [160 unidades Hounsfield]. Utilizando-se como referência os casos que apresentaram TEP na angio-TC, foram calculados a sensibilidade, a especificidade e os valores preditivos positivo e negativo para SVP. **Resultados:** No total, 119 pacientes (73 do sexo feminino; idade média de 62 anos) foram incluídos neste estudo. O TEP foi diagnosticado em 44 (35,8%) pacientes. O SVP estava presente em 16 dos 44 pacientes com TEP. A sensibilidade foi de 36,36% (intervalo de confiança de 95% (IC) 22,83-52,26%); a especificidade, 98,67% (IC 95% 91,79-99,93%); o valor preditivo positivo, 94,12% (IC 95% 69,24-99,69%); o valor preditivo negativo, 72,55% (IC 95% 62,67-80,70%). O índice Kappa para o SVP foi bom (0,801; IC 95% 0,645-0,957). O SVP foi correlacionado com embolia pulmonar lobar e segmentar (p \ 0,01). **Conclusões:** Apesar de uma baixa sensibilidade; a presença do sinal da veia pulmonar foi altamente específica para TEP, com uma boa concordância entre os leitores. Este sinal pode contribuir para o diagnóstico de TEP em estudos de angio-TC.

ABSTRACT

Introduction: Pulmonary thromboembolism (PE) is the third leading cause of mortality among acute cardiovascular diseases, after myocardial infarction and stroke. Computed Tomography Pulmonary angiography (CTPA) is the gold standard for diagnosing PE, making it possible to identify filling defects in the pulmonary veins in areas adjacent to the PE. **Objective:** Considering that pulmonary arterial obstruction decreases venous flow, we have hypothesized that filling defects in pulmonary veins can be identified in areas adjacent to pulmonary embolism (PE); this sign has been called "pulmonary vein sign" (PVS), therefore, we evaluated its prevalence and performance for PE diagnosis in CTPA. **Casuistic and Method:** This retrospective study enrolled consecutive patients with clinical suspicion of PE who underwent CTPA scan. The PVS was defined by the following criteria: (a) presence of a homogeneous filling defect of at least 2 cm in a pulmonary vein; (b) attenuation of the left atrium [160 Hounsfield units. Using the cases that presented PE on CTPA as reference, sensitivity, specificity, and positive and negative predictive values were calculated for PVS. **Results:** In total, 119 patients (73 female; mean age, 62 years) were included in this study. PE was diagnosed in 44 (35.8%) patients. The PVS was present in 16 out of the 44 patients with PE. Sensitivity was 36.36% (95% confidence interval (CI) 22.83–52.26%); specificity, was 98.67% (95% CI 91.79–99.93%); positive predictive value, 94.12% (95% CI 69.24–99.69%); negative predictive value, 72.55% (95% CI 62.67–80.70%). The Kappa Index for the PVS was good (0.801; 95% CI 0.645–0.957). PVS was correlated with lobar and segmental pulmonary embolism (p \ 0.01). **Conclusions:** Despite a low sensitivity; the presence of the pulmonary vein sign was highly specific for PE, with good agreement between readers. This sign could contribute to PE diagnosis in CTPA studies.

1-INTRODUÇÃO

Tromboembolismo pulmonar (TEP) caracteriza-se por quadro grave, que tem início quando trombo (coágulo ou êmbolo) localizado em uma das veias dos membros inferiores ou da pelve que se desloca e obstrui artéria pulmonar.[1] TEP é a terceira causa de mortalidade entre as doenças cardiovasculares agudas, após o infarto miocárdico e acidente vascular cerebral.[2-3] É a causa mais comum de morte evitável em pacientes internados.[4-5] Acredita-se que a doença tenha sido suspeitada em apenas 30% de pacientes que morrem devido ao TEP.[6-8]

Estima-se que, nos Estados Unidos, cerca de cinco milhões de pacientes apresentem trombose venosa profunda (TVP) todos os anos.[9-10] Destes, cerca de 650 mil (13%) evoluem para TEP e cerca de 100 a 200 mil (15,3 a 30,7%) morrem em decorrência da doença.[9-11]

Estudos epidemiológicos sobre TEP no Brasil são raros, quase todos oriundos de necrópsia, mostrando prevalência em torno de 3,9 a 16,6% [12]. Golin *et al.*,[8] avaliando 16.466 autópsias consecutivas no hospital da Faculdade de Medicina da Santa Casa de São Paulo mostraram que a incidência de TEP foi 4,7%. Em 68% desses casos, TEP foi considerado fatal.[8]

As apresentações clínicas mais comuns do TEP são dispneia e dor torácica, mas tosse, febre, hemoptise e síncope podem ocorrer.[13] Como muitas vezes estes sinais e sintomas do TEP são inespecíficos; necessitam de alto grau de suspeição. O diagnóstico precoce para tratamento adequado é fundamental para se evitar complicações, inclusive o óbito. Torres-Machado *et al.*[14] relataram que até 33,5% dos pacientes que chegam a uma unidade de emergência tem retardo no diagnóstico de TEP, sendo que até 11,9% deles são encaminhados para casa com diagnóstico clínico incorreto. Segundo estes

autores, pacientes com diagnóstico de TEP que apresentam 48 horas da chegada até o hospital, apresentam melhor prognóstico.

Casazza *et al*.[15] relataram 3,9% de mortes por TEP em pacientes hospitalizados e diagnosticados com TEP agudo. Óbitos ocorreram dentro de 24; 48 e 72 horas, após apresentação clínica em 27%, 39% e 49%, respectivamente; foi considerada como causa TEP agudo em 100%, 95% e 89% dos casos nestes intervalos. Faixa etária acima de 75 anos, sexo feminino, instabilidade hemodinâmica, imobilização nos quatro dias prévios, trauma recente e história prévia de doenças vasculares, coronárias ou arteriais foram fatores de risco para evolução para óbito ou deterioração clínica.[15]

Achados clínicos e de radiografia de tórax são inespecíficos, havendo necessidade de angiografia ou exame de imagem menos invasivo, a angiotomografia das artérias pulmonares (angio-TC). A angio-TC é o padrão ouro no diagnóstico de TEP, substituindo a angiografia, especialmente, com os avanços dos aparelhos de tomografia computadorizada (TC) [16]. Recentemente, ressonância magnética tem sido utilizada em pacientes com TEP e com contraindicação a angio-TC.[17]

A detecção pela angio-TC de falhas de enchimento luminais arteriais é o achado essencial para diagnóstico e avaliação da extensão da doença. Além disso, a TC permite também análise do parênquima pulmonar, mediastino e da cavidade pleural.

Angio-TC é um dos métodos de diagnóstico por imagem mais específicos para diagnóstico e quantificação de TEP.[18-19] O critério diagnóstico para TEP agudo inclui oclusão arterial com falha de enchimento de sua luz e aumento de calibre da artéria comparada aos vasos pérvios adjacentes. Alguns sinais têm sido usados para diagnóstico indireto de TEP.[20-21] Estes incluem oligoemia regional (sinal de

Westmark); opacidade triangular com base pleural (corcova de Hampton) e proeminência da artéria pulmonar central (sinal de Fleischner).[22]

A principal consequência hemodinâmica do TEP é a redução do fluxo pulmonar, a qual resulta em aumento da resistência vascular pulmonar e pressão arterial pulmonar, sobrecarregando o ventrículo direito.[23-24] Além disso, observa-se nos casos de TEP redução do fluxo da drenagem venosa.[23-25]

Devido a falta de suprimento causado pela obstrução da artéria pulmonar opacificada pelo contraste (TEP), existe falha da drenagem deste sangue, de uma determinada região, pelas veias pulmonares, ocasionando falha na opacificação da veia pulmonar central. Esta falha de enchimento em veia pulmonar central, com extensão igual ou maior que 2 cm, nos denominamos SINAL DA VEIA PULMONAR (SVP) e corresponde a sangue não opacificado pelo contraste, representando sinal secundário de TEP.

Diante deste contexto, justifica-se o estudo da associação entre sinal da veia pulmonar e diagnóstico de tromboembolismo pulmonar agudo, pois a identificação de defeitos de enchimento nas veias pulmonares em áreas adjacentes ao TEP. O SVP poderá contribuir sobremaneira no diagnóstico de TEP e, por conseguinte, melhorar a qualidade e quantidade de vida destes pacientes. Do ponto de vista científico, na literatura não foram encontrados trabalhos com este enfoque.

1.1- Objetivo

O objetivo deste estudo foi investigar a associação entre sinal da veia pulmonar e o diagnóstico de tromboembolismo pulmonar agudo.

2- CASUÍSTICA E MÉTODO

2-1. Casuística

Foram estudados, retrospectivamente, pacientes que apresentaram suspeita de TEP submetidos a angio-TC, independente de sexo e raça, no período de março/2012 e fevereiro/2013. Os pacientes foram atendidos no Instituto de Radiodiagnóstico Rio Preto, São José do Rio Preto-SP e na Santa Casa de Misericórdia de Porto Alegre-RS.

Foram excluídos pacientes com alguma contraindicação a angio-TC como insuficiência renal ou alergia ao meio de contraste iodado, e aqueles com suspeita clínica maior que 48 horas.

Este estudo foi aprovado pelo Comitê de Ética em Pesquisa em Seres Humanos (CEP) da Faculdade de Medicina de São José do Rio Preto (FAMERP) (Anexo 1).

2-2. Método

A angio-TC foi realizada em tomógrafo multidetectores de 64 canais LightSpeed VCT XT scanner (GE Healthcare Technologies, Waukesha, WI, Estados Unidos) (Figura 1). Os cortes tomográficos foram realizados da base até o ápice pulmonar em direção caudocefálica, usando os seguintes parâmetros: 225mAs, 120 kV, colimação de 0,5 mm, tempo de rotação de 0,75s com um 3,5 cm/s de movimento da mesa por rotação do *gantry*. A administração do meio de contraste foi realizada usando bomba injetora (CT Injector, Ulrich Medical, Ulm-Jungingen, Alemanha) com fluxo de 4,5 mL/s. Todos os pacientes receberam 1 mL de Ominipaque 350 mg/mL por Kg de peso corpóreo (Amersham Health, Cork, Irlanda). A administração de cada bolo foi seguida

imediatamente por 60 mL de soro fisiológico. A aquisição helicoidal foi iniciada, após início da administração do meio de contraste, a qual foi determinada pela região de interesse (ROI) com limiar de 130 unidades Hounsfield (UH) no átrio esquerdo (SmartPrep, GE Medical Systems, Milwaukee, WI, Estados Unidos). Este protocolo foi utilizado para aumentar o enchimento de contraste nos vasos subsegmentares.

As imagens foram avaliadas por dois radiologistas com experiência em diagnóstico por imagem torácica. Depois destes dois radiologistas analisarem independentemente, eles revisaram as imagens conjuntamente com um terceiro radiologista torácico, visando a obtenção de consenso.

Para diagnóstico de TEP agudo foram adotados os seguintes critérios: (a) oclusão arterial com falha de enchimento de todo o lúmen; (b) defeito de enchimento parcial circundado por meio de contraste, produzindo sinal do trombo “a cavaleiro” nas imagens adquiridas perpendicularmente ao eixo longo e sinal do “trilho de trem” nas imagens longitudinais do vaso e, (c) defeito de enchimento intraluminal periférico que apresenta ângulos agudos com a parede arterial.

Para identificação do sinal da veia pulmonar foram consideradas as seguintes características: (a) defeito de enchimento homogêneo na veia pulmonar com no mínimo 2 cm e, (b) atenuação do átrio esquerdo [160 UH] para melhor visualização das veias pulmonares.

2-3. Análise Estatística

A prevalência foi obtida para todos achados radiológicos com base nas imagens de TC. Usando os casos que apresentaram TEP na angio-TC como referência, sensibilidade, especificidade e os valores preditivos positivo e negativo foram calculados para o SVP. Valores para razão de verossimilhança para um teste positivo

foram calculados como a sensibilidade, divididos por um (1), menos a especificidade. Os valores da razão de verossimilhança para um teste negativo foram calculados como um (1) menos, a sensibilidade, divididos pela especificidade.[26-27]

Concordância entre radiologistas foi analisada usando teste de Kappa. A interpretação deste teste baseou-se nos seguintes parâmetros: < 0,20 (baixa); 0,21-0,40 (razoável); 0,41-0,60 (moderada); 0,61-0,80 (boa); 0,81-1,00 (muito boa).[28] Para avaliar associação entre SVP e outros achados parenquimatosos foi utilizado o teste exato de Fisher.

Intervalos de confiança de 95% (IC) foram calculados para as proporções, conforme intervalo do escore de Wilson com correção contínua.[29]

Todos os resultados foram analisados usando programas computacionais SPSS versão 20 (SPSS Inc., Chicago, IL, Estados Unidos) e Excel 2010 (Microsoft Corporation, Redmond, WA, Estados Unidos). Valores bicaudais de $p < 0,05$ foram considerados estatisticamente significativos.

Figura 1: Fotografia mostrando tomógrafo multidetectores de 64 canais LightSpeed VCT XT scanner utilizado nesta pesquisa. (Fonte:https://www.clinicalimagingsystems.com/product/ge-lightspeed-vct-64-slice-scanner/).

3- RESULTADOS

Dos 119 pacientes estudados; 73 (61,34%) eram do sexo feminino e 46 (38,66%) do masculino. A faixa etária dos pacientes variou de 11 a 88 anos (média 62 anos).

O tempo total da angio-TC foi 7,40 ± 1,45 min. para todo o tórax, variando de acordo com volume estudado. O intervalo de tempo para reposicionar o paciente da cama para o aparelho e o inverso não foram calculados. Todos os achados foram de qualidade suficiente para interpretação conclusiva.

O tromboembolismo pulmonar foi diagnosticado em 44 (35,8%) pacientes. Dentre estes pacientes, considerando a possibilidade de êmbolo em diferentes níveis no mesmo indivíduo; 10,92% (n = 13) tiveram êmbolos no tronco pulmonar; 11,76% (n = 14) em artérias lobares; 20,17% (n = 24) segmentares, e 6,72% (n = 8) subsegmentares, conforme Tabela1 e Figura 2.

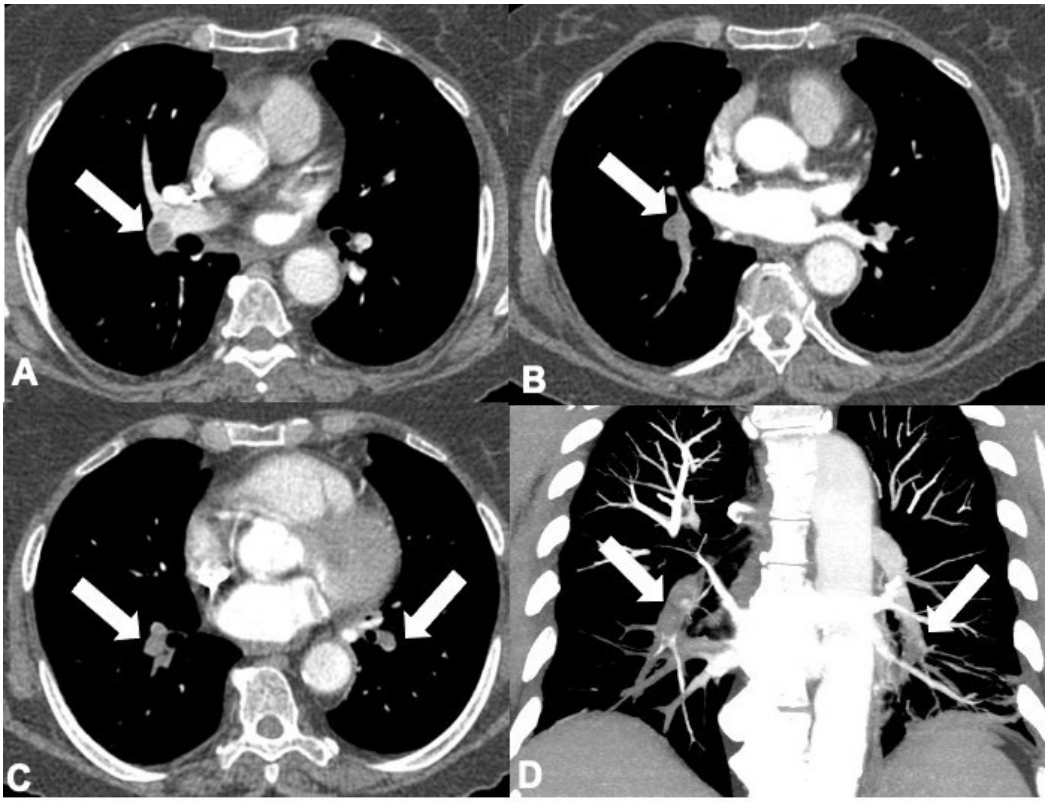

Figura 2: Cortes axiais na angio-TC em A,B,C e reconstrução coronal em D. Podemos notar falhas de enchimento em ramos interlobares da artéria pulmonar direita, bem como, em ramos segmentares e subsegmentares das artérias pulmonares bilaterais (setas brancas).

Tabela 1. Prevalência e localização de embolia pulmonar em 119 pacientes submetidos à angiotomografia das artérias pulmonares.

Parâmetros	**N (%)**
Prevalência	44 (36,97)
Localização	
central	13 (10,92)
lobar	14 (11,76)
segmentar	24 (20,17)
subsegmentar	8 (6,72)

N= número de indivíduos.

O SVP foi detectado em 16 (36,36%) pacientes num total de 44 com TEP. A Figura 3 representa exemplo de SVP associado a TEP. A sensibilidade foi 36,36% (intervalo de confiança (IC) 95% 22,83-52,26%); especificidade, 98,67% (IC 95% 91,79-99,93%); valor preditivo positivo, 94,12% (IC 95% 69,24-99,69%), valor preditivo negativo; 72,55% (95% IC 3,74-198,66). Razão de verossimilhança positiva foi 27,27 (IC 95% 3,74-198,66) e razão de verossimilhança negativa foi 0,64 (IC 95% 0,52-0,81).

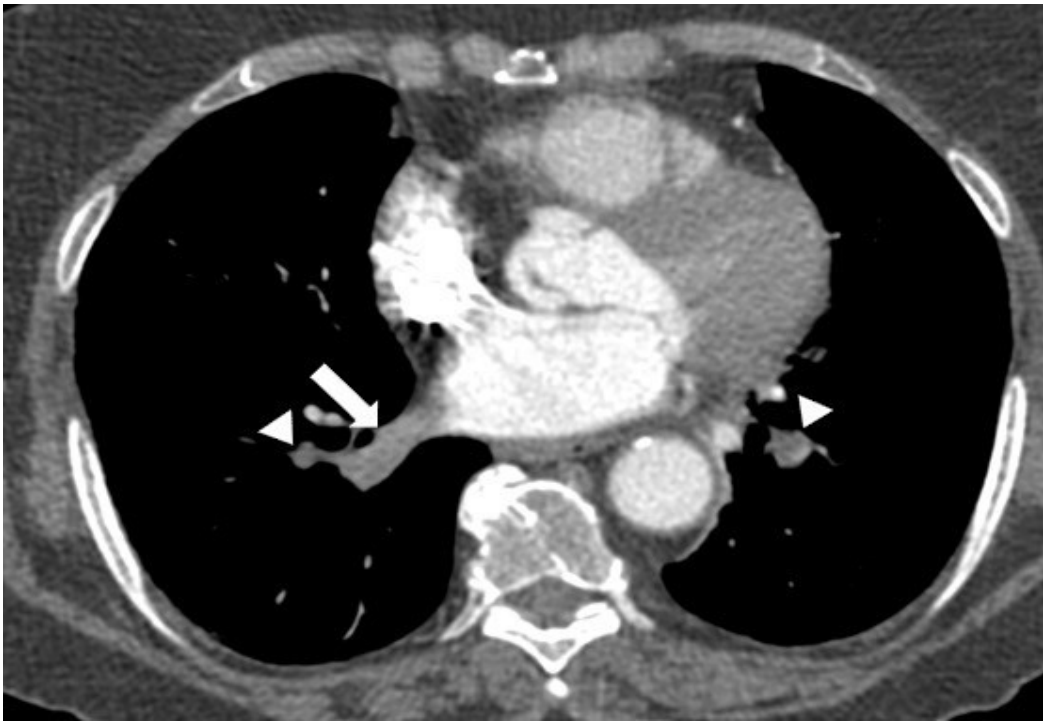

Figura 3: Corte axial de angio-TC com TEP em ramos lobares inferiores das artérias pulmonares inferiores bilaterais (cabeças de seta) e demonstrando o SVP na veia pulmonar inferior direita (seta branca).

Já O índice de Kappa para o SVP entre os dois radiologistas foi bom (0,801; IC 95% 0,645-0,957), conforme demonstra a Tabela 2 a seguir:

Tabela 2. Sensibilidade, especificidade, valores preditivos positivo e negativo, razões de verossimilhança e teste de Kappa para sinal da veia pulmonar em 119 pacientes submetidos à angiotomografia das artérias pulmonares.

.**Sinal da veia pulmonar**	**%**	**IC 95%**
Sensibilidade	36,36	22,83-52,26
Especificidade	98,67	91,79-99,93
VPP	94,12	69,24-99,93
VPN	72,55	62,67-80,70
RV+	27,27	3,74-198,66
RV-	0,64	0,52-0,81
Índice de Kappa	0,80	0,64-0,96

N = número de indivíduos; IC = intervalo de confiança; VPP = valor preditivo positivo; VPN = valor preditivo negativo; RV+ = razão de verossimilhança positiva; RV- = razão de verossimilhança negativa

Houve associação estatisticamente significativa entre SVP e TEP de localização lobar e segmentar ($P < 0,01$). Entre os 44 pacientes com TEP; seis tiveram êmbolos localizados (unilobar) e a sua localização não foi correlacionada com o SVP ($P = 0,21$). Houve associação significativa entre TEP unilateral e SVP ($P < 0,05$), conforme a Figura 4 a seguir:

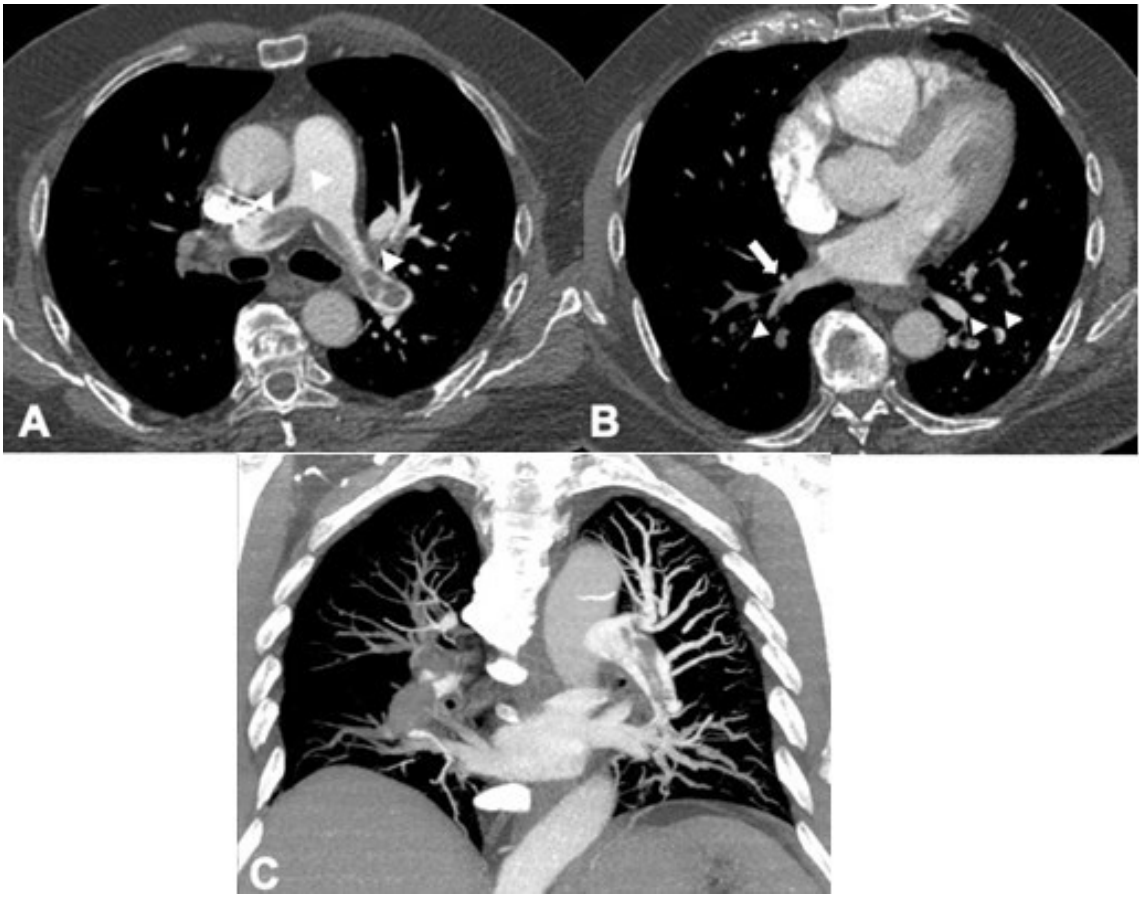

Figura 4: Cortes axiais de angio-TC em A e B, reconstrução em MIP (projeção de intensidade máxima) coronal em C. Foram notadas falhas de enchimento em ramos centrais das artérias pulmonares com formação de "trombo a cavaleiro", bem como, em ramos interlobares, segmentares e subsegmentares das artérias pulmonares bilaterais (cabeças de seta). Presença do SVP à direita demonstrado em B,C (setas brancas).

Prevalências de outros achados pulmonares encontram-se na Tabela 3. Nódulo pulmonar, espessamento de paredes de brônquios e bandas lineares foram os achados adicionais mais comuns (prevalências de 37,5, 22 e 20%, respectivamente). Nenhuma correlação entre esses achados e TEP foram estatisticamente significativos.

Tabela 3: Prevalência de outros achados pulmonares em 119 pacientes submetidos à angiotomografia das artérias pulmonares.

Achados	**Prevalência n (%)**	**Unilateral n (%)**	**Bilateral n (%)**
Consolidação	12 (10,0)	8 (66,7)	4 (33,3)
Derrame pleural	15 (12,6)	3 (20,0)	12 (80,0)
Fibrose pulmonar	8 (6,7)	0	8 (100)
Atelectasia	12 (10,0)	2 (16,7)	10 (83,3)
Bandas lineares	24 (20,0)	9 (37,5)	15 (62,5)
Massa pulmonar	6 (5,0)	0	6 (100)
Espessamento de brônquios	26 (22,0)	0	26 (100)
Bronquiectasia	2 (1,6)	2 (100)	0
Nódulo pulmonar	45 (37,8)	5 (11,1)	40 (88,9)

Não houve correlação estatisticamente significativa entre estes achados e tromboembolismo pulmonar.

4- DISCUSSÃO

Neste estudo os resultados mostraram que a prevalência do sinal da veia pulmonar foi altamente específica para tromboembolismo pulmonar agudo. Houve concordância satisfatória entre os resultados da avaliação radiológica inicial e revisão de imagens. O sinal da veia pulmonar, detectado por angiotomografia das artérias pulmonares, pode contribuir para o diagnóstico de tromboembolismo pulmonar agudo.

Embora o SVP não tenha sido relatado previamente na literatura, alguns autores têm estudado outros sinais tomográficos de TEP.[20,22] Worsley *et al*. descreveram sinais clássicos de TEP, como sinais de Westmark, Fleischner e corcova de Hampton, apresentando sensibilidades variando de 8 a 22%, e especificidades de 80 a 96%.[22] No entanto, neste estudo estes sinais foram avaliados na radiografia de tórax para pacientes em que o TEP tinha sido confirmado angiograficamente. Apesar das diferenças metodológicas, nesta pesquisa a sensibilidade foi baixa (36,4%) e a especificidade alta (98,7%); equiparável para o SVP. Além disso, a prevalência foi similar do TEP (36,97%) a diversas séries anteriores de angio-TC.[20,30]

Recentemente, Ermin *et al*. [31], estudando 286 pacientes com TEP, encontraram o SVP em 32,7% deles, sendo a especificidade de 88,46%. No presente estudo, o SVP foi identificado em 36,36% dos pacientes com TEP, sendo a especificidade de 98,67%. Apesar da frequência de ocorrência do SVP ser próxima entre estes trabalhos, é importante ressaltar que existem diferenças como quantidade de detectores dos tomógrafos; sendo 16 no de Ermin *et al*.[31] e 64 no presente estudo. Além disso, o protocolo da angio-TC foi distinto. Neste trabalho foi padronizada a administração do meio de contraste, determinada pelo ROI com 130 UH no átrio esquerdo, enquanto Ermin *et al*.[31] otimizaram a opacificação da artéria pulmonar.

Considerando que os critérios para detecção exata do SVP incluem atenuação do átrio esquerdo maior que 160 UH. Nem todos os exames possibilitarão a identificação do SVP, pois a drenagem das veias pulmonares ocorre em direção ao átrio esquerdo.

Zhang *et al.*[32] investigaram valor preditivo do preenchimento insuficiente do meio de contraste em veias pulmonares de pacientes com TEP agudo por meio de angio-TC. Entretanto, os autores não especificaram os critérios tomográficos para a detecção dessa falha no preenchimento. Nesta pesquisa, um dos critérios foi defeito de enchimento homogêneo na veia pulmonar com no mínimo 2 cm.

Nesta investigação, houve correlação estatisticamente significativa do SVP e êmbolos lobares e segmentares, mas não para coágulos no tronco pulmonar nem em TEP subsegmentar (6,72%). Vale ressaltar que alguns mecanismos fisiopatológicos podem ser responsáveis por esta associação. Usualmente alterações hemodinâmicas iniciais por TEP ocorrem devido a mecanismo de reflexo, que causa vasoconstricção de artérias pulmonares pequenas aumentando a resistência arteriolar pulmonar.[33] Quando o TEP é maciço ou repetitivo, um mecanismo de bloqueio do leito vascular pulmonar pode resultar em hipertensão pulmonar sustentada.[33] Este mecanismo também pode afetar o SVP, o qual pode ser transitório com TEPs pequenos. Recentemente, Koike *et al.*,[33] utilizando TC com dupla energia para avaliar perfusão pulmonar no TEP, verificaram que a diferença do volume de perfusão sanguínea pulmonar em pacientes com e sem TEP tende a ser maior na fase precoce do que na fase tardia. A provável explicação para este achado é que na fase inicial existe avaliação da perfusão da artéria pulmonar, enquanto em fase tardia existe a participação de artérias colaterais sistêmicas. Além disso, salientaram o importante papel das artérias colaterais sistêmicas em portadores de TEP. Isso também pode interferir no SVP, como aumento na perfusão de

volume sanguíneo pulmonar, devido ao fluxo sistêmico de colaterais durante a aquisição de imagens tardias que poderia também aumentar o fluxo venoso, modificando a apresentação do SVP.

Apesar dos achados pulmonares adicionais serem frequentes, não foi encontrada correlação estatisticamente significativa com TEP. Coche *et al.*[20] investigando o valor dos achados parenquimatosos e pleurais dos pacientes com clínica suspeita para TEP, observaram diferença significativa somente em consolidações com formato triangular e bandas lineares. Nesta série, apesar de não analisar consolidações de acordo com seu aspecto morfológico, estes achados não foram associados com TEP em nossas sequências.

Algumas limitações deste estudo incluem amostra de tamanho reduzido. Estudos prospectivos adicionais podem também tentar avaliar alguma correlação entre SVP e indicadores clínicos de TEP, como o escore de Wells e/ou risco de mortalidade. Além disso, estimar o tempo médio do evento do TEP e da apresentação do sinal pode ser útil para caracterizar futuramente este achado. Nesta pesquisa, foi investigado o SVP em pacientes com TEP agudo. Estudos adicionais podem investigar este achado em TEP crônico e/ou embolia não trombótica. Alguns pacientes incluídos em nossa amostra apresentaram anormalidades estruturais nos pulmões, como fibrose e massas pulmonares, o que pode afetar a circulação pulmonar, influenciando na acurácia do SVP. O SVP deveria também ser investigado em situações de fluxo venoso reduzido, como disfunção cardíaca esquerda e doença pulmonar veno-oclusiva, a qual provavelmente afeta a prevalência e acurácia deste sinal.

5- CONCLUSÕES

Nesse sentido, diante da literatura científica da área, dos resultados obtidos e da discussão realizada, é possível concluir que:

1- A prevalência do sinal da veia pulmonar foi altamente específica para tromboembolismo pulmonar;

2- O sinal da veia pulmonar, detectado por angiotomografia das artérias pulmonares, pode contribuir para o diagnóstico de tromboembolismo pulmonar agudo.

6- REFERÊNCIAS BIBLIOGRÁFICAS

1. Giordano NJ, Jansson PS, Young MN, Hagan KA, Kabrhel C. Epidemiology, Pathophysiology, Stratification, and Natural History of Pulmonary Embolism. Tech Vasc Interv Radiol 2017;20:135-140.

2. Cronin P, Dwamena BA. A clinically meaningful interpretation of the Prospective Investigation of Pulmonary Embolism Diagnosis (PIOPED) II and III data. Acad Radiol. 2018;25:561-572.

3. Bryce YC, Perez-Johnston R, Bryce EB, Homayoon B, Santos-Martin EG. Pathophysiology of right ventricular failure in acute pulmonary embolism and chronic thromboembolic pulmonary hypertension: a pictorial essay for the interventional radiologist. Insights Imaging 2019;10:18.

4. Mançano AD, Rodrigues RS, Barreto MM, Zanetti G, Moraes TC, Marchiori E. Incidence and morphological characteristics of the reversed halo sign in patients with acute pulmonary embolism and pulmonary infarction undergoing computed tomography angiography of the pulmonary arteries. J Bras Pneumol 2019;45:e20170438.

5. Beckman MG, Hooper WC, Critchley SE, Ortel TL. Venous thromboembolism: a public health concern. Am J Prev Med 2010;38:S495-501.

6. Giuntini C, Di Ricco G, Marini C, et al. Updates on pulmonary embolism: epidemiology. Chest 1995;107:3S-9S.

7. Goldhaber SZ, Visani L, De Rosa M. Acute pulmonar embolism: clinical outcomes in the International Cooperative Pulmonary Embolism Registry (ICOPER). Lancet 1999;353:1386-1389.

8. Golin V, Sprovieri SRS, Salles MJC. Pulmonary thromboembolism: retrospective study of necropsies performed over 24 years in an university hospital in Brazil. Rev Paul Med 2002;120:105-108.

9. He H, Stein MW, Zalta B, et al. Pulmonary infarction: spectrum of findings on multidetector helical CT. J Thorac Imaging 2006;21:1-7.

10. Stein PD, Matta F, Musani MH, et al. Silent pulmonary embolism in patients with deep venous thrombosis: a systematic review. Am J Med 2010;123;426-431.

11. Fred HL. Unsuspected pulmonar thromboembolism: a continuing clinical challenge. Tex Heart Inst J 2013;40:9-12.

12. Terra Filho M, Menna-Barreto SS. Comissão de circulação pulmonar da Sociedade Brasileira de Pneumologia e Tisiologia. Recomendações para o manejo de tromboembolia pulmonar. J braspneumol 2010;36(supl.1):S1-S68.

13. Pollack CV, Schreiber D, Goldhaber SZ, et al. Clinical characteristics, management, and outcomes of patients diagnosed with acute pulmonary embolism in the emergency department: initial report of EMPEROR (Multicenter Emergency Medicine Pulmonary Embolism in the Real World Registry). J Am Coll Cardiol2011;57:700-706.

14. Torres-Macho J, Mancebo-Plaza AB, Crespo-Giménez A, et al. Clinical features of patients inappropriately undiagnosed of pulmonar embolism. Am J Emerg Med 2013;31:1646-1650.

15. Casazza F, Becattini C, Bongarzoni A, et al Clinical features and short term outcomes of patients with acute pulmonary embolism: The Italian Pulmonary Embolism Registry (IPER).Thromb Res 2012;130:847-52.

16. Osman AM, Abdeldayem EH. Value of CT pulmonary angiography to predict short-term outcomes in patients with pulmonary embolism. Int J Cardiovasc Imaging 2018;34:975-983.

17. Ufuk F, Kaya F, Herek D, Sagtas E, Cakmak P, Yagci B. Pulmonary vein sign on unenhanced-MRI as a sign of severe pulmonary embolism. Iran J Radiol 2019;16: e85998.

18. Schoepf U, Holzknecht N, Helmberger TK, et al. Subsegmental pulmonary emboli: improved detection with thin-collimation multidetector row spiral CT. Radiology 2002;222:483-490.

19. Stein PD, Fowler SE, Goodman LR, et al. Multidetector computed tomography for acute pulmonary embolism. N Engl J Med 2006;354:2317-2327.

20. Coche EE, Muller NL, Kim K, et al. Acute pulmonary embolism: ancillary findings at spiral CT. Radiology 1998;207:753-758.

21. Marchiori E, Zanetti G, Escuissato DL, et al. Reversed halo sign: high-resolution CT scan findings in 79 patients. Chest 2012;141:1260-1266.

22. Worsley DF, Alavi A, Aronchick JM, et al. Chest radiographic findings in patients with acute pulmonary embolism: observations from the PIOPED study. Radiology 1993;189:133-136.

23. 23-Feihl F. Hemodynamics and gas exchange in pulmonary embolism: physiopathology and treatment. Schweiz MedWochenschr1991;121:1645-1653.

24. Riedel M, Rudolph W. Hemodynamics and gas exchange in acute lung embolism. Herz1989;14:109-114.

25. Yamamoto T. Management of patients with high-risk pulmonary embolism: a narrative review. J Intensive Care 2018;6:16.

26. Lijmer JG, Mol BW, Heisterkamp S, Gouke JB, Prins MH, van der Meulen JHP et al. Empirical Evidence of Design-Related Bias in studies of Design Tests. JAMA 1999;282:1061-1066.

27. Jaeschke R, Guyatt GH, Sackett DL. What Are the Results and Will They Help me in Caring for My Patients?. JAMA 1994;271: 703-707.

28. Landis JR, Koch GG. The measurement of observer agreement for categorical data. Biometrics 1977;33:159-74.

29. Newcombe RG. Explanatory and Pragmatic Estimates of the Treatment Effect when Deviations from allocated Treatment occur. Statistics in Medicine 1988; 7:1179-1186.

30. Donohoo, J H, Mayo-Smith W, Pezzullo J; Egglin TK. Utilization Patterns and Diagnostic Yield of 3421 Consecutive Multidetector Row Computed Tomography Pulmonary Angiograms in a Busy Emergency Department. Journal of Computer Assisted Tomography 2008; 32:421-425.

31. Emin, S, Çinkooğlu A, Susam S, Batum Ö, Yılmaz, U. A new perspective for pulmonary thromboembolism radiology: 'Pulmonary vein sign'. Clin Respir J. 2018;12:2653-2658.

32. Zhang H, Ma Y, Song Z, Lv J, Yang Y. Predictive value of insufficient contrast medium filling in pulmonary veins in patients with acute pulmonary embolism.Medicine (Baltimore) 2017;96:e7926.

33. Parmley LF, north RL, Ott BS. Hemodynamic Alterations of Acute Pulmonary Thromboembolism. Circulation Rettarch. 1911; 9:450-465.

34. Koike K, Sueyoshi E, Sakamoto I, Uetani M. Clinical Significance of Late Phase of Lung Perfusion Blood Volume (Lung Perfusion Blood Volume) Quantified by Dual-Energy Computed Tomography in Patients With Pulmonary Thromboembolism. J Thorac Imaging 2017;32:43-49.

ANEXOS

ANEXO 01. APROVAÇÃO DO COMITÊ DE ÉTICA HUMANO

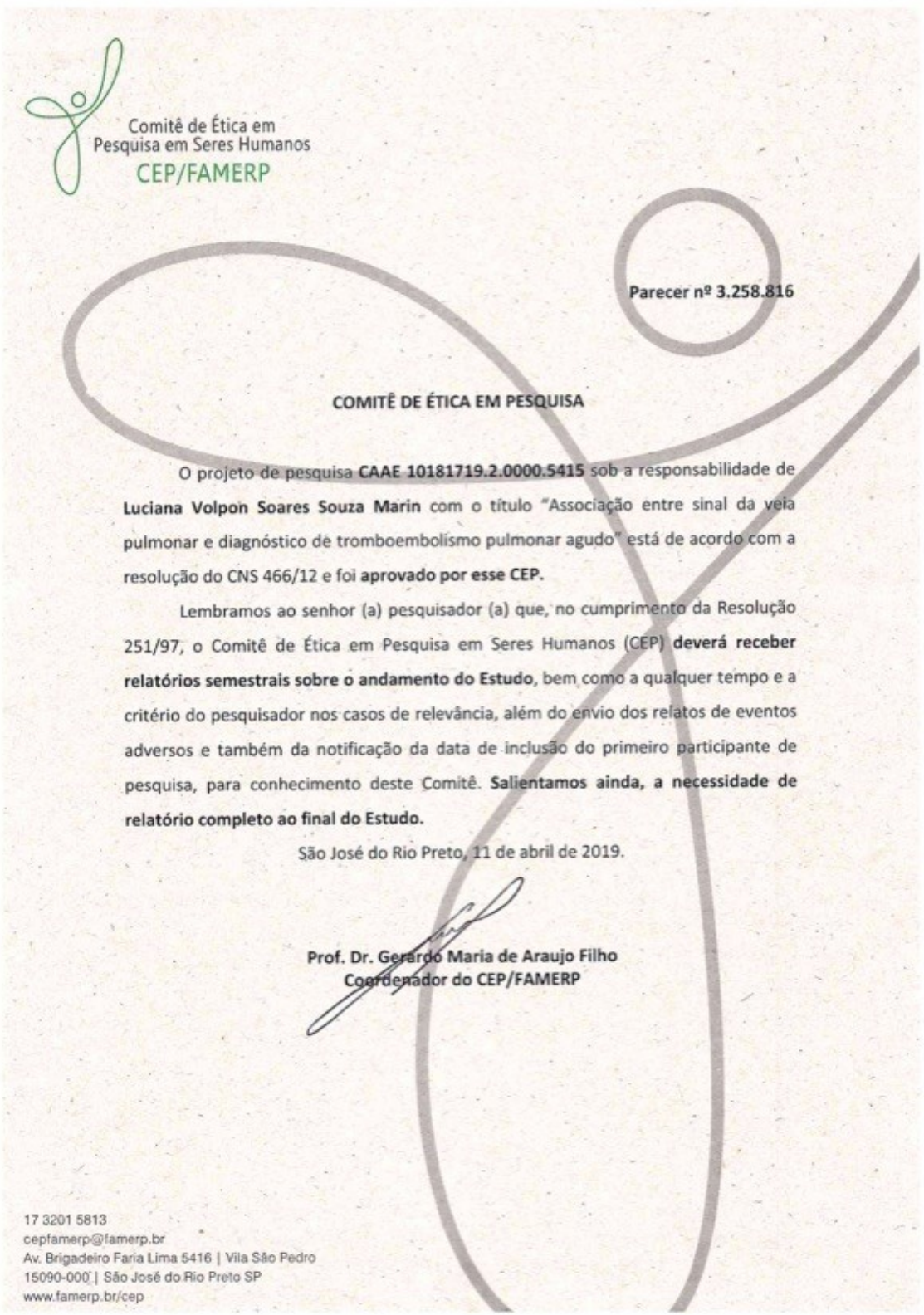

Comitê de Ética em
Pesquisa em Seres Humanos
CEP/FAMERP

Parecer nº 3.258.816

COMITÊ DE ÉTICA EM PESQUISA

O projeto de pesquisa **CAAE 10181719.2.0000.5415** sob a responsabilidade de **Luciana Volpon Soares Souza Marin** com o título "Associação entre sinal da veia pulmonar e diagnóstico de tromboembolismo pulmonar agudo" está de acordo com a resolução do CNS 466/12 e foi **aprovado por esse CEP.**

Lembramos ao senhor (a) pesquisador (a) que, no cumprimento da Resolução 251/97, o Comitê de Ética em Pesquisa em Seres Humanos (CEP) **deverá receber relatórios semestrais sobre o andamento do Estudo**, bem como a qualquer tempo e a critério do pesquisador nos casos de relevância, além do envio dos relatos de eventos adversos e também da notificação da data de inclusão do primeiro participante de pesquisa, para conhecimento deste Comitê. **Salientamos ainda, a necessidade de relatório completo ao final do Estudo.**

São José do Rio Preto, 11 de abril de 2019.

Prof. Dr. Gerardo Maria de Araujo Filho
Coordenador do CEP/FAMERP

17 3201 5813
cepfamerp@famerp.br
Av. Brigadeiro Faria Lima 5416 | Vila São Pedro
15090-000 | São José do Rio Preto SP
www.famerp.br/cep

APÊNDICES

APÊNDICE 01. ARTIGO CIENTÍFICO RESULTANTE DA TESE PUBLICADO EM PERIÓDICO INTERNACIONAL

Lung
DOI 10.1007/s00408-017-0057-7

PULMONARY VASCULAR DISEASE

"Pulmonary Vein Sign" for Pulmonary Embolism Diagnosis in Computed Tomography Angiography

Luciana Volpon Soares Souza[1] · Matheus Zanon[2,3] · Arthur Soares Souza[1] · Klaus Irion[4] · Diana Penha[4] · Giordano Rafael Tronco Alves[5] · Edson Marchiori[5] · Bruno Hochhegger[2,3]

Received: 21 May 2017 / Accepted: 11 September 2017

Abstract
Purposes Considering that pulmonary arterial obstruction decreases venous flow, we hypothesized that filling defects in pulmonary veins can be identified in areas adjacent to pulmonary embolism (PE). This sign was named the "pulmonary vein sign" (PVS), and we evaluated its prevalence and performance for PE diagnosis in computed tomography pulmonary angiography (CTPA).
Methods This retrospective study enrolled consecutive patients with clinical suspicion of PE who underwent CTPA scan. The PVS was defined by the following criteria: (a) presence of a homogeneous filling defect of at least 2 cm in a pulmonary vein; (b) attenuation of the left atrium > 160 Hounsfield units. Using the cases that presented PE on CTPA as reference, sensitivity, specificity, and positive and negative predictive values were calculated for PVS.
Results In total, 119 patients (73 female; mean age, 62 years) were included in this study. PE was diagnosed in 44 (35.8%) patients. The PVS was present in 16 out of 44 patients with PE. Sensitivity was 36.36% (95% confidence interval (CI) 22.83–52.26%); specificity, 98.67% (95% CI 91.79–99.93%); positive predictive value, 94.12% (95% CI 69.24–99.69%); negative predictive value, 72.55% (95% CI 62.67–80.70%). The Kappa index for the PVS was good (0.801; 95% CI 0.645–0.957). PVS was correlated with lobar and segmental pulmonary embolism ($p < 0.01$).
Conclusion Despite a low sensitivity, presence of the pulmonary vein sign was highly specific for PE, with a good agreement between readers. This sign could contribute for PE diagnosis on CTPA studies.

Keywords Pulmonary embolism · Computed tomography pulmonary angiography · Pulmonary vein sign

✉ Matheus Zanon
mhgzanon@hotmail.com

Luciana Volpon Soares Souza
luvolpon@gmail.com

Arthur Soares Souza
asouzajr@gmail.com

Klaus Irion
klaus.irion@btinternet.com

Diana Penha
dianapenha@gmail.com

Giordano Rafael Tronco Alves
grtalves@gmail.com

Edson Marchiori
edmarchiori@gmail.com

Bruno Hochhegger
brunohochhegger@gmail.com

[1] Rio Preto Radiodiagnostic Intitute - Rua Cila, 3033, Sao Jose Do Rio Preto 15015-800, Brazil

[2] LABIMED – Medical Imaging Research Lab, Department of Radiology, Pavilhão Pereira Filho Hospital, Irmandade Santa Casa de Misericórdia of Porto Alegre - Av. Independência, 75, Porto Alegre 90020-160, Brazil

[3] Department of Diagnostic Methods, Federal University of Health Sciences of Porto Alegre - R. Sarmento Leite, 245, Porto Alegre 90050-170, Brazil

[4] Department of Radiology, Liverpool Heart and Chest Hospital, NHS Foundation Trust - Thomas Drive, Broadgreen, Liverpool L143PE, UK

[5] Department of Radiology, Federal University of Rio de Janeiro Medical School - Av. Carlos Chagas Filho, 373, Rio De Janeiro 21941-902, Brazil

Published online: 14 October 2017

Introduction

Pulmonary embolism (PE) is a relatively common medical emergency. Characterized by partial or total obstruction of pulmonary arteries usually due to a thrombus, PE results in a sudden reduction or cessation of perfusion in the corresponding zone [1]. The most common clinical presentations are shortness of breath and chest pain, but cough, fever, hemoptysis, and syncope can occur [2]. As these symptoms are non-specific, imaging plays a fundamental role in the diagnosis of PE [3].

Computed tomographic pulmonary angiography (CTPA) is one of the most accurate imaging modalities for PE diagnosis [4, 5]. The diagnostic criteria for acute PE include an arterial occlusion with failure to enhance the entire lumen due to a filling defect, and the artery could be enlarged compared to adjacent patent vessels. Some ancillary signs have been used for indirect diagnosis of PE [6, 7]. These include regional oligemia (Westermark sign); peripheral, pleural-based, wedge-shaped area of increased opacity (Hampton hump); and prominence of the central pulmonary artery (Fleischner sign) [8]. Determination of the diagnostic value of these ancillary signs may permit more reliable diagnoses when emboli are suboptimally visualized, or they can suggest the diagnosis when PE is not suspected.

The main hemodynamic consequence of PE is an acute mechanical reduction of the pulmonary vascular cross-sectional area, which results in sudden increase in pulmonary vascular resistance and pulmonary arterial pressure, intensifying right ventricular work [9, 10]. In addition, all PE cases show an ipsilateral reduction in venous drainage [9, 10]. Based on the theory that the pulmonary arterial obstruction decreases venous flow, our hypothesis is that we can identify filling defects in the pulmonary veins in areas adjacent to the PE. This sign was named the "pulmonary vein sign" (PVS). The aim of this study was to evaluate the prevalence and performance of this sign to diagnose PE in CTPA.

Materials and Methods

Patient Selection

This study was performed with the approval of our Institutional Review Board (ISCMPA Committee, IRB00002509), and informed consent was waived. We retrospectively analyzed CTPA scans performed between March 2012 and February 2013 of patients who presented in our emergency department with clinical suspicion of PE. All examinations were completed within 48 h of clinical presentation. Subjects were excluded if there were any contraindications for CTPA, such as chronic renal failure or allergy to iodine medium.

Computed Tomography Protocol

Computed tomography angiography was performed using a multidetector scanner (64-slice LightSpeed VCT XT scanner, GE Healthcare Technologies, Waukesha, Wisconsin, United States of America). Lungs were scanned from the base to the apex in the caudocephalic direction using the following parameters: using the following scan parameters: 225 mAs, 120 kV, 0.5 mm collimation, rotation time of 0.75 s with a 3.5 cm/s table movement per gantry rotation. Administration of contrast material was performed using an automatic power injector (CT Injector, Ulrich Medical, Ulm-Jungingen, Germany) at a flow rate of 4.5 mL/s. All patients received 1 mL of Omnipaque 350 mg/mL per kilogram body weight (Amersham Health, Cork, Ireland). Administration of each bolus was followed immediately by a 60 mL saline flush. The helical acquisition was initiated after the start of the bolus administration of contrast medium, which was determined by a region of interest (ROI) with a threshold of 130 HU in the left atrium. (Smart Prep; GE Medical Systems). We routinely use this protocol to increase the contrast fill in subsegmental vessels.

Imaging Evaluation

Image interpretation was performed by two radiologists specifically trained in thoracic imaging, with 10 and 9 years of experience. After these two radiologists had conducted independent analyses, they reviewed the images together with a third senior chest radiologist with more than 20 years of experience to reach final consensus. Findings were analyzed according to the Fleischner Society's Glossary of Terms [11].

For acute PE diagnosis, the following criteria had to be included: (a) arterial occlusion with failure to enhance the entire lumen due to a large filling defect, and artery could be enlarged compared to adjacent patent vessels; (b) partial filling defect surrounded by contrast material, producing the "polo mint" sign on images acquired perpendicular to the long axis of a vessel and the "railway track" sign on longitudinal images of the vessel; (c) a peripheral intraluminal filling defect that forms acute angles with the arterial wall.

The PVS was defined by the following criteria: (a) presence of a homogeneous filling defect in the least 2 cm of a pulmonary vein; and (b) attenuation of the left atrium > 160 HU. We hypothesized that this filling defect would be a consequence of a decreased venous flow due to

pulmonary arterial obstruction. Likewise, we have settled this threshold for attenuation of the left atrium for a better visualization of pulmonary veins.

Statistical Analysis

All results were analyzed using commercial software (SPSS ver. 20, SPSS Inc., Chicago, IL, USA; Excel 2010, Microsoft Corporation, Redmond, WA, USA). Two-tailed p values < 0.05 were considered to indicate statistical significance. Based on the CT images, prevalences were obtained for all radiological findings. Using the cases that presented PE on CTPA as reference, sensitivity, specificity, and positive and negative predictive values were calculated for the PVS. Values for likelihood ratios for a positive test were calculated as the sensitivity, divided by 1 minus the specificity; and likelihood ratios for a negative test were calculated as 1 minus the sensitivity, divided by the specificity [12, 13]. Agreement between radiologists was assessed using kappa statistics. Interpretation was conducted based on the following parameters: kappa < 0.20, poor agreement; kappa $= 0.21$–0.40, fair agreement; kappa $= 0.41$–0.60, moderate agreement; kappa $= 0.61$–0.80, good agreement; kappa $= 0.81$–1.00, very good agreement [14]. Fisher´s exact test was used to assess any associations between the PVS and other parenchymal findings. 95% confidence intervals (CI) were calculated for the proportions, according to Wilson score interval with continuity correction [15].

Results

The study protocol included 119 patients (female, $n = 73$ (61.34%); mean age, 62 years; age range, 11–88 years). Median total CTPA scanning time was about 7.40 min (SD ± 1.45 min) for the entire chest, varying according to the covered volume. The time interval for repositioning the patient from bed to the magnet and back has not been assessed. All findings were of sufficient quality for conclusive interpretation.

Pulmonary embolism was diagnosed in 44 (35.8%) patients. Among these patients, considering the possibility of emboli in different levels in the same subject, 10.92% ($n = 13$) had emboli in the pulmonary trunk, 11.76% ($n = 14$) in lobar arteries, 20.17% ($n = 24$) in the segmental level, and 6.72% ($n = 8$) were subsegmental PE (Table 1).

The PVS was present in 16 out of 44 patients with PE. Figure 1 depicts an example of the PVS associated with PE in the right lower lobe. Sensitivity was 36.36% (95% confidence interval (CI) 22.83–52.26%); specificity, 98.67% (95% CI 91.79–99.93%); positive predictive value, 94.12% (95% CI 69.24–99.69%); negative predictive value, 72.55% (95% CI 62.67–80.70%). Positive likelihood ratio was 27.27 (95% CI 3.74–198.66), and negative likelihood ratio was 0.64 (95% CI: 0.52–0.81). The Kappa index for the pulmonary vein sign between the two radiologists was good (0.801; 95% CI 0.645–0.957).

Table 1 Pulmonary embolism prevalence and the "pulmonary vein sign" performance in 119 patients

Parameters	n (%)	95% CI
Prevalence	44 (36.97)	–
Location		
Main	13 (10.92)	–
Lobar	14 (11.76)	–
Segmental	24 (20.17)	–
Subsegmental	8 (6.72)	–
"Vein sign" performance		
Sensitivity	36.36%	22.83–52.26
Specificity	98.67%	91.79–99.93
PPV	94.12%	69.24–99.69
NPV	72.55%	62.67–80.70
LR+	27.27	3.74–198.66
LR−	0.64	0.52–0.81
Kappa index	0.80	0.64–0.96

CI confidence interval, *LR+* positive likelihood ratio, *LR−* negative likelihood ratio, *NPV* negative predictive value, *PPV* positive predictive value

There was a statically significant association between the PVS and PE location at lobar and segmental levels ($p < 0.01$). Among the 44 patients with PE, six had localized (unilobar) embolisms and this location was not correlated with the PVS ($p = 0.21$). There was a statistically significant association between unilateral PE and the PVS ($p < 0.05$).

Prevalences of other pulmonary findings are presented in Table 2. Pulmonary nodule, bronchial thickening, and linear brands were the most common additional pulmonary findings (prevalences, 37.5, 22, and 20%, respectively). None of the correlations between these features and PE was statistically significant.

Discussion

In this study, we have tried to demonstrate an association between the PVS in CTPA scans and pulmonary embolism. Although this sign had not been reported previously in literature, other authors have studied the diagnostic performance of other ancillary CT signs of PE [8, 16]. Worsley et al. described classic signs for PE, such as Westermark, Fleischner, and Hampton hump signs, presenting sensitivities ranging from 8 to 22%, and

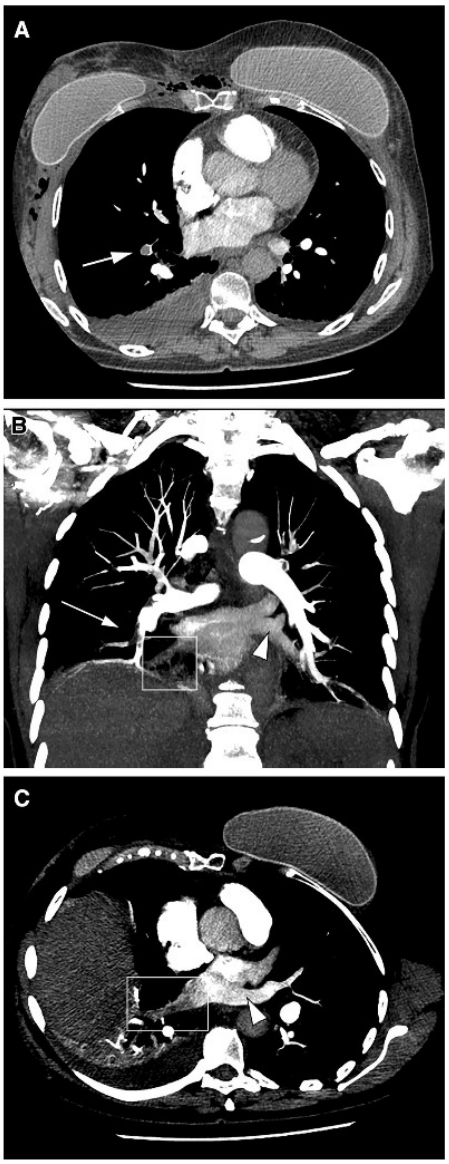

◀**Fig. 1** Images from a 46-year-old woman on the seventh postoperative day after bilateral breast augmentation surgery, with history of mastectomy due to breast cancer. Patient presented at the emergency department with sudden chest pain and dyspnea. Axial (**a**) and coronal (**b**) computed tomography images demonstrating a filling defect on a segmental pulmonary artery of the right lower lobe (white arrow). A filling defect greater than 2 cm is also noted in the adjacent pulmonary vein on the coronal (**b**) and oblique (**c**) CT reconstructions (white square), characterizing the "pulmonary vein sign." Comparatively, the other pulmonary veins are normally filled with contrast media (white arrowhead)

specificities ranging from 80 to 96% [8]. However, this study evaluated these signs at chest radiographies for patients that PE was angiographically confirmed. Despite methodological differences, our study demonstrated comparable low sensitivity (36.4%) and high specificity (98.7%) for the PVS. Additionally, we demonstrated a PE prevalence (36.97%) similar to several previous CTPA series [16–21].

There was a statistically significant correlation for the PVS and lobar and segmental pulmonary emboli but not for clots in the pulmonary trunk neither for subsegmental PE. This could be due to the small sample size and low prevalence of subsegmental PE (6.72%). However, some physiopathology mechanisms might be also accountable for this association. Usually initial pulmonary hemodynamic changes due to PE occurs from a reflex mechanism that causes vasoconstriction of small pulmonary arteries, increasing pulmonary arteriolar resistance [22]. When PE is massive or repetitive, mechanical blockage of the pulmonary vascular bed might result in sustained pulmonary hypertension [22]. This mechanism could also affect the PVS, which could be transient with small PEs. In a recent study by Koike et al. [23] that used dual-energy CT to assess lung perfusion in PE, the authors have found that difference in perfusion blood volume of the lung between patients with and those without PE tend to be larger in the early phase than in the late phase (respectively, 14 vs. 40 s from the start of injection of contrast media). This result might have reflected the reduction of pulmonary perfusion from the pulmonary artery and an enhanced role of systemic collaterals in patients with PE. This could also interfere in the PVS, as an increase in perfusion blood volume of the lung due to systemic collateral flow during late acquisition images could also increase venous flow, modifying PVS presentation.

Despite frequent additional pulmonary findings, no statistically significant correlation was found with pulmonary embolism. In a study by Coche et al. that tried to determine the value of lung parenchymal and pleural findings in patients with clinical suspicion of PE, a statistically significant difference was found only for wedge-shaped consolidations and linear bands [16]. Although we have not analyzed consolidations

Table 2 Prevalence of other pulmonary findings

Imaging findings	Prevalence *n* (%)	Unilateral *n* (%)	Bilateral *n* (%)
Consolidation	12 (10.0)	8 (66.7)	4 (33.3)
Pleural effusion	15 (12.6)	3 (20.0)	12 (80.0)
Pulmonary fibrosis	8 (6.7)	0	8 (100)
Atelectasis	12 (10.0)	2 (16.7)	10 (83.3)
Linear bands	24 (20.0)	9 (37.5)	15 (62.5)
Lung mass	6 (5.0)	0	6 (100)
Bronchial thickening	26 (22.0)	0	26 (100)
Bronchiectasis	2 (1.6)	2 (100)	0
Pulmonary nodule	45 (37.8)	5 (11.1)	40 (88.9)

None of the correlations between these features and PE was statistically significant

according to their morphology likewise, these findings were not associated with PE in our series.

Some limitations of this study include a small sample size. Further prospective studies should also try to evaluate any correlation between the PVS and clinical indicators of pulmonary embolism, such as the Wells score and/or mortality risk. In addition, estimating a mean time between the PE event and the sign presentation could be helpful to further characterize this finding. We have analyzed the PVS in patients with acute PE. Further studies could investigate this finding in chronic PE and/or non-thrombotic embolism. Some patients included in our sample presented structural abnormalities in the lungs, such as pulmonary fibrosis and lung masses, what could affect pulmonary circulation, influencing on the accuracy of the PVS. The PVS should also be investigated in situations of decreased venous flow, such as left heart dysfunction and pulmonary veno-occlusive disease, which probably affect this sign prevalence and accuracy.

In summary, despite a low sensitivity, presence of the "pulmonary vein sign" was highly specific for PE, with a good agreement between readers. This sign could contribute for PE diagnosis on CTPA studies.

Compliance With Ethical Standards

Conflict of interest The authors declare that they have no conflict of interest.

Ethical Approval All procedures performed in studies involving human participants were in accordance with the ethical standards of the institutional and/or national research committee and with the 1964 Helsinki declaration and its later amendments or comparable ethical standards.

References

1. McCaig LF, Nawar EW (2006) National hospital ambulatory medical care survey: 2004 emergency department summary. Adv Data 372:1–29
2. Pollack CV, Schreiber D, Goldhaber SZ et al (2011) Clinical characteristics, management, and outcomes of patients diagnosed with acute pulmonary embolism in the emergency department: initial report of EMPEROR (multicenter emergency medicine pulmonary embolism in the real world registry). J Am Coll Cardiol 57:700–706
3. Roy PM, Meyer G, Vielle B et al (2006) Appropriateness of diagnostic management and outcomes of suspected pulmonary embolism. Ann Intern Med 144:157–164
4. Schoepf U, Holzknecht N, Helmberger TK et al (2002) Subsegmental pulmonary emboli: improved detection with thin-collimation multi–detector row spiral CT. Radiology 222:483–490
5. Stein PD, Fowler SE, Goodman LR et al (2006) Multidetector computed tomography for acute pulmonary embolism. N Engl J Med 354:2317–2327
6. Coche EE, Muller NL, Kim K et al (1998) Acute pulmonary embolism: ancillary findings at spiral CT. Radiology 207:753–758
7. Marchiori E, Zanetti G, Escuissato DL et al (2012) Reversed halo sign: high-resolution CT scan findings in 79 patients. Chest 141:1260–1266
8. Worsley DF, Alavi A, Aronchick JM et al (1993) Chest radiographic findings in patients with acute pulmonary embolism: observations from the PIOPED study. Radiology 189:133–136
9. Riedel M, Rudolph W (1989) Hemodynamics and gas exchange in acute lung embolism. Herz 14:109–114
10. Feihl F (1991) Hemodynamics and gas exchange in pulmonary embolism: physiopathology and treatment. Schweiz Med Wochenschr 121:1645–1653
11. Hansell DM, Bankier AA, MacMahon H et al (2008) Fleischner society: glossary of terms for thoracic imaging. Radiology 246:697–722
12. Lijmer JG, Mol BW, Heisterkamp S et al (1999) Empirical evidence of design-related bias in studies of diagnostic tests. JAMA 282:1061–1066
13. Jaeschke R, Guyatt GH, Sackett DL (1994) Users' guides to the medical literature. III. How to use an article about a diagnostic test. B. What are the results and will they help me in caring for my patients? the evidence-based medicine working group. JAMA 271:703–707
14. Landis JR, Koch GG (1977) The measurement of observer agreement for categorical data. Biometrics 33:159–174
15. Newcombe RG (1998) Interval estimation for the difference between independent proportions: comparison of eleven methods. Stat Med 17:873–890
16. Coche EE, Müller NL, Kim KI et al (1998) Acute pulmonary embolism: ancillary findings at spiral CT. Radiology 207:753–758

17. Revel MP, Sanchez O, Couchon S et al (2012) Diagnostic accuracy of magnetic resonance imaging for an acute pulmonary embolism: results of the 'IRM-EP' study. J Thromb Haemost 10:743–750
18. Revel MP, Sanchez O, Lefort C et al (2013) Diagnostic accuracy of unenhanced, contrast-enhanced perfusion and angiographic MRI sequences for pulmonary embolism diagnosis: results of independent sequence readings. Eur Radiol 23:2374–2382
19. Weir ID, Drescher F, Cousin D et al (2010) Trends in use and yield of chest computed tomography with angiography for diagnosis of pulmonary embolism in a Connecticut hospital emergency department. Conn Med 74:5–9
20. Pasin L, Zanon M, Moreira J et al (2017) Magnetic Resonance Imaging of Pulmonary Embolism: diagnostic Accuracy of Unenhanced MR and Influence in Mortality Rates. Lung 195:193–199
21. Donohoo J, Mayo-Smith W, Pezzullo J, Egglin T (2008) Utilization patterns and diagnostic yield of 3421 consecutive multidetector row computed tomography pulmonary angiograms in a busy emergency department. J Comput Assist Tomogr 32:421–425
22. Parmley LF Jr, North RL, Ott BS (1962) Hemodynamic alterations of acute pulmonary thromboembolism. Circ Res 11:450–465
23. Koike H, Sueyoshi E, Sakamoto I, Uetani M (2017) Clinical significance of late phase of lung perfusion blood volume (lung perfusion blood volume) quantified by dual-energy computed tomography in patients with pulmonary thromboembolism. J Thorac Imaging 32:43–49

APÊNDICE 02. LISTA DE ARTIGOS CIENTÍFICOS QUE CITAM O ARTIGO RESULTANTE DA TESE PUBLICADO EM PERIÓDICO INTERNACIONAL

1. Hochhegger B, Zanon M, Altmayer S, Mandelli NS, Stüker, Mohammed TL et al. COVID-19 mimics on chest CT: a pictorial review and radiologic guide. British Journal of Radiology. 2021; 94:1-8.

2. Gopalan D, Nordgren-Rogberg A, Vi Le EP, Pavey H, Tarkin J, Nyrén S, Auger W et al. Abnormal Pulmonary Venous Filling: An Adjunct Feature in the Computed Tomography Pulmonary Angiogram Assessment of Chronic Thromboembolic Pulmonary Hypertension. J Am Heart Assoc.2020; 9:1-11.

3. Gopalan D, Riley JYJ, Leong K, Guo HH, Zamanian RT, Hsi ABS, et al. Pulmonary Vein Sign on Computed Tomography Pulmonary Angiography in Proximal and Distal Chronic Thromboembolic Pulmonary Hypertension With Hemodynamic Correlation. Journal of Thoracic Imaging.2023; 38:159-164.

4. Halloran T, Gutierrez M. Slow flow mimicking pulmonary embolism. BMJ case reports. 2023; 16: e255056.

5. Ermin, S, Çinkooğlu A, Susam S, Batum Ö, Yılmaz, U. A new perspective for pulmonary thromboembolism radiology:'Pulmonary vein sign'. Clin Respir J. 2018;12:2653-2658.

6. Hausmann D, Maher A, Sieroń DA, Huber AT, Obmann VC, Ebner L et al. Detection of pulmonary embolism on CT-angiography using contrast attenuation of pulmonary veins.Acta Angiologica. 2021; 27:1-9.

7. 吴长蓉, 陈毅斐, 陶兆武. 急性肺栓塞患者可溶性血栓调节蛋白, D-二聚体水平与CT 肺动脉阻塞指数的关系分析. *中国 CT 和 MRI 杂志*. 2019; 17: 29-31.

8. Huo Y R, Chan MV, Ridley L. Measuring right ventricular lateral wall thickness on CTPA and inpatient mortality in patients with acute PE-promising but more evidence required. Emergency Radiology.2021; 28: 863-864.

9. Ufuk F, Kaya F, Herek D, Sagtas E, Cakmak P, Yagci B. Pulmonary vein sign on unenhanced-MRI as a sign of severe pulmonary embolism. Iran J Radiol 2019;16: e85998.

Arch Bronconeumol. 2018;54(11):579

Sociedad Española de Neumología y Cirugía Torácica SEPAR

ARCHIVOS DE Bronconeumología

www.archbronconeumol.org

Clinical Image

A Complex Pulmonary Vascularization: Bilateral Meandering Pulmonary Veins

Una vascularización pulmonar compleja: venas pulmonares sinuosas bilaterales

Arthur Soares Souza Jr.[a,b], Luciana Volpon Soares Souza[a], Edson Marchiori[b,*]

[a] Ultra X, São José do Rio Preto, SP, Brazil
[b] Universidade Federal do Rio de Janeiro, Rio de Janeiro, Brazil

A 22-year-old asymptomatic female was referred to our hospital due to an abnormal finding on a chest radiograph during a routine check-up (Fig. 1A). Physical examination was unremarkable. She underwent enhanced chest computed tomography (CT) examination (Fig. 1B–D), which demonstrated bilateral pulmonary veins with anomalous routes in the lower pulmonary regions, and normal drainage into the left atrium. The diagnosis of bilateral meandering pulmonary veins (MPV) was made based on the CT findings, and the patient was discharged with no further investigation.

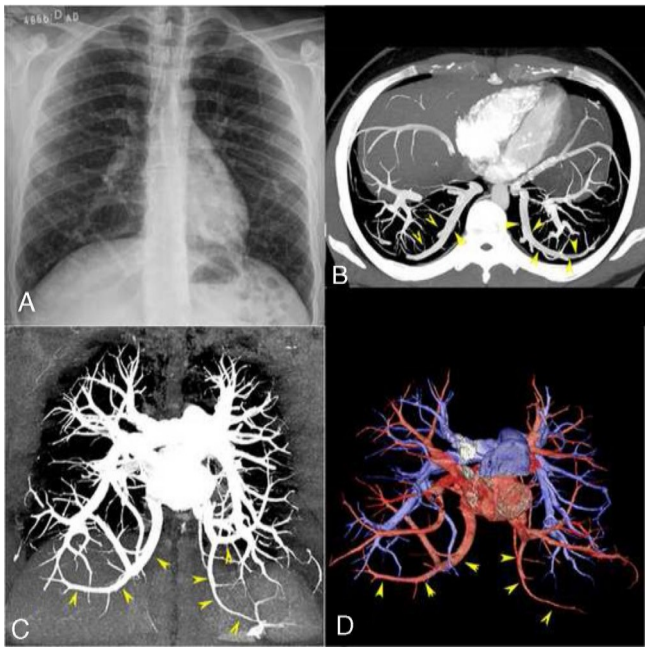

Fig. 1. Posteroanterior chest radiograph (A) showing bilateral anomalous curvilinear vessels in the lower pulmonary regions. Enhanced chest computed tomography (CT) examination with axial (B) and coronal (C) maximum intensity projection imaging, which demonstrated bilateral pulmonary veins with anomalous routes in the lower pulmonary regions (yellow arrowheads), but draining normally into the left atrium. Coronal volume-rendering 3D reconstruction (D) shows the anomalous veins (red) and normal pulmonary arteries (blue).

It is important to distinguish between pulmonary venous return malformation (PVRM) and MPV. PVRM (e.g., scimitar syndrome) results in a left-to-right shunt, which can lead to cyanosis and may require surgical correction. Consequently, patients are often symptomatic and present at a young age. In contrast, MPV involves no left-to-right shunt.[1,2] As in our case, patients with MPV are usually asymptomatic, with the diagnosis made incidentally. Recognition of these variations is important for the clinician to avoid unnecessary investigation when the differential diagnosis includes vascular malformations requiring surgical or interventional treatment. Furthermore, when patients with MPV require surgery for other reasons, thoracic surgeons should be aware of the anomaly to avoid injury to the anomalous vein. Treatment has not been required in any reported case of MPV.

References

1. Souza AS Jr, de Souza LS, Zanetti G, Marchiori E. A unique pulmonary vascular pattern: bilateral anomalous single pulmonary veins. Thorax. 2014;69:687.
2. Rodrigues MA, Ritchie G, Murchison JT. Incidental meandering right pulmonary vein, literature review and proposed nomenclature revision. World J Radiol. 2013;5:215–9.

* Corresponding author.
E-mail address: edmarchiori@gmail.com (E. Marchiori).

https://doi.org/10.1016/j.arbres.2018.05.017

J Bras Pneumol. 2019;45(1):e20180006
http://dx.doi.org/10.1590/1806-3713/e20180006

Solitary fibrous tumor of the pleura: a rare cause of elevation of the right lung base

Arthur Soares Souza Jr[1,2,a], Luciana Volpon Soares Souza[1,b], Gláucia Zanetti[3,c], Edson Marchiori[3,d]

DEAR EDITOR:

A 42-year-old female nonsmoker with no history of comorbidities was admitted to the hospital with a 6-month history of right-sided chest pain and dyspnea. A chest X-ray showed marked elevation of the right lung base (Figures 1A and 1B). Laboratory test results were unremarkable. A magnetic resonance imaging scan of the chest revealed a heterogeneous mass in the right hemithorax, with intermediate signal intensity on T1- and T2-weighted images (Figures 1C and 1D). A transthoracic needle biopsy was performed, and the results were inconclusive. The patient underwent radical surgical resection by open thoracotomy. The tumor was pedunculated, with free margins, measuring approximately 12 × 11 × 6 cm, and the pedicle was connected to the mediastinal pleura. The final diagnosis was solitary fibrous tumor of the pleura (SFTP). The postoperative evolution was uneventful.

Elevation of the right lung base may occur associated with elevation of the right hemidiaphragm or with the diaphragm in normal position. In the first condition, the main causes are phrenic paralysis[1] and the presence of an expansive lesion (e.g., a hepatic tumor or a subphrenic abscess) below the diaphragm. In the second condition, the main cause is infrapulmonary pleural effusion, although other, uncommon, causes include pleural tumors, such as SFTP.

A solitary fibrous tumor is defined as a mesenchymal neoplasm that has fibroblastic characteristics and clear peripheral vascular tumor-like branching vascularization. Although such tumors most commonly affect the pleura, they can occur in other thoracic areas (i.e., the mediastinum, pericardium, and lung), as well as in extrathoracic areas (i.e., the abdomen, head/neck, and central nervous system).[2-4]

An SFTP is often asymptomatic and discovered incidentally by radiography performed for other reasons. When signs and symptoms (including digital clubbing and hypertrophic osteoarthropathy) are present, they are usually associated with larger tumors. Patients with SFTP occasionally have hypoglycemia, which is seen more often in patients with malignant SFTP and is known as Doege-Potter syndrome. Doege-Potter syndrome is believed to be a type of non-insulin-dependent hypoglycemia.[2,3]

Computed tomography (CT) of a small SFTP frequently demonstrates a homogeneous, well-defined, noninvasive, lobular soft-tissue mass, usually adjacent to the chest wall or within a fissure. Larger lesions are typically heterogeneous and may not exhibit CT features suggestive of focal pleural tumors.[4] Heterogeneous areas of low attenuation on unenhanced CT scans may be caused by hemorrhage, necrosis, or cystic changes.[3,4] Changes in tumor location can be detected and are often related to the attachment of a benign SFTP to the pleural tissue through the pedicle.[3] Most localized fibrous tumors arise from the visceral pleura, and nearly half are pedunculated, the vascular supply to the tumor being contained within the pedicle.[4]

SFTPs show variable signal intensity on magnetic resonance imaging. The masses have predominantly low or intermediate signal intensity on T1- and T2-weighted images. They may also present high signal intensity on T2-weighted images. It has been suggested that this variable signal intensity is mainly dependent on the relative amounts of collagen and fibroblasts, as well as on the presence of areas of hemorrhage, necrosis, or cystic degeneration within the tumor. Intense heterogeneous enhancement after intravenous administration of gadolinium is typical and is generally due to high vascularity.

Making the differential diagnosis between benign and malignant SFTP is usually problematic. Although some imaging aspects, such as changes in the tumor location (suggesting the presence of a pedicle) and homogeneous attenuation of the lesion, are often associated with benign tumors, most authors have found that malignant lesions are indistinguishable from those with benign histological characteristics on imaging methods.[2,3-5] Currently, SFTP is primarily diagnosed on the basis of microscopic pathology findings, especially those obtained with immunohistochemical techniques.[2,4] On histological analysis, localized fibrous tumors appear as low-grade neoplasms with variable cellularity. The tumor cells are ovoid to spindle-shaped with round to oval nuclei, evenly distributed fine chromatin, inconspicuous nucleoli, and bipolar faintly eosinophilic cytoplasm with indistinct cell borders. Nuclear pleomorphism is minimal, and mitoses are usually rare or absent. Cellularity is variable and is inversely related to collagen content. Areas of necrosis, hemorrhage, or cystic degeneration may be evident, particularly in lesions that are large or in malignant lesions. Immunohistochemical staining shows that tumor cells are immunoreactive for CD34 and Bcl-2, albeit they typically lack expression for cytokeratin or S-100 protein.[2-4] Complete surgical excision is the treatment of choice and is the only effective treatment.

1. Ultra X, São José do Rio Preto (SP) Brasil.
2. Faculdade de Medicina de Rio Preto, São José do Rio Preto (SP) Brasil.
3. Universidade Federal do Rio de Janeiro, Rio de Janeiro (RJ) Brasil.
a. http://orcid.org/0000-0001-8079-6712; b. http://orcid.org/0000-0003-0261-1860; c. http://orcid.org/0000-0001-8797-7380

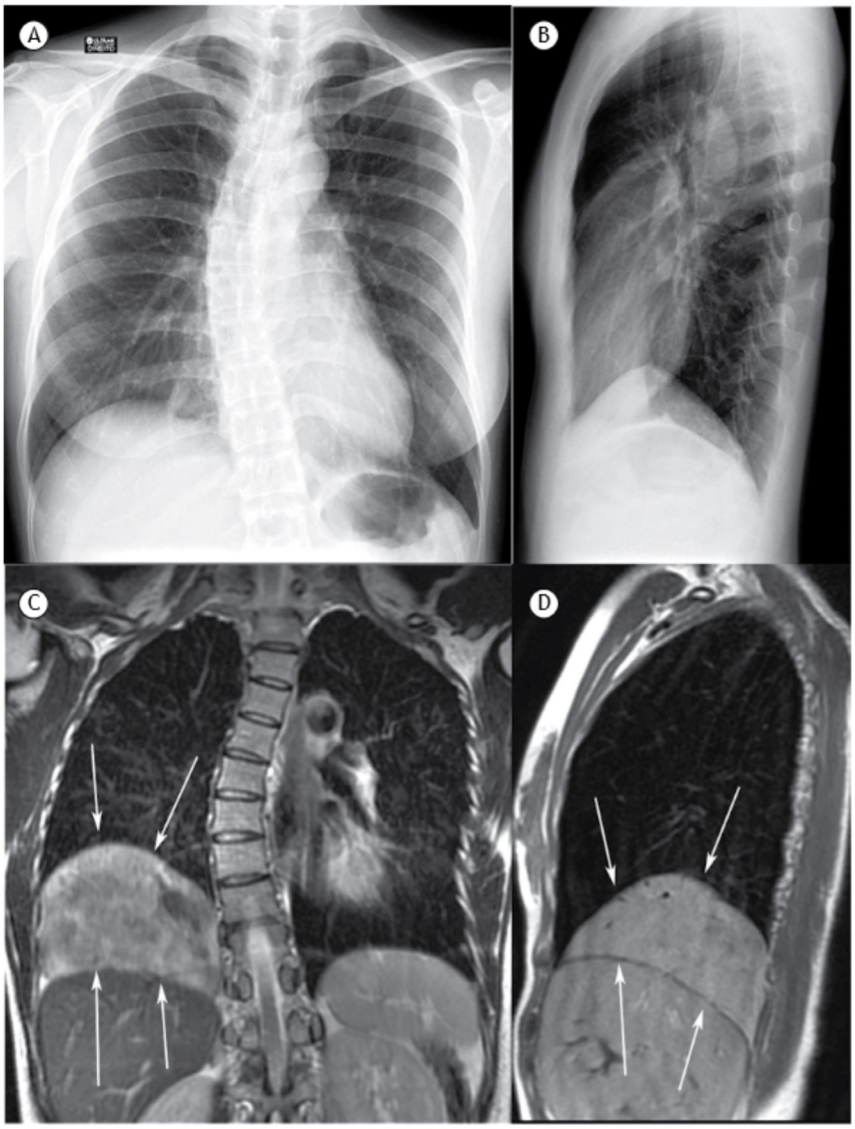

Figure 1. Frontal and lateral chest X-rays (A and B, respectively) showing elevation of the right lung base. Unenhanced coronal T2-weighted and sagittal T1-weighted magnetic resonance imaging scans (C and D, respectively) showing a large mass (arrows) occupying the inferior region of the right hemithorax with a heterogeneous, intermediate signal. The mass lies between the right lung base and the liver, with a well-defined cleavage plane between the two.

The prognosis for patients with SFTP is generally favorable. However, in a small number of cases, the lesions recur, undergo malignant transformation, or metastasize.[2,3]

REFERENCES

1. Ko MA, Darling GE. Acquired paralysis of the diaphragm. Thorac Surg Clin. 2009;19(4):501-10. https://doi.org/10.1016/j.thorsurg.2009.08.011
2. Chu X, Zhang L, Xue Z, Ren Z, Sun YE, Wang M, et al. Solitary fibrous tumor of the pleura: An analysis of forty patients. J Thorac Dis. 2012;4(2):146-54. https://doi.org/10.3978/j.issn.2072-1439.2012.01.05
3. Rosado-de-Christenson ML, Abbott GF, McAdams HP, Franks TJ, Galvin JR. From the archives of the AFIP: Localized fibrous tumor of the pleura. Radiographics. 2003;23(3):759-83. https://doi.org/10.1148/rg.233025165
4. Cardinale L, Ardissone F, Garetto I, Marci V, Volpicelli G, Solitro F, et al. Imaging of benign solitary fibrous tumor of the pleura: a pictorial essay. Rare Tumors. 2010;2(1):e1. https://doi.org/10.4081/rt.2010.e1
5. Lococo F, Cafarotti S, Treglia G. Is 18F-FDG-PET/CT really able to differentiate between malignant and benign solitary fibrous tumor of the pleura? Clin Imaging. 2013;37(5):976. https://doi.org/10.1016/j.clinimag.2013.03.003

Respiratory Medicine 149 (2019) 9–15

Contents lists available at ScienceDirect

Respiratory Medicine

journal homepage: www.elsevier.com/locate/rmed

Review article

Neurofibromatosis type 1: State-of-the-art review with emphasis on pulmonary involvement

Sérgio Ferreira Alves Júnior[a], Gláucia Zanetti[a], Alessandro Severo Alves de Melo[b], Arthur Soares Souza Jr.[c], Luciana Soares Souza[c], Gustavo de Souza Portes Meirelles[d], Klaus Loureiro Irion[e], Bruno Hochhegger[f], Edson Marchiori[a,*]

[a] Federal University of Rio de Janeiro, Rio de Janeiro, Brazil
[b] Universidade Federal Fluminense, Rio de Janeiro, Brazil
[c] Faculdade de Medicina de São José do Rio Preto (Famerp) and Ultra X, São José do Rio Preto, SP, Brazil
[d] Universidade Federal de São Paulo (UNIFESP) and Grupo Fleury, São Paulo, SP, Brazil
[e] The University of Manchester, Manchester, United Kingdom
[f] Santa Casa de Porto Alegre, Porto Alegre, Rio Grande do Sul, Brazil

ARTICLE INFO

Keywords:
Neurofibromatosis type 1
Interstitial lung disease
Computed tomography
Pulmonary hypertension
Pulmonary diseases

ABSTRACT

Neurofibromatosis type 1 (NF-1), also known as von Recklinghausen's disease, is an autosomal dominant dysplasia of the ectoderm and mesoderm with a variable clinical expression, but near-complete penetrance before the age of 5 years. The estimated incidence is 1 in 3000 births. NF-1 is characterized by collections of neurofibromas, café-au-lait spots, axillary and inguinal freckling, and pigmented hamartomas in the iris (Lisch nodules). Pulmonary manifestations of NF-1, which usually include bilateral basal reticulations and apical bullae and cysts, are reported in 10–20% of adult patients. Clinically, neurofibromatosis-associated diffuse lung disease (NF-DLD) usually presents with nonspecific respiratory symptoms, including dyspnea on exertion, shortness of breath, and chronic cough or chest pain, at the time of diagnosis. Computed tomography (CT) is highly accurate for the identification and characterization of NF-DLD; it is the most reliable method for the diagnosis of this lung involvement. Various CT findings of NF-DLD, including cysts, bullae, ground-glass opacities, bibasilar reticular opacities, and emphysema, have been described in patients with NF-1. The typical CT pattern, however, is characterized by upper-lobe cystic and bullous disease, and basilar interstitial lung disease. Currently, the goal of NF-DLD treatment is the earliest possible diagnosis, focusing on symptom relief and interventions that positively alter the course of the disease, such as smoking cessation. The aim of this review is to describe the main clinical, pathological, and imaging aspects of NF-1, with a focus on pulmonary involvement.

1. Introduction

Neurofibromatosis type 1 (NF-1) is a genetic syndrome characterized by clinical manifestations of systemic and progressive involvement that mainly affect the skin, nervous system, bones, and eyes, and can affect any other organ [1,2]. Collections of neurofibromas, café-au-lait spots, axillary and inguinal freckling, and pigmented hamartomas in the iris (Lisch nodules) are the main features of NF-1 and represent some of the diagnostic criteria for this disease [1–4]. Less common features include bone deformities (pseudarthrosis, dysplasia), scoliosis, short stature, cognitive deficits, seizure disorders, peripheral neuropathies, and more serious manifestations, such as plexiform neurofibromas, malignant peripheral nerve sheath tumors (MPNSTs), and optic nerve and other central nervous system gliomas [3,5].

The thorax and lungs can be affected in several ways, including by the development of cutaneous and subcutaneous neurofibromas on the chest wall, kyphoscoliosis, ribbon deformity of the ribs, posterior vertebral scalloping, intrathoracic neurogenic neoplasms, meningoceles, bullous lung disease, pulmonary hypertension (PH), and interstitial lung disease [1,6,7]. The aim of this review is to describe the main clinical, pathological, and imaging aspects of NF-1, focusing on thoracic and pulmonary involvement.

* Corresponding author. Rua Thomaz Cameron, 438. Valparaiso, CEP 25685, 120.Petrópolis, Rio de Janeiro, Brazil.
E-mail addresses: sergio_faj@hotmail.com (S.F. Alves Júnior), glauciazanetti@gmail.com (G. Zanetti), alesevero@gmail.com (A.S. Alves de Melo), asouzajr@gmail.com (A.S. Souza), luciana.soaressouza@gmail.com (L.S. Souza), gmeirelles@gmail.com (G. de Souza Portes Meirelles), klaus.irion@btinternet.com (K.L. Irion), brunohochhegger@gmail.com (B. Hochhegger), edmarchiori@gmail.com (E. Marchiori).

https://doi.org/10.1016/j.rmed.2019.01.002
Received 11 August 2018; Received in revised form 4 January 2019; Accepted 11 January 2019
Available online 17 January 2019

2. Epidemiology and genetic aspects

NF-1 traditionally exhibits autosomal dominant inheritance, being the most common of the phakomatoses (neurocutaneous syndromes) and the most common autosomal dominant disorder. It has a reported incidence of 1 in 3000 births; in 30–50% of cases, affected individuals have no family history of the disease, and NF-1 is caused by the spontaneous appearance of *de novo* mutations in (usually paternal) germ cells [4,8–11]. Penetrance is nearly complete before the age of 5 years, but the clinical expression of NF-1 is highly variable, even within the same family. Conversely, members of different affected families frequently show similarity in the distribution of lesions [2,12]. At least 1 million individuals worldwide are believed to be living with NF-1 [2]. The disease has no predilection for sex, and several studies have failed to establish any significant racial difference in its incidence [2,9].

NF-1 results from a mutation in the *NF1* tumor-suppressor gene, located on the long arm of chromosome 17 (at locus 17q11.2) and encoding a cytoplasmic protein called neurofibromin type 1. This protein is a negative regulator of the *Ras* proto-oncogene, and is predominantly expressed in neurons, Schwann cells, oligodendrocytes, and astrocytes [2,9,12].

A central region of neurofibromin is structurally and functionally homologous to GTPase-activating proteins, which accelerate the hydrolysis of p21Ras-GTP (the active form) to p21Ras-GDP (the inactive form) by stimulating intrinsic p21Ras-GTPase activity. As p21Ras proteins play central roles in cell differentiation and growth, inactivation of the *NF1* gene favors the active state (p21Ras-GTP), resulting in the permanent stimulation of a cascade of signals and excessive cell division due to non-regulated activation of the MAP kinase pathway. This pathway could play a role in the development of benign neurofibroma-type tumors, MPNSTs, PH with hyperplasia of pulmonary artery smooth-muscle cells, and interstitial disease, such as hyperplasia/metaplasia of interstitial pulmonary fibroblastic cells [2,12].

3. Diagnosis

The diagnosis of NF-1 is based on the presence of two or more of the following seven criteria, determined by the clinical evaluation and family history of the patient: six or more café-au-lait spots (diameter > 5 mm before puberty and > 15 mm after puberty), two or more neurofibromas of any type or one plexiform neurofibroma, axillary freckling, two or more iris hamartomas (Lisch nodules), optic glioma, typical bone lesions (sphenoid dysplasia or tibial pseudarthrosis), and one or more first-degree relatives with NF-1. These diagnostic criteria were defined in 1987 by the United States National Institutes of Health and have been proven to be strong and reliable, as they have stood well over time [13–16]. Approximately 50% of patients meet the diagnostic criteria for NF-1 up to the age of 1 year, 97% meet the criteria by the age of 8 years, and virtually all patients fulfill them by the age of 20 years [16].

Café-au-lait spots (Fig. 1) are symmetrical flat areas of cutaneous hyperpigmentation (classically described as being light brown in color) with rounded edges, usually seen at birth. They are typically the initial clinical manifestation of NF-1 and tend to increase in size and number throughout childhood and puberty. By adulthood, about 95% of patients with NF-1 have café-au-lait spots [8,17]. In addition, 70% of patients with NF-1 show freckling in the intertriginous areas of the axilla and in the inguinal region [8].

Cutaneous and subcutaneous neurofibromas (Fig. 2) are other frequent skin manifestations of NF-1, usually developing in the late teens or early twenties but occasionally emerge in early childhood. They occur in more than 95% of patients, with variation in number and size among individuals and within families [8,15,16,18]. Lisch nodules, which are hamartomas of the iris pigment epithelium, are the most common ophthalmological feature of NF-1, although they are not pathognomonic. They appear as multiple pale, yellowish-brown, oval to round, dome-shaped papules projecting from the surface of the iris. Optic pathway gliomas, seen in about 15–20% of patients with NF-1, are usually low-grade astrocytomas that can grow in the optic nerve, optic chiasm, optic tract, and hypothalamus [8,15,19].

Cognitive problems are the most common neurological complications in individuals with NF-1. Severe intellectual disability with an intellectual quotient < 70 (mental retardation) is rare and only slightly more frequent than in the general population [8,15]. Epilepsy occurs in approximately 6–7% of individuals with NF-1 [15]. Plexiform neurofibromas are classic neurogenic tumors that occur outside the central nervous system and are the pathognomonic feature of NF-1. They can affect a range of organs and, given the rich distribution of peripheral nerves throughout the thorax, NF-1–related thoracic neurofibromas may involve the ribs, chest wall, lungs, and mediastinum [11]. They typically manifest at birth, increase particularly in the first decade of life, and can grow during adolescence and early adulthood. They differ from other neurofibromas in arising from multiple nerve fascicles; they grow along the length of the involved nerve (compromising long segments), infiltrate the nerve, and extend to surrounding structures [8,9]. Plexiform neurofibromas carry a lifetime risk of malignant transformation to MPNSTs, although such transformation is rare [8,20].

Mutational and molecular analyses are helpful in confirming the clinical diagnosis of NF-1, notably in patients with paucisymptomatic forms: segmental forms in pediatric cases (café-au-lait spots are often the only clinical findings in young children) and Legius syndrome. Such analyses are also useful for prenatal diagnosis. However, genetic testing is not routinely recommended to establish the diagnosis in the daily clinical care of patients with typical NF-1, and consultation with medical specialists is advised before the test is performed [15,16,21]. One limitation of genetic testing is the lack of genotype–phenotype correlation. Therefore, although useful for diagnostic confirmation, a positive test result cannot be used to predict the severity or outcome of the disease [15,16].

4. Thoracic involvement

4.1. Pulmonary involvement

Pulmonary manifestations of NF-1 observed in imaging examinations include nodular, bullous, cystic, and/or interstitial parenchymal lesions, and are reported in 10–20% of adults with the disease (Figs. 3 and 4) [12,22,23]. NF-1–associated interstitial lung disease is generally bilateral, symmetrical, and predominantly basal. Typically, it occurs in association with thin-walled bullae, which are located in the upper lung zones [4]. This combination has been considered to be the hallmark of NF-1, although it is not pathognomonic of the disease [24].

Although NF-1 is congenital, pulmonary fibrosis and neurofibromatosis-associated diffuse lung disease (NF-DLD) are traditionally not evident before the patient reaches adulthood, typically appearing in the third or fourth decade of life [12,25]. Chest CT rarely reveals the typical honeycombing pattern representative of advanced-stage fibrosis; it more frequently shows different forms of injury, such as linear opacities, predominantly peripheral lung base reticulations, and ground-glass opacities [12]. The existence of an interstitial pneumonia type that is truly specific to NF-1 remains under debate, as most studies have provided little evidence to establish a reliable association between NF-1 and pulmonary fibrosis, and fibrotic changes may be smoking-induced manifestations [3,12,23,26]. Interstitial lung disease in patients with NF-1 is pathologically similar to that seen in other diseases that produce interstitial fibrosis [27]. It is characterized in its initial stages by thickening and lymphoplasmocytic cellular infiltration of the alveolar wall, with enlargement and desquamation of alveolar lining cells [25,27]. Subsequently, this cellular response is replaced by fibrosis, resulting in destruction of the alveoli, confluence of air spaces, formation of bullae, and obliteration of blood vessels [27]. This histopathology, defined by the expansion of the alveolar septa by

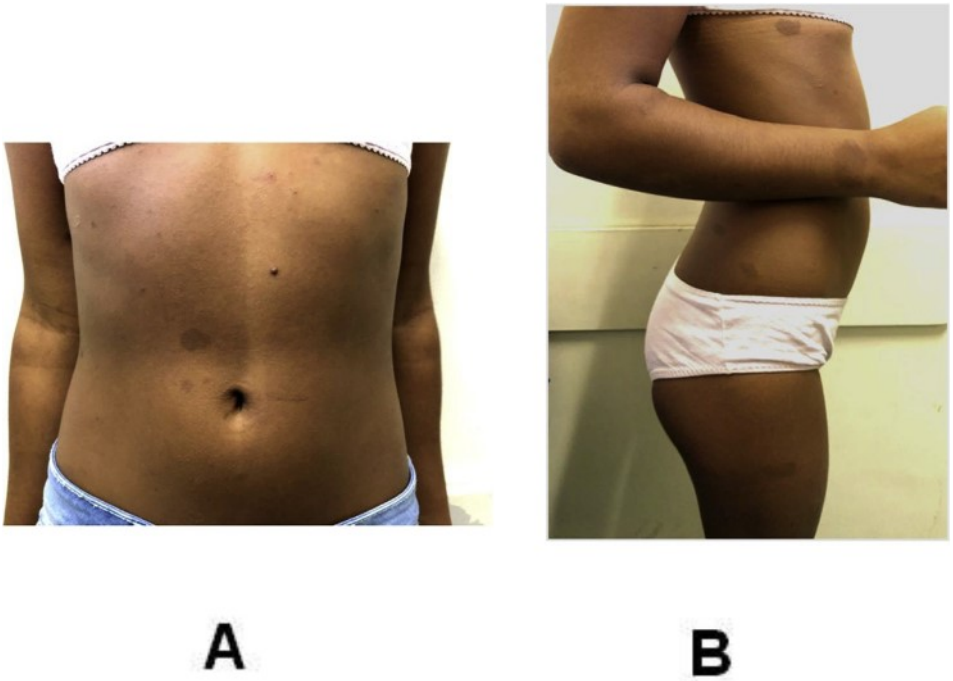

Fig. 1. A 12-year-old girl with neurofibromatosis type 1. Ectoscopic examination (a and b) shows multiple light-brown macules with rounded edges representing typical café-au-lait spots, coexisting with hypopigmented macules on the skin surface. (For interpretation of the references to color in this figure legend, the reader is referred to the Web version of this article.)

Fig. 2. A 70-year-old woman with neurofibromatosis type 1. Ectoscopic examination shows multiple pedunculated cutaneous neurofibromas on the skin surface.

lymphocytic inflammatory cells, with variable and increased amounts of interstitial smooth muscle and fibrosis, is consistent with a non-specific interstitial pneumonia pattern. Massaro and Katz [27] also reported increased numbers of intra-alveolar eosinophils and desquamated pneumocytes, rather than pigmented macrophages, as would be expected in desquamative interstitial pneumonia or respiratory bronchiolitis, entities linked to smoking. Thus, these findings support the hypothesis that NF-DLD (interstitial/cystic) is a distinct manifestation of NF-1, rather than a disease related purely to smoking. However, NF-1 may increase the sensitivity of the lungs to cigarette smoke, increasing the severity of NF-DLD in smokers and causing early development of emphysema-like changes in these patients [4,26].

Centrilobular nodules and parenchymal cysts show an apical predominance, with some subpleural cysts capable of simulating paraseptal emphysema. In the advanced stages of NF-1, the lesions are clustered, potentially leading to erroneous diagnosis of centrilobular emphysema [4,12]. Also, in advanced-stage disease, damage from diffuse cystic disease may progress to chronic respiratory failure, and may even lead to more serious complications, such as spontaneous pneumothorax or PH, mostly secondary to hypoxemia [12,28,29].

PH associated with NF-1 (PH-NF1) is a rare, but severe, complication of NF-1. It is classified as pre-capillary group 5 PH, defined as "PH with unclear and/or multifactorial mechanisms" [12,30]. PH-NF1 is characterized by female predominance, diagnosis at an advanced age, association with parenchymal lung disease in two-thirds of cases, and a poor long-term prognosis. Severe PH-NF1 is generally associated with lung lesions, mostly cysts or bullae in the upper lobes, diffuse ground-glass opacities (sometimes with a mosaic pattern), and reticular opacities. However, parenchymal lung disease is absent in one-third of PH-NF1 cases, and the severity of PH is disproportionate to the degree of NF-DLD in other cases, supporting the hypothesis of a specific vascular disease, rather than disease secondary to hypoxemia [12,30–33].

Extending beyond the frequent reporting of nodular and cystic lesions in smokers, Oikonomou et al. [23] reported the CT finding of upper-lobe-predominant cystic lesions in all of six non-smokers with NF-1, and centrilobular nodules in five of the six patients. Given that none of these six patients was ever a smoker, the observed cystic changes cannot be attributed to emphysema. The random distribution of the cystic changes, the cysts' thin but well-defined walls, and the absence of any centrilobular artery in their centers also do not support the diagnosis of emphysema [23].

In 2007, Zamora et al. [4] carried out an extensive literature review in which 64 cases of NF-DLD were analyzed by chest radiography (available in 63 cases) and/or chest CT (available in 8 cases), with the aims of estimating the frequency and describing the pattern of pulmonary radiological findings. Chest CT revealed bullae (50%), bibasilar reticular abnormalities (50%), ground-glass opacities (37%), emphysema (25%), and cysts (25%), but not honeycombing [4]. The review showed no significant difference in age, pulmonary function pattern, or radiographic abnormalities between non-smokers and smokers. Emphysema was not seen in any of the 4 non-smoking patients and was seen in 2 of the 12 smokers. The remaining cases had no smoking

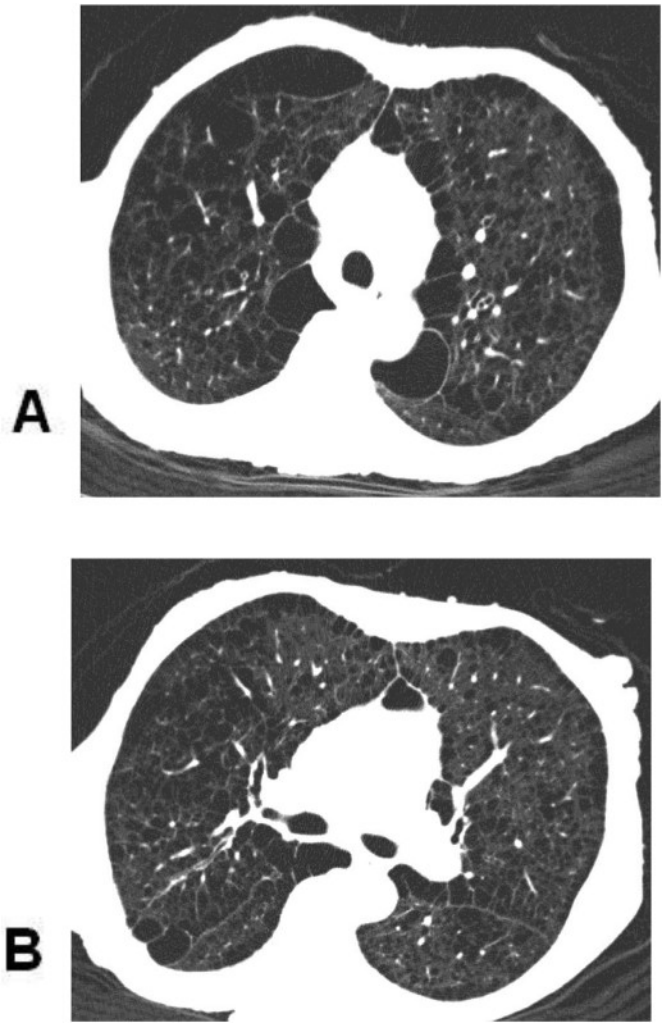

Fig. 3. A 64-year-old female smoker with neurofibromatosis type 1. Axial high-resolution CT images obtained with lung window settings at the levels of the upper lobes (a) and the tracheal bifurcation (b) show numerous large subpleural bullae and emphysema with predominance in the upper lobes. Note also bilateral, variably sized, thin-walled cysts distributed without peripheral–central predominance. Multiple cutaneous neurofibromas are visible in the thoracic wall.

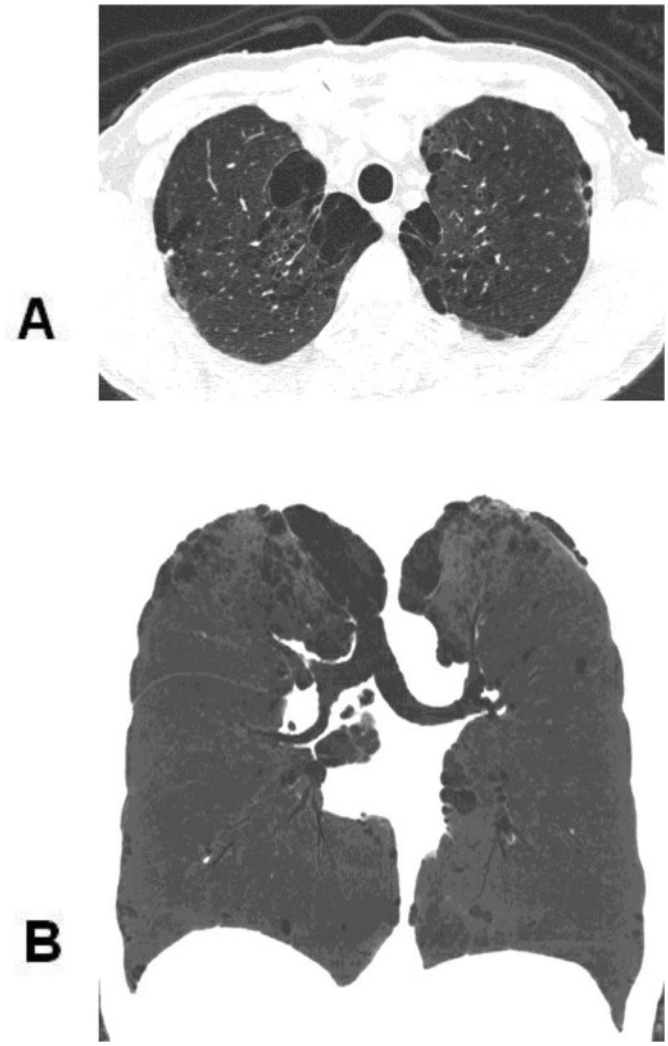

Fig. 4. A 55-year-old non-smoking woman with neurofibromatosis type 1. Axial high-resolution CT image obtained with lung window settings at the level of the upper lobes (a) and coronal reformatted minimum intensity projection image (b) shows upper- and peripheral-dominant distribution of centrilobular and paraseptal emphysema and some bilateral subpleural bullae. Some scattered thin-walled cysts are also visible in the upper zones. Multiple cutaneous neurofibromas are visible in the thoracic wall.

history available [4].

In 2015, Ueda et al. [3] reviewed chest CT images of 88 patients with NF-1; 44 (51%) were positive for subcutaneous nodules, 34 (39%) for skin nodules, 20 (23%) for scoliosis, 16 (18%) for emphysema, 13 (15%) for cysts, 13 (15%) for mediastinal masses, 8 (9%) for nodules, and 8 (9%) for ground-glass nodules. No patient had interstitial pneumonia. This series showed an upper-lobe-dominant distribution of cysts, in agreement with all previous reports and with no significant difference in the rate of cysts between smoking and non-smoking patients, suggesting that smoking does not affect the appearance of cysts in patients with NF-1 [3]. Furthermore, it showed an upper- and peripheral-dominant distribution of emphysema. Although 2 of 16 emphysema cases were never-smokers, the study findings implied that emphysema is strongly affected by a history of smoking, as reported previously by Ryu et al. [26]. Still, one can say that the association between smoking and emphysema in patients with NF-1 remains unclear [3].

A pulmonary association that is uncommon, but worth noting, is that between NF-1 and lung cancer. Two predominant theories have been postulated to explain this association: the development of tumors from previous scar tissue or bullae secondary to interstitial fibrosis, and the deletions on chromosome 17p, where the p53 tumor suppressor gene is located [34,35]. Our review of the literature yielded reports on only a few scattered cases of NF-1 with lung cancer. Adenocarcinoma was the most frequent histological diagnosis, followed by other types of non-small cell cancer, small cell cancer, poorly differentiated cancer, and carcinosarcoma [36]. Hence, NF-1 should be considered as an underlying risk factor for the development of lung cancer, although additional studies with larger cohorts are required.

4.2. Mediastinal involvement

Neurogenic tumors growing in the posterior mediastinum are frequently seen in patients with NF-1 [12,18]. Plexiform neurofibromas usually appear as well-delimited, smooth, round or elliptical masses in the paravertebral region or along the path of the vagus, phrenic, recurrent laryngeal, or intercostal nerve [11] (Fig. 5).

Plexiform neurofibromas are usually extensive fusiform or infiltrating masses that tend to surround mediastinal vessels with loss of normally visible fat planes and can result in diffuse mediastinal widening. They demonstrate variable contrast material enhancement and may calcify. Both types can remodel, erode, invade, or even destroy

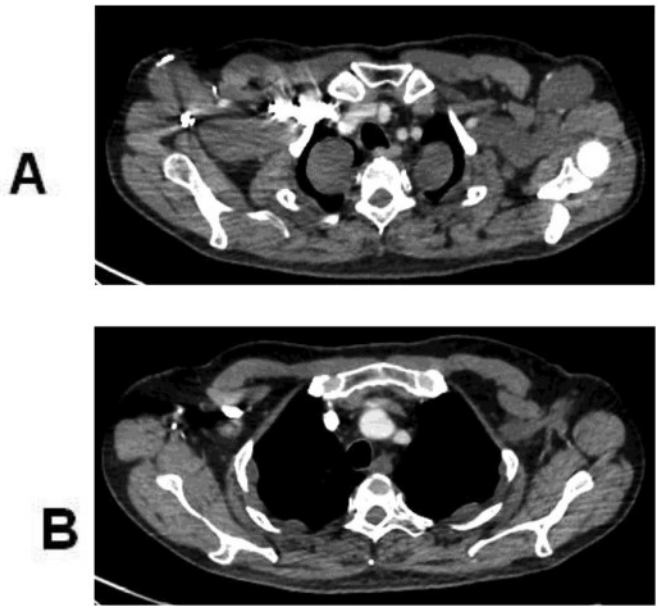

Fig. 5. A 56-year-old man with neurofibromatosis type 1. Contrast-enhanced axial (a and b) high-resolution chest CT images obtained with mediastinal window settings demonstrate multiple hypodense, well-delimited round masses in the intercostal spaces, protruding to both lungs. These masses did not enhance with contrast and were ultimately diagnosed as neurofibromas. Other similar lesions are visible in the deep axillary region.

adjacent bone structures, thereby simulating more aggressive lesions [11,12]. Of particular concern is that these lesions can apply pressure to mediastinal structures, such as the trachea, esophagus, nerves, or blood vessels. The symptoms are mainly those of compression, with chest pain and cough being the most frequent. Digestive and other respiratory symptoms, or even superior vena cava syndrome, can also be present in rare cases [12].

Intrathoracic meningocele associated with NF-1 is a relatively rare entity, and an estimated 60–85% of all thoracic meningoceles are associated with NF-1. These cystic formations of the posterior mediastinum originate by saccular protrusion of the meninges into the thoracic cavity through a pathologically dilated intervertebral foramen or a bone defect in a thoracic vertebra. The accepted etiopathogenesis in patients with NF-1 is that of dural dysplasia and intervertebral foraminal enlargement. Most patients become symptomatic between 30 and 50 years of age, and the disease has a slight female predominance [37–39]. Lateral or anterior thoracic meningoceles are unilobed cystic formations of variable dimensions, filled by cerebrospinal fluid, which appear on CT images as well-circumscribed paravertebral masses with low attenuation due to their liquid content. Meningoceles usually occur in association with scoliosis of the thoracic spine (typically on the convex side of the scoliotic curve), expand the intervertebral foramen, and occasionally exhibit peripheral enhancement by iodinated contrast [11,37]. Magnetic resonance imaging (MRI) findings are usually diagnostic, showing meningoceles with the same signal intensity as the cerebrospinal fluid in all sequences and defining better relationships between the cystic lesion and the spinal canal, nerve root, and spinal cord compared with evaluation by CT [11,37]. Thoracic meningoceles should be differentiated from solid tumors, especially mediastinal tumors that usually arise from the posterior mediastinum, such as neurofibroma, neuroblastoma, ganglioneuroma, and posterior mediastinal cystic hygroma [38].

4.3. Skeletal involvement

Musculoskeletal thoracic involvement in NF-1 comprises focal thoracic scoliosis, posterior vertebral scalloping, enlargement of neural foramina (Fig. 6), and characteristic rib deformities due to bone dysplasia or erosion by adjacent neurofibromas [11].

Muniz et al. [40] studied 141 chest radiographs of NF-1 individuals and found that the following findings were very frequent: rib erosion (19.8%), pectus excavatum (12.0%), kyphoscoliosis (3.5%), and posterior mediastinal masses (7.1%). The spinal column and ribs are the components of the skeletal system most commonly affected by NF-1 [41]. Thoracic spinal curvature affects approximately 10% of patients with NF-1, appearing early in childhood and often requiring corrective surgery. Scoliosis associated with NF-1 more commonly involves the lower cervical and upper thoracic spine, and may be idiopathic or dystrophic. Dystrophic scoliosis typically involves four to six segments, causes distortion of the vertebral bodies and ribs, and is rapidly progressive. Scoliosis with rotation may also occur, producing a reduction in lung volume, which, if severe, may result in respiratory failure [8,15]. Pectus excavatum and carinatum occur in up to 30% of patients

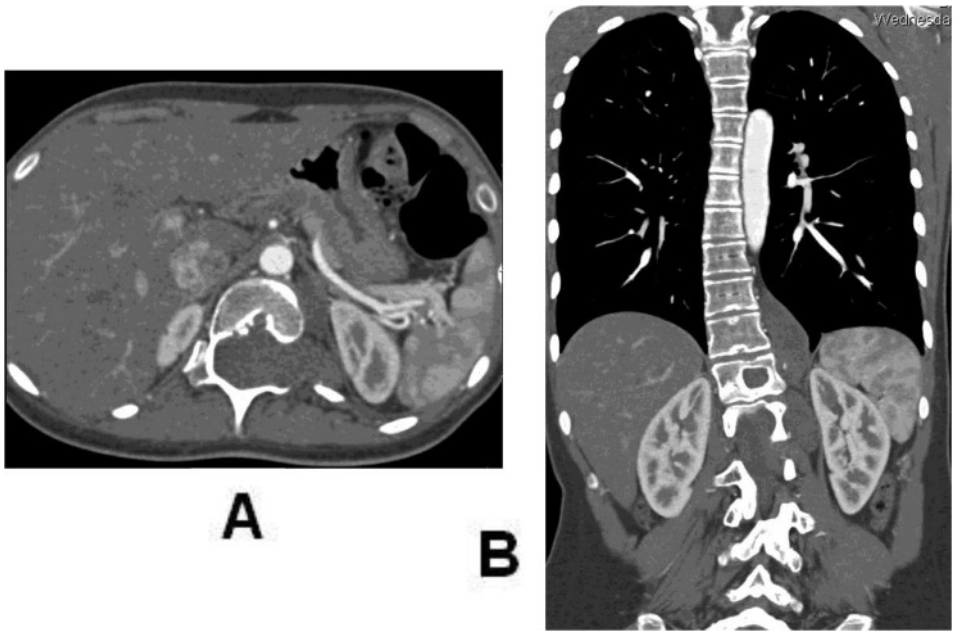

Fig. 6. A 19-year-old woman with neurofibromatosis type 1 presenting with left lumbar pain. Contrast-enhanced thoracoabdominal CT images with axial (a) and coronal (b) reconstruction demonstrate an elliptical, hypodense, well-delimited, non-enhancing mass (plexiform neurofibroma) extending through an enlarged thoracic neural foramen to the left paravertebral region of the inferior region of the posterior mediastinum. Note also the presence of scoliosis.

with NF-1, but they do not contribute to respiratory symptoms or complications [8]. Posterior vertebral scalloping most commonly occurs due to dural ectasia (caused by mesodermal dysplasia of the meninges), but may also be secondary to neurofibromas or thoracic meningoceles. It is observed on lateral radiographs of the spine and on coronal sections of spinal CT and MRI images as an exaggeration of the normal concavity of the posterior surface of one or more vertebral bodies [42]. Costal arch irregularities may occur due to a primary dysplastic defect in bone formation or by erosion of an intercostal neurofibroma. In patients with NF-1, ribs corresponding to abnormal and dysplastic vertebral bodies often have a "twisted ribbon" appearance on images. In the initial description of the radiographic appearance of NF-1, such deformities were attributed to the pressure exerted by intercostal neurofibromas. Now, it is known that some patients exhibiting such changes do not present intercostal neurofibromas. Respiratory symptoms are not associated directly with these defects [40,43].

5. Management and treatment

Given that NF-1 is a genetic syndrome, effective clinical monitoring of these patients with evaluation by a multidisciplinary team is the basis of treatment [16]. The management of patients with NF-1 is focused on the age-specific monitoring of disease manifestations and the education of patients regarding the disease, its possible complications, and the importance of regular clinical follow-up. Individuals with NF-1 need to be encouraged to seek medical help if they experience any unusual symptoms and to ask whether these symptoms are related to NF-1, increasing knowledge about their condition. An important fact reflecting the need for such patient awareness and regular follow-up is that severe disease complications, such as MPNST, are most likely to become symptomatic in the inter-appointment period in patients of all ages [15,44].

Since routine radiological screening is not recommended by most NF-1-management guidelines, neither MRI of the neuro axis, nor routine images of the chest and abdomen should be performed to identify asymptomatic tumors or to be use as basal exams. Imaging surveillance of patients with NF-1 is guided by positive findings of physical examination [9,15,45]. Currently, no effective medical treatment is available to reverse or prevent lesions characteristic of NF-1. Genetic counseling and regular clinical follow-up for the early detection of treatable complications are employed in current practice [44,46]. Targeted treatment depends on and is specific to each manifestation of the syndrome that a patient develops. Therefore, for each involvement found in NF-1 patients an expectant or surgical management may be chosen. Effective medical treatments for NF-1–related neurogenic tumors are lacking. Dombi et al. [47] reported early-phase data suggesting that children with NF-1 and inoperable plexiform neurofibromas benefited from long-term treatment with selumetinib. Fischer-Huchzermeyer et al. [48] suggested that MPNSTs might be treated successfully by combined therapy with all-trans retinoic acid and MEK inhibitors. Pre-conception genetic counseling is essential for adult patients and is recommended for all individuals with NF-1 [15,17].

6. Conclusion

NF-1 is the most common multisystem neurocutaneous syndrome. It may present with various phenotypes and a wide variety of clinical and imaging manifestations. NF-1 should be suspected in the presence of classic diagnostic lesions, such as café-au-lait spots, skin-fold freckling, neurofibromas, iris hamartomas (Lisch nodules), and typical bone lesions. In affected patients, although interstitial lung disease can develop into pulmonary fibrosis, as well as to cystic, emphysematous, or bullous lesions, our literature review showed that the strongest and most reliable pulmonary association is between cystic lung disease and NF-1, allowing characterization of NF-DLD as a distinct clinical entity. Still, whether emphysematous, bullous, and fibrotic changes can be attributed essentially to lung involvement of NF-1 or to variable degrees of smoke-induced alteration remains under debate. Recognition of the various clinical and imaging features of NF-1 and, more specifically, NF-DLD is pivotal in making a presumptive associative diagnosis, as well as in defining the extent of pulmonary involvement; it also aids decision making about disease management.

Contributions of each author

Dr. Alves Júnior: contributed to data interpretation, and preparation and revision of the manuscript.

Dr Zanetti: contributed to CT scan evaluation, literature review, and revision of the manuscript.

Dr Alves de Melo: contributed to the collection of the data and preparation of the manuscript.

Dr Souza Jr: contributed to literature review and final review of the manuscript.

Soares Souza: contributed to the data interpretation, literature review, and revision of the manuscript.

Dr Meirelles: contributed to CT scan evaluation, and final review of the manuscript.

Dr Irion: contributed to literature review and revision of the manuscript.

Dr Hochhegger: contributed to the design of study, CT scan evaluation, and final review of the manuscript.

Dr Marchiori was the principal investigator and is the guarantor of the entire manuscript. He contributed to the coordination and design of the study, data interpretation, and preparation and revision of the manuscript.

Conflicts of interest

All authors inform that there are none conflicts of interest.

References

[1] V.M. Riccardi, Von recklinghausen neurofibromatosis, N. Engl. J. Med. 305 (27) (1981) 1617–1627.
[2] J.R. Antônio, E.M. Goloni-Bertollo, L.A. Trídico, Neurofibromatosis: chronological history and current issues, An. Bras. Dermatol. 88 (3) (2013) 329–343.
[3] K. Ueda, O. Honda, Y. Satoh, et al., Computed tomography (CT) findings in 88 neurofibromatosis 1 (NF1) patients: prevalence rates and correlations of thoracic findings, Eur. J. Radiol. 84 (6) (2015) 1191–1195.
[4] A.C. Zamora, H.R. Collard, P.J. Wolters, W.R. Webb, T.E. King, Neurofibromatosis associated lung disease: a case series and literature review, Eur. Respir. J. 29 (1) (2007) 210–214.
[5] M.Y. Shino, S. Rabbani, J.A. Belperio, J.P. Lynch 3rd, S.S. Weigt, Neurofibromatosis-associated diffuse lung disease: case report, Semin. Respir. Crit. Care Med. 33 (5) (2012) 572–575.
[6] G.F. Louza, G. Zanetti, E. Marchiori, Neurofibromatosis type I with pulmonary involvement, Arch. Bronconeumol. 54 (2) (2018) 106–107.
[7] A. Fernández Plaza, A. Sánchez González, Diffuse cystic lung disease as a manifestation of neurofibromatosis, Radiologí 56 (4) (2014) 376–377.
[8] N.P. Hirsch, A. Murphy, J.J. Radcliffe, Neurofibromatosis: clinical presentations and anaesthetic implications, Br. J. Anaesth. 86 (4) (2001) 555–564.
[9] C. Vijapura, E. Saad Aldin, A.A. Capizzano, B. Policeni, Y. Sato, T. Moritani, Genetic syndromes associated with central nervous system tumors, Radiographics 37 (1) (2017) 258–280.
[10] J.H. Tonsgard, Clinical manifestations and management of neurofibromatosis type 1, Semin. Pediatr. Neurol. 13 (1) (2006 Mar) 2–7.
[11] B.J. Fortman, B.S. Kuszyk, B.A. Urban, E.K. Fishman, Neurofibromatosis type 1: a diagnostic mimicker at CT, Radiographics 21 (3) (2001) 601–612.
[12] L. Reviron-Rabec, B. Girerd, A. Seferian, et al., Pulmonary complications of type 1 neurofibromatosis, Rev. Mal. Respir. 33 (6) (2016) 460–473.
[13] National Institutes of Health consensus development conference statement: neurofibromatosis. Bethesda, Md., USA, July 13-15, 1987, Neurofibromatosis 1 (3) (1988) 172–178.
[14] P. Nalepa, M. Wolnicka, Neurofibromatosis type 1 with interstitial pulmonary lesions diagnosed in adult patient. A case study and literature review, Pneumonol. Alergol. Pol. 80 (2) (2012) 152–157.
[15] R.E. Ferner, S.M. Huson, N. Thomas, et al., Guidelines for the diagnosis and management of individuals with neurofibromatosis 1, J. Med. Genet. 44 (2) (2007) 81–88.

[16] K.P. Boyd, B.R. Korf, A. Theos, Neurofibromatosis type 1, J. Am. Acad. Dermatol. 61 (1) (2009) 1–16.
[17] C. Lu-Emerson, S.R. Plotkin, The neurofibromatoses. Part 1: NF1, Rev. Neurol. Dis. 6 (2) (2009) E47–E53.
[18] T. Arazi-Kleinmann, Y. Mor, N. Brand, et al., Neurofibromatosis diagnosed on CT with MR correlation, Eur. J. Radiol. 42 (2002) 69–73.
[19] J.W. Chan, Neuro-ophthalmic features of the neurocutaneous syndromes, Int. Ophthalmol. Clin. 52 (3) (2012) 73–85.
[20] M. Farid, E.G. Demicco, R. Garcia, et al., Malignant peripheral nerve sheath tumors, Oncol. 19 (2) (2014) 193–201.
[21] E. Pasmant, B. Parfait, A. Luscan, et al., Neurofibromatosis type 1 molecular diagnosis: what can NGS do for you when you have a large gene with loss of function mutations? Eur. J. Hum. Genet. 23 (5) (2015) 596–601.
[22] P.D.B. Davies, Diffuse pulmonary involvement in von Recklinghausen's disease: a new syndrome, Thorax 18 (1963) 198.
[23] A. Oikonomou, K. Vadikolias, T. Birbilis, D. Bouros, P. Prassopoulos, HRCT findings in the lungs of non-smokers with neurofibromatosis, Eur. J. Radiol. 80 (3) (2011) e520–e523.
[24] W.R. Webb, P.C. Goodman, Fibrosing alveolitis in patients with neurofibromatosis, Radiology 122 (2) (1977) 289–293.
[25] A.S. Patchefsky, W.G. Atkinson, W.S. Hoch, G. Gordon, H.I. Lipshitz, Interstitial pulmonary fibrosis and von Recklinghausen's disease. An ultrastructural and immunofluorescent study, Chest 64 (4) (1973) 459–464.
[26] J.H. Ryu, J.G. Parambil, P.S. McGrann, G.L. Aughenbaugh, Lack of evidence for an association between neurofibromatosis and pulmonary fibrosis, Chest 128 (4) (2005) 2381–2386.
[27] D. Massaro, S. Katz, Fibrosing alveolitis: its occurrence, roentgenographic, and pathologic features in von Recklinghausen's neurofibromatosis, Am. Rev. Respir. Dis. 93 (6) (1966) 934–942.
[28] S. Ayed Della, A. Kotti, H. BenSik Ali, S. Ayed, M. Fekih Hassen, S. Elatrous, Pneumothorax spontané et maladie de Recklinghausen: À propos d'un cas, Rev. Pneumol. Clin. 68 (2012) 202–204.
[29] R. Bouchentouf, A rare aetiology of lung cystic lesions: neurofibromatosis type 1, Tunis. Med. 94 (5) (2016) 412–413.
[30] E.M. Jutant, B. Girerd, X. Jaïs, et al., Pulmonary hypertension associated with neurofibromatosis type 1, Eur. Respir. Rev. 27 (149) (2018 Aug 29).
[31] D. Montani, F. Coulet, B. Girerd, et al., Pulmonary hypertension in patients with neurofibromatosis type I, Medicine (Baltim.) 90 (3) (2011) 201–211.
[32] D. Rodrigues, H. Oliveira, C. Andrade, et al., Interstitial lung disease and pre-capillary pulmonary hypertension in neurofibromatosis type 1, Respir. Med. Case Rep. 24 (2018) 8–11.
[33] U. Chaddha, I. Puscas, A. Prosper, S. Ganesh, B. Yaghmour, A 63-year-old woman with neurofibromatosis type 1 and pulmonary hypertension with worsening hypoxemia, Chest 152 (4) (2017) e89–e93.
[34] E. Shimizu, T. Shinohara, N. Mori, et al., Loss of heterozygosity on chromosome arm 17p in small cell lung carcinomas, but not in neurofibromas, in a patient with von Recklinghausen neurofibromatosis, Cancer 71 (3) (1993) 725–728.
[35] A. Hsu, S. Han, Synchronous neuroendocrine tumor and non-small-cell lung cancer in neurofibromatosis type 1, Clin Case Rep 3 (12) (2015) 990–996.
[36] A. Oikonomou, D. Mikroulis, P. Mintzopoulou, L. Lukman, P. Prassopoulos, Lung cancer associated with neurofibromatosis type I, Case Rep Radiol 2013 (2013) 869793.
[37] G.C. Andrade, O.P. Braga, M.K. Hisatugo, M.A. De Paiva Neto, E. Succi, F.M. Braga, Giant intrathoracic meningoceles associated with cutaneous neurofibromatosis type I: case report, Arq Neuropsiquiatr 61 (3) (2003) 677–681.
[38] T. Zuo, Z. Ni, M. Zhou, C. Huang, Z. Tang, Z. Yang, Large intrathoracic meningocele in a patient with neurofibromatosis type 1, Asian Cardiovasc. Thorac. Ann. 22 (2) (2014) 219–221.
[39] D.G. Cho, Y.J. Chang, K.D. Cho, J.T. Hong, Collaborative treatment of huge intrathoracic meningoceles associated with neurofibromatosis type 1: a case report, J. Cardiothorac. Surg. 10 (2015 Nov 10) 161.
[40] M.P. Muniz, A.S. Souza, D.A.B. Criado, et al., Type 1 neurofibromatosis: radiological findings of the chest, Radiol. Bras. 43 (3) (2010) 167–170.
[41] S.E. Rossi, J.J. Erasmus, H.P. McAdams, L.F. Donnelly, Thoracic manifestations of neurofibromatosis-I, AJR Am. J. Roentgenol. 173 (6) (1999) 1631–1638.
[42] S.L. Wakely, The posterior vertebral scalloping sign, Radiology 239 (2) (2006) 607–609.
[43] J.C. Hunt, D.G. Pugh, Skeletal lesions in neurofibromatosis, Radiology 76 (1961) 1–20.
[44] A.F. Espig, A.A. Slomp, A.Q. Campagnolo, et al., Neurofibromatosis type 1: update, Rev. Bras. Ciência Mov. 6 (2008) 243–249.
[45] R. Listernick, R.E. Ferner, G.T. Liu, D.H. Gutmann, Optic pathway gliomas in neurofibromatosis-1: controversies and recommendations, Ann. Neurol. 61 (3) (2007) 189–198.
[46] A. Casal, N. Rodríguez-Núñez, A. Martínez-Alegría, S. Candamio, J. Álvarez, L. Valdés, Neurofibromatosis type I with lung involvement in a cancer patient, Pulmonology 24 (4) (2018) 269–271.
[47] E. Dombi, A. Baldwin, L.J. Marcus, et al., Activity of selumetinib in neurofibromatosis type 1-related plexiform neurofibromas, N. Engl. J. Med. 375 (26) (2016) 2550–2560.
[48] S. Fischer-Huchzermeyer, A. Dombrowski, G. Wilke, et al., MEK inhibitors enhance therapeutic response towards ATRA in NF1 associated malignant peripheral nerve sheath tumors (MPNST) in-vitro, PLoS One 12 (11) (2017) e0187700.

European Journal of Cardio-Thoracic Surgery 56 (2019) 816
doi:10.1093/ejcts/ezz108 Advance Access publication 8 April 2019

IMAGES IN CARDIO-THORACIC SURGERY

Cite this article as: Souza ASJr, Soares Souza LV, Marchiori E. Asymptomatic arterio-arterial fistula between pulmonary and phrenic arteries. Eur J Cardiothorac Surg 2019;56:816.

Asymptomatic arterio-arterial fistula between pulmonary and phrenic arteries

Arthur Soares Souza Jr[a,b], Luciana Volpon Soares Souza[a] and Edson Marchiori[c,*]

[a] Ultra X, São José do Rio Preto, São Paulo, Brazil
[b] Department of Radiology, Faculdade de Medicina de Rio Preto, São José do Rio Preto, São Paulo, Brazil
[c] Department of Radiology, Universidade Federal do Rio de Janeiro, Rio de Janeiro, Brazil

* Corresponding author. Department of Radiology, Universidade Federal do Rio de Janeiro,Rua Thomaz Cameron, 438, Valparaiso, CEP 25685.120, Petrópolis, Rio de Janeiro, Brazil. Tel: +55-24-22492777; fax: +55-21-26299017; e-mail: edmarchiori@gmail.com (E. Marchiori).

Received 4 February 2019; received in revised form 27 February 2019; accepted 13 March 2019

Keywords: Arterio-arterial fistula • Computed tomography • Pulmonary vascularization

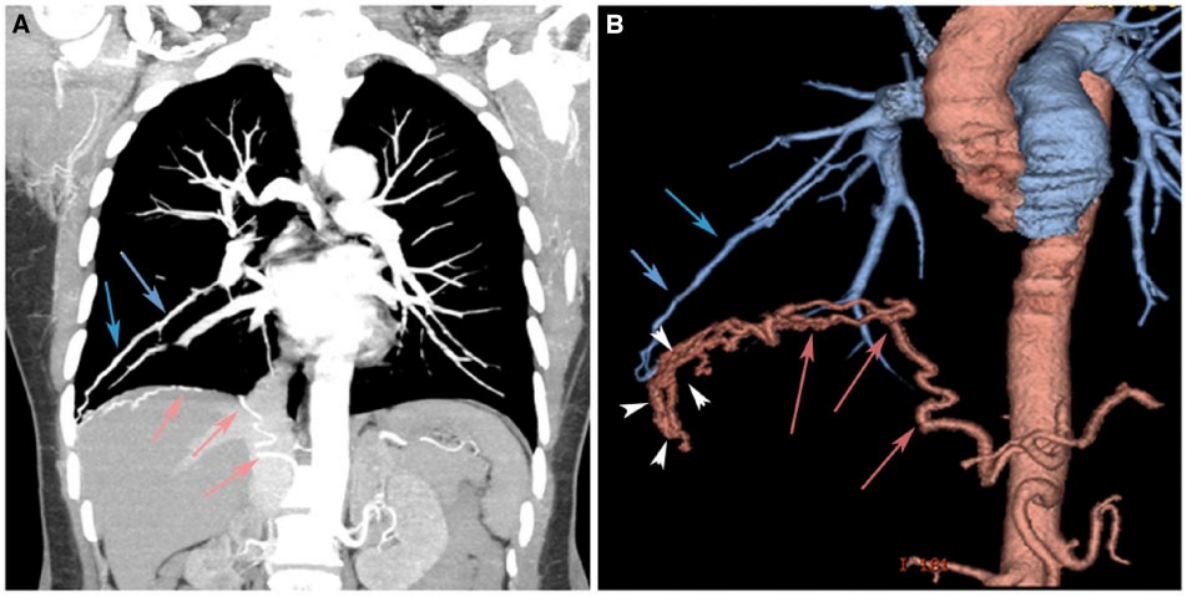

Figure 1: A 52-year-old woman underwent computed tomography (CT) during follow-up for colon carcinoma. CT coronal (**A**) and 3-dimensional reconstruction (**B**) revealed a vascular tangle (arrowheads) adjacent to the diaphragm, originating from a phrenic artery (pink arrows) and draining to a dilated interlobar pulmonary artery (blue arrows). The vascular malformation was embolized.

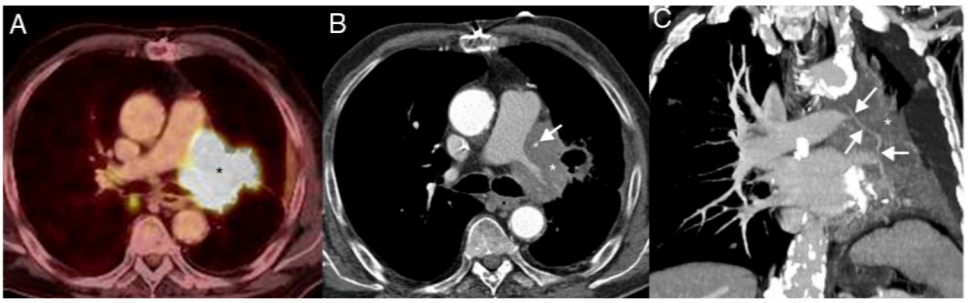

Fig. 2. Axial fused PET/CT image (A) demonstrates a hypermetabolic mass (asterisk). Axial CT image (mediastinal window) from the CT portion of the PET/CT (B) study shows an increase in the size of the left hilar mass (asterisk) and a greater secondary encasement of the left internal mammary artery graft (arrow) with respect to the previous imaging study. Coronal CT image (mediastinal window) from the CT portion of the PET/CT (C) better depicts the encasement of the coronary artery bypass graft (arrows) by the mass (asterisk).

Bibliografía

1. Basso C, Rizzo S, Valente M, Thiene G. Cardiac masses and tumours. Heart. 2016;102:1230–45.
2. Khaji A, Kowey PR. Update on atrial fibrillation. Trends Cardiovasc Med. 2017;27:14–25.
3. Juan O, Esteban E, Sotillo J, Alberola V. Atrial flutter and myocardial infarction-like ECG changes as manifestations of left ventricle involvement from lung carcinoma. Clin Transl Oncol. 2008;10:125–7.

Luis Gorospe [a,*], Ana María Ayala-Carbonero [a,b], Odile Ajuria-Illarramendi [c], Alberto Cabañero-Sánchez [d]

[a] *Department of Radiology, Ramón y Cajal University Hospital, Madrid, Spain*

[b] *Department of Pathology, Ramón y Cajal University Hospital, Madrid, Spain*

[c] *Department of Nuclear Medicine, Ramón y Cajal University Hospital, Madrid, Spain*

[d] *Department of Thoracic Surgery, Ramón y Cajal University Hospital, Madrid, Spain*

* Corresponding author.
E-mail address: luisgorospe@yahoo.com (L. Gorospe).

https://doi.org/10.1016/j.arbres.2019.03.018
0300-2896/

Mucormycotic Pulmonary Pseudoaneurysm Causing Fatal Hemoptysis

Hemoptisis letal causada por un pseudoaneurisma pulmonar mucomircótica

Dear Editor:

A 40-year-old diabetic man with 40 pack-years smoking exposure presented to the emergency department with a 30-day history of fever, dyspnea, and productive cough with thick yellowish sputum, later associated with hemoptysis. The patient had type 2 diabetes mellitus and reported unmeasured weight loss over the last month. Laboratory tests revealed leukocytosis (18,500 cells/mm^3); the patient's blood glucose level was 296 mg/dL and his glycosylated hemoglobin concentration was 12.8%. His basal oxygen saturation was 89%. Other laboratory findings were unremarkable. A chest-X ray showed three cavitary lesions with air-fluid levels (Fig. 1A). The patient's sputum was negative for acid-fast bacilli.

Contrast-enhanced chest computed tomography (CT) disclosed thick-walled cavitary lesions, one with solid content and a pseudoaneurysm inside, located on a peripheral ramification of the right pulmonary artery (Fig. 1B–D). Fiberoptic bronchoscopy revealed necrotic material covering the right main bronchial mucosa. Bronchoalveolar lavage (BAL) demonstrated the presence of fungal hyphae suggestive of zygomycosis. Cultures confirmed the presence of *Rhizopus* species. The patient was treated with amphotericin B. During hospitalization, he had several episodes of hemoptysis, and he died of massive hemoptysis on the second day after the internation admission.

Mucormycosis (also known as zygomycosis) is a fulminant opportunistic fungal infection caused by fungi of the order Mucorales, class Zygomycetes. Mucormycosis is far less common than other opportunistic fungal infections, such as *Aspergillus* and *Candida* infections, although the mortality rate is much higher. Although Classically described in patients with diabetes (especially diabetic ketoacidosis), in the modern era it is seen most commonly in patients with hematological malignancies, particularly those who have undergone stem cell transplantation.[1–3] Lin et al.[4] described 35 patients with confirmed pulmonary mucormycosis; hematological malignances were found in 68% and diabetes in 20% of the cases.

Mucormycosis manifests in the sinuses (39%), lung (24%), skin (19%), brain (9%), and gastrointestinal tract (7%), and as disseminated disease (6%). The respiratory symptoms of pulmonary mucormycosis are diverse, including fever, cough, expectoration, chest pain, and breathing difficulties.[1,2] Mucorales species are angioinvasive, which leads to vessel rupture with massive hemorrhage and infarction of the distal tissue. Hemoptysis is a common complication and can be massive, causing sudden death.[1] The clinical diagnosis of mucormycosis is difficult, and is often made at a late stage or postmortem. The diagnosis relies on the identification of organisms in tissues by pathological examination, with confirmation by culture.[1,2,5] However, some authors have reported, as in our case, initial diagnosis by identification of the fungus in sputum or BAL fluid, with subsequent confirmation by culture. In one case series, 25% of sputum or BAL specimens allowed positive identification.[6] The main differential diagnosis is pulmonary aspergillosis. On pathological examination, hyphae characteristics differ between *Mucor* and *Aspergillus* species. The hyphae of *Mucor*

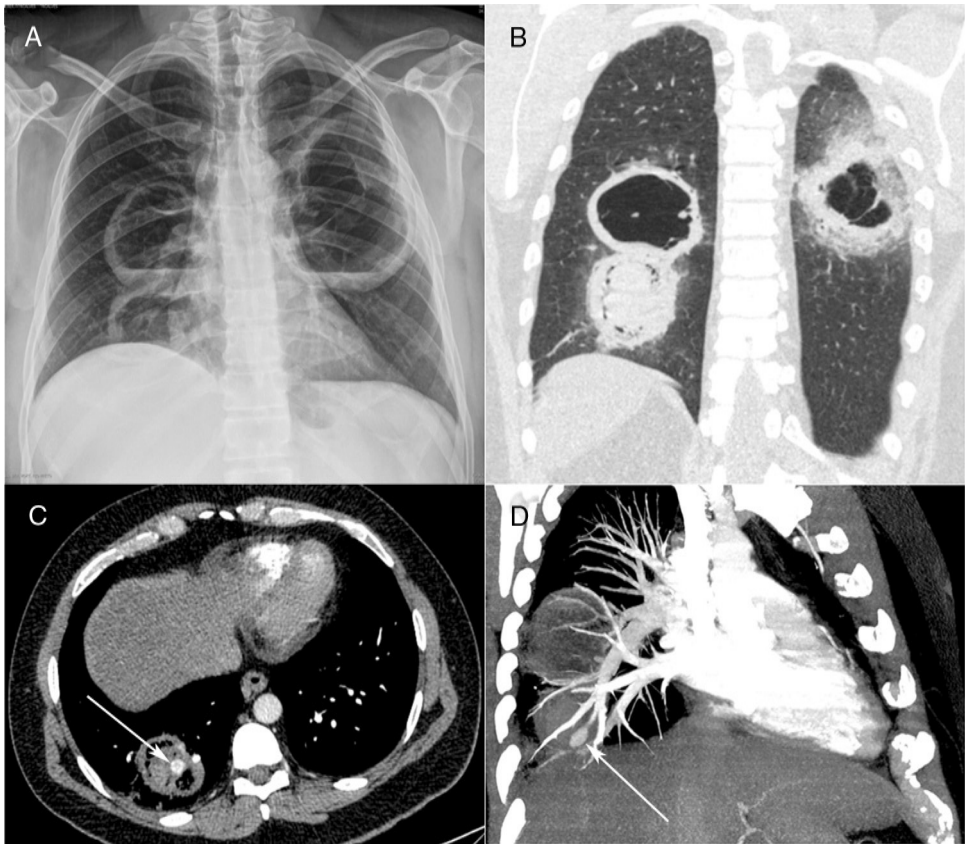

Fig. 1. Posteroanterior chest radiograph (A) showing three large cavitary lesions, two on the right lung and one on the left, with air-fluid levels. Coronal computed tomography image (B) obtained with the lung window setting demonstrating the thick-walled cavitary lesions, with solid content in one lesion on the right. Axial contrast-enhanced image (C) obtained with the mediastinal window setting depicting the solid content in the lower cavity, with a highly enhancing nodule inside (arrow), compatible with an aneurysm. Computed tomography–pulmonary angiography image (D) demonstrating that the pseudoaneurysm is related to a peripheral pulmonary artery (arrow).

species are thick and non-septate, and have larger diameters than the hyphae of *Aspergillus* (which have fewer, irregular branches and form right or obtuse angles).[2]

Most patients with pulmonary mucormycosis show consistent sequential morphological changes on serial follow-up imaging, consisting initially of consolidation or nodules/masses with the CT halo sign, followed by the reversed halo sign or central necrosis and, finally, the air-crescent sign. These changes are related to recovery of the absolute neutrophil count.[3] Aneurysms affecting the pulmonary arteries are extremely uncommon. The most common cause of this complication is infection. Other causes are pulmonary hypertension, pulmonary arteritis, cystic medial necrosis, and thoracic trauma. The most common organisms are bacteria. Fungal invasion of pulmonary artery walls, resulting in pseudoaneurysm formation, is exceedingly rare.[1,7,8] Physicians should consider pulmonary mucormycosis in immunocompromised patients with unresolved pneumonia. In addition, the high fatality rates associated with pulmonary artery pseudoaneurysm warrant aggressive management with surgery and antifungal agents.

Bibliografía

1. Kim YI, Kang HC, Lee HS, Choi JS, Seo KH, Kim YH, et al. Invasive pulmonary mucormycosis with concomitant lung cancer presented with massive hemoptysis by huge pseudoaneurysm of pulmonary artery. Ann Thorac Surg. 2014;98:1832–5.
2. Li YH, Sun P, Guo JC. Clinical analysis of diabetic combined pulmonary mucormycosis. Mycopathologia. 2017;182:1111–7.
3. Nam BD, Kim TJ, Lee KS, Kim TS, Han J, Chung MJ. Pulmonary mucormycosis: serial morphologic changes on computed tomography correlate with clinical and pathologic findings. Eur Radiol. 2018;28:788–95.
4. Lin E, Moua T, Limper AH. Pulmonary mucormycosis: clinical features and outcomes. Infection. 2017;45:443–8.
5. Espíldora-Hernández J, Pérez-López C, Abarca-Costalago M, Nuño-Álvarez E. Pulmonary mucormycosis at onset of diabetes in a young patient. Arch Bronconeumol. 2017;53:531–3.
6. Kontoyiannis DP, Wessel VC, Bodey GP, Rolston KV. Zygomycosis in the 1990s in a tertiary-care cancer center. Clin Infect Dis. 2000;30:851–6.
7. Vaideeswar P. Fatal haemoptysis due to mucormycotic intrapulmonary arterial aneurysm. Int J Cardiol. 2002;83:273–4.
8. Ramachandran L, Dewan S, Kumar V, Wankhade B. Mucormycosis causing pulmonary artery aneurysm. Respir Med Case Rep. 2015;16:71–3.

Luciana Volpon Soares Souza[a], Arthur Soares Souza[a,b], Edson Marchiori[b,*]

[a] *Ultra X, Brazil*
[b] *Universidade Federal do Rio de Janeiro, Rio de Janeiro, Brazil*

Corresponding author.
E-mail address: edmarchiori@gmail.com (E. Marchiori).

https://doi.org/10.1016/j.arbres.2019.03.019
0300-2896/

Arch Bronconeumol. 2021;57(12):767

Sociedad Española de Neumología y Cirugía Torácica SEPAR

ARCHIVOS DE Bronconeumología

www.archbronconeumol.org

Clinical Image

Bronchial and Tracheal Mucosa-Associated Lymphoid Tissue Lymphoma

Linfoma del tejido linfoide asociado a mucosas bronquial y traqueal

Luciana Volpon Soares Souza[a], Arthur Soares Souza Jr[a,b], Edson Marchiori[c,*]

[a] Ultra X, São José do Rio Preto, SP, Brazil
[b] Faculdade de Medicina de Rio Preto, SP, Brazil
[c] Universidade Federal do Rio de Janeiro, Rio de Janeiro, Brazil

A 72-year-old man presented with a 1-year history of progressive dyspnea. Chest radiography findings were normal. Chest computed tomography showed nodular lesions in the trachea and left main bronchus, with irregular luminal narrowing and severe stenosis (Fig. 1A–C). Pulmonary function testing revealed a variable intrathoracic obstruction. ^{18}F-fluorodeoxyglucose (FDG) positron emission tomography/computed tomography showed increased FDG uptake in the left main bronchus, with a maximum standard uptake value of 8.4 (Fig. 1D). Fiberoptic bronchoscopy revealed multiple small mucosal lesions along the trachea and left main bronchus (Fig. 1E). Histopathology showed proliferation of atypical small lymphoid cells infiltrating the bronchial mucosa and submucosa (Fig. 1F). Immunohistochemical staining supported the diagnosis of extranodal marginal-zone mucosa-associated lymphoid tissue (MALT) lymphoma. The patient was referred for radiotherapy.

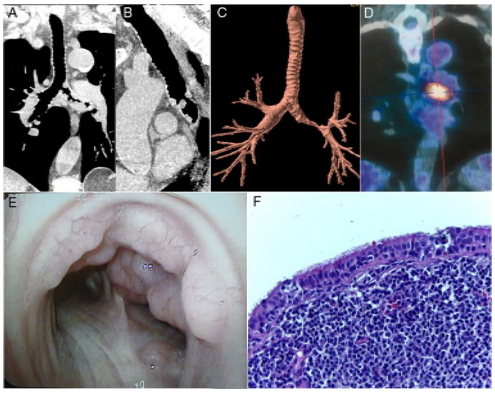

Fig. 1. Coronal (A) and sagittal (B) reformatted images and a three-dimensional external rendering (C) of a chest computed tomography image show nodular lesions in the trachea and left main bronchus, with irregular luminal narrowing and severe stenosis. (D) ^{18}F-fluorodeoxyglucose positron emission tomography/computed tomography demonstrated increased fluorodeoxyglucose uptake in the left main bronchus, with a maximum standard uptake value of 8.4. (E) Fiberoptic bronchoscopy revealed multiple small nodular mucosal lesions with a cobblestone appearance along the trachea and left main bronchus. (F) A histopathological section demonstrating the proliferation of atypical small lymphoid cells, compatible with lymphoma (hematoxylin and eosin stain, 100× magnification).

MALT refers to the lymphoid tissue underlying the epithelia of the gastrointestinal, respiratory, and urogenital tracts. MALT related to the respiratory tract epithelia is called bronchus-associated lymphoid tissue. MALT lymphoma comprises a group of low-grade extranodal B-cell neoplasms. These tumors arising in the bronchial or tracheal wall are extremely rare. The treatment strategy for this condition has not been completely elucidated, and surgery, radiotherapy, or chemotherapy has been used, alone or in combination.[1,2]

Conflicts of interest

The authors declare that they have no conflicts of interest to express.

References

1. Minami D, Ando C, Sato K, Moriwaki K, Sugahara F, Nakasuka T, et al. Multiple mucosa-associated lymphoid tissue lymphoma of the trachea. Intern Med. 2017;56:2907–11, http://dx.doi.org/10.2169/internalmedicine.8269-16.
2. Yoon RG, Kim MY, Song JW, Chae EJ, Choi CM, Jang S. Primary endobronchial marginal zone B-cell lymphoma of bronchus-associated lymphoid tissue: CT findings in 7 patients. Korean J Radiol. 2013;14:366–74, http://dx.doi.org/10.3348/kjr.2013.14.2.366.

* Corresponding author.
E-mail address: edmarchiori@gmail.com (E. Marchiori).

https://doi.org/10.1016/j.arbres.2020.05.026

European Journal of Cardio-Thoracic Surgery 59 (2021) 276–277
doi:10.1093/ejcts/ezaa271 Advance Access publication 25 August 2020

CASE REPORT

Cite this article as: Soares Souza LV, Souza AS, Morales MM, Marchiori E. Superior vena cava aneurysm: an unusual mediastinal mass. Eur J Cardiothorac Surg 2021;59:276–7.

Superior vena cava aneurysm: an unusual mediastinal mass

Luciana Volpon Soares Souza[a], Arthur Soares Souza Jr [a,b], Márcia Maria Morales [c] and Edson Marchiori [d,*]

[a] Departamento de Radiologia, Ultra X, São José do Rio Preto, São Paulo, Brazil
[b] Departamento de Radiologia, Faculdade de Medicina de Rio Preto, São José do Rio Preto, São Paulo, Brazil
[c] Departamento de Cirurgia, Hospital Israelita Albert Einstein, São Paulo, São Paulo, Brazil
[d] Departamento de Radiologia, Universidade Federal do Rio de Janeiro, Rio de Janeiro, Brazil

* Corresponding author. Universidade Federal do Rio de Janeiro, Rua Thomaz Cameron, 438, Valparaiso, Petrópolis, Rio de Janeiro CEP 25685.120, Brazil. Tel: +55-24-22492777; fax: +55-21-26299017; e-mail: edmarchiori@gmail.com (E. Marchiori).

Received 11 April 2020; received in revised form 15 June 2020; accepted 27 June 2020

Abstract

Superior vena cava aneurysms are rare mediastinal vascular lesions. Aneurysms are classified as fusiform and saccular, with the latter being rarer than the former. We report the case of an asymptomatic 75-year-old woman who presented with a superior mediastinal mass. She underwent chest computed tomography angiography, which demonstrated a saccular aneurysm in the superior vena cava.

Keywords: Superior vena cava • Aneurysm • Computed tomography

INTRODUCTION

The majority of aneurysms in the chest involve the aorta and its branches; aneurysms of the superior vena cava (SVC) are rare mediastinal vascular lesions. They are generally asymptomatic and are often found incidentally on imaging studies. Two types of SVC aneurysm have been described: fusiform and saccular [1–3]. The majority of these aneurysms are fusiform. The development of complications, such as rupture, thrombus formation and pulmonary embolism, has been described, particularly in saccular aneurysms, and may necessitate surgery and anticoagulation therapy [1, 4, 5]. We report the case of an asymptomatic 75-year-old woman with a mediastinal mass detected during a routine check-up. Contrast-enhanced chest computed tomography (CT) angiography demonstrated an SVC aneurysm. Surgical resection of the aneurysm was performed successfully.

CASE REPORT

A 75-year-old asymptomatic woman presented with a mediastinal mass detected on a chest radiograph acquired during a routine check-up. No prior chest imaging was available for this patient. She had a past history of hypertension, diabetes and a 30-pack-year smoking habit. She denied any history of chest trauma, thoracic surgery or previous central venous catheterization. On physical examination, she was eupnoeic in room air, with normal pulmonary and cardiac auscultation. Laboratory test results were unremarkable.

Unenhanced chest CT was performed and revealed a right mediastinal mass (Fig. 1A). Contrast-enhanced CT angiography revealed a saccular aneurysm arising from the anterior surface of the SVC (Fig. 1B). Three-dimensional volume-rendered coronal imaging (Fig. 1C) demonstrated the relationships between the aneurysm and adjacent vascular structures. The aneurysm contained no filling defect, and the other mediastinal veins were normal. Considering the risk of rupture or thrombus formation, surgical resection was performed, and the aneurysm was excised successfully (Fig. 1D).

Median sternotomy was performed. The patient underwent extracorporeal circulation with the arterial site in the ascending aorta and bicaval venous cannulation of the inferior vena cava and left venous brachiocephalic trunk. This strategy permitted isolation of the SVC. The azygous vein was isolated and closed to prevent blood flow to the upper vena cava. The saccular aneurysm, which measured 5.7 cm, was approached in the middle portion of the upper vena cava and extended to the right pleural space. The aneurysmatic sac was opened and removed, and the upper vena cava was reconstructed with a bovine pericardial patch. During this reconstruction of the upper vena cava with extracorporeal support, cardiac arrest and myocardial protection were not needed. Cardiopulmonary bypass was achieved with no complication. The patient's postoperative period was uneventful, and she was discharged on the fifth day after the procedure.

DISCUSSION

SVC aneurysms are very rare and usually asymptomatic; most are detected incidentally by imaging examinations, on which they appear as mediastinal masses. The SVC aneurysms are mainly either fusiform (comprising the majority of cases) or saccular [1–5]. SVC aneurysms may be congenital or acquired, but in most cases their cause is unknown. They have been associated with cystic

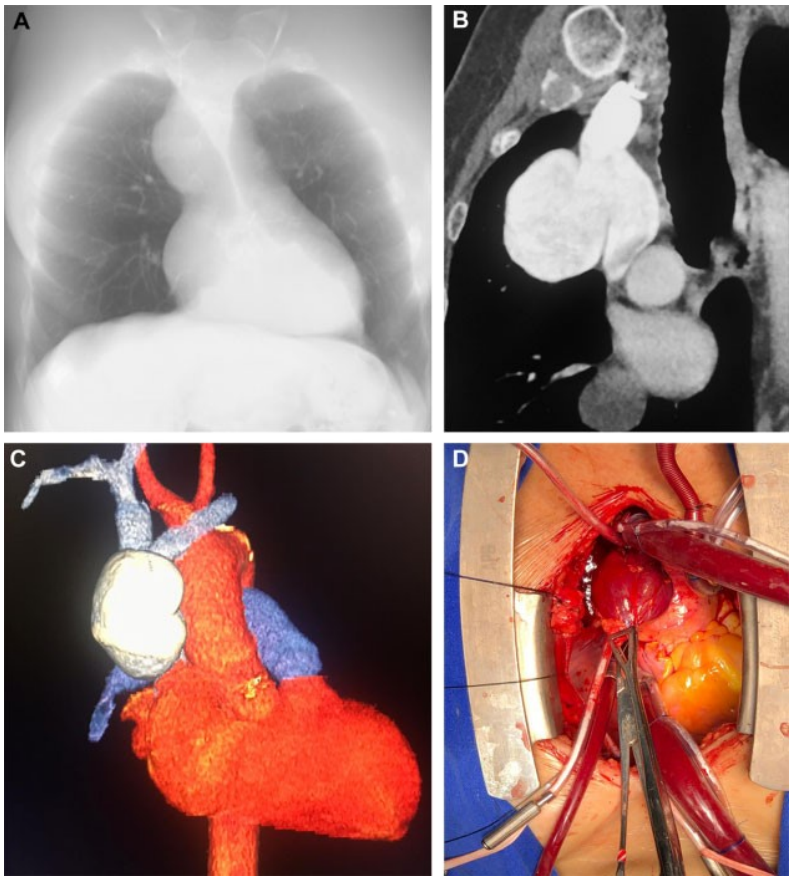

Figure 1: Unenhanced chest computed tomography (CT) revealed a right mediastinal mass (**A**). Contrast-enhanced CT angiography showed a saccular aneurysm arising from the anterior surface of the superior vena cava (**B**). Three-dimensional volume-rendered coronal (**C**) image demonstrated the relationships between the aneurysm and adjacent vascular structures. There were no filling defects in the aneurysm sac, and the other mediastinal veins were normal. The aneurysm (**D**) was excised successfully.

hygromas, which may be related to the similar embryological origins of the venous and lymphatic systems. Other possible aetiologies are trauma and previous surgery [2–5]. Contrast-enhanced CT clearly depicts the fusiform or saccular dilatation of SVCs, allowing for a definitive diagnosis. Filling defects in an aneurysm may indicate thrombus. Changes in the size of an aneurysm with different degrees of respiration and patient positions are highly suggestive of a venous, rather than arterial, aneurysm [2]. Reported complications of SVC aneurysms are rare and include aneurysmal rupture, thrombosis and acute pulmonary thromboembolism [1, 4, 5]. Therapeutic guidelines for SVC aneurysms are not well-established. Treatment decisions are influenced by the aneurysm type. For most fusiform aneurysms, a conservative approach with regular follow-up imaging is sufficient because possible complications are rare. For saccular SVC aneurysms, even asymptomatic ones, prophylactic surgical resection is recommended.

Other factors prompting the recommendation of surgical treatment of SVC aneurysms are the presence of symptoms (caused by partial or total venous compression with subsequent obstruction), sudden rapid aneurysm growth and the risk of rupture or internal thrombus formation (as a thrombus increases the risk of pulmonary embolism). If resection is not performed, long-term anticoagulation to prevent venous thromboembolism may be considered [1–5].

Conflict of interest: none declared.

Reviewer information

European Journal of Cardio-Thoracic Surgery thanks the anonymous reviewer(s) for their contribution to the peer review process of this article.

REFERENCES

[1] Oh SG, Kim KH, Seon HJ, Yoon HJ, Ahn Y, Jeong MH *et al.* Unusual cause of acute right ventricular dysfunction: rapid progression of superior vena cava aneurysm complicated by thrombosis and pulmonary thromboembolism. J Korean Med Sci 2011;26:690–3.

[2] Enright TR, Kanne JP. Saccular superior vena cava aneurysm—incidental diagnosis by MDCT. Clin Radiol 2010;65:421–2.

[3] Sharma R, Ravi M, Unni TG. Primary fusiform superior vena cava aneurysm. Cardiol Res 2017;8:176–8.

[4] Patel A, Cobb R, Rivera V, Simpson S. Untreated superior vena cava aneurysm: radiological significance and review of the literature. Case Rep Radiol 2016;2016:1–3.

[5] Janczak D, Skiba J, Gemel M, Mak M, Ziomek A, Malinowski M *et al.* Giant saccular superior vena cava aneurysm-a rare and difficult clinical case. J Thorac Dis 2016;8:E247–9.

European Journal of Cardio-Thoracic Surgery 59 (2021) 723
doi:10.1093/ejcts/ezaa303 Advance Access publication 3 November 2020

Cite this article as: Soares Souza LV, Souza AS Jr, Marchiori E. Left-sided scimitar syndrome. Eur J Cardiothorac Surg 2021;59:723.

Left-sided scimitar syndrome

Luciana Volpon Soares Souza[a], Arthur Soares Souza Jr[a,b] and Edson Marchiori [c,*]

[a] Ultra X, São José do Rio Preto, SP, Brazil
[b] Faculdade de Medicina de Rio Preto, São José do Rio Preto, SP, Brazil
[c] Universidade Federal do Rio de Janeiro, Rio de Janeiro, Brazil

* Corresponding author. Universidade Federal do Rio de Janeiro, Rua Thomaz Cameron 438, Valparaiso, CEP 25685.120, Petrópolis, Rio de Janeiro, Brazil. Tel: +55-24-22492777; e-mail: edmarchiori@gmail.com (E. Marchiori).

Received 14 July 2020; accepted 18 July 2020

Keywords: Left scimitar syndrome • Computed tomography • Thoracic vascularization

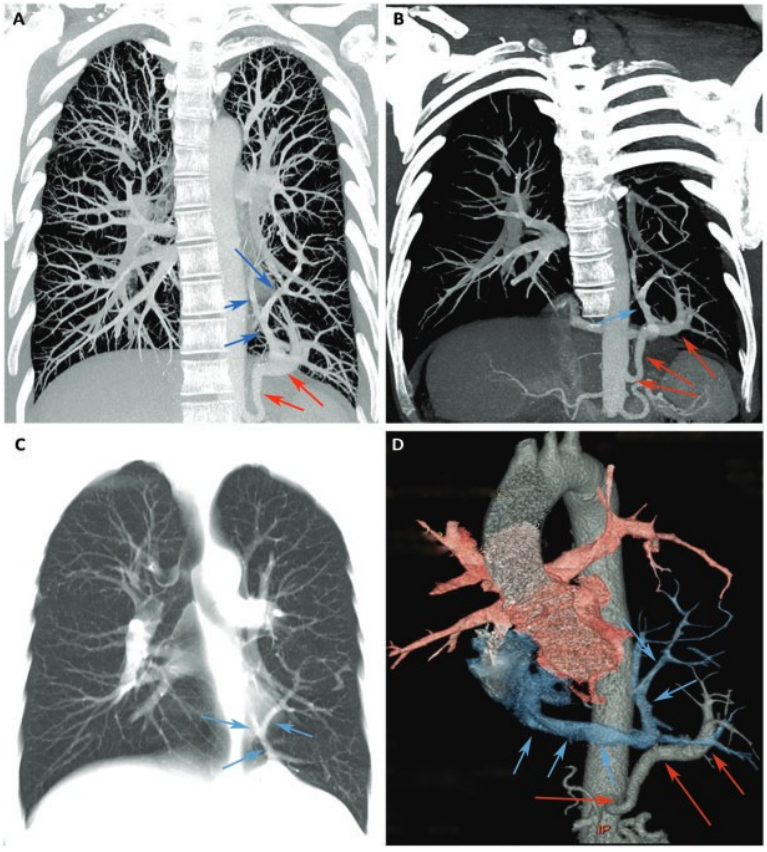

Figure 1: A chest CT of a 52-year-old asymptomatic man revealed a systemic arterial supply to the left lower lobe, arising from the abdominal aorta (red arrows). The lower portion of the left lung was drained into the inferior vena cava by an anomalous vein that crossed the mediastinum (blue arrows). The diagnosis was left scimitar syndrome.

Reviewer information

European Journal of Cardio-Thoracic Surgery thanks Daniel Zimpfer and the other, anonymous reviewer(s) for their contribution to the peer review process of this article.

J Bras Pneumol. 2021;47(1):e20200462
https://dx.doi.org/10.36416/1806-3756/e20200462

Calcified metastases of teratoma

Luciana Volpon Soares Souza[1], Arthur Soares Souza Jr[1,2], Edson Marchiori[3]

A 37-year-old male patient was admitted for oncological follow-up. He had undergone right orchiectomy via the scrotal pouch two years prior for the resection of a tumor mass; the histopathological diagnosis was a combination of germ cell tumor, teratoma components, and areas of malignant degeneration. At that time, he had venous vascular invasion with metastases in the abdominal lymph nodes and the lungs (Figures 1A and 1B). The lung metastases were noncalcified. He underwent palliative treatment with chemotherapy, which resulted in stabilization of the tumor. A recent CT showed masses and nodules in both lungs, predominating in the right base, containing foci of calcification (Figures 1C and 1D). Biopsy of a pulmonary nodule was compatible with a post-pubertal metastatic teratoma with adenocarcinomatous transformation. At presentation, the patient was stable and receiving a new chemotherapy regimen.

Malignant transformation of teratomas is rare, occurring in only 3-6% of testicular germ cell tumors. The most common types of malignant transformation include sarcoma, carcinoma, and primitive neuroectodermal tumor. Teratomas with malignant transformation are usually metastatic at presentation, have a high recurrence rate, and are more aggressive than are teratomas without malignant transformation. The most common sites of metastasis are the lymph nodes, liver, and lungs. The treatment of teratomas with malignant transformation remains challenging. The standard treatment is radical orchiectomy, with or without chemotherapy and/or radiotherapy.[1,2]

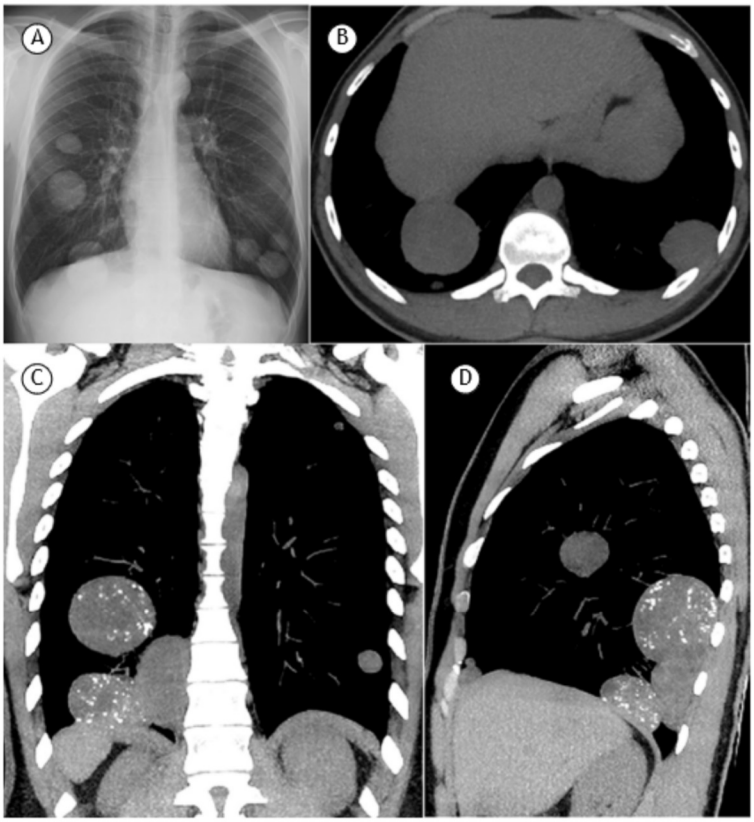

Figure 1. A chest radiograph (in A) and a chest CT scan (in B) obtained in October of 2017 showing multiple noncalcified nodules and masses in both lungs, predominantly in the lower regions. A chest CT performed two years later in the coronal (in C) and sagittal (in D) planes demonstrated growth of the nodules and masses, which contained calcification foci.

REFERENCES

1. 1. Ibrahim DY, Sun H. Somatic Malignant Transformation of a Testicular Teratoma: A Case Report and an Unusual Presentation. Case Rep Pathol. 2019;2019:5273607. https://doi.org/10.1155/2019/5273607
2. 2. Cabral FC, Krajewski KM, Rosenthal MH, Hirsch MS, Howard SA. Teratoma with malignant transformation: report of three cases and review of the literature. Clin Imaging. 2014;38(5):589-593. https://doi.org/10.1016/j.clinimag.2014.04.011

1. Ultra X, São José do Rio Preto (SP) Brasil.
2. Faculdade de Medicina de Rio Preto, SP, Brazil. São José do Rio Preto (SP) Brasil.
3. Universidade Federal do Rio de Janeiro, Rio de Janeiro (RJ) Brasil.

ISSN 1806-3713

J Bras Pneumol. 2021;47(5):e20200595
https://dx.doi.org/10.36416/1806-3756/e20200595

Consenso de terminologia em radiologia torácica em português do Brasil e de Portugal

Bruno Hochhegger[1,2,3], Edson Marchiori[4], Rosana Rodrigues[5], Alexandre Mançano[6], Dany Jasinowodolinski[4], Rodrigo Caruso Chate[7], Arthur Soares Souza Jr[8], Alexandre Marchini Silva[9], Márcio Sawamura[10], Marcelo Furnari[6], Cesar Araujo-Neto[11], Dante Escuissato[12], Rogerio Pinetti[13], Luiz Felipe Nobre[14], Danny Warszawiak[15], Gilberto Szarf[16], Gustavo Borges da Silva Telles[7], Gustavo Meirelles[17], Pablo Rydz Santana[18], Viviane Antunes[13], Julia Capobianco[19], Israel Missrie[19], Luciana Volpon Soares Souza[8], Marcel Koeningan Santos[20], Klaus Irion[21], Isabel Duarte[22], Rosana Santos[23], Erique Pinto[23], Diana Penha[23]

1. Pontifícia Universidade Católica do Rio Grande do Sul – PUCRS – Porto Alegre (RS) Brasil.
2. Universidade Federal de Ciências da Saúde de Porto Alegre, Porto Alegre (RS) Brasil.
3. Thoracic Imaging Division, College of Medicine, University of Florida, Gainesville (FL) USA.
4. Universidade Federal do Rio de Janeiro – UFRJ – Rio de Janeiro (RJ) Brasil.
5. Universidade Federal do Rio Grande do Sul – UFRGS – Porto Alegre (RS) Brasil.
6. Sabin Medicina Diagnóstica, Brasília (DF) Brasil.
7. Hospital Israelita Albert Einstein, São Paulo (SP) Brasil.
8. Faculdade de Medicina de São José do Rio Preto, São José do Rio Preto (SP) Brasil.
9. Santa Casa de Misericórdia de São Paulo, São Paulo (SP) Brasil.
10. Universidade de São Paulo – USP – São Paulo (SP) Brasil.
11. Universidade Federal da Bahia – UFBA – Salvador (BA) Brasil.
12. Universidade Federal do Paraná – UFPR – Curitiba (PR) Brasil.
13. DASA Diagnósticos, São Paulo (SP) Brasil.
14. Universidade Federal de Santa Catarina, Florianópolis (SC) Brasil.
15. Diagnóstico Avançado por Imagem – DAPI – Curitiba (PR) Brasil.
16. Universidade Federal de São Paulo – Unifesp – São Paulo (SP) Brasil.
17. Alliar Diagnóstico por Imagem, São Paulo (SP) Brasil.
18. Hospital Beneficência Portuguesa de São Paulo, São Paulo (SP) Brasil.
19. Fleury Medicina e Saúde, São Paulo (SP) Brasil.
20. Faculdade de Medicina de Ribeirão Preto, Universidade de São Paulo – USP – Ribeirão Preto (SP) Brasil.
21. Manchester National Health Service, Manchester, United Kingdom.
22. Instituto Português de Oncologia de Lisboa Francisco Gentil, Lisboa, Portugal.
23. Universidade da Beira Interior, Covilhã, Portugal.

Recebido: 24 novembro 2020.
Aprovado: 27 maio 2021.

RESUMO

A comunicação eficiente entre a equipe médica é um fator importante no diagnóstico e tratamento precoce e adequado dos pacientes. A terminologia utilizada em relatórios de exames radiológicos aparece nesse contexto como um elo importante entre radiologistas e os demais integrantes da equipe médica. Portanto, a heterogeneidade no uso de termos em relatórios é importante mas ainda pouco discutida. Este artigo é resultado de uma extensa revisão da nomenclatura radiológica em radiologia torácica, englobando pela primeira vez termos utilizados em vários métodos (radiografia, TC e RM), desenvolvida por radiologistas brasileiros e portugueses. O objetivo desta revisão da terminologia médica foi criar uma linguagem padronizada para os profissionais médicos e as equipes multidisciplinares.

Descritores: Tomografia computadorizada por raios X; Radiografia; Imagem por ressonância magnética; Terminologia como assunto.

INTRODUÇÃO

O objetivo da terminologia médica é fornecer uma linguagem padronizada para os profissionais médicos e equipes multidisciplinares. Essa terminologia permite uma comunicação multidisciplinar médica eficiente, maior rapidez na partilha e discussão dos casos clínicos e integração dos dados no registro clínico dos pacientes. Deve-se ainda salientar que uma linguagem adequada pode ajudar a reduzir erros de comunicação e documentação inadequada, o que garante às equipes médicas a análise dos processos dos pacientes com maior rapidez e precisão e, assim, maior rapidez no diagnóstico e tratamento.[1,2]

Com o objetivo de sumarizar criticamente as recentes evidências dos descritores de imagem, foram reunidos 25 especialistas brasileiros e 4 portugueses participantes da comissão de imagem da Sociedade Brasileira de Pneumologia e Tisiologia para elaborar o presente consenso. A seleção dos temas foi feita por um painel de especialistas que selecionou tópicos ou perguntas relativas às mudanças mais significativas nos conceitos previamente publicados, incluindo a terminologia de radiografia e RM de tórax, termos que até então não foram abordados previamente. A cada especialista convidado coube revisar ou responder a um tópico ou pergunta neste consenso. Em uma segunda fase, 3 especialistas discutiram e estruturaram todos os textos encaminhados pelos demais e, em uma terceira fase, todos os especialistas revisaram e discutiram as presentes recomendações. O presente consenso traz um incremento de mais de 50% nas terminologias previamente publicadas e engloba termos em uso em radiografia de tórax, TC e RM.[2]

Na radiologia torácica, o relatório radiológico escrito é o instrumento mais importante, e muitas vezes o único, de comunicação entre o radiologista e o médico

Endereço para correspondência:
Bruno Hochhegger. Departamento de Radiologia, Pavilhão Pereira Filho, Irmandade Santa Casa de Misericórdia de Porto Alegre, Avenida Independência, 75, CEP 90020-160, Porto Alegre, RS, Brasil.
Tel.: 55 51 3214-8300. E-mail: brunohochhegger@gmail.com
Apoio financeiro: Nenhum.

requisitante. O objetivo do presente consenso foi padronizar a terminologia usada na descrição das imagens torácicas em português do Brasil (subtítulo principal) e de Portugal, que, quando diferente, está identificada por (PT).

ÁCINO

O ácino é a unidade estrutural anatômica do pulmão. Localiza-se distalmente ao bronquíolo terminal e contém os ductos alveolares e alvéolos. O ácino participa das trocas gasosas e mede entre 6-10 mm. Um lóbulo secundário contém de 3 a 25 ácinos. Os ácinos somente são visíveis quando acumulam material (patológico) e aparecem como opacidades nodulares mal definidas em radiografias, TC e RM.[1]

APRISIONAMENTO AÉREO OU APRISIONAMENTO GASOSO (PT)

O aprisionamento aéreo corresponde à retenção de ar (gás) nas vias aéreas distais e é identificado na TC e RM. É reconhecido na fase expiratória e corresponde a uma redução da atenuação do parênquima pulmonar, apresentando menor valor do que a densidade habitual do parênquima e sem redução de volume (Figura 1).[1-3] É habitualmente resultado de uma obstrução parcial ou completa de vias aéreas ou de uma anormalidade focal da complacência pulmonar.[2]

ATELECTASIA OU COLAPSO

Atelectasia é o termo que descreve a redução de volume de ar do pulmão atingido. O mecanismo de origem mais frequente é a obstrução da via aérea com reabsorção do ar distal. Traduz-se por perda de volume com opacidade ou aumento da atenuação e desvio das fissuras, brônquios, vasos, diafragma, coração ou mediastino (Figura 2). A atelectasia passiva resulta da compressão por derrame pleural ou massa. A definição imagética é uma área pulmonar hiperdensa (ou com hipersinal no caso da RM) que apresenta redução do volume pulmonar, broncograma aéreo e perda da definição dos vasos. Pode ser identificada na radiografia, TC e RM de tórax.

ATELECTASIA REDONDA

Atelectasia redonda refere-se à presença de colapso pulmonar focal que ocorre em associação a uma variedade de condições.[4] Está tipicamente relacionada à doença pleural, sendo, portanto, um achado relativamente comum em pacientes com exposição ao asbesto,[5] nos quais costuma ter relação com um derrame pleural exsudativo prévio ou ser resultado de fibrose pleural adjacente ou espessamento pleural difuso.[4-7] Nos métodos axiais, a atelectasia redonda apresenta formato arredondado ou ovalado, localização periférica e em contato com a superfície pleural geralmente espessada, com ou sem derrame. A atelectasia redonda está caracteristicamente associada à redução volumétrica do lobo envolvido e a um aspecto curvilíneo das estruturas vasculares e brônquicas adjacentes às margens da lesão, formando o sinal da cauda do cometa (Figura S1).[2,5] Por representar parênquima pulmonar colapsado, a atelectasia redonda pode demonstrar intenso realce após a injeção de meio de contraste na TC e RM, uma característica útil na diferenciação com neoplasias pulmonares, que geralmente não apresentam captação tão intensa nos exames contrastados.

BANDA PARENQUIMATOSA

A banda parenquimatosa é definida como uma opacidade linear alongada, com espessura de 1-3 mm e até 5 cm de comprimento, que pode ser observada em pacientes com fibrose ou outras causas de espessamento intersticial.[1] Geralmente essas bandas são periféricas e frequentemente entram em contato com a superfície pleural, que pode estar espessada e retraída no local. Podem representar septos interlobulares espessados contíguos, fibrose peribroncovascular, cicatrizes grosseiras ou atelectasias relacionadas a áreas de fibrose pulmonar ou pleural de causa não específica (Figura S2).[5] As bandas parenquimatosas são observadas,

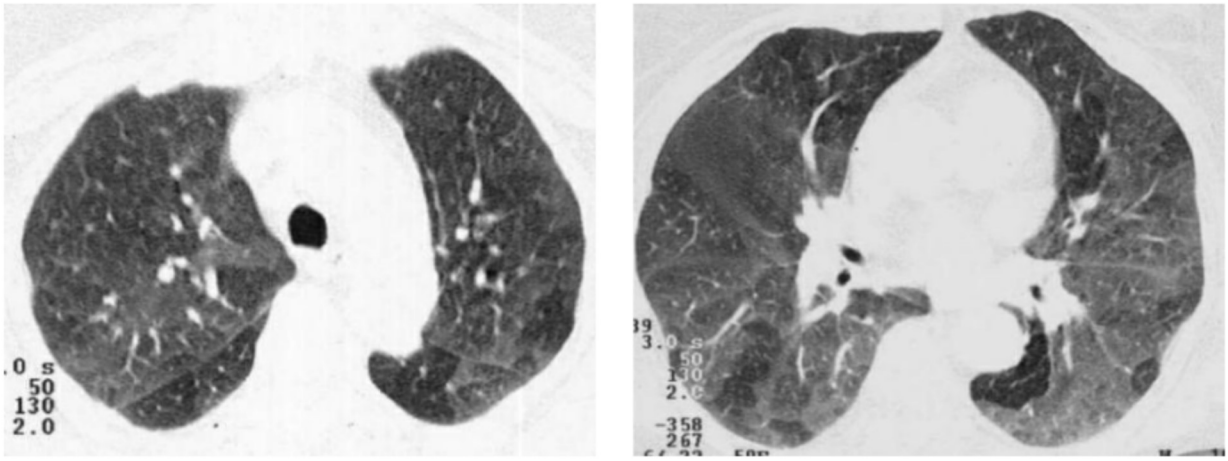

Figura 1. Imagens axiais de TC de tórax em janela de pulmão adquiridas em fase expiratória, revelando nos segmentos posteriores dos lobos inferiores diferentes densidades parenquimatosas, com áreas de redução de atenuação relacionadas com áreas de aprisionamento aéreo por obstrução de pequenas vias aéreas.

com maior frequência, em pacientes com exposição ao asbesto e sarcoidose.

BOLA FÚNGICA

A bola fúngica patologicamente representa um conglomerado de hifas entrelaçadas, geralmente de uma espécie de *Aspergillus*, colonizando uma cavidade contendo muco, fibrina e detritos celulares. Geralmente ocorre com doença fibrocavitária anterior (por exemplo, tuberculose ou sarcoidose) e eventualmente com cistos e bolhas e em brônquios. A bola fúngica pode ser móvel e apresentar mobilidade dependente da gravidade com a mudança de decúbito e pode mostrar um sinal do crescente aéreo (Figura 3). Ela pode mostrar uma atenuação heterogênea que lembra a textura de esponja e exibir focos de calcificação em TC e RM. É sinônimo de aspergiloma.[8] Vide "Sinal do crescente do aéreo".

BOLHA

A bolha patologicamente corresponde a um espaço aéreo medindo mais de 1 cm de diâmetro, podendo apresentar vários centímetros, demarcada por uma parede fina que não ultrapassa 1 mm de espessura. A bolha está geralmente associada a enfisema e alterações no pulmão adjacente. (Vide "Enfisema bolhoso"). A bolha aparece como uma hipertransparência focal arredondada ou área de hipoatenuação ≥ 1 cm de diâmetro delimitada por uma fina parede em radiografia, RM e TC (Figura 4). As bolhas múltiplas são frequentes e estão associadas a enfisema pulmonar (centrolobular e parasseptal).[5]

BRONCOCELE OU BRONCOCELO (PT)

Broncocele corresponde patologicamente a uma dilatação brônquica segmentar, habitualmente cilíndrica e de aspecto ramificado, que se apresenta total ou parcialmente preenchida por secreção, geralmente mucoide. A causa pode ser doença obstrutiva, de etiologia congênita, tumoral ou por corpo estranho; ou não obstrutiva, como asma, aspergilose broncopulmonar alérgica ou fibrose cística. Na radiografia aparece como uma opacidade alongada, com morfologia ramificada, mais evidente nas regiões centrais do pulmão. Em TC e RM a broncocele apresenta-se como uma imagem alongada de morfologia cilíndrica, podendo apresentar aspecto ramificado em Y ou V (Figura S3 e Figura 5). Tal aspecto muitas vezes configura imagem de "dedo

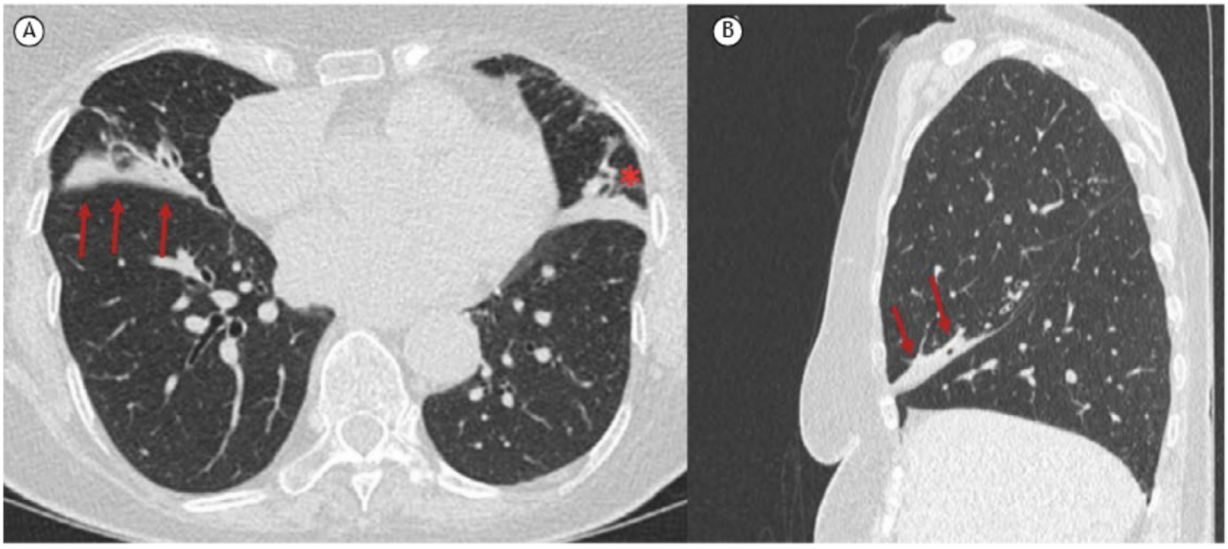

Figura 2. Em A, imagem axial de TC em janela de pulmão revelando atelectasia do lobo médio direito (setas) e da língula (asterisco) onde se observa, no plano coronal (em B), ligeiro desvio da fissura obliqua, brônquios e vasos adjacentes (setas).

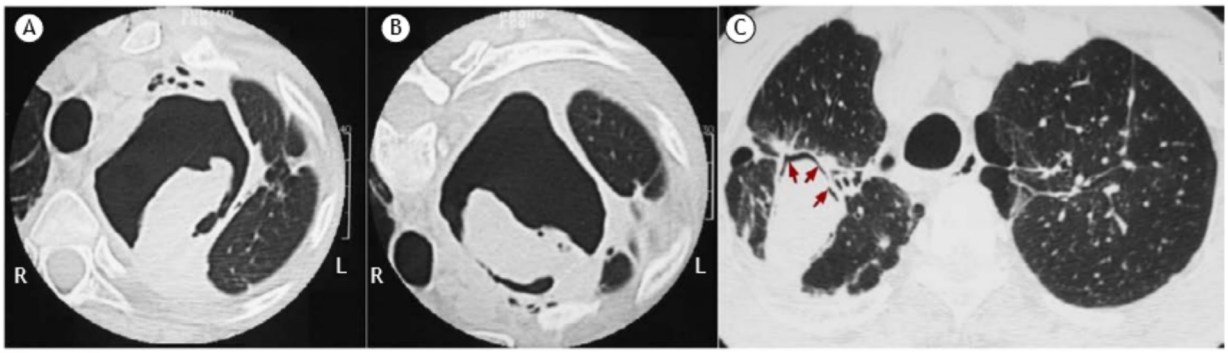

Figura 3. Imagens axiais de TC em janela de pulmão com paciente em decúbito dorsal (A) e decúbito ventral (B) mostrando mobilidade da bola fúngica no interior de cavidade no lobo superior esquerdo. Em C, sinal do crescente aéreo (setas) em cavidade com bola fúngica no lobo superior direito.

de luva". Na TC, a hipoatenuação do parênquima pulmonar distal à alteração, principalmente nos casos de atresia brônquica devida à redução da ventilação e perfusão, e o aumento da atenuação do conteúdo da broncocele, que pode ser um indicativo de aspergilose broncopulmonar alérgica, podem estar associados.[9]

BRONCOGRAMA AÉREO

O broncograma aéreo é uma imagem aérea de aspecto ramificado no interior de uma área com aumento da atenuação do parênquima pulmonar, refletindo estruturas brônquicas aeradas em regiões com ausência de ar alveolar, ou seja, com preenchimento do espaço aéreo (consolidação) ou absorção do ar (atelectasia).

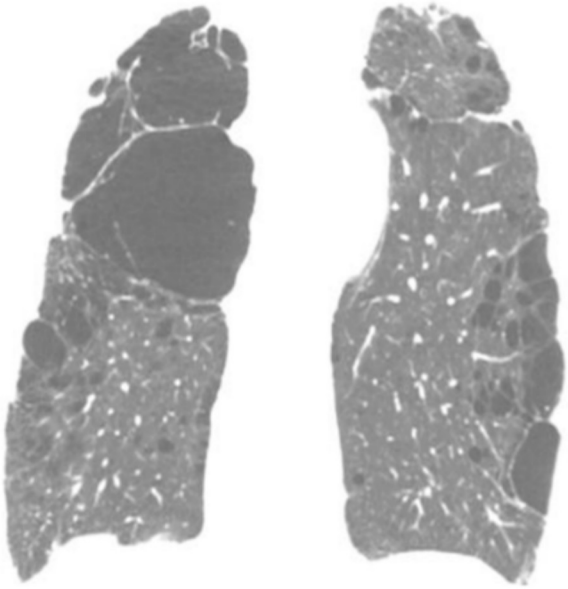

Figura 4. Imagem coronal de TC em janela de pulmão de paciente com enfisema centrolobular e parasseptal que apresenta várias bolhas, sendo as maiores no ápice pulmonar direito.

Na radiografia aparece como uma imagem aérea ramificada no interior de opacidades. Quando observado na radiografia, o broncograma aéreo é indicativo de que a alteração se localiza no parênquima pulmonar. Em TC e RM o broncograma aéreo corresponde a imagem brônquica aerada no interior de uma consolidação ou atelectasia do parênquima pulmonar (Figura 6). Quando associado a atelectasias, o broncograma aéreo pode indicar ausência de obstrução de vias aéreas proximais. Eventualmente podem ser observados em adenocarcinomas e linfomas pulmonares.[10]

BRONCOLITO

O broncolito é patologicamente definido como material calcificado ou ossificado no interior da árvore traqueobrônquica. A TC é superior à radiografia e à RM para o diagnóstico. O aspecto típico é de uma imagem calcificada junto à parede brônquica ou no interior do brônquio e sem componente de partes moles, o que o distingue de outras lesões como hamartoma ou tumor carcinoide (Figura S4). Os broncolitos são mais comuns nos brônquios do lobo superior direito e do lobo médio e podem causar atelectasias, aprisionamento aéreo e bronquiectasias devido à obstrução brônquica.[11]

BRONQUIECTASIA

Esta entidade é patologicamente definida como uma dilatação brônquica irreversível, focal ou difusa, geralmente secundária à inflamação e/ou infecção, obstrução brônquica ou anomalia congênita. Na radiografia os achados podem ser inespecíficos e incluem opacidades lineares e/ou reticulares, espessamento de paredes brônquicas ou mesmo a visualização da dilatação brônquica. Na TC o diagnóstico é realizado quando o diâmetro interno do brônquio é maior do que o da artéria pulmonar adjacente (sinal do anel de sinete), quando há perda do afilamento gradual do

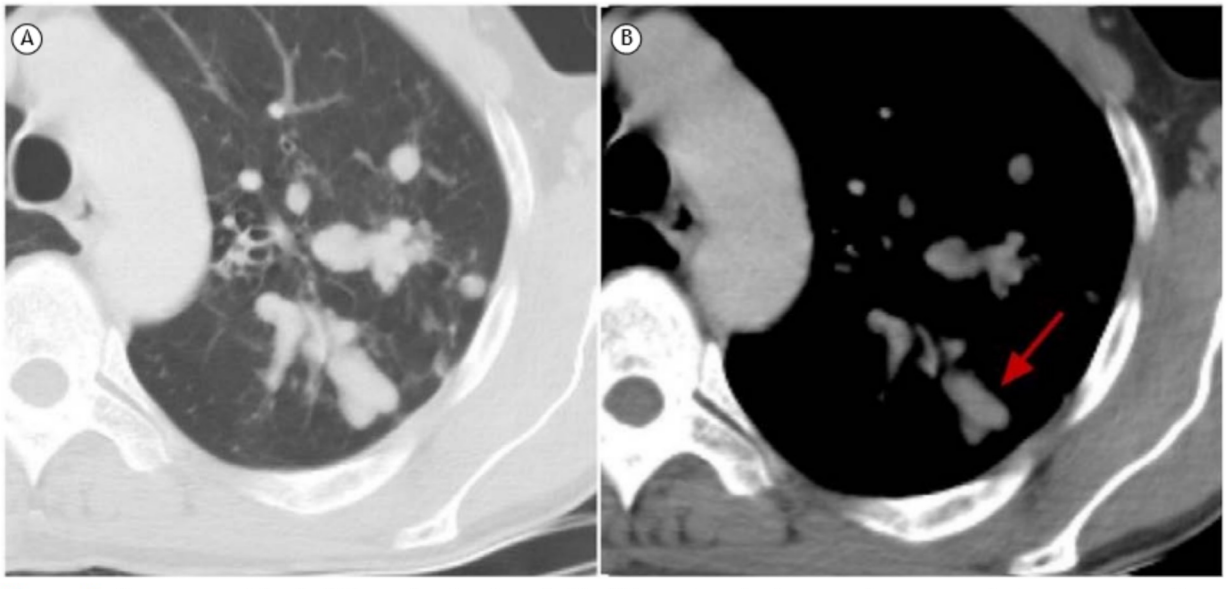

Figura 5. Imagens axiais de TC em janela de pulmão (A) mostrando broncoceles em paciente com aspergilose broncopulmonar alérgica (ABPA) e, em janela de mediastino (B), mostrando conteúdo com atenuação aumentada (seta vermelha) no interior da broncocele, o que sugeriu o diagnóstico de ABPA.

brônquio, definido como a manutenção do seu calibre por mais que 2 cm distalmente à bifurcação brônquica (aspecto de trilho de trem) e quando há a identificação de vias aéreas a menos de 1 cm da superfície pleural (Figura 7). A RM também pode detectar os mesmos achados de dilatação brônquica descritos na TC mas com menor acurácia. As bronquiectasias são classificadas morfologicamente em cilíndricas, quando apresentam uma dilatação uniforme do brônquio; varicosas, quando apresentam uma dilatação brônquica irregular, alternando áreas de maior e menor calibre; e císticas, quando apresentam uma grande dilatação focal, formando cistos.[12,13]

BRONQUIOLECTASIA

A bronquiolectasia é patologicamente definida como uma dilatação dos bronquíolos, originária tanto de atividade inflamatória (portanto, potencialmente reversível) ou mais frequentemente em decorrência de fibrose; nesse caso é denominada "bronquiolectasia de tração". Os bronquíolos diferem dos brônquios por não possuírem cartilagem ou glândulas nas suas paredes. Os bronquíolos maiores têm diâmetro entre 0,8 e 1,0 mm, reduzindo-se progressivamente até o nível dos bronquíolos respiratórios (os mais distais, que apresentam sacos alveolares nas suas paredes)

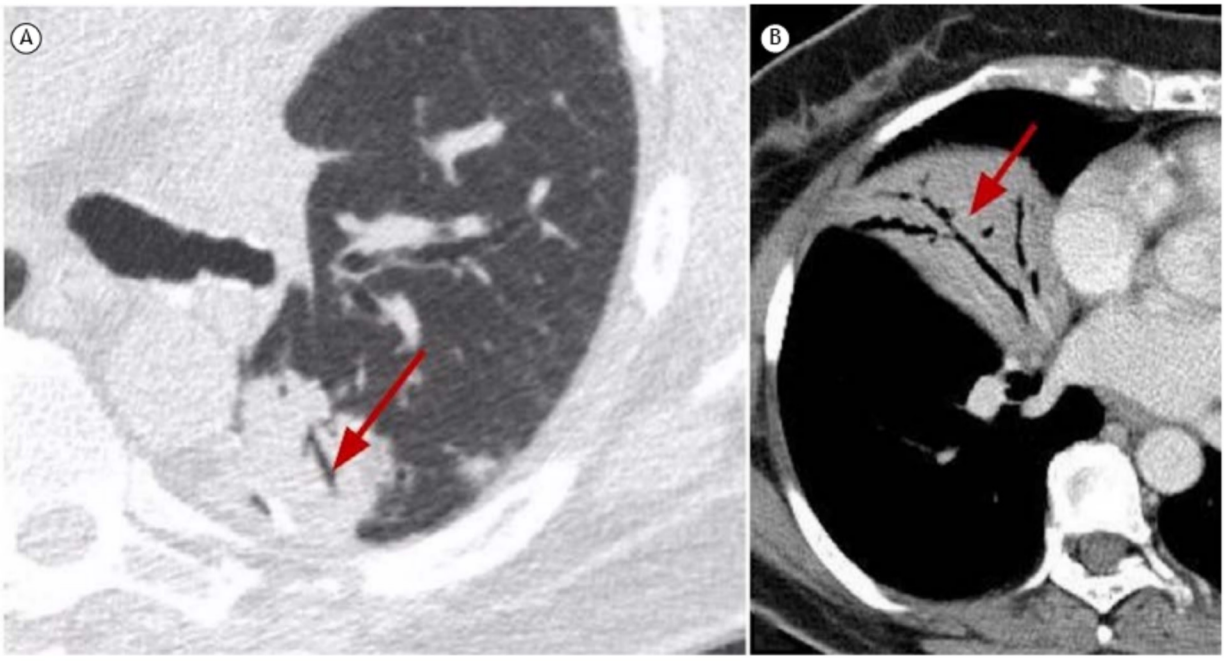

Figura 6. Imagens axiais de TC em janela de pulmão (A) revelando broncograma aéreo (seta) em foco de consolidação no lobo inferior esquerdo e, em janela de mediastino (B), mostrando broncograma aéreo (seta) em consolidação no lobo médio.

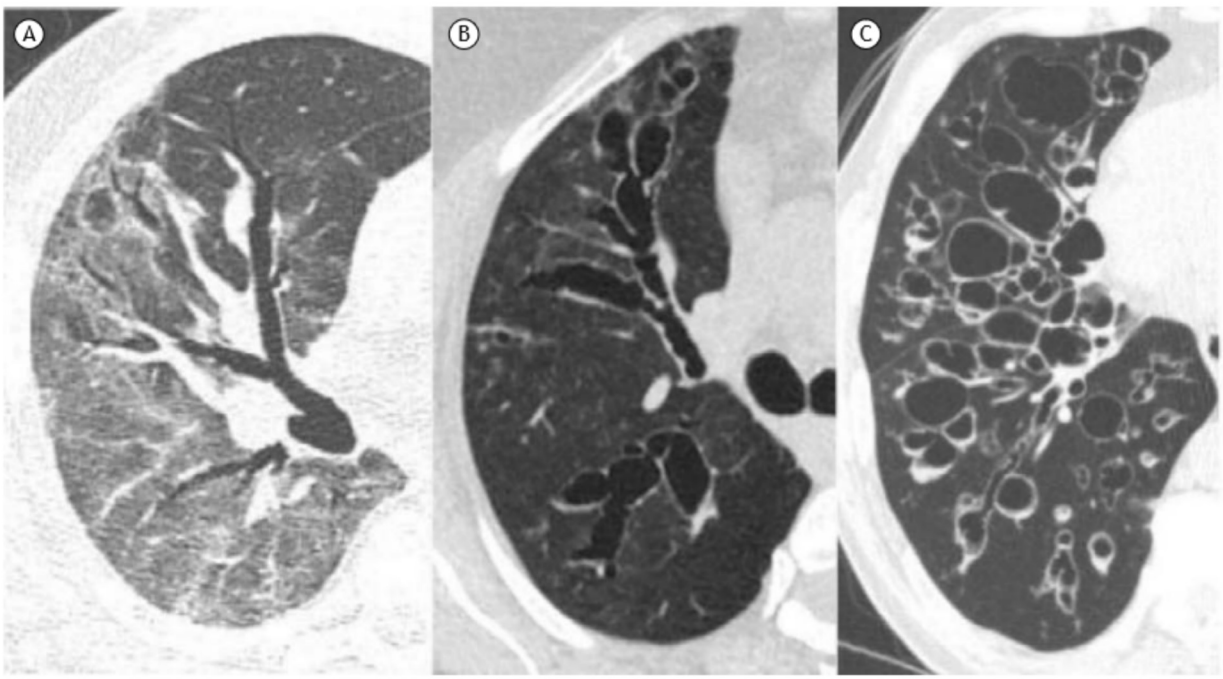

Figura 7. Imagens axiais de TC em janela de pulmão, mostrando bronquiectasias cilíndricas (A), varicosas (B) e císticas (C).

cujo diâmetro varia entre 0,4 e 0,5 mm.[4,12,13] Os bronquíolos normais não são vistos à TCAR, cujo limite de resolução permite ver brônquios com até 2-3 mm de calibre.[14]. Quando dilatados e com secreção, os bronquíolos podem ser vistos como nódulos centrolobulares ou como "árvore em brotamento". As bronquiolectasias de tração aparecem como pequenos espaços aéreos císticos ou tubulares rodeados por fibrose (Figura S5).[1,14-16]

As bronquiolectasias de tração são de difícil caracterização na radiografia e, quando isso ocorre, são geralmente observadas na periferia das bases pulmonares. Na TC as bronquiectasias de tração apresentam-se como uma imagem brônquica dilatada, de aspecto tubular, cístico ou arredondado, dependendo do eixo da imagem. As bronquiolectasias de tração são predominantemente periféricas (justapleurais), de menor calibre e relacionadas a alterações intersticiais pulmonares fibrosantes (Figura S6). Na RM as bronquiolectasias de tração raramente são caracterizadas e, quando evidentes, apresentam-se como estruturas tubulares de hipossinal associadas a áreas de distorção arquitetural do parênquima pulmonar.

CAVIDADE

A cavidade é patologicamente definida como um espaço preenchido por gás, visível como transparência ou baixa atenuação no interior de uma massa, consolidação ou nódulo.[1,2] Na radiografia, TC e RM a cavidade é um espaço aéreo, medindo mais de 1 cm de diâmetro (podendo apresentar vários centímetros) e demarcado por uma parede espessa maior > 2 mm de espessura (Figura S7).[15]

CISTO OU QUISTO (PT)

A descrição patológica de cisto é de um espaço arredondado, bem circunscrito, que é circundado por uma parede epitelizada ou fibrosa, de espessura variável.[17,18] Na radiografia de tórax a identificação de cistos é pouco frequente e muitas vezes duvidosa.[17,18] Na TC caracteriza-se por uma área arredondada de baixo coeficiente de atenuação no parênquima pulmonar com uma interface bem definida com o pulmão normal adjacente (Figura 8).[17,18] A espessura da parede do cisto é fina e não maior que 2 mm. A RM é utilizada para o estudo das lesões císticas não aéreas de mediastino e tórax, tendo um papel interessante no seu diagnóstico diferencial e na determinação de componente hemorrágico e componente de gordura. Os cistos geralmente contêm ar, mas, ocasionalmente, podem conter líquido (por exemplo, cisto broncogênico) ou mesmo algum material sólido. Cistos aéreos pulmonares isolados são achados incidentais comuns e aumentam com a idade.[17,18] A presença de cinco cistos pulmonares ou mais é utilizada como critério para a investigação de doenças pulmonares císticas.[5] As doenças pulmonares císticas cursam geralmente com múltiplos cistos pulmonares, frequentemente com aumento do volume pulmonar, e incluem linfangioliomiomatose, histiocitose de células de Langerhans, pneumonia intersticial linfocítica e síndrome de Birt-Hogg-Dubé.[17,18] Entretanto, existem doenças pulmonares fibrosantes que desenvolvem cistos, a exemplo dos cistos de faveolamento/favo de mel. Vide "Faveolamento".

DISTORÇÃO ARQUITETURAL

A distorção arquitetural do parênquima pulmonar corresponde patologicamente à disposição anormal e desorganizada de brônquios, vasos, fissuras ou septos e está relacionada com doenças localizadas ou difusas, particularmente associadas à fibrose e com perda de volume.[1,2] Esse termo pode ser descrito em laudos de radiografia, TC e RM em regiões onde há uma desorganização anatômica extensa que dificulta o reconhecimento anatômico exato das estruturas (Figura S8).

ENFISEMA

O enfisema é caracterizado patologicamente pelo alargamento anormal e permanente dos espaços aéreos distais ao bronquíolo terminal com destruição das suas paredes, sem fibrose bem definida. O critério histológico adicional de "ausência de fibrose óbvia" tem sido questionado porque algum grau de fibrose intersticial pode estar presente em consequência do tabagismo. A classificação patológica do enfisema é tradicionalmente baseada na localização microscópica da doença em relação ao ácino ou ao lóbulo secundário. Os principais tipos são enfisema centroacinar ou centrolobular, parasseptal ou acinar distal e panacinar ou panlobular.[1,18-31] Os achados tomográficos são de áreas de baixa atenuação, tipicamente sem paredes visíveis.[2]

ENFISEMA BOLHOSO

O enfisema bolhoso não representa uma entidade histológica específica, mas indica um enfisema caracterizado primariamente pela presença de uma grande bolha. Frequentemente é associado a enfisema centrolobular e parasseptal (Figura S9).[18] Denomina-se enfisema bolhoso gigante quando as bolhas ocupam pelo menos um terço do hemitórax e localizam-se assimetricamente nos lobos superiores, podendo variar de 1 a mais de 20 cm de diâmetro.[19] Na TC a bolha é caracterizada como área focal hipodensa, medindo 1 cm ou mais de diâmetro, delimitada por parede fina, que não ultrapassa 1 mm de espessura. Geralmente tem conteúdo gasoso, mas pode ocasionalmente ter nível líquido.[1] Bolhas menores que 1 cm e localizadas na pleura visceral ou na região pulmonar subpleural são denominadas *blebs* na língua inglesa. As *blebs* ou vesículas de localização apical são frequentemente responsáveis pelo pneumotórax espontâneo primário.[20]

ENFISEMA CENTROLOBULAR/CENTROACINAR

Esse tipo de enfisema corresponde patologicamente à dilatação seletiva de elementos da porção central do

ácino, particularmente dos bronquíolos respiratórios e dos alvéolos correspondentes. O processo é mais desenvolvido nos lobos superiores e na região superior dos lobos inferiores, sendo fortemente associado com tabagismo e bronquite crônica. As alterações inflamatórias nas pequenas vias aéreas são comuns, com tamponamento, infiltração parietal e fibrose, que causam estenose e bloqueio do fluxo aéreo, além de distorção e destruição da anatomia do centro do ácino.[21-23] A TC demonstra múltiplos pequenos focos parenquimatosos arredondados de reduzida atenuação em localização centrolobular, sem paredes definidas (Figura 9). Uma delgada orla opaca pode ser reconhecida na transição entre a área enfisematosa e o pulmão normal devido à compressão do parênquima adjacente pelo espaço aéreo dilatado. As artérias centrolobulares podem frequentemente ser identificadas no interior das áreas hipodensas.[22] Os achados de enfisema centrolobular na radiografia e RM são apenas indiretos, demonstrando aumento do volume pulmonar, sem achados diagnósticos seguros.

ENFISEMA INTERSTICIAL

O enfisema intersticial é a dissecção do interstício pulmonar por ar, podendo ser espontâneo ou traumático. É mais frequentemente identificado em neonatos submetidos à ventilação mecânica.[24] Nas radiografias do tórax, é raramente identificado e pode apresentar-se como formações de aspecto cístico intrapulmonares ou subpleurais, imagens radiolucentes lineares que se estendem ao mediastino e halo perivascular decorrente das coleções aéreas.[22] Na TC apresenta-se por coleções aéreas focais, difusas, uni ou bilaterais, que podem simular cistos ou bolhas, localizadas ao longo do interstício adjacente aos vasos, brônquios e septos interlobulares (Figura S10).[25,26] Os achados de enfisema intersticial na radiografia e RM são inespecíficos, sem achados diagnósticos seguros.

ENFISEMA PANACINAR OU PANLOBULAR

O enfisema panacinar é caracterizado patologicamente pelo alargamento de espaços aéreos do ácino pulmonar,

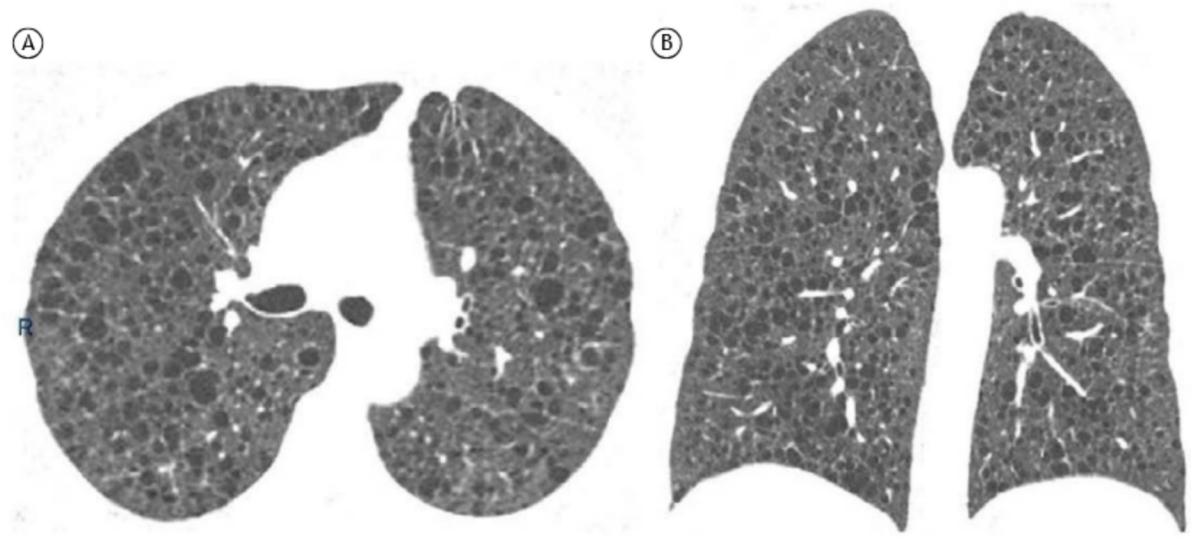

Figura 8. Imagens de TC em janela de pulmão no plano axial (A) e no plano coronal (B) revelando múltiplos cistos pulmonares em uma paciente com linfangioliomiomatose.

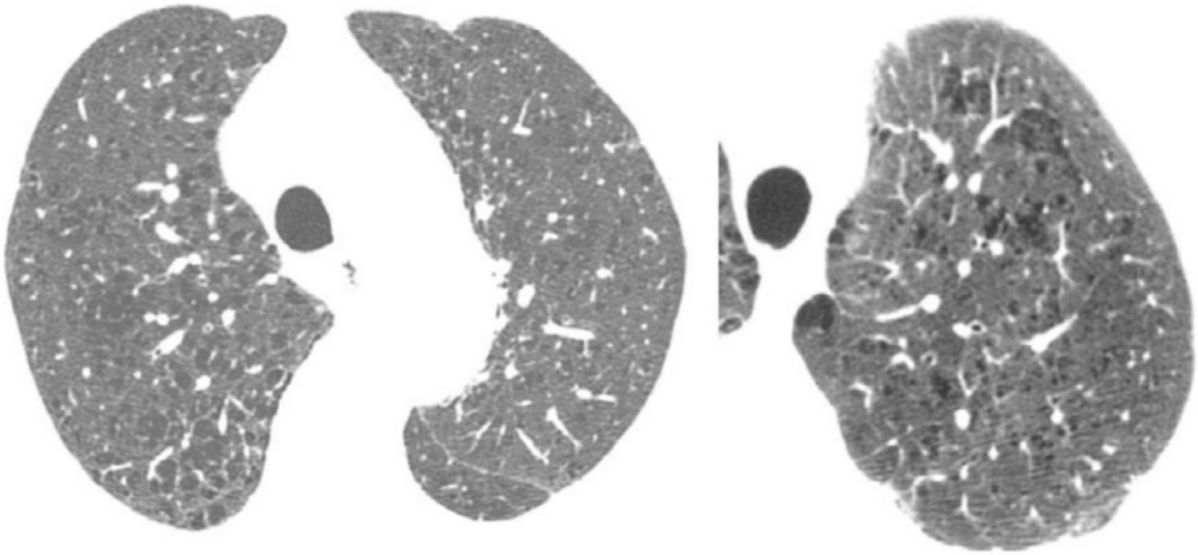

Figura 9. Imagens axiais de TC em janela de pulmão revelando enfisema centrolobular nos lobos superiores em paciente com hábitos tabágicos.

comprometendo as estruturas desde os bronquíolos respiratórios até os alvéolos. De modo mais ou menos uniforme todos os elementos do lóbulo secundário são comprometidos.[23] A deficiência de alfa-1-antitripsina está associada a esse tipo de enfisema. O enfisema panacinar pode ser encontrado em fumantes, associado a enfisema centrolobular, bem como em usuários de drogas endovenosas (efeito crônico) e em volta de broncoceles na atresia brônquica. As radiografias de tórax podem ser normais nas fases mais precoces da doença. Nas formas mais avançadas há distorção e rarefação vascular. Outros achados incluem retificação do diafragma e aumento do diâmetro anteroposterior do tórax e do espaço retroesternal.[27] Na TC as lesões são homogeneamente distribuídas com predomínio em lobos inferiores e caracterizam-se por redução difusa da atenuação do parênquima pulmonar com rarefação vascular nas áreas afetadas (Figura S11). Podem também ser encontradas bronquiectasias. Pode ser difícil a diferenciação entre áreas onde o parênquima pulmonar é normal e onde há enfisema. O enfisema panacinar é indistinguível da bronquiolite obliterante (constritiva).[28] Os achados de enfisema na RM são apenas indiretos, demonstrando aumento do volume pulmonar, sem achados diagnósticos seguros.

ENFISEMA PARASSEPTAL OU ACINAR DISTAL

Nesse tipo de enfisema há patologicamente um alargamento permanente do ácino distal com destruição de ductos e sacos alveolares com alvéolos dilatados em localização subpleural junto aos septos interlobulares.[29] Nas radiografias do tórax o enfisema parasseptal é de difícil detecção nas formas menos graves. Imagens radiolucentes com paredes finas podem ser vistas na periferia dos pulmões.[27] Na TC são vistas formações císticas subpleurais e peribroncovasculares eventualmente separadas por septos interlobulares intactos. As porções anteriores e posteriores dos lobos superiores e as porções posteriores dos lobos inferiores são mais frequentemente afetadas. Bolhas podem estar associadas a essa forma de enfisema (Figura S12). O uso de reconstruções com projeção de intensidade mínima facilita a detecção das lesões.[30] Os achados de enfisema parasseptal na RM são apenas indiretos, demonstrando aumento do volume pulmonar, sem achados diagnósticos seguros.

ESPAÇOS AÉREOS

O termo "espaço aéreo" é uma descrição genérica que se refere à parte aerada dos pulmões onde há troca gasosa, ou seja, os bronquíolos respiratórios, ductos alveolares e alvéolos. É excluída dessa denominação a parte exclusivamente condutora das vias aéreas, desde a traqueia até o bronquíolo terminal. Os espaços aéreos representam a maior parte de um pulmão normal. Normalmente esse termo é usado em conjunto com patologias que ocupam e substituem o conteúdo gasoso do pulmão por produtos patológicos, sejam células ou líquido. Patologias pulmonares diversas ocupam o espaço aéreo de uma maneira uniforme ou preservando focos de pulmão aerado no interior da lesão.[2,32] Na radiografia a presença de broncogramas aéreos pode indicar o preenchimento do espaço aéreo ao redor do brônquio. Na TC lesões como consolidações, massas e nódulos comprometem vários compartimentos pulmonares, inclusive o espaço aéreo. Na maioria das vezes o termo "espaço aéreo" é usado referindo-se à substituição do mesmo por produto patológico ou quando há pulmão aerado no interior dessas lesões (Figura S13). É importante a diferenciação com escavação, onde não há conteúdo gasoso sem parênquima pulmonar.[1,2,32] Vide "Cavidade".

ESPESSAMENTO DE SEPTOS INTERLOBULARES

Os septos interlobulares anatomicamente fazem parte do esqueleto intersticial pulmonar periférico, delimitam um lóbulo pulmonar secundário e são compostos por tecido conectivo, veias e vasos linfáticos. Usualmente não são visualizados em exames de imagem em pessoas saudáveis. Quando espessados, são caracterizados na radiografia como finas opacidades lineares periféricas, perpendiculares à superfície pleural e mais facilmente visualizados nas regiões laterais das bases pulmonares. São também chamados de linhas B de Kerley.[1,2,32] Na TC e RM são caracterizados por opacidades lineares periféricas/subpleurais perpendiculares à superfície pleural, distando aproximadamente 1,0-2,5 cm entre si. Quando há espessamento de septos de vários lóbulos pulmonares secundários contíguos, esses podem tomar um aspecto de arcadas poligonais (Figura 10).[4,18,30]

FAVEOLAMENTO OU FAVO DE MEL (PT)

O achado de faveolamento é anatomopatologicamente representado por ácinos dilatados por fibrose formando imagens císticas devido ao colapso de outros ácinos periféricos. Esses cistos apresentam-se com paredes espessas fibrosas com epitélio brônquico metaplásico

Figura 10. Imagem axial de TC em janela de pulmão revelando espessamento difuso de septos interlobulares, formando arcadas poligonais.

adjacente. Na TC é definido como um agrupamento de imagens cistoides associadas à redução volumétrica pulmonar, de dimensões geralmente subcentimétricas e de localização subpleural. Na RM os achados são semelhantes, mas a acurácia de detecção desse achado é menor que na TC.[18] Apesar de ser representado por múltiplas camadas de cistos na maioria dos casos, a junção de dois a três cistos em meio a outros achados de fibrose já pode caracterizar esse achado.[4,18] O faveolamento representa a fase final de várias doenças com perda completa da arquitetura pulmonar, como pneumonia intersticial usual e sarcoidose (Figura S14).[4,18]

FISSURA

Corresponde anatomicamente à invaginação da pleura visceral que reveste a superfície externa do pulmão, separando um lobo (ou parte de um lobo) de outro. O termo "fissura" é também sinônimo do termo "cissura". Cada fissura interlobar é formada pela aposição de duas camadas de pleura visceral. Em geral, identificam-se as fissuras maiores (oblíquas), que separam os lobos inferiores dos demais, e a fissura menor (horizontal), que separa o lobo médio do lobo superior direito. Fissuras supranumerárias geralmente separam segmentos ao invés de lobos. As fissuras podem ser incompletas. Nos exames de imagem as fissuras podem aparecer como opacidades lineares onde ocorre a separação dos lobos ou segmentos pulmonares.[1,33]

INFILTRADO

É considerado um termo impreciso e inespecífico, frequentemente utilizado para descrever uma região de opacificação pulmonar, identificada em radiografia, RM ou TC, que é causada por doença de vias aéreas ou do interstício. Como apresenta diferentes significados para diversas pessoas, é considerado um termo controverso e não recomendado. Sugerimos que seja substituído pelo termo "opacidade".[34]

INTERFACE

É um termo anatômico definido como o limite entre duas estruturas ou tecidos de diferentes densidades. Quando duas estruturas torácicas com diferentes densidades radiológicas se justapõem, seus limites são nítidos. Em imagem esse termo é utilizado apenas no estudo das doenças intersticiais por TCAR. O sinal da interface é caracterizado pela presença de irregularidades nas bordas de contato entre os pulmões e brônquios, vasos e pleura visceral, sendo sugestivo de espessamento intersticial, geralmente associado a outras alterações, que conjuntamente permitem o diagnóstico.[33,35,36]

INTERSTÍCIO

É um termo de anatomia e consiste na rede de tecido conjuntivo distribuída ao longo dos pulmões, servindo para sua sustentação. Seus componentes são: (a) interstício axial (ou broncovascular), que envolve brônquios, artérias e veias desde os hilos até o nível dos bronquíolos respiratórios; (b) interstício periférico, que é o tecido conjuntivo contíguo às superfícies pleurais (subpleural) e septos interlobulares; e (c) interstício intralobular (também chamado acinar ou parenquimatoso), que é uma rede de fibras finas interposta entre as paredes dos alvéolos e dos septos alveolares.[1,36] Nos métodos de imagem não é identificado em pacientes sadios.

LINHA CURVILÍNEA SUBPLEURAL

Corresponde à compressão passiva pulmonar fisiológica na porção pendente do pulmão (por exemplo, na superfície posterior em pacientes em decúbito dorsal), que é revertido após a mudança de decúbito. Pode também ser encontrada em casos de edema pulmonar ou fibrose (Figura S15).[1] É um termo imagético demonstrado em TC e RM e representado como uma opacidade curvilínea de 1-3 mm de espessura, normalmente a menos de 1 cm da superfície pleural, com distribuição paralela a essa.

LÓBULO PULMONAR SECUNDÁRIO

É um termo anatômico definido como a menor unidade anatômica pulmonar, delimitada por septos de tecido conjuntivo denominados septos interlobulares. Apresenta aspecto poliédrico, mede de 1,0-2,5 cm de diâmetro e contém um número variado de ácinos. O centro do lóbulo é formado pelo conjunto de bronquíolo, arteríola pulmonar e vasos linfáticos, com interstício circunjacente. Nos septos interlobulares encontram-se pequenas veias pulmonares e vasos linfáticos (Figura 10).[37,38] Não é identificado nos estudos de imagem em seu aspecto normal.

MASSA

Massa é um termo imagético definido como qualquer lesão expansiva pulmonar, pleural, mediastinal ou da parede torácica, com densidade de partes moles, de gordura ou de cálcio, maior que 3 cm, com contornos pelo menos parcialmente definidos, independentemente das características de seus contornos ou da heterogeneidade de seu conteúdo.[1,39] O termo pode ser aplicado em radiografia, TC e RM. As massas pulmonares (Figura 11) frequentemente estão relacionadas a lesões neoplásicas, primárias ou metastáticas; contudo, podem também representar lesões inflamatórias, como pseudotumores e pneumonia em organização (PO), ou infecciosas, como tuberculomas ou criptococomas, por exemplo.[40] Massas mediastinais podem ser classificadas quanto a sua origem no mediastino anterior (pré-vascular), médio (visceral) ou posterior (paravertebral) para aumentar a acurácia do diagnóstico diferencial.[41]

MICETOMA

Micetoma caracteristicamente representa um grupo de infecções crônicas subcutâneas causadas pela

inoculação traumática na pele de material contaminado com actinomicetos, principalmente espécies dos gêneros *Nocardia, Streptomyces* e *Actinomadura*, ou fungos verdadeiros (eumicetos), incluindo os gêneros *Acremonium, Fusarium, Leptosphaeria* e *Madurella*, resultando em actinomicetomas e eumicetomas, respectivamente.[42,43] Apresenta tendência a invadir os tecidos adjacentes, formando nódulos ou massas com cavidades e trajetos fistulosos, com eliminação de secreção purulenta contendo grãos constituídos por novelos de hifas e filamentos. Na maioria dos casos, localiza-se nos membros inferiores, podendo levar a deformidades e fraturas. O acometimento pulmonar e pleural é raro.[42] Quando invadem o pulmão, têm o aspecto de consolidação com necrose, e derrame pleural pode ser identificado.[43] Geralmente acometem agricultores, sendo endêmicos na América Latina, Índia e África.[42-46] O micetoma não representa uma colonização de cavidade pulmonar preexistente; portanto, a utilização desse termo como sinônimo de "bola fúngica" deve ser evitada. Vide "Bola fúngica".

NÓDULO

Nódulo é definido como uma opacidade focal aproximadamente arredondada, ou pelo menos parcialmente delimitada, com densidade de partes moles, gordura ou cálcio e medindo até 3 cm de diâmetro (a partir de 3 cm deve-se empregar o termo "massa"; Figura 12).[1,41] O termo pode ser aplicado em radiografia, TC e RM. Sugere-se a denominação de "pequeno nódulo" a medida de até 10 mm do diâmetro médio (média dos dois maiores diâmetros perpendiculares entre si, preferencialmente no plano axial) ou do diâmetro em outro plano ortogonal caso o nódulo seja maior no sentido longitudinal. Nódulos com mais de 10 mm devem ter o seu maior e menor diâmetro ortogonal descritos. Nódulos com menos de 3 mm não precisam ter suas dimensões descritas, podendo ser chamados de micronódulos.[47,48] Podem ser divididos em nódulos sólidos, quando obscurecem completamente os contornos de vasos e de paredes brônquicas (Figura 12); nódulos com atenuação pura em vidro fosco, quando não obscurecem as margens vasculares e as paredes brônquicas (Figura 12); e nódulos parcialmente sólidos, quando há áreas com atenuação de partes moles e outras com atenuação em vidro fosco (Figura 12).[47] Os nódulos devem, ainda, ser descritos quanto às suas margens, morfologia e localização. Nódulos perifissurais e com morfologia alongada ou poligonal, por exemplo, indicam benignidade (linfonodos pulmonares).[48] Quando múltiplos, os nódulos devem ser classificados quanto a sua distribuição (padrão nodular randômico, padrão nodular perilinfático e padrão nodular centrolobular, este último com ou sem padrão de árvore em brotamento). Vide "Massa", "Padrão nodular centrolobular", "Padrão nodular", "Padrão miliar" e "Padrão de árvore em brotamento".

OLIGOEMIA

Oligoemia é um termo que representa redução focal, regional ou generalizada, do volume sanguíneo pulmonar. A oligoemia é demonstrada em TC e RM mas dificilmente em radiografia. Apresenta-se como uma diminuição do calibre e do número de vasos pulmonares em regiões específicas ou difusamente, indicando que o fluxo sanguíneo é menor que o habitual (Figura S16).[1,2] Ocasionalmente as áreas de maior perfusão pulmonar podem simular aspecto de opacidade em vidro fosco, devendo se notar que há redução no número e calibre dos vasos nas regiões de maior transparência dos pulmões para se fazer o diagnóstico diferencial (Figura S17) [49-51]

OPACIDADE

Opacidade é um termo genérico para descrever uma imagem que se distingue, pelo menos parcialmente, das estruturas que a circundam ou se superpõem, por

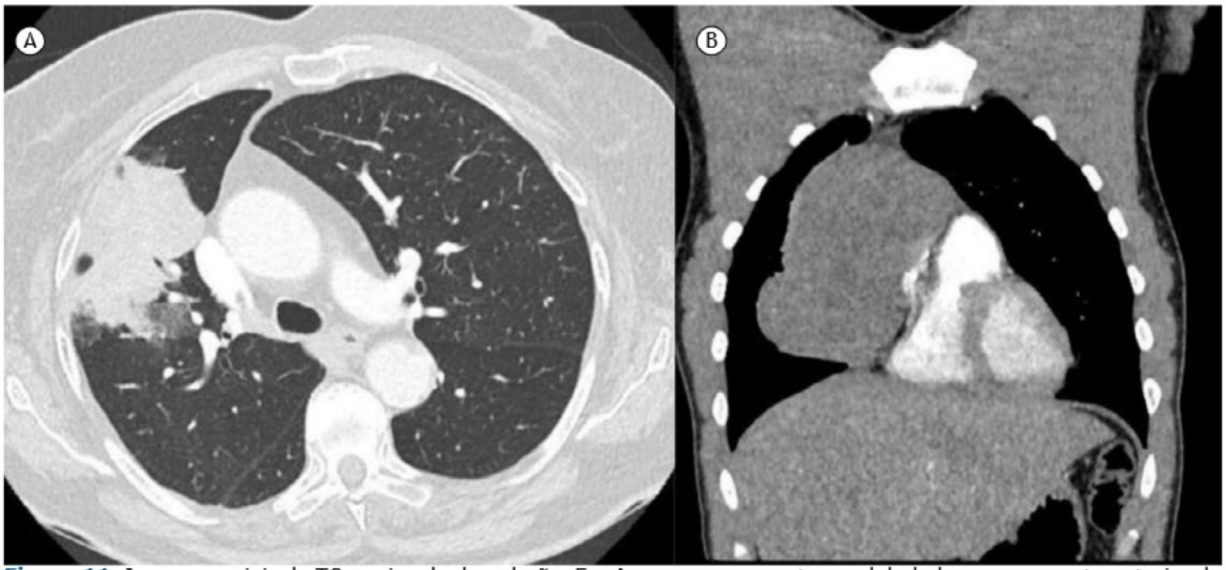

Figura 11. Imagens axiais de TC em janela de pulmão. Em A, massa com contornos lobulados no segmento anterior do lobo superior do pulmão direito em paciente com adenocarcinoma de pulmão Em B, massa no compartimento mediastinal anterior (pré-vascular), com atenuação de partes moles, em paciente com seminoma mediastinal.

apresentar maior densidade. Na radiografia do tórax esse termo não implica sua natureza do ponto de vista patológico, de seu tamanho ou de localização específica, podendo ser de origem pulmonar, pleural, da parede torácica ou de origem externa ao paciente. Na TC as opacidades pulmonares podem obscurecer totalmente as estruturas vasculares e paredes brônquicas (como na consolidação, nos nódulos sólidos e nas massas) ou podem ter atenuação em vidro fosco (quando as estruturas vasculares e paredes brônquicas permanecem visíveis).[1,2] Esse termo não é recomendado na RM. O termo "opacidade" tem algumas derivações que merecem ser discutidas. Vide "Consolidação", "Opacidade em vidro fosco" e "Massa".

OPACIDADE EM VIDRO FOSCO OU DESPOLIDO (PT)

A definição de opacidade em vidro fosco ou despolido corresponde ao aumento da densidade pulmonar (opacidade) em atenuação sem obscurecer as estruturas vasculares no seu interior.

Na radiografia de tórax apresenta-se como opacidade pulmonar mal definida, de baixa densidade, dentro da qual as margens dos vasos pulmonares podem ser indistintas. A grande sobreposição de estruturas na radiografia pode levar à interpretação inadequada desse achado, devendo-se, portanto, evitar o uso desse termo. Na TC corresponde ao aumento da densidade do parênquima pulmonar com preservação dos contornos dos vasos e brônquios (Figura 13). Pode representar espessamento intersticial, preenchimento parcial dos espaços aéreos (devido a líquido, células e/ou fibrose), colapso parcial de alvéolos, aumento do volume sanguíneo capilar ou ainda uma combinação desses mecanismos.[52,53]

A opacidade em vidro fosco é menos densa e deve ser distinguida da consolidação, na qual os vasos não são identificáveis no interior da área de pulmão comprometido (vide "Consolidação"). Quando a opacidade em vidro fosco é superposta por linhas intralobulares e septos interlobulares espessados, configura o padrão de pavimentação em mosaico ou *crazy paving* (vide "Pavimentação em mosaico"). Quando assume morfologia arredondada/nodular, pode ser chamada de nódulo subssólido, que inclui nódulos puramente em vidro fosco, ou seja, não sólidos (Figura 13), ou semissólidos, quando exibem componente com densidade de partes moles de permeio.

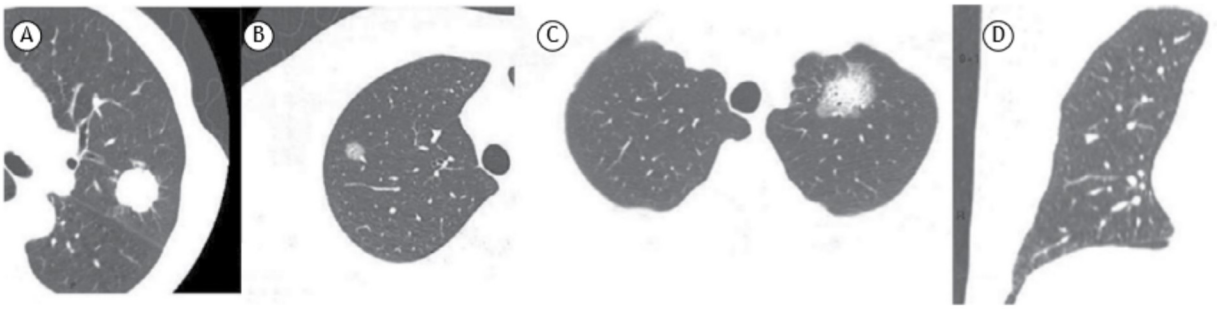

Figura 12. Imagens axiais de TC em janela de pulmão. Em A, nódulo sólido com contornos lobulados e espiculados no segmento apicoposterior do lobo superior do pulmão esquerdo. Em B, nódulo com atenuação pura em vidro fosco no segmento apical do lobo superior do pulmão direito. Em C, nódulo com atenuação mista (parcialmente sólido e parcialmente em vidro fosco) no lobo superior do pulmão esquerdo. Em D, nódulo perifissural e morfologia poligonal junto da cissura horizontal do pulmão direito (linfonodo pulmonar).

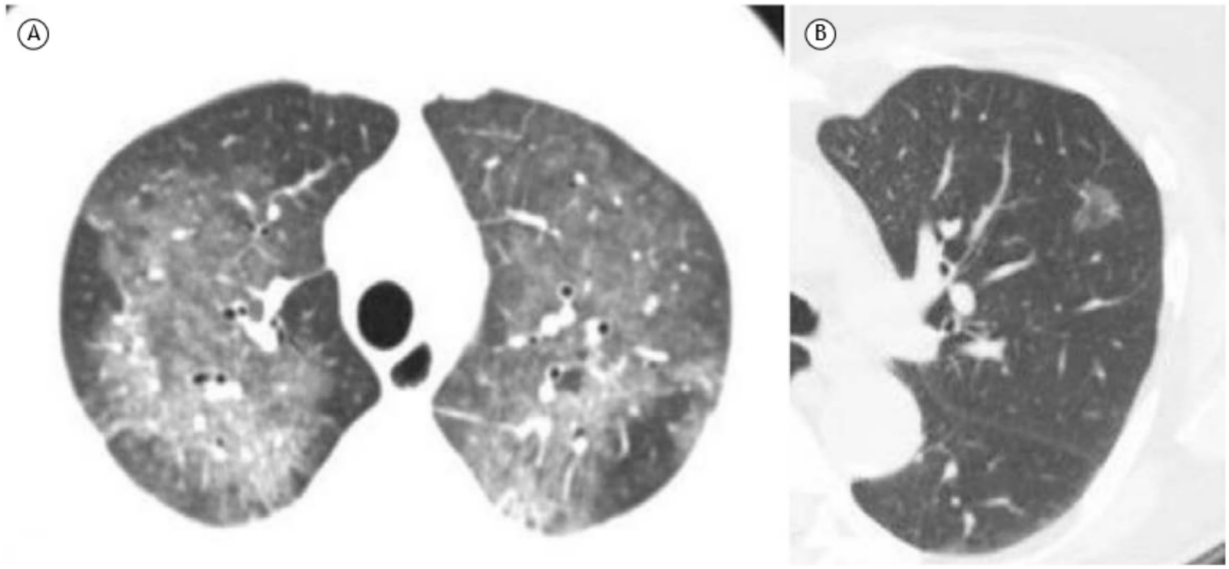

Figura 13. Imagens axiais de TC em janela de pulmão demonstrando opacidades em vidro fosco em ambos os pulmões, de distribuição predominantemente central em paciente com edema pulmonar (A) e revelando um nódulo com atenuação em vidro fosco (subssólido) que foi diagnosticado como adenocarcinoma de crescimento lepídico (B).

Na RM a opacidade em vidro fosco apresenta-se com aumento de sinal nas imagens em T2, o que é comumente observado nos processos patológicos, e tem alta correlação com a TC.[1]

OPACIDADE LINEAR

Na radiografia e TC, representa uma imagem linear fina e alongada de maior densidade em relação ao parênquima pulmonar (maior atenuação ao feixe de raios X), com etiologias diversas. Recomenda-se, sempre que possível, o uso de termos mais específicos como "bandas parenquimatosas", "atelectasias lineares" ou "espessamento de septos interlobulares" (Figura S18).[2]

OPACIDADE PARENQUIMATOSA OU OPACIFICAÇÃO PARENQUIMATOSA

Na radiografia e TC esse tipo de opacidade representa qualquer área de maior atenuação ao feixe de raios X em relação ao parênquima pulmonar. O aumento da atenuação do parênquima pulmonar pode ou não obscurecer os contornos dos vasos e brônquios (Figura 14). O termo "consolidação" indica a perda da definição das margens dos vasos e brônquios (exceto pelos broncogramas aéreos) no interior da opacidade, enquanto o termo "opacidade em vidro fosco" indica um aumento menor da atenuação do parênquima, que preserva os contornos das estruturas no seu interior.[1,2,54,55]

OPACIDADE PENDENTE

Na radiografia e TC a opacidade pendente representa um aumento da densidade (maior atenuação ao feixe de raios X) do parênquima pulmonar nas regiões subpleurais posteriores (quando em decúbito dorsal) ou anteriores (quando em decúbito ventral), correspondendo a atelectasias relacionadas ao decúbito. Desaparece com a mudança de decúbito (Figura S18).[1,2]

PAVIMENTAÇÃO EM MOSAICO

É um termo específico da TC que representa um padrão misto que associa o espessamento dos septos interlobulares com opacidade intralobular do espaço aéreo na forma de vidro fosco. Aparece em situações que envolvem o interstício e o espaço aéreo. Ocorre em várias patologias como proteinose alveolar, hemorragia alveolar, SDRA ou infecções, como por *Pneumocystis carinii* ou pelo recente SARS-CoV-2 (Figura S19).[56,57]

PADRÃO DE ÁRVORE EM BROTAMENTO OU EM BOTÃO (PT)

O padrão de árvore em brotamento pode ser utilizado em radiografia, TC e RM e corresponde a opacidades/

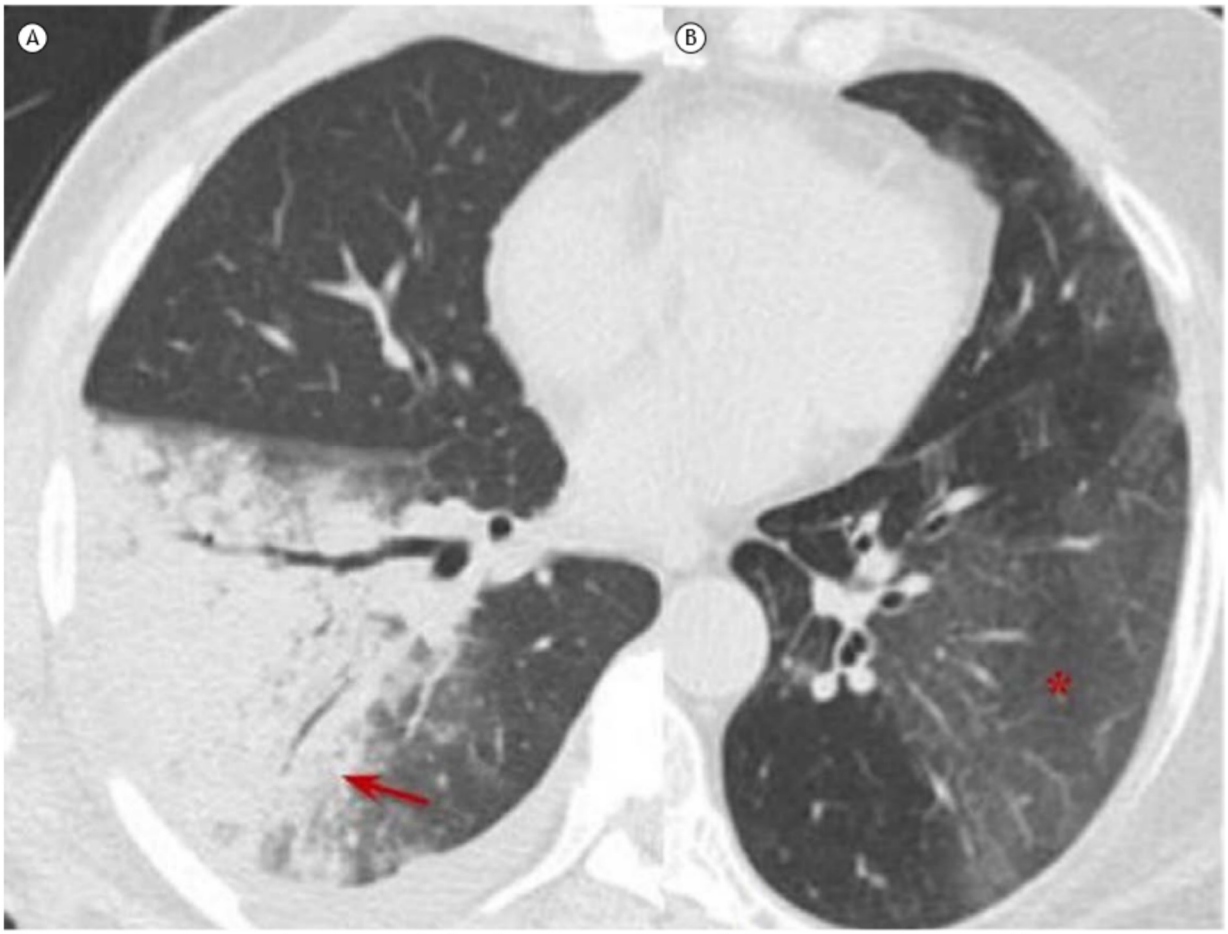

Figura 14. Imagens axiais de TC em janela de pulmão mostrando opacidades parenquimatosas que obliteram os contornos dos vasos e brônquios no lobo inferior direito (seta), indicando consolidação, sendo também visível broncograma aéreo nessa opacidade (A), e opacidades parenquimatosas que preservam os contornos dos vasos e brônquios no lobo inferior esquerdo (asterisco) indicando opacidades em vidro fosco (B).

nódulos ramificados centrolobulares, com pequenas nodularidades nas extremidades, assemelhando-se ao aspecto do brotamento de algumas árvores (Figura 15). Esse padrão decorre do preenchimento das estruturas centrolobulares ramificadas, seja o bronquíolo, seja a artéria centrolobular. Reflete um espectro alargado de alterações endo e perilobulares com inflamação e exsudação.[1,58]

Na maior parte dos casos, esse padrão representa bronquíolos dilatados e preenchidos por material patológico, embora possa também estar relacionado com a infiltração do tecido conjuntivo peribroncovascular centrolobular ou, ocasionalmente, com a dilatação ou o preenchimento (por exemplo, metástases intravasculares) das artérias pulmonares centrolobulares.[58]

PADRÃO MILIAR

O padrão miliar é um padrão de imagem descrito em radiografia, TC e RM. Ele é composto por nódulos < 3 mm (micronódulos) com distribuição difusa e aleatória e são uniformes entre si.[59] É frequentemente produto da disseminação hematogênica, como tuberculose e metástases (Figura S20).[1,2,,60]

PADRÃO DE PERFUSÃO EM MOSAICO

O padrão de perfusão em mosaico é descrito em TC e é caracterizado por áreas com diferentes atenuações intercaladas. Resulta da obliteração das pequenas vias aéreas ou de doença vascular oclusiva, ambas ocasionando áreas de oligoemia (redução da atenuação) alternando com áreas de pulmão normal, ventilado e perfundido. No caso de doença obliterativa das pequenas vias aéreas, a TC em fase expiratória mostra acentuação dos focos parenquimatosos que se apresentam hipodensos (redução da atenuação) pelo componente de aprisionamento aéreo.[1,2,61] O uso do termo "atenuação em mosaico" não é mais recomendado pois aumenta as chances de erros de interpretação com relação ao termo "perfusão em mosaico". O termo "opacidade em vidro fosco não homogênea" deve ser utilizado em substituição à atenuação em mosaico.

PADRÃO NODULAR

Padrão nodular refere-se à presença de múltiplas opacidades pulmonares arredondadas < 3 cm com densidade de partes moles e pode ser descrito em radiografias, TC e RM. Pequenos nódulos (ou micronódulos) são aqueles com diâmetro < 1 cm. Eles podem ser classificados quanto à distribuição pelo parênquima pulmonar em nódulos perilinfáticos, aleatórios ou centrolobulares. A distribuição centrolobular caracteriza-se pela presença de nódulos ocupando a porção central do lóbulo pulmonar secundário, a poucos milímetros da superfície pleural e das cissuras, sem, no entanto, tocá-las. Em geral, esse tipo de distribuição está associado a doenças bronquiolares ou arteriolares ou doenças da bainha conjuntiva peribroncovascular.[60] As principais doenças que se apresentam com o padrão nodular são a silicose, a

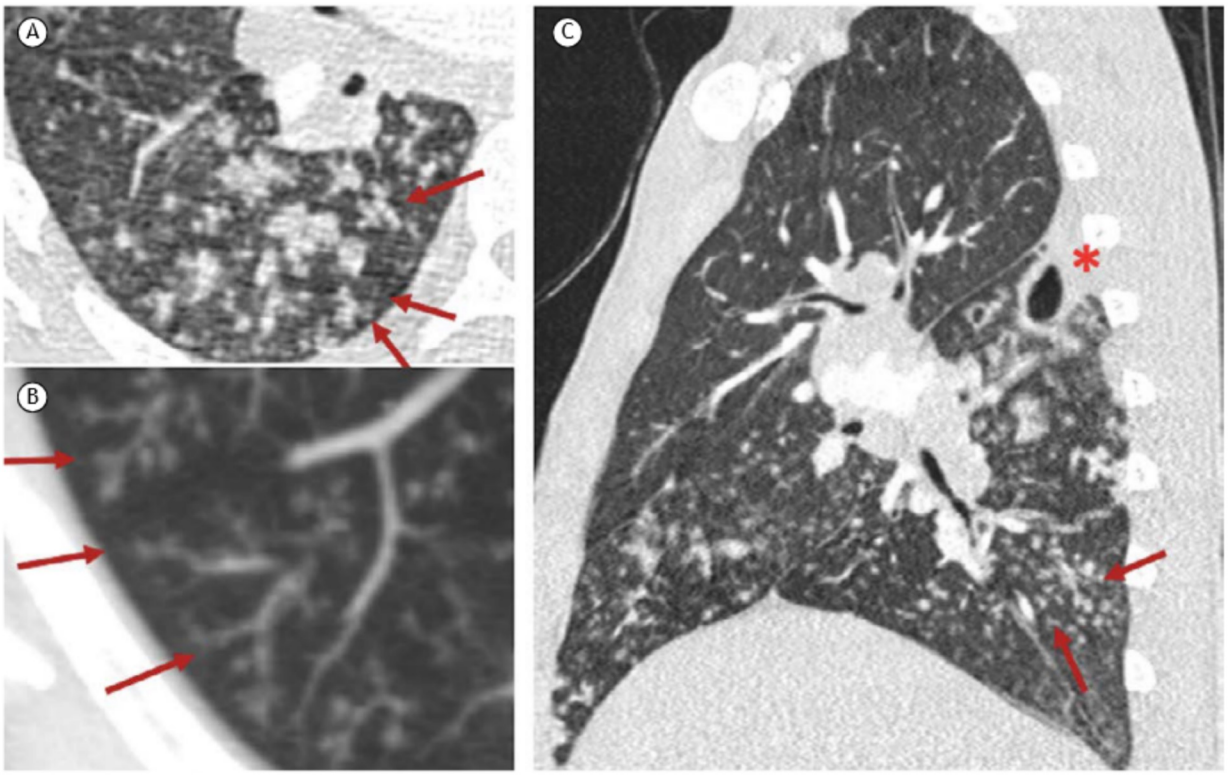

Figura 15. Imagens de TC em janela de pulmão de um paciente com tuberculose pulmonar. Em A, imagem no plano axial onde se observam várias opacidades centrolobulares com pequenos nódulos e imagens ramificadas (setas). Em B, em reconstrução em projeção de intensidade máxima, as imagens opacificadas correspondem ao preenchimento endobrônquico dos bronquíolos distais (setas). Em C, imagem no plano sagital indicando, além de nódulos centrolobulares e padrão de árvore em brotamento (setas), a presença de cavidade no segmento superior do lobo inferior direito, localização característica para a cavitação da tuberculose pulmonar (asterisco).

pneumonite por hipersensibilidade e algumas formas de bronquiolite. Na maioria dos casos os nódulos de pneumonite por hipersensibilidade e de bronquiolites têm atenuação em vidro fosco.[61,62]

PADRÃO PERILOBULAR (OPACIDADES PERILOBULARES, ESPESSAMENTO PERILOBULAR)

O padrão perilobular representa o envolvimento da periferia do lóbulo pulmonar secundário (região perilobular) por substrato histopatológico variável.[63,64] Na TC e RM demonstra opacidades lineares/curvilíneas contornando septos interlobulares, sendo maiores e menos definidas que esses, em geral determinando aparência poligonal ou em arcada (Figura S21).[63-66] O diagnóstico diferencial inclui PO, sendo esse padrão observado com frequência variável (22-57%), representando acumulação de material inflamatório em organização na periferia do lóbulo pulmonar, associado ou não a espessamento septal.[63-65] Na PO, o padrão perilobular é frequentemente associado a outros achados típicos, como consolidações, ao invés de ser um achado isolado.[66]

PADRÃO RETICULAR

O padrão reticular representa o envolvimento dos interstícios pulmonares com substrato histopatológico variável. Na radiografia é caracterizado por imagens lineares, por vezes entrelaçadas, mais facilmente vistas na periferia dos campos pulmonares. Na TC e RM corresponde geralmente a espessamento septal que pode ser inter ou intralobular, mas por vezes pode decorrer de cistos cujas paredes se apresentam como linhas na radiografia (Figura S22). Frequentemente, embora não invariavelmente, está associado a doenças fibrosantes, quando também se observam sinais de perda volumétrica no parênquima pulmonar.[1,67]

PSEUDOPLACA

A pseudoplaca é uma opacidade contígua à pleura visceral formada por pequenos nódulos coalescentes, simulando uma placa pleural. Essa entidade pode ser identificada em TC e RM e é encontrada mais frequentemente na sarcoidose, silicose e pneumoconiose dos mineiros de carvão.[1]

PLACA PLEURAL

Representa patologicamente uma área alongada de tecido conjuntivo denso na superfície pleural que corresponde a espessamento focal visto na radiografia ou mais comumente na TC e RM (Figura S23).[1,68-70] Pode corresponder a um achado incidental, porém quando múltiplas, faz-se necessário o diagnóstico diferencial entre a exposição ao asbesto e a sequela de empiema/tuberculose (geralmente unilateral e extensa). Por vezes podem se apresentar calcificadas, quando são mais facilmente detectadas na radiografia como imagens lineares verticais paralelas à parede torácica.

PNEUMATOCELE OU PNEUMATOCELO (PT)

Pneumatocele é um termo que pode ser identificado na radiografia, TC e RM e é definido como uma imagem cística arredondada de paredes finas (< 1 mm) e conteúdo gasoso, que muda de tamanho num curto espaço de tempo (Figura S24). Ela é decorrente de um mecanismo valvular obstrutivo da via aérea. Eventualmente pode apresentar conteúdo líquido interno. Geralmente resolvem de maneira espontânea. É mais frequentemente vista em crianças, associada a processos infecciosos, especialmente nas pneumonias por *Staphylococcus* sp. e em imunossuprimidos com pneumonia por *Pneumocystis jirovecii*.[71] Também pode ser vista em neonatos prematuros com desconforto respiratório.[72]

PSEUDOCAVIDADE

É um termo utilizado em TC e caracterizado como uma lesão cistoide arredondada ou ovalada de baixo coeficiente de atenuação, geralmente < 1 cm de diâmetro, entremeada a nódulos ou massas pulmonares ou em uma área de consolidação. Em algumas ocasiões é de difícil diferenciação com cavidade pulmonar. Este achado pode ser decorrente de brônquios dilatados ou mesmo com calibre normal ou de uma área de enfisema no interior da lesão, ou ainda pode representar uma porção de parênquima pulmonar preservado (Figuras S25 e S26). A presença de pseudocavidade em nódulos está frequentemente associada a adenocarcinoma e pode ser vista em pneumonia com necrose nas consolidações (Figura S26).[71-73]

PNEUMOMEDIASTINO

Pneumomediastino é um achado de imagem caracterizado pela presença de ar/gás no mediastino. O ar ou gás pode atingir os espaços mediastinais por aumento súbito da pressão intra-alveolar, com consequente ruptura de alvéolos e passagem de gás para o interstício peribroncovascular, que disseca até o hilo e entra no mediastino. A TC é o padrão ouro de diagnóstico, que também pode ser realizado por radiografia (Figura S27). A RM não é utilizada. A presença de pneumomediastino pode também advir da ruptura de víscera oca, como esôfago, traqueia, brônquios ou até mesmo pescoço ou cavidade abdominal. A associação com pneumotórax é frequente.[74]

PNEUMOTÓRAX

Pneumotórax refere-se à presença de ar no espaço pleural. É habitualmente classificado em espontâneo, traumático, diagnóstico/iatrogênico ou de tensão, conforme a etiologia do mesmo. Pode ser identificado em radiografia, TC e RM (Figura S28). Quando de dimensões significativas (> 2 cm entre a superfície pleural e o contorno pulmonar), há indicação para a colocação de dreno pleural.[1,2,74] Na maioria dos casos, o pneumotórax é causado por trauma como fratura dos arcos costais ou trauma torácico penetrante. O

pneumotórax hipertensivo é uma emergência médica, pois o ar na cavidade pleural encontra-se sob pressão, o que causa colapso vascular associado e redução do retorno venoso à aurícula esquerda. No caso do pneumotórax iatrogênico, esse frequentemente resulta de procedimentos torácicos como biopsia pulmonar, inserção de cateter venoso central ou cirurgia torácica.[75]

SINAL DO ALVO

O sinal do alvo é caracterizado por uma opacidade periférica em anel em conjunto com uma opacidade central nodular em vidro fosco. O termo pode ser descrito em TC e RM. Este achado foi inicialmente descrito como associado à pneumonia por SARS-CoV-2 (Figura S29).[76] No entanto, referências recentes apontam para semelhante etiopatogênese entre o sinal do halo invertido e o sinal do alvo como sinal radiológico de PO.[77]

SINAL DA ARCADA (ESPESSAMENTO SEPTAL PERILOBULAR)

O sinal da arcada é caracterizado por uma opacidade linear de distribuição perilobular, com conformação de arco ou arcada, ao redor do lóbulo pulmonar secundário. Esse padrão, à semelhança dos sinais do alvo e do halo invertido, aponta para PO (Figura S30).[77,78] O termo pode ser descrito em TC e RM.

SINAL DO ANEL DE SINETE

O sinal do anel de sinete é composto por uma opacidade em formato de anel, representando um brônquio dilatado no corte axial, e uma opacidade adjacente menor, representando a artéria pulmonar correspondente, o qual lembra um anel de sinete (ou anel de pérola). Esse sinal é descrito na TC para diagnóstico de bronquiectasia (Figura S31). O sinal de anel de sinete pode ser visto também em doenças caracterizadas por redução anormal do fluxo arterial pulmonar como interrupção proximal da artéria pulmonar ou tromboembolismo pulmonar crônico. Ocasionalmente, uma opacidade vascular pequena em contato com o brônquio é determinada por artéria brônquica ao invés da artéria pulmonar.[79-82] Vide "Bronquiectasia".

SINAL DO CRESCENTE AÉREO

O sinal do crescente aéreo é descrito em TC e é caracterizado por uma coleção de ar de tamanho variado e em forma de menisco ou de meia-lua localizada na periferia de um nódulo ou de massa com densidade de partes moles (Figura S32). É comum na descrição de achados radiográficos ou tomográficos de bola fúngica (aspergiloma), em que se observa uma coleção de ar interposta entre a parede da cavidade pré-existente e a lesão intracavitária pendente. O sinal do crescente aéreo também já foi descrito em outras doenças, tais como aspergilose pulmonar angioinvasiva, abscesso pulmonar, câncer de pulmão e outras infecções fúngicas.[72-74]

SINAL DO HALO

O sinal do halo é um achado tomográfico não específico, caracterizado pela presença de um halo de opacidade em vidro fosco circundando um nódulo ou, menos frequentemente, uma massa ou uma área de consolidação arredondada (Figura S33). Na maior parte dos casos, o halo em vidro fosco é causado por hemorragia perinodular.[4] Por exemplo, na aspergilose angioinvasiva (AAI) o nódulo representa um enfarte pulmonar secundário à angioinvasão pelo fungo, e o halo resulta da hemorragia alveolar perinodular. Em outros processos infecciosos, o halo deve-se à infiltração inflamatória perilesional. Nos adenocarcinomas, o halo ocorre por proliferação das células tumorais ao longo dos septos alveolares, preservando a arquitetura pulmonar (crescimento lepídico).[1] O mesmo aspecto pode ser observado em algumas metástases de adenocarcinomas (principalmente originadas no tubo digestivo ou no pâncreas). Uma informação útil para a abordagem diagnóstica inicial é se o paciente é imunocompetente ou imunocomprometido. Em pacientes imunodeficientes, predominam as causas infecciosas, especialmente as doenças fúngicas invasivas, como AAI. Assim, na presença de neutropenia febril, especialmente em pacientes com doenças hematológicas malignas ou após transplante de medula óssea, a causa mais importante é AAI.[1] Nesses casos, o achado do sinal do halo é considerado uma evidência precoce de AAI mesmo antes da positivação dos testes sorológicos, permitindo, segundo alguns autores, o início da terapia antifúngica.

SINAL DO HALO INVERTIDO

O sinal do halo invertido (SHI) é definido como uma área arredondada de opacidade em vidro fosco circundada por um anel de consolidação.[1] O SHI foi inicialmente descrito como específico para PO. Publicações posteriores identificaram-no num amplo espectro de doenças infecciosas e não infecciosas.[4,83-86] As causas infecciosas mais comuns são a tuberculose, a paracoccidioidomicose e as doenças fúngicas invasivas (aspergilose pulmonar invasiva e mucormicose).[87] Entre as causas não infecciosas, a mais comum é a PO, tanto na sua forma idiopática como na forma secundária. Outras causas importantes são o enfarto pulmonar e a sarcoidose (Figura S34).[1] Embora seja considerado um sinal pouco específico, a análise cuidadosa das características morfológicas do SHI pode estreitar o diagnóstico diferencial, ajudando o médico no diagnóstico definitivo. Dois aspectos de imagem devem ser considerados na tentativa de tornar o diagnóstico mais específico: a presença de nódulos compondo a parede e/ou o interior do halo (SHI nodular), assim como o aspecto reticulado no interior do halo (SHI reticulado). Deve ser lembrado que esses dois aspectos não são observados na PO, que

é a causa mais comum do SHI. Essas considerações são importantes porque o tratamento dessas condições é completamente diferente.

SINAL DO SEPTO NODULAR (SINAL EM CONTAS/SINAL EM ROSÁRIO/ ESPESSAMENTO SEPTAL NODULAR)

Os septos interlobulares delimitam o lóbulo pulmonar secundário, sendo formados por tecido conjuntivo, veias pulmonares e vasos linfáticos. Os septos normais geralmente não são identificados nas imagens radiológicas, por vezes podendo ser vistos na TCAR em pequena quantidade, finos e na periferia pulmonar.[33] Edema, infiltrados inflamatórios, fibrose e disseminação neoplásica podem levar ao espessamento dos septos interlobulares, que pode ser liso, irregular ou nodular. O espessamento septal nodular está frequentemente relacionado a linfangite carcinomatosa ou sarcoidose, podendo também ser identificado em menor frequência em outras doenças linfoproliferativas, pneumoconioses e na amiloidose.[1] Na radiografia é difícil diferenciar se o espessamento é liso ou irregular/ nodular, normalmente identificando-se padrão septal ou reticular de opacidades intersticiais. A TC e a RM permitem identificar o espessamento nodular do septo, que adquire o aspecto em contas ou em rosário. Na linfangite carcinomatosa, o sinal do septo nodular é mais frequentemente focal e unilateral, estando associado a adenopatia hilar/mediastinal unilateral e a outras alterações suspeitas em pacientes com história de malignidade (Figura S35). Na sarcoidose, o sinal é visto mais comumente de forma bilateral e simétrica, predominando em campos médios e superiores dos pulmões associado a adenopatia hilar bilateral, assim como nas estações paratraqueais à direita. Tipicamente, a sarcoidose afeta mulheres negras com idade entre 20 e 40 anos.[88]

TORACOLITO/TORACOLITÍASE

O toracolito corresponde a uma pequena estrutura/ nódulo livre e móvel, com ou sem calcificação na cavidade pleural (Figura S36). A toracolitíase é uma condição benigna rara, caracterizada pela presença de um ou mais toracolitos na cavidade pleural. O achado radiológico mais característico é a mobilidade da pequena estrutura/nódulo, que pode ser demonstrada nos estudos de imagem sequenciais ou com alteração de posicionamento do paciente. A toracolitíase raramente é sintomática, sendo um achado incidental em radiografias e TC, e não requer nenhum tratamento específico, muito menos ressecção cirúrgica.[89]

CONSIDERAÇÃO FINAL

Apesar de não definitivo, acreditamos que o presente artigo possa ajudar os radiologistas a tentar uma padronização dos relatórios, o que deve melhorar o entendimento dos mesmos e resultar em melhor assistência aos pacientes.

CONTRIBUIÇÃO DOS AUTORES

BH, CNA e ASSJ: concepção e planejamento do estudo e interpretação dos resultados. Todos os autores: redação ou revisão das versões preliminares e final e aprovação da versão final.

REFERÊNCIAS

1. Hansell DM, Bankier AA, MacMahon H, McLoud TC, Müller NL, Remy J. Fleischner Society: glossary of terms for thoracic imaging. Radiology. 2008;246(3):697-722. https://doi.org/10.1148/radiol.2462070712
2. Silva CI, Marchiori E, Souza Júnior AS, Müller NL; Comissão de Imagem da Sociedade Brasileira de Pneumologia e Tisiologia. Illustrated Brazilian consensus of terms and fundamental patterns in chest CT scans. J Bras Pneumol. 2010;36(1):99-123. https://doi.org/10.1590/s1806-37132010000100016
3. Arakawa H, Webb WR, McCowin M, Katsou G, Lee KN, Seitz RF. Inhomogeneous lung attenuation at thin-section CT: diagnostic value of expiratory scans. Radiology. 1998;206(1):89-94. https://doi.org/10.1148/radiology.206.1.9423656
4. Woodring JH, Reed JC. Types and mechanisms of pulmonary atelectasis. J Thorac Imaging. 1996;11(2):92-108. https://doi.org/10.1097/00005382-199621000-00002
5. Roach HD, Davies GJ, Attanoos R, Crane M, Adams H, Phillips S. Asbestos: when the dust settles an imaging review of asbestos-related disease. Radiographics. 2002;22 Spec No:S167-S184. https://doi.org/10.1148/radiographics.22.suppl_1.g02oc10s167
6. Hillerdal G. Rounded atelectasis. Clinical experience with 74 patients. Chest. 1989;95(4):836-841. https://doi.org/10.1378/chest.95.4.836
7. Gevenois PA, de Maertelaer V, Madani A, Winant C, Sergent G, De Vuyst P. Asbestosis, pleural plaques and diffuse pleural thickening: three distinct benign responses to asbestos exposure. Eur Respir J. 1998;11(5):1021-1027. https://doi.org/10.1183/09031936.98.11051021
8. Roberts CM, Citron KM, Strickland B. Intrathoracic aspergilloma: role of CT in diagnosis and treatment. Radiology. 1987;165(1):123-128. https://doi.org/10.1148/radiology.165.1.3628758
9. Occelli A, Soize S, Ranc C, Giovannini-Chami L, Bailly C, Leloutre B, et al. Bronchocele density in cystic fibrosis as an indicator of allergic broncho-pulmonary aspergillosis: A preliminary study. Eur J Radiol. 2017;93:195-199. https://doi.org/10.1016/j.ejrad.2017.05.047
10. Choi JA, Kim JH, Hong KT, Kim HS, Oh YW, Kang EY. CT bronchus sign in malignant solitary pulmonary lesions: value in the prediction of cell type. Eur Radiol. 2000;10(8):1304-1309. https://doi.org/10.1007/s003300000315
11. Alshabani K, Ghosh S, Arrossi AV, Mehta AC. Broncholithiasis: A Review. Chest. 2019;156(3):445-455. https://doi.org/10.1016/j.chest.2019.05.012
12. Barker AF. Bronchiectasis. N Engl J Med. 2002;346(18):1383-1393. https://doi.org/10.1056/NEJMra012519
13. Cantin L, Bankier AA, Eisenberg RL. Bronchiectasis. AJR Am J Roentgenol. 2009;193(3):W158-W171. https://doi.org/10.2214/AJR.09.3053
14. Akira M, Inoue Y, Kitaichi M, Yamamoto S, Arai T, Toyokawa K. Usual interstitial pneumonia and nonspecific interstitial pneumonia with and without concurrent emphysema: thin-section CT findings. Radiology. 2009;251(1):271-279. https://doi.org/10.1148/radiol.2511080917
15. Souza Jr AS, Araujo Neto C, Jasinovodolinsky D, Marchiori E, Kavakama J, Irion KL, et al. Terminologia para a Descrição de Tomografia Computadorizada do Tórax. Radiol Bras. 2002:35(2):125-128. https://doi.org/10.1590/S0100-39842002000200016
16. Funari MBG. Tomografia Computadorizada do Tórax Normal In: Funari MBG. Diagnóstico por Imagem das Doenças Torácicas. São Paulo: Guanabara Koogan; 2012. p. 87-106.
17. Seaman DM, Meyer CA, Gilman MD, McCormack FX. Diffuse

cystic lung disease at high-resolution CT. AJR Am J Roentgenol. 2011;196(6):1305-1311. https://doi.org/10.2214/AJR.10.4420

18. Raoof S, Bondalapati P, Vydyula R, Ryu JH, Gupta N, Raoof S, et al. Cystic Lung Diseases: Algorithmic Approach. Chest. 2016;150(4):945-965. https://doi.org/10.1016/j.chest.2016.04.026
19. Thurlbeck WN. Chronic airflow obstruction in lung disease. In: Bennington JL. Editor. Major Problems in Pathology, vol. 5. Philadelphia: Saunders; 1976. p. 221-302.
20. Stern EJ, Webb WR, Weinacker A, Müller NL. Idiopathic giant bullous emphysema (vanishing lung syndrome): imaging findings in nine patients. AJR Am J Roentgenol. 1994;162(2):279-282. https://doi.org/10.2214/ajr.162.2.8310909
21. Irion KL, Hochhegger B, Marchiori E, Porto Nda S, Baldisserotto Sde V, Santana PR. Chest X-ray and computed tomography in the evaluation of pulmonary emphysema [Article in Portuguese]. J Bras Pneumol. 2007;33(6):720-732. https://doi.org/10.1590/S1806-37132007000600017
22. Hruban RH, Meziane MA, Zerhouni EA, Khouri NF, Fishman EK, Wheeler PS, et al. High resolution computed tomography of inflation-fixed lungs. Pathologic-radiologic correlation of centrilobular emphysema. Am Rev Respir Dis. 1987;136(4):935-940. https://doi.org/10.1164/ajrccm/136.4.935
23. Takahashi M, Fukuoka J, Nitta N, Takazakura R, Nagatani Y, Murakami Y, et al. Imaging of pulmonary emphysema: a pictorial review. Int J Chron Obstruct Pulmon Dis. 2008;3(2):193-204. https://doi.org/10.2147/COPD.S2639
24. Sherren PB, Jovaisa T. Pulmonary interstitial emphysema presenting in a woman on the intensive care unit: case report and review of literature. J Med Case Rep. 2011;5:236. https://doi.org/10.1186/1752-1947-5-236
25. Kemper AC, Steinberg KP, Stern EJ. Pulmonary interstitial emphysema: CT findings. AJR Am J Roentgenol. 1999;172(6):1642. https://doi.org/10.2214/ajr.172.6.10350307
26. Donnelly LF, Lucaya J, Ozelame V, Frush DP, Strouse PJ, Sumner TE, et al. CT findings and temporal course of persistent pulmonary interstitial emphysema in neonates: a multiinstitutional study. AJR Am J Roentgenol. 2003;180(4):1129-1133. https://doi.org/10.2214/ajr.180.4.1801129
27. Pipavath SN, Schmidt RA, Takasugi JE, Godwin JD. Chronic obstructive pulmonary disease: radiology-pathology correlation. J Thorac Imaging. 2009;24(3):171-180. https://doi.org/10.1097/RTI.0b013e3181b32676
28. Litmanovich D, Boiselle PM, Bankier AA. CT of pulmonary emphysema–current status, challenges, and future directions. Eur Radiol. 2009;19(3):537-551. https://doi.org/10.1007/s00330-008-1186-4
29. Araki T, Nishino M, Zazueta OE, Gao W, Dupuis J, Okajima Y, et al. Paraseptal emphysema: Prevalence and distribution on CT and association with interstitial lung abnormalities. Eur J Radiol. 2015;84(7):1413-1418. https://doi.org/10.1016/j.ejrad.2015.03.010
30. Brauner M, Brillet P. Pathophysiological approach to infiltrative lung diseases on CT [Article in French]. J Radiol. 2009;90(11 Pt 2):1841-1853. https://doi.org/10.1016/s0221-0363(09)73287-1
31. The definition of emphysema. Report of a National Heart, Lung, and Blood Institute, Division of Lung Diseases workshop. Am Rev Respir Dis. 1985;132(1):182-185.
32. Webb WR, Muller NL, Naidich DP, editors. High-resolution CT of the lung. 4th ed. Philadelphia: Lippincott Williams & Wilkins; 2008.
33. Tuddenham WJ. Glossary of terms for thoracic radiology: recommendations of the Nomenclature Committee of the Fleischner Society. AJR Am J Roentgenol. 1984;143(3):509-517. https://doi.org/10.2214/ajr.143.3.509
34. Patterson HS, Sponaugle DN. Is infiltrate a useful term in the interpretation of chest radiographs? Physician survey results. Radiology. 2005;235(1):5-8. https://doi.org/10.1148/radiol.2351020759
35. Naidich DP. Webb WR, Müller N, Vlahos I, Krinski GA, editors. Computed tomography and magnetic resonance of the thorax. 4th ed. Philadelphia: Lippincott Williams & Wilkins; 2007. p. 683.
36. Webb WR, Müller NL, Naidich DP. Airways diseases. In: Webb WR, Müller NL, Naidich DP, editors. High-resolution CT of the lung. 5th ed. Philadelphia: Lippincott Williams & Wilkins; 2014. p. 585-602.
37. Webb WR. Thin-section CT of the secondary pulmonary lobule: anatomy and the image--the 2004 Fleischner lecture. Radiology. 2006;239(2):322-338. https://doi.org/10.1148/radiol.2392041968
38. Webb RW, Müller NL, Naidich DP. Illustrated glossary of high-resolution computed tomography terms. In: Webb WR, Muller NL, Naidich DP, editors. High-resolution CT of the lung. 5th ed. Philadelphia: Lippincott Williams & Wilkins; 2014. p. 660-677.
39. MacMahon H, Naidich DP, Goo JM, Lee KS, Leung ANC, Mayo JR, et al Guidelines for Management of Incidental Pulmonary Nodules Detected on CT Images: From the Fleischner Society 2017. Radiology. 2017;284(1):228-243. https://doi.org/10.1148/radiol.2017161659
40. Giménez A, Franquet T, Prats R, Estrada P, Villalba J, Bagué S. Unusual primary lung tumors: a radiologic-pathologic overview. Radiographics. 2002;22(3):601-619. https://doi.org/10.1148/radiographics.22.3.g02ma25601
41. Carter BW, Benveniste MF, Madan R, Godoy MC, de Groot PM, Truong MT, et al. ITMIG Classification of Mediastinal Compartments and Multidisciplinary Approach to Mediastinal Masses. Radiographics. 2017;37(2):413-436. https://doi.org/10.1148/rg.2017160095
42. Ameen M, Arenas R. Developments in the management of mycetomas. Clin Exp Dermatol. 2009;34(1):1-7. https://doi.org/10.1111/j.1365-2230.2008.03028.x
43. Welsh O, Vera-Cabrera L, Salinas-Carmona MC. Mycetoma. Clin Dermatol. 2007;25(2):195-202. https://doi.org/10.1016/j.clindermatol.2006.05.011
44. Abd El-Bagi ME, Fahal AH. Mycetoma revisited. Incidence of various radiographic signs. Saudi Med J. 2009;30(4):529-533.
45. Muñoz-Hernández B, Noyola MC, Palma-Cortés G, Rosete DP, Galván MA, Manjarrez ME. Actinomycetoma in arm disseminated to lung with grains of Nocardia brasiliensis with peripheral filaments. Mycopathologia. 2009;168(1):37-40. https://doi.org/10.1007/s11046-009-9189-5
46. Lacaz CS. Geographic distribution of mycetoma in Brazil [Article in Portuguese]. An Bras Dermatol. 1981;56(3):167-172.
47. Bankier AA, MacMahon H, Goo JM, Rubin GD, Schaefer-Prokop CM, Naidich DP. Recommendations for Measuring Pulmonary Nodules at CT: A Statement from the Fleischner Society. Radiology. 2017;285(2):584-600. https://doi.org/10.1148/radiol.2017162894
48. American College of Radiology (ACR) [homepage on the Internet. Reston, VA: ACR. Lung CT Screening Reporting & Data System (Lung-RADS). Available from: https://www.acr.org/Clinical-Resources/Reporting-and-Data-Systems/Lung-Rads
49. Martin KW, Sagel SS, Siegel BA. Mosaic oligemia simulating pulmonary infiltrates on CT. AJR Am J Roentgenol. 1986;147(4):670-673. https://doi.org/10.2214/ajr.147.4.670
50. Ameli-Renani S, Rahman F, Nair A, Ramsay L, Bacon JL, Weller A, et al. Dual-energy CT for imaging of pulmonary hypertension: challenges and opportunities. Radiographics. 2014; 34 (7): 1769-90. https://doi.org/10.1148/rg.347130085
51. Lu GM, Wu SY, Yeh, BM, Zhang LJ. Dual-energy CT for imaging of pulmonary hypertension: challenges and opportunities. Radiographics. 2014;34(7):1769-1790. https://doi.org/10.1148/rg.347130085
52. Remy-Jardin M, Remy J, Giraud F, Wattinne L, Gosselin B. Computed tomography assessment of ground-glass opacity: semiology and significance. J Thorac Imaging. 1993;8(4):249-264. https://doi.org/10.1097/00005382-199323000-00001
53. Remy-Jardin M, Giraud F, Remy J, Copin MC, Gosselin B, Duhamel A. Importance of ground-glass attenuation in chronic diffuse infiltrative lung disease: pathologic-CT correlation. Radiology. 1993;189(3):693-698. https://doi.org/10.1148/radiology.189.3.8234692
54. Barreto MM, Rafful PP, Rodrigues RS, Zanetti G, Hochhegger B, Souza AS Jr, et al. Correlation between computed tomographic and magnetic resonance imaging findings of parenchymal lung diseases. Eur J Radiol. 2013;82(9):e492-e501. https://doi.org/10.1016/j.ejrad.2013.04.037
55. Leung AN, Miller RR, Müller NL. Parenchymal opacification in chronic infiltrative lung diseases: CT-pathologic correlation. Radiology. 1993;188(1):209-214. https://doi.org/10.1148/radiology.188.1.8511299
56. Rossi SE, Erasmus JJ, Volpacchio M, Franquet T, Castiglioni T, McAdams HP. "Crazy-paving" pattern at thin-section CT of the lungs: radiologic-pathologic overview. Radiographics. 2003;23(6):1509-1519. https://doi.org/10.1148/rg.236035101
57. El Homsi M, Chung M, Bernheim A, Jacobi A, King MJ, Lewis S, et al. Review of chest CT manifestations of COVID-19 infection. Eur J Radiol Open. 2020;7:100239. https://doi.org/10.1016/j.ejro.2020.100239
58. Franquet T, Giménez A, Prats R, Rodríguez-Arias JM, Rodríguez C.

Thrombotic microangiopathy of pulmonary tumors: a vascular cause of tree-in-bud pattern on CT. AJR Am J Roentgenol. 2002;179(4):897-899. https://doi.org/10.2214/ajr.179.4.1790897

59. Marchiori E, Hochhegger B, Zanetti G. Tree-in-bud pattern. J Bras Pneumol. 2017;43(6):407. https://doi.org/10.1590/s1806-37562017000000303
60. Marchiori E, Zanetti G, Hochhegger B. Small interstitial nodules. J Bras Pneumol. 2015;41(3):250. https://doi.org/10.1590/S1806-37132015000000059
61. Almeida Junior JG, Marchiori E, Escuissato DL, Souza Jr AS, Gasparetto L, Nobre LF, et al. Pneumonite por hipersensibilidade (alveolite alérgica extrínseca): achados na tomografia computadorizada de alta resolução. Rev Imagem. 2003;25(4):231-237.
62. Marchiori E, Ferreira A, Saez F, Gabetto JM, Souza Jr AS, Escuissato DL, et al. Conglomerated masses of silicosis in sandblasters: high-resolution CT findings. Eur J Radiol. 2006;59(1):56-59. https://doi.org/10.1016/j.ejrad.2006.01.015
63. Ujita M, Renzoni EA, Veeraraghavan S, Wells AU, Hansell DM. Organizing pneumonia: perilobular pattern at thin-section CT. Radiology. 2004;232(3):757-761. https://doi.org/10.1148/radiol.2323031059
64. Johkoh T, Müller NL, Ichikado K, Nakamura H, Itoh H, Nagareda T. Perilobular pulmonary opacities: high-resolution CT findings and pathologic correlation. J Thorac Imaging. 1999;14(3):172-177. https://doi.org/10.1097/00005382-199907000-00003
65. Faria IM, Zanetti G, Barreto MM, Rodrigues RS, Araújo-Neto CA, Silva JL, et al. Organizing pneumonia: chest HRCT findings. J Bras Pneumol. 2015;41(3):231-237. https://doi.org/10.1590/S1806-37132015000004544
66. Torrealba JR, Fisher S, Kanne JP, Butt YM, Glazer C, Kershaw C, et al. Pathology-radiology correlation of common and uncommon computed tomographic patterns of organizing pneumonia. Hum Pathol. 2018;71:30-40. https://doi.org/10.1016/j.humpath.2017.10.028
67. Marten K. Reticular pattern in thin-section CT: from morphology to differential diagnosis [Article in German]. Radiologe. 2009;49(9):873-882. https://doi.org/10.1007/s00117-009-1829-8
68. Lynch DA, Gamsu G, Aberle DR. Conventional and high resolution computed tomography in the diagnosis of asbestos-related diseases. Radiographics. 1989;9(3):523-551. https://doi.org/10.1148/radiographics.9.3.2727359
69. Friedman AC, Fiel SB, Fisher MS, Radecki PD, Lev-Toaff AS, Caroline DF. Asbestos-related pleural disease and asbestosis: a comparison of CT and chest radiography. AJR Am J Roentgenol. 1988;150(2):269-275. https://doi.org/10.2214/ajr.150.2.269
70. Aberle DR, Gamsu G, Ray CS, Feuerstein IM. Asbestos-related pleural and parenchymal fibrosis: detection with high-resolution CT. Radiology. 1988;166(3):729-734. https://doi.org/10.1148/radiology.166.3.3340770
71. Kim TH, Kim SJ, Ryu YH, Chung SY, Seo JS, Kim YJ, et al. Differential CT features of infectious pneumonia versus bronchioloalveolar carcinoma (BAC) mimicking pneumonia. Eur Radiol. 2006;16(8):1763-1768. https://doi.org/10.1007/s00330-005-0101-5
72. Tailor TD, Schmidt RA, Eaton KD, Wood DE, Pipavath SN. The Pseudocavitation Sign of Lung Adenocarcinoma: A Distinguishing Feature and Imaging Biomarker of Lepidic Growth. J Thorac Imaging. 2015;30(5):308-313. https://doi.org/10.1097/RTI.0000000000000168
73. Penha D, Pinto E, Taborda-Barata L, Irion K, Marchiori E. Lung cancer associated with cystic airspaces: a new radiological presentation of lung cancer. J Bras Pneumol. 2020;46(6):e20200156. https://doi.org/10.36416/1806-3756/e20200156
74. O'Connor AR, Morgan WE. Radiological review of pneumothorax. BMJ. 2005;330(7506):1493-1497. https://doi.org/10.1136/bmj.330.7506.1493
75. Sakai M, Hiyama T, Kuno H, Mori K, Saida T, Ishiguro T, et al. Thoracic abnormal air collections in patients in the intensive care unit: radiograph findings correlated with CT. Insights Imaging. 2020;11(1):35. https://doi.org/10.1186/s13244-020-0838-z
76. Müller CIS, Müller NL. Chest CT target sign in a couple with COVID-19 pneumonia. Radiol Bras. 2020;53(4):252-254. https://doi.org/10.1590/0100-3984.2020.0089
77. Marchiori E, Penha D, Nobre LF, Hochhegger B, Zanetti G. Differences and Similarities between the Double Halo Sign, the Chest CT Target Sign and the Reversed Halo Sign in Patients with COVID-19 Pneumonia. Korean J Radiol. 2021;22(4):672-676. https://doi.org/10.3348/kjr.2020.1150
78. Chiarenza A, Esposto Ultimo L, Falsaperla D, Travali M, Foti PV, Torrisi SE, et al. Chest imaging using signs, symbols, and naturalistic images: a practical guide for radiologists and non-radiologists. Insights Imaging. 2019;10(1):114. https://doi.org/10.1186/s13244-019-0789-4
79. Ouellette H. The signet ring sign. Radiology. 1999;212(1):67-68. https://doi.org/10.1148/radiology.212.1.r99jl2067
80. Ryu JH, Swensen SJ. Cystic and cavitary lung diseases: focal and diffuse. Mayo Clin Proc. 2003;78(6):744-752. https://doi.org/10.4065/78.6.744
81. McGuinness G, Naidich DP, Leitman BS, McCauley DI. Bronchiectasis: CT evaluation. AJR Am J Roentgenol. 1993;160(2):253-259. https://doi.org/10.2214/ajr.160.2.8424327
82. Ryu DS, Spirn PW, Trotman-Dickenson B, Hunsaker A, Jung SM, Park MS, et al. HRCT findings of proximal interruption of the right pulmonary artery. J Thorac Imaging. 2004;19(3):171-175. https://doi.org/10.1097/01.rti.0000130598.86945.b9
83. Abramson S. The air crescent sign. Radiology. 2001;218(1):230-232. https://doi.org/10.1148/radiology.218.1.r01ja19230
84. Marshall GB, Farnquist BA, MacGregor JH, Burrowes PW. Signs in thoracic imaging. J Thorac Imaging. 2006;21(1):76-90. https://doi.org/10.1097/01.rti.0000189192.70442.7a
85. Wang LF, Chu H, Chen YM, Perng RP. Adenocarcinoma of the lung presenting as a mycetoma with an air crescent sign. Chest. 2007;131(4):1239-1242. https://doi.org/10.1378/chest.06-1551
86. Marchiori E, Zanetti G, Hochhegger B. Reversed halo sign. J Bras Pneumol. 2015;41(6):564. https://doi.org/10.1590/s1806-37562015000000235
87. Marchiori E, Hochhegger B, Zanetti G. Reversed halo sign in invasive fungal infections. J Bras Pneumol. 2016;42(3):232. https://doi.org/10.1590/S1806-37562016000000119
88. Ganeshan D, Menias CO, Lubner MG, Pickhardt PJ, Sandrasegaran K, Bhalla S. Sarcoidosis from Head to Toe: What the Radiologist Needs to Know. Radiographics. 2018;38(4):1180-1200. https://doi.org/10.1148/rg.2018170157
89. Escuissato DL, Zanetti G, Marchiori E. A mobile calcified nodule in the pleural cavity: thoracolithiasis. J Bras Pneumol. 2019;45(4):e20190113. https://doi.org/10.1590/1806-3713/e20190113

Archivos de Bronconeumología 58 (2022) 714

Sociedad Española de Neumología y Cirugía Torácica SEPAR

ARCHIVOS DE
Bronconeumología

www.archbronconeumol.org

Clinical Image

Brachiocephalic Vein Aneurysm: An Unusual Cause of an Anterior Mediastinal Mass

Luciana Volpon Soares Souza[a], Arthur Soares Souza Jr[a,b], Edson Marchiori[c,*]

[a] Ultra X, São José do Rio Preto, SP, Brazil
[b] Faculdade de Medicina de Rio Preto, São José do Rio Preto, SP, Brazil
[c] Universidade Federal do Rio de Janeiro, Rio de Janeiro, Brazil

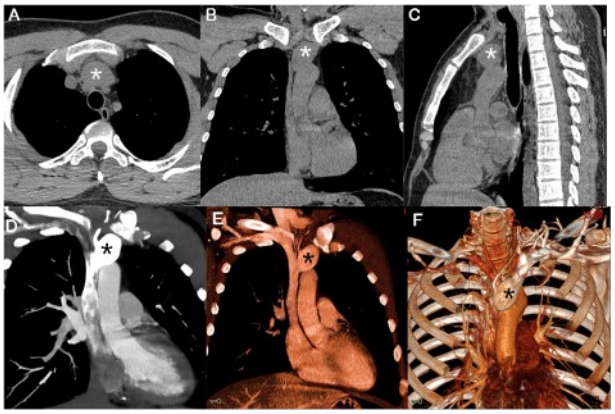

Fig. 1. Non-enhanced chest CT (A–C) showed a prevascular mediastinal mass (asterisks). Enhanced CT with coronal reconstruction (D, E) and 3D volumetric reconstruction (F) demonstrated a fusiform aneurysm of the brachiocephalic vein, beginning 1.5 cm distal to the internal jugular vein and extending to the superior vena cava (asterisks).

A 33-year-old man with no significant past medical history presented with a mediastinal mass that had been found incidentally on a chest CT examination performed as part of the investigation of a respiratory infection. Non-enhanced chest CT showed a prevascular mediastinal mass (Fig. 1A–C). Enhanced CT with coronal reconstruction (Fig. 1D–E) and 3D volumetric reconstruction (Fig. 1F) demonstrated a fusiform aneurysm of the brachiocephalic vein, extending to the superior vena cava, measuring 2.5 cm × 2.7 cm × 3.8 cm; its neck was 1.1 cm in diameter. A final diagnosis of left brachiocephalic vein aneurysm (BCVA) was made. Some treatment options were offered to the patient, especially antithrombotic treatments. The patient refused any kind of treatment, and is being followed on an outpatient basis. After 3 years, he remains asymptomatic.

Aneurysms of the brachiocephalic (or innominate) vein are very rare. About 40 cases have been reported to date. They may be completely asymptomatic, presenting as incidental findings on imaging examinations or as a result of complications that they cause, including thromboembolism and venous obstruction, rupture, and compression of adjacent structures. The most common BCVA presentation is a widened mediastinum on a chest radiograph. The accurate diagnosis of a mediastinal aneurysm is essential to avoid complications secondary to biopsy or surgical intervention. Imaging is usually sufficient for the identification and characterization of such aneurysms.[1,2]

The two main types of BCVA are fusiform (comprising the majority of cases) and saccular. Treatment is largely determined by clinical presentation, morphological characteristics of the aneurysm (saccular or fusiform, condition of the neck and the size of the aneurysm), patient decisions, and surgical conditions. Current treatment approaches include conservative management and open surgery. Endovascular treatment is also becoming a therapeutic option. For larger saccular BCVA, even those that are asymptomatic, prophylactic surgical resection has been recommended. Fusiform aneurysms like that identified in our patient pose a much lower risk of complication and can be treated conservatively.[1,2]

Conflict of interest

The authors declare that they have no conflicts of interest to express.

References

1. Ueno H, Yazawa M, Tsubouchi H, Nakanishi K, Sugiyama T, Kadomatsu Y, et al. Left brachiocephalic vein aneurysm: a case report. Surg Case Rep. 2021;7:66, http://dx.doi.org/10.1186/s40792-021-01148-0.
2. Nguyen Q, Olive JK, Vervoort D, Phan K, Luc JGY. Brachiocephalic vein aneurysm: a systematic review of the literature. J Thorac Dis. 2020;12:2747–58, http://dx.doi.org/10.21037/jtd.2020.04.39.

* Corresponding author.
E-mail address: edmarchiori@gmail.com (E. Marchiori).

https://doi.org/10.1016/j.arbres.2022.02.011

J Bras Pneumol. 2024;50(2):e20240080
https://dx.doi.org/10.36416/1806-3756/e20240080

Tracheobronchial amyloidosis and multiple myeloma

Luciana Volpon Soares Souza[1], Arthur Soares Souza Jr[1,2], Edson Marchiori[3]

An 86-year-old man was admitted with cough and weight loss. He reported episodes of mild hemoptysis and denied fever or other symptoms. He was a smoker (40 pack-years) with a previous history of multiple myeloma. Physical examination demonstrated wheezing. Laboratory test results were unremarkable. Chest CT revealed tracheal and bronchial wall thickening, and lytic lesions on the ribs and vertebral bodies with partial collapse (Figure 1).

The patient was referred for fiberoptic bronchoscopy with BAL. Bronchoscopy showed tracheal and bronchial wall thickening, with swelling and hypertrophy of a brittle, and easily bleeding mucosa, as well as submucosal plaques. BAL fluid was negative for neoplastic cells, bacteria, and fungi. Biopsy of the tracheal walls revealed a stroma occupied by an amorphous eosinophilic material that was positive on Congo red staining and exhibited apple-green birefringence under polarized light, consistent with amyloidosis.

Multiple myeloma and amyloidosis are characterized by abnormal accumulation and deposition of monoclonal plasma cells and extracellular protein fibrils. Multiple myeloma is often complicated with amyloidosis.[1] In the thoracic compartment, amyloidosis typically affects the heart, but it can also involve the pulmonary parenchyma, tracheobronchial tree, and other sites. Pulmonary involvement is rare, and amyloidosis is reported as tracheobronchial, diffuse/alveolar-septal, or nodular.[2]

AUTHOR CONTRIBUTIONS

All author equally contributed to this manuscript.

CONFLICTS OF INTEREST

None declared.

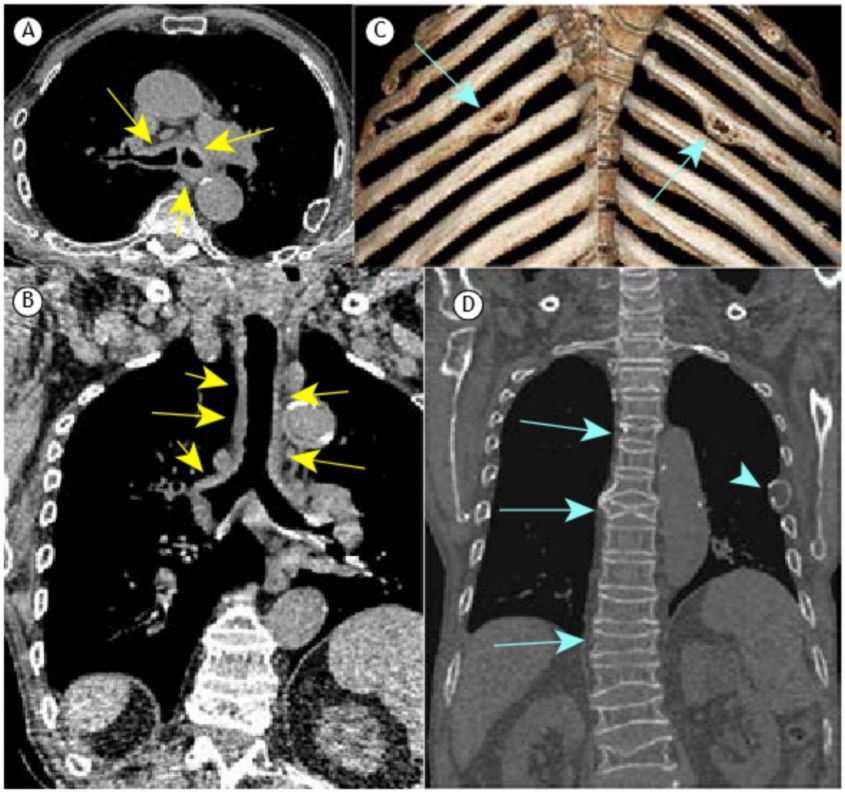

Figure 1. Axial CT of the chest (mediastinal window) at the level of the proximal segment of the bronchial bifurcation (in A) and a coronal reconstruction scan (in B) showing thickening of the tracheal wall and main bronchi (yellow arrows). In C, three-dimensional reconstruction of the chest wall demonstrating bilateral lytic lesions on the ribs (blue arrows). In D, coronal reconstruction showing partial collapse of multiple vertebral bodies (green arrows) and a lytic lesion on a left rib (arrowhead).

REFERENCES

1. Suzuki K. Diagnosis and Treatment of Multiple Myeloma and AL Amyloidosis with Focus on Improvement of Renal Lesion. Clin Exp Nephrol. 2012;16(5):659-671. https://doi.org/10.1007/s10157-012-0684-5
2. Torres PPTES, Rabahi M, Pinto SA, Curado KCMA, Rabahi MF. Primary tracheobronchial amyloidosis. Radiol Bras. 2017;50(4):267-268. https://doi.org/10.1590/0100-3984.2015.0177

1. Ultra X, São José do Rio Preto (SP) Brasil.
2. Faculdade de Medicina de Rio Preto, São José do Rio Preto (SP) Brasil.
3. Universidade Federal do Rio de Janeiro, Rio de Janeiro (RJ) Brasil.

J Bras Pneumol. 2023;49(4):e20230053
https://dx.doi.org/10.36416/1806-3756/e20230053

Pulmonary emphysema associated with skin nodules

Luciana Volpon Soares Souza[1], Arthur Soares Souza Jr[1,2], Edson Marchiori[3]

A 55-year-old nonsmoking female patient with a known diagnosis of neurofibromatosis type 1 (NF1) since adolescence presented with a two-month history of dyspnea and cough. During adolescence, she developed subcutaneous and cutaneous neurofibromas predominantly on the chest wall (Figure 1A). In addition, she had café au lait spots on the skin. The patient's brother also had NF1. She denied fever. Laboratory test findings, including alpha-1 antitrypsin levels, were normal. No pulmonary function testing was performed. A chest X-ray showed multiple soft-tissue nodules on the chest wall (Figure 1B). Chest CT demonstrated bilateral emphysematous changes with subpleural bullae, predominantly in the upper lobes, along with several cutaneous and subcutaneous nodules (Figures 1C and 1D). A diagnosis of neurofibromatosis-associated diffuse lung disease was established.

NF1 or von Recklinghausen's disease is a genetic disorder characterized by multiple tumors of ectodermal and mesodermal tissues. The disease has a varied clinical presentation, with subcutaneous and cutaneous neurofibromas, café au lait spots on the skin, and iris

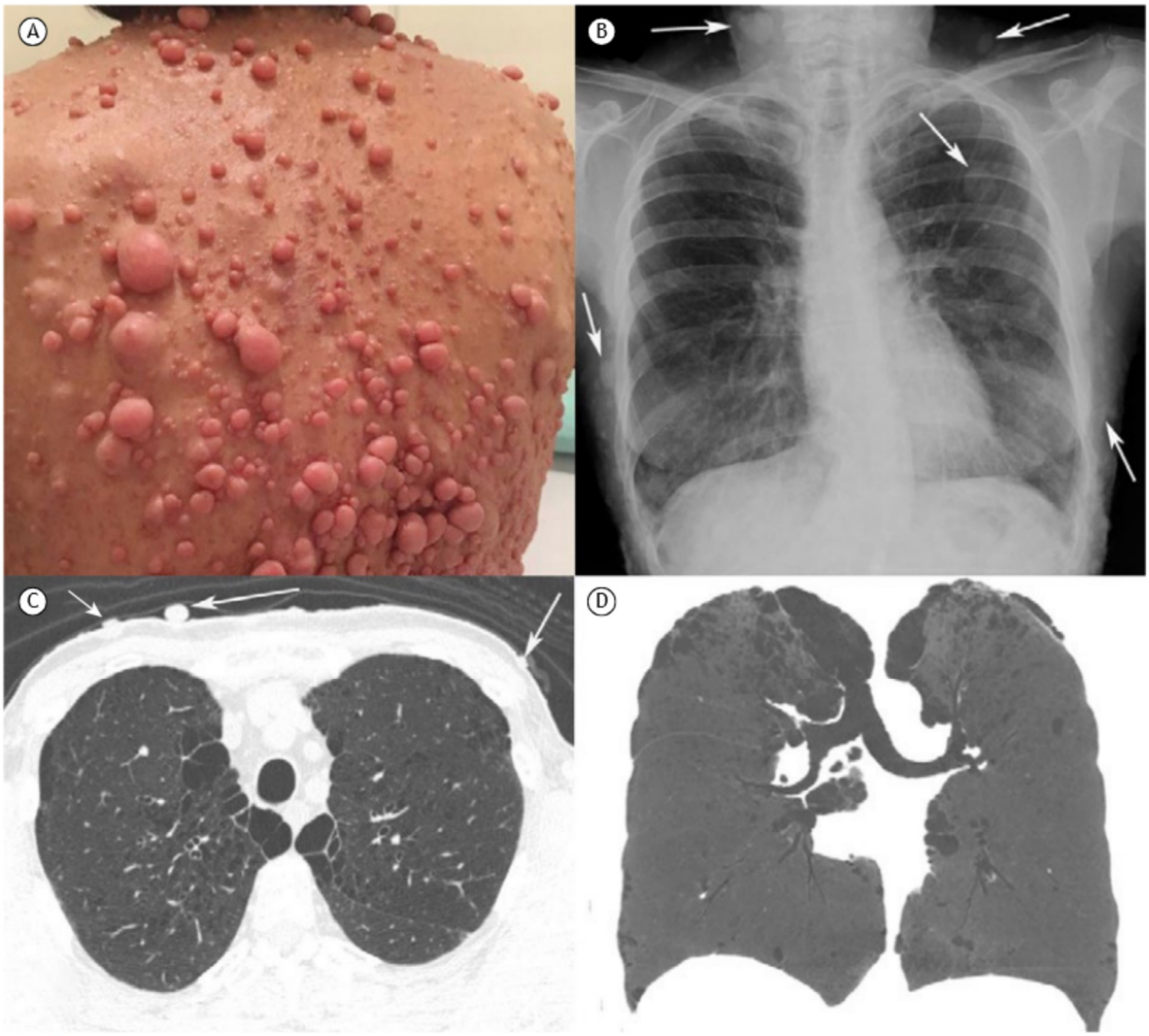

Figure 1. In A, a photograph of the dorsal region of the chest showing multiple cutaneous neurofibromas. In B, a chest X-ray shows multiple soft-tissue nodules on the chest wall (arrows). In C and D, respectively, an axial chest CT image (lung window) at the level of the upper lobes and a coronal minimum intensity projection image show emphysematous lesions predominantly in the upper lobes. Note also nodules (neurofibromas) on the chest wall (arrows in C).

1. Ultra X, São José do Rio Preto (SP) Brasil.
2. Faculdade de Medicina de Rio Preto, São José do Rio Preto (SP) Brasil.
3. Universidade Federal do Rio de Janeiro, Rio de Janeiro (RJ) Brasil.

hamartomas (Lisch nodules) being most common. Diffuse lung disease associated with NF1 consists of an emphysematous, cystic, or bullous process with upper lobe predominance. Varying amounts of fibrosis and ground-glass opacity are also present.[1-3]

AUTHOR CONTRIBUTIONS

The authors equally contributed to this work.

CONFLICTS OF INTEREST

None declared.

REFERENCES

1. Zamora AC, Collard HR, Wolters PJ, Webb WR, King TE. Neurofibromatosis-associated lung disease: a case series and literature review. Eur Respir J. 2007;29(1):210-214. https://doi.org/10.1183/09031936.06.00044006
2. Shino MY, Rabbani S, Belperio JA, Lynch JP 3rd, Weigt SS. Neurofibromatosis-associated diffuse lung disease: case report. Semin Respir Crit Care Med. 2012;33(5):572-575. https://doi.org/10.1055/s-0032-1325165
3. Ueda K, Honda O, Satoh Y, Kawai M, Gyobu T, Kanazawa T, et al. Computed tomography (CT) findings in 88 neurofibromatosis 1 (NF1) patients: Prevalence rates and correlations of thoracic findings. Eur J Radiol. 2015;84(6):1191-1195. https://doi.org/10.1016/j.ejrad.2015.02.024

J Bras Pneumol. 2023;49(1):e20220466
https://dx.doi.org/10.36416/1806-3756/e20220466

Tomographic pleuropulmonary manifestations in rheumatoid arthritis: a pictorial essay

Guilherme das Posses Bridi[1], Márcio Valente Yamada Sawamura[2], Mark Wanderley[1], Luciana Volpon Soares Souza[3], Ronaldo Adib Kairalla[1,4], Letícia Kawano-Dourado[1,5,6], Bruno Guedes Baldi[1,7]

1. Divisão de Pneumologia, Instituto do Coração – InCor – Hospital das Clínicas, Faculdade de Medicina, Universidade de São Paulo, São Paulo (SP) Brasil.
2. Instituto de Radiologia, Hospital das Clínicas, Faculdade de Medicina, Universidade de São Paulo, São Paulo (SP) Brasil.
3. Ultra X, São José do Rio Preto (SP) Brasil.
4. Núcleo de Tórax, Hospital Sírio-Libanês, São Paulo, Brasil.
5. Hcor Research Institute, Hospital do Coração, São Paulo (SP) Brasil.
6. MAGIC Evidence Ecosystem Foundation, Oslo, Norway.
7. Hospital do Coração, São Paulo (SP) Brasil.

Submitted: 11 December 2022.
Accepted: 30 December 2022.

Study carried out in the Divisão de Pneumologia, Instituto do Coração – InCor – Hospital das Clínicas, Faculdade de Medicina, Universidade de São Paulo, São Paulo (SP) Brasil.

ABSTRACT

Rheumatoid arthritis (RA) is an autoimmune inflammatory and heterogeneous disease that affects several systems, especially the joints. Among the extra-articular manifestations of RA, pleuropulmonary involvement occurs frequently, with different presentations, potentially in all anatomic thoracic compartments, and may determine high morbidity and mortality. The most common pleuropulmonary manifestations in patients with RA include interstitial lung disease (ILD), pleural disease, pulmonary arterial hypertension, rheumatoid lung nodules, airway disease (bronchiectasis and bronchiolitis), and lymphadenopathy. Pulmonary hypertension and ILD are the manifestations with the greatest negative impact in prognosis. HRCT of the chest is essential in the evaluation of patients with RA with respiratory symptoms, especially those with higher risk factors for ILD, such as male gender, smoking, older age, high levels of rheumatoid factor, or positive anti-cyclic citrullinated peptide antibody results. Additionally, other etiologies that may determine tomographic pleuropulmonary manifestations in patients with RA are infections, neoplasms, and drug-induced lung disease. In these scenarios, clinical presentation is heterogeneous, varying from being asymptomatic to having progressive respiratory failure. Knowledge on the potential etiologies causing tomographic pleuropulmonary manifestations in patients with RA coupled with proper clinical reasoning is crucial to diagnose and treat these patients.

Keywords: Lung diseases, interstitial; Lung diseases; Pleural diseases; Pulmonary arterial hypertension; Arthritis, rheumatoid; Tomography.

INTRODUCTION

Rheumatoid arthritis (RA) is an autoimmune rheumatic disease that most commonly affects the joints. Pleuropulmonary manifestations are common and significantly contribute to increase morbidity and mortality in RA, affecting up to 60% of the patients during the disease course. All anatomic thoracic compartments can be involved in RA, including the pleura and pulmonary parenchyma, as well as small and large airways.[1-3] Clinical presentation is heterogeneous, varying from being asymptomatic to having progressive respiratory failure, and may have acute or insidious onset.[1,4] Pulmonary involvement in RA usually occurs within five years after the diagnosis of RA, but it is important to reinforce that it may precede the articular involvement.[2,3]

To evaluate the different pleuropulmonary manifestations of RA, CT is essential because it allows not only the detailing of the lesions, but also their precise location. Additionally, CT is important to assess other etiologies that may determine pulmonary lesions in patients with RA, such as infections, drug-induced lung disease (DILD), neoplasms, and response to treatment.[5]

Although there is no formal recommendation to screen patients with RA for the presence of pleuropulmonary involvement, screening may be recommended in those with respiratory symptoms and/or changes in pulmonary examinations, CT scans, or pulmonary function tests. Additionally, patients with a higher risk of pulmonary involvement due to factors such as male gender, older age, smoking, positive results for anti-cyclic citrullinated peptide antibodies, or high titers of rheumatoid factor should undergo CT and pulmonary function evaluation.

The main pleuropulmonary manifestations that may occur in patients with RA include interstitial lung disease (ILD), pleural disease, pulmonary arterial hypertension (PAH), rheumatoid lung nodules, airway disease (bronchiectasis and bronchiolitis), lymphadenopathy, and DILD.

The objective of this pictorial essay was to present the main tomographic pleuropulmonary manifestations that may be identified in patients with RA (Chart 1).

ILD

ILD is one of the most common pulmonary manifestations of RA and the second leading cause of mortality, primarily

Correspondence to:
Bruno Guedes Baldi. Avenida Dr. Enéas de Carvalho Aguiar, 44, 8º andar, Bloco II, Cerqueira César, CEP 05403-900, São Paulo, SP, Brasil.
Tel.: 55 11 2661-5695. Fax: 55 11 2661-5695. E-mail: bruno.baldi@hc.fm.usp.br
Financial support: None.

Chart 1. Summary of the main pleuropulmonary manifestations of rheumatoid arthritis.

Disease pattern	Radiological manifestations	Other features
Usual interstitial pneumonia	Basilar and peripheral traction bronchiectasis, with or without honeycombing	Most common ILD pattern (60%)
		Worst prognosis among all ILD patterns
	Exuberant honeycombing, straight edge sign, and anterior upper lobe involvement	
Nonspecific interstitial pneumonia	Basilar and peripheral ground-glass opacities and fine reticulation; traction bronchiectasis	Association with longer duration of joint disease, lower risk of disease progression, and greater treatment response
	Usually symmetric	
	Subpleural sparing may occur	
Organizing pneumonia	Peripheral and peribronchovascular consolidation; ground-glass opacities	Abnormalities are often fleeting or migratory
	Nodules and reversed halo sign may occur less frequently	Usually has good prognosis
Lymphocytic interstitial pneumonia	Lower lobe-predominant and peribronchovascular thin-walled cysts	More commonly associated with Sjögren's syndrome
	Ground-glass opacities and septal thickening	
Desquamative interstitial pneumonia	Ground-glass opacities and mild reticulation	Rare and may precede the onset of RA by years
	Cysts may be found	
	Basal and peripheral predominance	
Inflammatory pleural effusion	Usually unilateral with small pleural enhancement	Most patients are asymptomatic
		Usually exudative with low glucose levels, low pH levels, high LDH levels, high rheumatoid factor titers, low total complement activity, and low C3 and C4 levels
Pulmonary arterial hypertension	Enlarged pulmonary arteries, dilatation of right-sided cardiac chambers, and right ventricular hypertrophy	Rare and usually seen in older patients with long-standing RA-ILD
	Mosaic attenuation in the lungs as an indirect sign	
Rheumatoid lung nodules	Round opacities with variable size, usually multiple and cavitated	Usually asymptomatic and associated with subcutaneous nodules
	Usually in the subpleural region	
Bronchiectasis	Cylindrical, varicose, and cystic bronchiectasis may occur	Chronic suppurative infections, treatment with disease-modifying antirheumatic drugs, and genetic predisposition may be related to bronchiectasis
Constrictive bronchiolitis	Bronchial wall thickening, bronchiectasis, and mosaic attenuation pattern	More common in females and in those with long-standing untreated disease Airflow obstruction and air trapping in pulmonary function tests
Follicular bronchiolitis	Small centrilobular nodules with branching structures (tree-in-bud sign) Air trapping and peribronchovascular and septal thickening may also occur	Associated with RA or Sjögren's syndrome

Continue...▶

Chart 1. Summary of the main pleuropulmonary manifestations of rheumatoid arthritis. (Continued...)

Disease pattern	Radiological manifestations	Other features
Caplan Syndrome (rheumatoid pneumoconiosis)	Multiple peripheral lung nodules with cavitations or calcifications in some cases	Associated with exposure to coal, asbestos, or silica May precede the onset of RA by more than 10 years Most patients are asymptomatic
Lymphadenopathy	Mediastinal or axillary	Approximately 70% of patients with RA Patients may show signs of inflammatory activity
Drug-induced lung disease	Patterns suggestive of hypersensitivity pneumonitis, eosinophilic pneumonia, pulmonary edema, organizing pneumonia, and diffuse alveolar damage	Secondary to immune-mediated reaction or direct toxicity Diagnosis usually based on symptoms, tomographic pattern, and time between treatment initiation and drug discontinuation Symptoms usually improve with drug discontinuation

ILD: interstitial lung disease; and RA: rheumatoid arthritis.

owing to respiratory failure, superimposed infection, and lung cancer.[6,7] ILD is responsible for 10-20% of RA-related mortality, and approximately 10% of patients have clinically significant disease. RA-ILD may determine a variable spectrum of presentations, from acute to chronic ones, including diffuse alveolar damage (DAD), organizing pneumonia (OP), and fibrotic disorders.[8]

Risk factors for RA-ILD include smoking, male sex, older age, duration/activity of RA, and seropositivity for rheumatoid factor or anti-cyclic citrullinated peptide antibodies.[2,9] Patients with RA rarely need to undergo lung biopsy to confirm the diagnosis of ILD, which is most of the time based on tomographic patterns.

Usual interstitial pneumonia associated with RA

Usual interstitial pneumonia (UIP) is the most common ILD pattern in RA, with a prevalence of about 60%. UIP carries the worst prognosis among all patients with ILD secondary to RA, the surviving rates being quite similar to those of patients with idiopathic pulmonary fibrosis (IPF).[10] The main CT features are basilar and peripheral traction bronchiectasis and/or bronchiolectasis, with or without honeycombing, and minimal or absent ground-glass opacities.[2,11] The imaging presentation of RA-UIP and IPF may be identical. Chung et al.[12] have described three features favoring the presence of autoimmune rheumatic diseases as the etiology of UIP over IPF: exuberant honeycombing; straight edge sign, characterized as the isolation of fibrosis in the lower zones with sharp demarcation between fibrotic and normal lung in the craniocaudal plane and without substantial extension of fibrosis along the lateral margins at coronal imaging; and anterior upper lobe involvement (Figure 1).

Nonspecific interstitial pneumonia and other ILD patterns

Nonspecific interstitial pneumonia (NSIP) is the second most common ILD pattern in RA, occurring in around one-third of cases.[10] NSIP is associated with longer duration of joint disease, lower risk of disease progression, greater treatment response, and better outcomes when compared with UIP.[13] There is no difference in prognosis when comparing idiopathic NSIP with autoimmune rheumatic disease-associated NSIP.[7] CT findings in NSIP include basilar- and peripheral-predominant ground-glass opacities and reticulation, with or without immediate subpleural sparing, and traction bronchiectasis (Figure 2). The tomographic presentation of NSIP is typically homogeneous and symmetric, and traction bronchiectasis is often relatively central in comparison with UIP.[2,10,11]

The third most common ILD pattern in RA is OP, which tends to be more aggressive and to determine more symptoms than does cryptogenic OP.[7,14] Tomographic features of OP vary and commonly include peripheral and peribronchovascular consolidations, ground-glass opacities, and, less frequently, nodules (Figure 3). A reversed halo sign, characterized by a central ground-glass area surrounded by a complete or incomplete ring of peripheral consolidation, and perilobular opacities may also be identified. These abnormalities are often fleeting or migratory.[10,11]

Lymphocytic interstitial pneumonia (LIP) is a benign lymphoproliferative ILD that may occur in patients with RA, but more commonly occurs in association with Sjögren's syndrome (SS). Because secondary SS is the most common extra-articular manifestation in RA, affecting approximately 35% of patients, cases of LIP in RA may be associated with SS.[15] LIP is part of a continuum of reactive

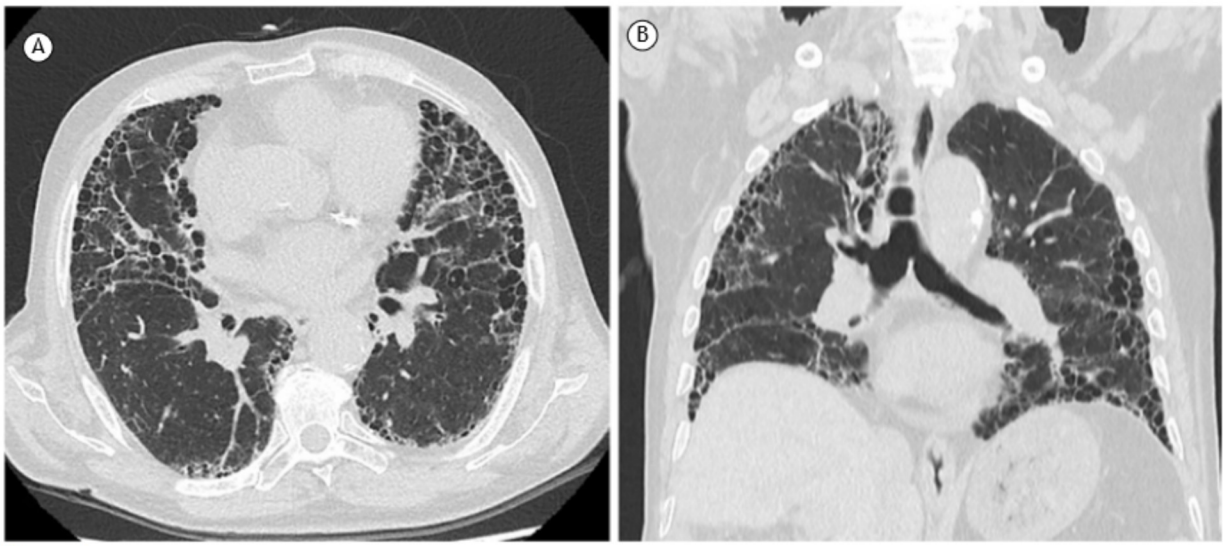

Figure 1. CT scans of an 87-year-old male patient with rheumatoid arthritis, usual interstitial pneumonia, and exuberant honeycombing. In A, axial reconstruction: large and predominantly peripheral cysts, and some areas with traction bronchiolectasis. In B, coronal reconstruction: lesions in the apicobasal axis.

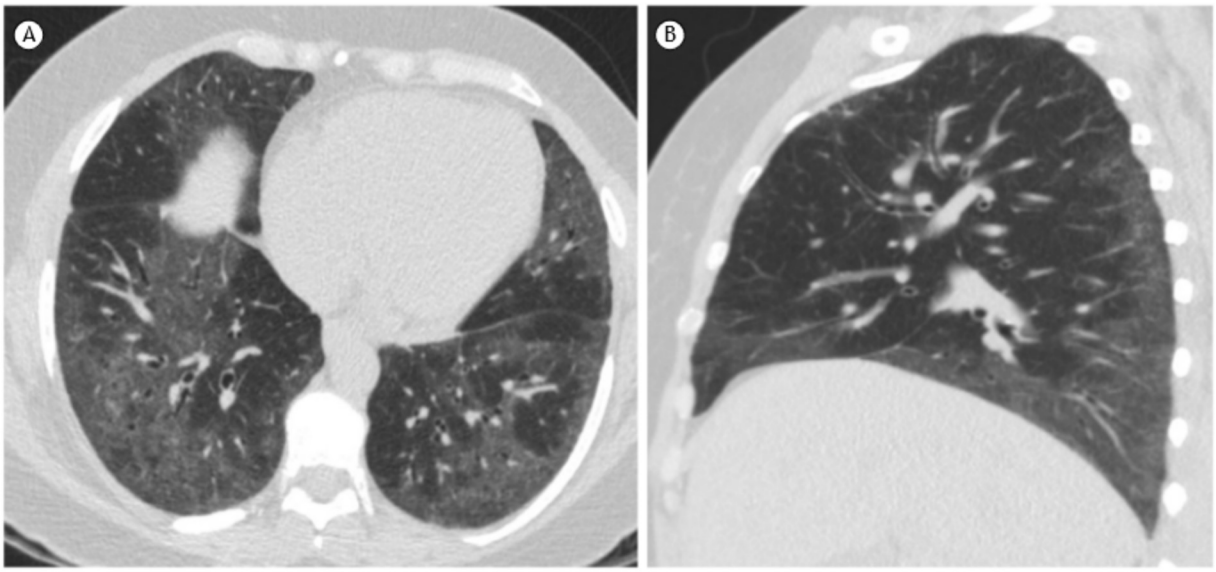

Figure 2. CT scans of a 37-year-old female patient with rheumatoid arthritis and nonspecific interstitial pneumonia. In A, axial reconstruction: diffuse ground-glass opacities and fine reticulation, predominantly in the lower lobes. In B, sagittal reconstruction showing subpleural sparing.

lymphoproliferation with follicular bronchiolitis. CT findings of LIP include lower lobe-predominant thin-walled cysts adjacent to vessels (perivascular distribution), with or without septal thickening and ground-glass opacities (Figure 4).[11,16]

Interstitial lung abnormalities (ILAs) and ILD are seen in up to 60% of individuals with RA, and some patients with such lesions may have disease progression with a significant impact on morbidity and mortality rates.[17,18] Estimates of the rate of imaging progression of ILAs range from 20% to 48% over five years. Additionally, the increase in the rate of mortality was most strongly associated with the imaging progression of ILAs, and specific imaging patterns indicative of pulmonary fibrosis were associated with earlier mortality.[19] Kawano-Dourado et al.,[17] in a retrospective study with patients with RA, quantified the initial CT pattern as compared to a second CT four years after the initial imaging. Of the 56 individuals with ILA/ILD, 21 (38%) had imaging evidence of disease progression. Subpleural distribution and higher baseline ILA/ILD extent were predictors of a higher risk of imaging progression. However, prospective longitudinal studies with patients with RA-ILA are necessary to better the understanding of the impact and the risk of progression of ILA.

Desquamative interstitial pneumonia (DIP) is a rare subtype of ILD. Although DIP is usually associated with exposure to tobacco smoke, some cases have been associated with autoimmune rheumatic diseases such as RA. Tomographic features of DIP[20] include ground-glass opacities with mild reticulation, basal and peripheral predominance, and, less frequently, cystic lesions (Figure 5).

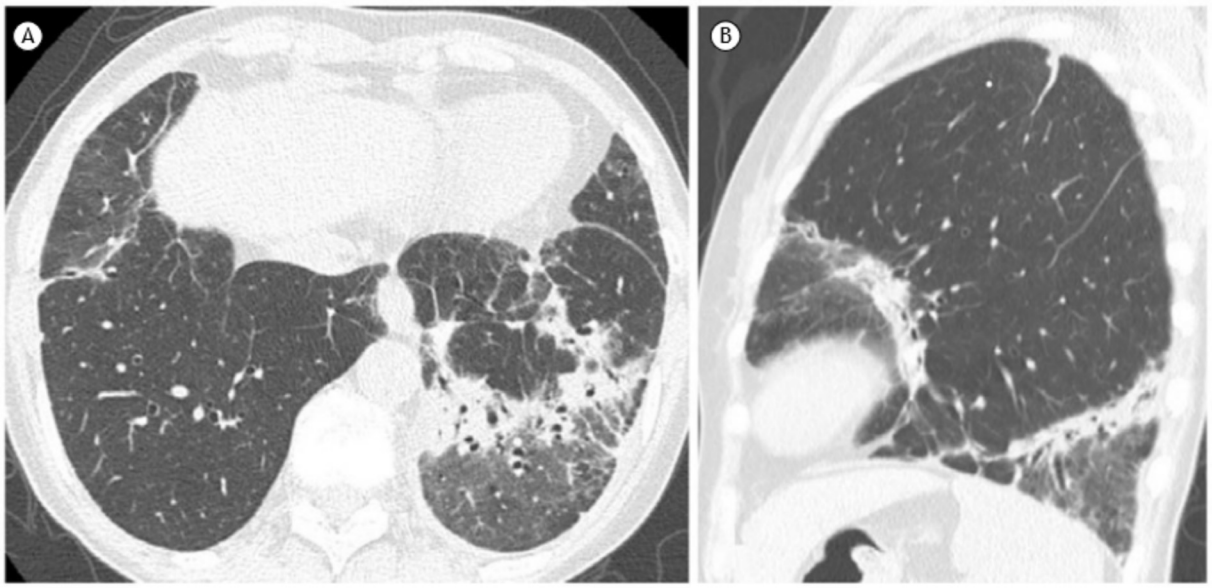

Figure 3. CT scans in axial (in A) and sagittal (in B) reconstructions of a male patient with rheumatoid arthritis. The scans demonstrate peripheral and peribronchovascular consolidations, which is compatible with organizing pneumonia.

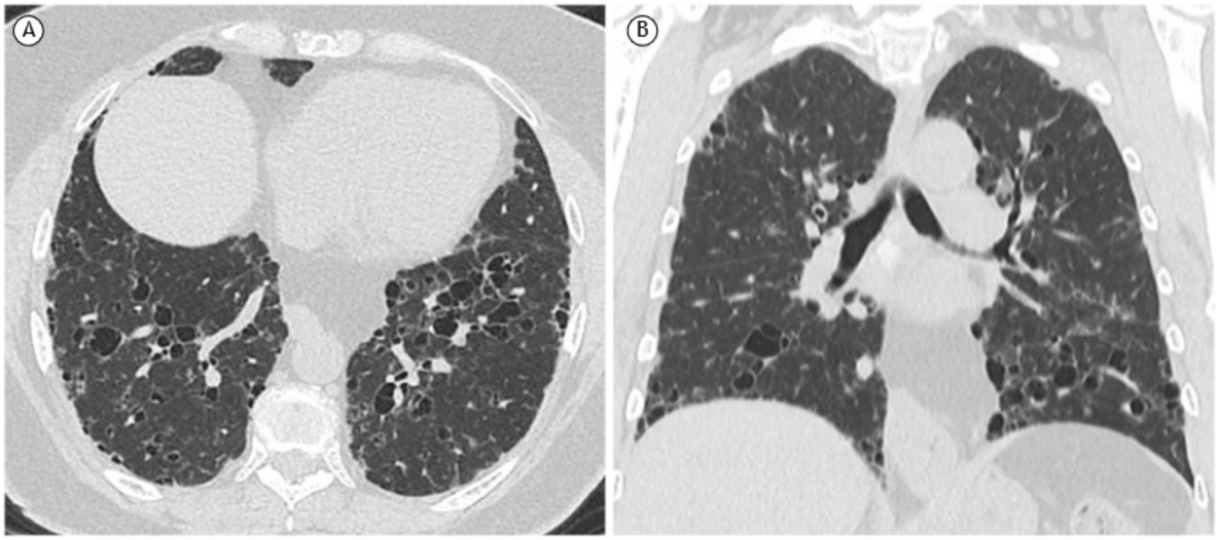

Figure 4. CT scans of a 60-year-old female patient with rheumatoid arthritis and lymphocytic interstitial pneumonia. Axial (in A) and coronal (in B) reconstructions show thin-walled cysts with variable sizes and discrete ground-glass opacities, predominating in the lower lobes and along the peribronchovascular bundle.

PLEURAL MANIFESTATIONS

Pleural disease is considered the most common thoracic manifestation in patients with RA and was identified in 73% of patients in a postmortem study.[21] However, most patients are asymptomatic, and few present with chest pain or dyspnea.[1,21] The most common pleural manifestations are effusions and pleurisy, with a prevalence of approximately 3% and 20%, respectively.[4]

Pleural effusion can occur due to pleural inflammation (Figure 6), infections, or RA-associated cardiac disease in patients with RA. Pleural effusions secondary to cardiac failure are usually bilateral, which is different from those secondary to pleural inflammation or infections, which are usually unilateral and present with small volume. Pleural effusion associated with inflammation is usually exudative with low glucose levels (≤ 25 mg/dL), low pH levels (< 7.3), high LDH levels (> 700 IU/L), high rheumatoid factor titers, and low total complement activity levels, as well as low C3 and C4 levels. Chronic pleural inflammation may result in pleural involvement with thickening of both parietal and visceral pleurae, which is quite similar to empyema. Pleural involvement can also be nodular, mimicking neoplasms.[4]

Pleural effusion may be transient, persistent, or relapsing, and when untreated or recurrent, pleuritis can lead to pleural fibrosis, trapped lung, and lung restriction.[1] Bronchopleural fistulae and pneumothorax are other less common findings that are usually associated with the rupture of rheumatoid lung nodules. Bronchopleural fistulae, immunosuppression, and chronic pleural disease fistulae increase the risk of empyema.[1,4]

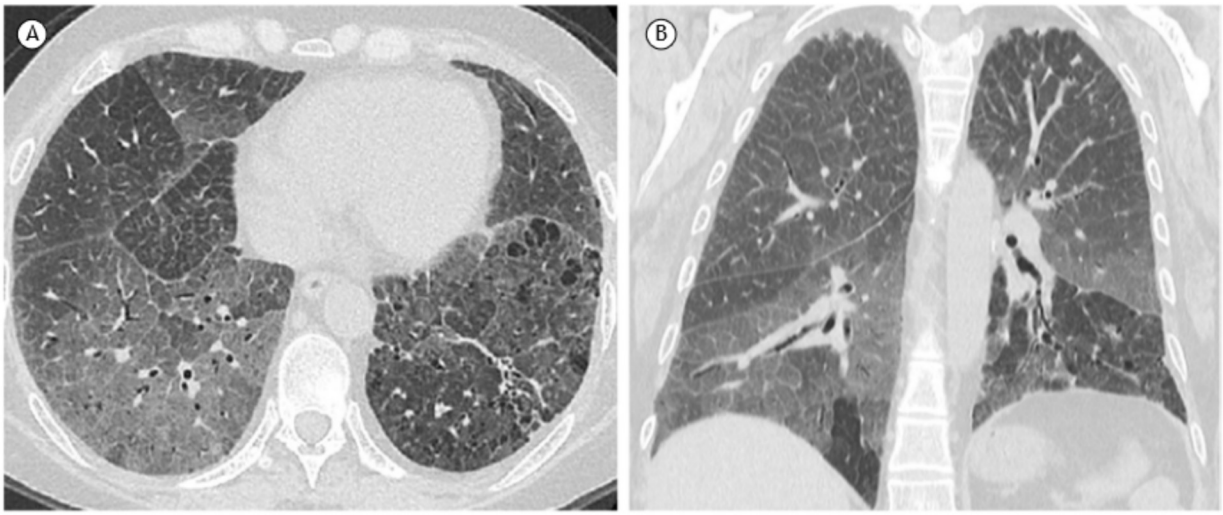

Figure 5. CT scans of a 45-year-old female patient with rheumatoid arthritis and desquamative interstitial pneumonia. Axial (in A) and coronal (in B) reconstructions demonstrate diffuse ground-glass opacities, interlobular septal thickening, and cysts, predominating in the lower lobes.

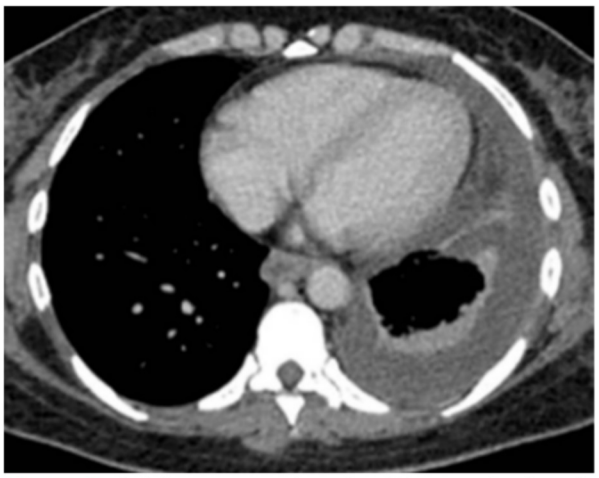

Figure 6. Axial reconstruction of a CT scan of a female patient with a left pleural effusion secondary to rheumatoid arthritis.

PAH

In patients with RA, PAH may be seen in isolation or in association with ILD. It is rare as an isolated finding in RA and is more common in older patients with long-standing ILD. PAH can lead to chronic respiratory failure and right heart failure, and it rarely occurs secondary to RA vasculitis.[1,4,22]

Direct CT findings of PAH are enlarged pulmonary arteries, main pulmonary artery diameter to ascending aorta diameter ratio > 1, dilatation of right-sided cardiac chambers, and right ventricular hypertrophy. Indirect signs in the lungs may be identified, such as mosaic attenuation, indicating regional differences in pulmonary perfusion.[1,4]

RHEUMATOID LUNG NODULES

Rheumatoid lung nodules or necrobiotic lung nodules are described in up to 20% of RA patients and are usually associated with subcutaneous nodules. Patients are frequently asymptomatic but may develop symptoms if nodules cavitate to the pleural space. Rheumatoid lung nodules are characterized on CT scans as round opacities, from few millimeters to several centimeters in size, typically located in the subpleural region, and are usually multiple and cavitated (Figure 7A).[23,24]

Because rheumatoid lung nodules have radiological characteristics quite similar to those of granulomatous and neoplastic diseases, they may represent a diagnostic challenge. Imaging features more commonly associated with rheumatoid lung nodules as compared to malignancy include multiplicity, smooth border, cavitation, satellite nodules, and pleural contact.[4,23] Histologically, rheumatoid nodules are composed of central fibrinoid necrosis surrounded by palisading epithelioid histiocytes and peripheral, chronic inflammatory cells.

The risk of malignancy in RA, such as primary lung cancer and lymphoproliferative disorders, particularly diffuse B-cell lymphoma, is overall 10% higher in comparison with that observed in the general population. Higher rates of malignancy may be explained by RA host factors, such as immune-mediated mechanisms, inflammation, viruses, and genetic predispositions, and non-RA risk factors, such as smoking, chronic lung inflammation, and pulmonary fibrosis.[4] Adenocarcinoma is the most common histopathological pattern of lung cancer in patients with RA,[23] followed by squamous cell carcinoma and small cell carcinoma (Figures 7B and 7C).

Caplan syndrome

Caplan syndrome (rheumatoid pneumoconiosis) was first described in a large cohort of coal miners with RA in 1953,[24] and it can be associated with exposure to coal, asbestos, or silica. The prevalence is less than 1% in the USA in autopsy series[25] and is more common in patients with silicosis. The disease is

characterized by the presence of multiple peripheral rheumatoid lung nodules and may precede the onset of arthritis by more than ten years. Radiographically, nodules tend to form rapidly and persist over years, approximately 10% of which developing cavitations or calcifications.[7] The nodules vary from 0.5 to 5 cm and may coalesce (Figure 7D).[4]

Most patients with Caplan syndrome are asymptomatic, and there is no impact on their pulmonary function test results.[3] Although a causal link between RA and dust exposure has not been completely established, it has been hypothesized that exposure to foreign particles leads to chronic immune activity that might facilitate the formation of autoantibodies, promoting the occurrence of RA. Indeed, pneumoconiosis may be associated with increased formation of immune complexes and increased rheumatoid factor levels, even without a definitive autoimmune diagnosis. The question of individual susceptibility remains unanswered.[2,26]

AIRWAY DISEASE

Bronchiectasis

Previous studies described bronchiectasis in 30-40% of RA patients.[4,27] Since bronchiectasis may be clinically silent, the real prevalence may be even greater (Figure 8). Chronic suppurative infections, treatment with disease modifying anti-rheumatic drugs, and genetic predisposition are some of the hypotheses associated with the development of bronchiectasis. Of note, a higher mortality rate was described in patients with RA and bronchiectasis than in those with either condition alone.[27]

Bronchiolitis

Constrictive and follicular bronchiolitis may occur in patients with RA. Constrictive bronchiolitis, also known as obliterative bronchiolitis, is characterized by bronchiolar inflammation with submucosal peribronchial fibrosis associated with luminal stenosis and occlusion. Although uncommon, it is a severe and

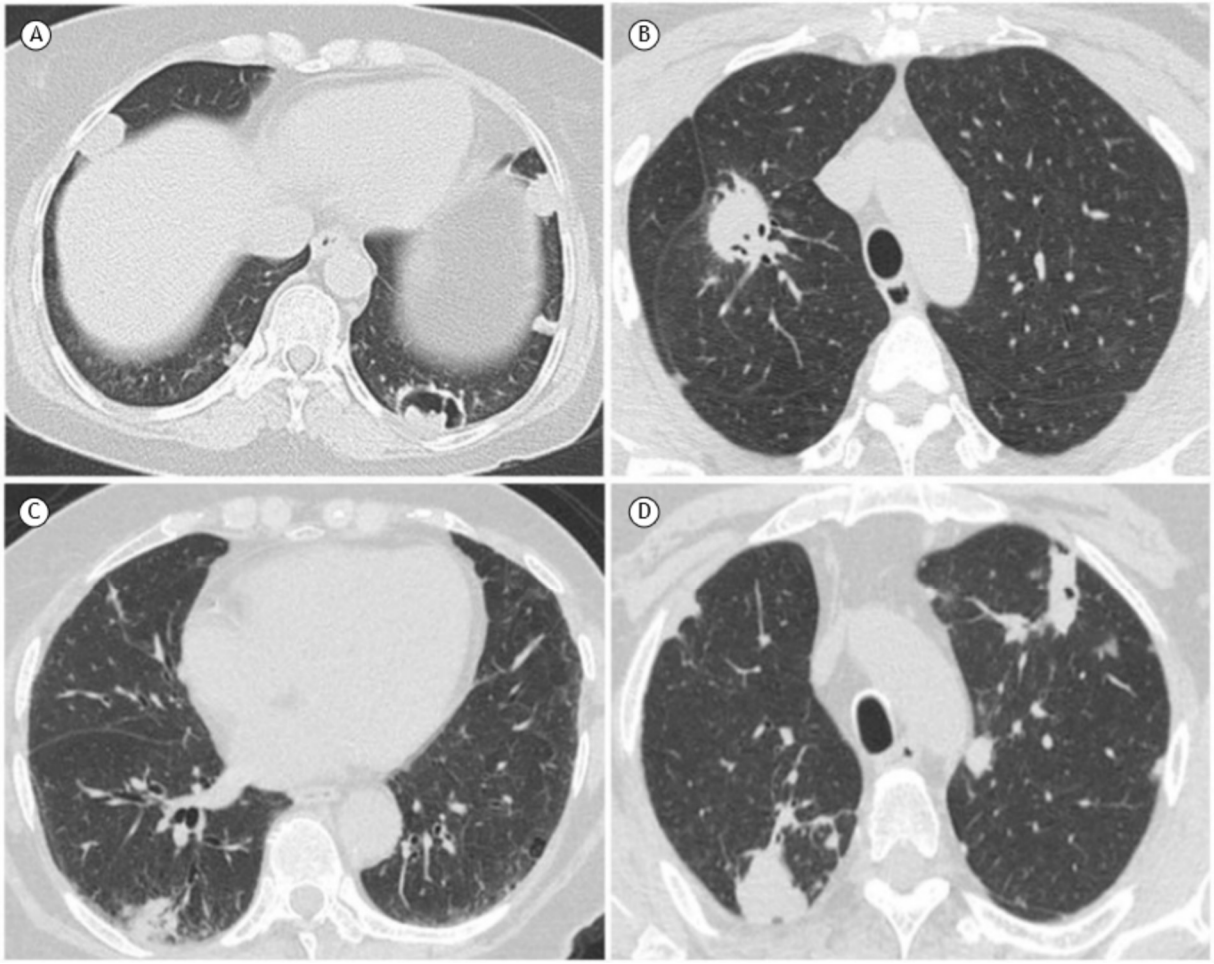

Figure 7. In A, a CT scan in axial reconstruction of a 50-year-old female patient with rheumatoid arthritis shows multiple bilateral subpleural nodules, the largest one being cavitated in the left lower lobe, which is compatible with rheumatoid nodules. In B, a CT scan in axial reconstruction of a patient with rheumatoid arthritis demonstrates a pulmonary nodule in the upper right lobe. Histopathological analysis was compatible with lung adenocarcinoma. In C, a CT scan in axial reconstruction of a patient with rheumatoid arthritis shows a pulmonary nodule in the lower right lobe. Histopathological analysis was compatible with lung adenocarcinoma. In D, a CT scan in axial reconstruction of a 68-year-old male patient with rheumatoid arthritis and Caplan syndrome demonstrates subpleural nodules predominantly in the upper lobes, one with central cavitation.

potentially fatal condition. Constrictive bronchiolitis in RA is more common in females and in those with positive rheumatoid factor results and long-standing untreated disease, but it may also occur secondary to use of medications, including sulfasalazine.[2,27] Patients usually develop progressive dyspnea, cough, and bronchorrhea, and it may occur in the absence of other systemic symptoms.[27] Pulmonary function tests usually show airflow obstruction and air trapping. Tomographic findings include bronchial wall thickening, bronchiectasis, and a mosaic attenuation pattern, with areas of decreased lung attenuation representing air trapping (Figure 9A). Additional expiratory CT images are helpful in this setting to confirm the presence of air trapping.[4]

Follicular bronchiolitis is characterized by reactive hyperplasia of bronchus-associated lymphoid tissue. It is usually secondary to autoimmune rheumatic diseases, mainly RA and SS, and has good prognosis. Tomographic features of follicular bronchiolitis include small centrilobular nodules with branching structures (tree-in-bud sign), corresponding to bronchial dilation, wall thickening, and mucoid impaction (Figure 9B). Air trapping and peribronchovascular and septal thickening may also be seen and correspond to proliferative lymphatic tissue.[4,27]

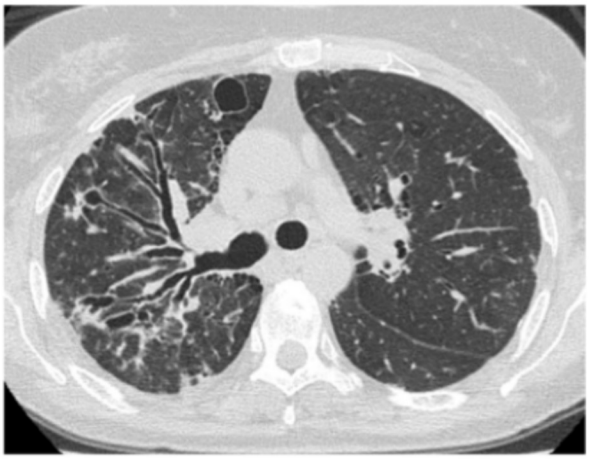

Figure 8. A CT scan in axial reconstruction of a 54-year-old female patient with rheumatoid arthritis demonstrates cylindrical, varicose, and cystic bronchiectasis in the right lung.

Lymphadenopathy

Axillary and mediastinal lymph node enlargement may occur in 20-70% of patients with RA, especially in those with RA-ILD.[4,28] The biology underpinning this enlargement remains unclear. However, migration of immune cells from the peripheral circulation through mediastinal lymph nodes to the lungs has been suggested to contribute to pulmonary fibrosis.[29] Furthermore, patients with either mediastinal or axillary lymphadenopathy showed significantly higher simple disease activity index than did those with no lymphadenopathy, which is a valid and sensitive tool to assess disease activity in patients with RA. Therefore, lymphadenopathy may be associated with signs of inflammatory activity in RA and is usually mild (Figure 10). Although lymphadenopathy in RA patients is mostly part of an inflammatory process, it is essential to exclude the presence of a malignant process or sarcoid reaction in those using TNF-α inhibitors.[4,30]

DILD

DILD in patients with RA can occur by immune-mediated reactions related to the mechanism of action of the drug or due to its direct toxicity and is usually associated with use of disease-modifying antirheumatic drugs and nonsteroidal anti-inflammatory agents.[1,4] The onset of DILD can be within days or years after treatment initiation with the suspected drug, but symptoms are nonspecific. The most common radiologic patterns of drug toxicity are: hypersensitivity reaction, resembling hypersensitivity pneumonitis,

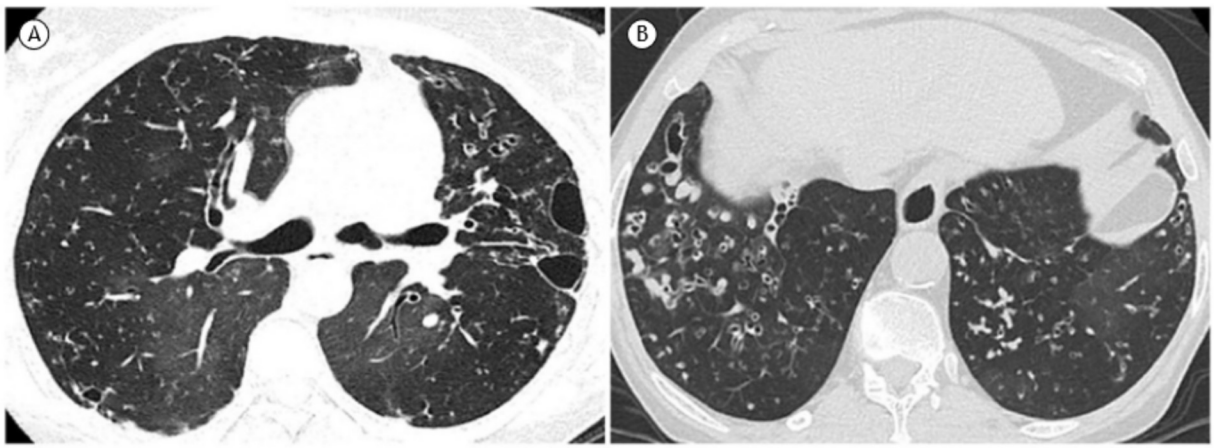

Figure 9. In A, a CT scan in axial reconstruction of a 60-year-old female patient with rheumatoid arthritis and constrictive bronchiolitis demonstrates bronchial wall thickening, bilateral centrilobular opacities, bronchiectasis, and mosaic attenuation pattern, compatible with air trapping. In B, a CT scan in axial reconstruction of a 50-year-old female patient with rheumatoid arthritis and follicular bronchiolitis shows diffuse small centrilobular nodules, tree-in-bud opacities, some bronchiolectasis, and bronchiolar wall thickening, predominating in the lower lung zones.

eosinophilic pneumonia, pulmonary edema, OP, and DAD. The diagnosis is based on clinical and imaging findings, as well as the time between treatment initiation and drug discontinuation and, less frequently, on histopathological findings. The main differential diagnoses include RA-ILD progression or exacerbation, infection, and cardiogenic pulmonary edema.[4]

Methotrexate-induced lung disease is the archetype of drug-induced pulmonary toxicity in patients with RA, usually occurring early with the beginning of therapy. The most common CT and histologic findings of methotrexate-induced lung disease are similar to those of hypersensitivity pneumonitis (Figures 11A and 11B). Other patterns include OP and DAD. Symptoms usually improve with drug discontinuation.[4] In a case-control study[31] with discovery and international replication samples, the association of methotrexate exposure with ILD was evaluated in 410 patients with chronic fibrotic ILD associated with RA (RA-ILD), and 673 patients with RA without ILD. The results suggested that methotrexate use was not associated with an increased risk of RA-ILD in patients with RA and that ILD was often detected later in methotrexate-treated patients.[31]

The use of TNF-α inhibitors is frequently associated with infectious and noninfectious granulomatous lung disease, DAD, and, less often, pulmonary fibrosis. Sarcoidosis-like disease in patients with RA is more common in those that received etanercept. Tomographic features are similar to the typical findings of sarcoidosis, including micronodules and lymphadenopathy (Figures 11C and 11D). Another pattern that can occur is OP, associated with DAD or as a distinct DILD. Rituximab is used in patients with an inadequate TNF-α inhibitor response and can also lead to DAD and OP.[4]

Leflunomide can lead to ILD exacerbation, accelerated formation of pulmonary rheumatoid nodules, and diffuse alveolar hemorrhage. Nonsteroidal anti-inflammatory drugs, including ibuprofen, aspirin, and acetaminophen, have been reported as potential etiologies for DILD and may present as allergic-type reactions, such as eosinophilic pneumonia and pulmonary edema.[1,4]

FINAL CONSIDERATIONS

It is essential to evaluate the presence of respiratory symptoms and objective pleuropulmonary involvement regularly in patients with RA due to the high prevalence of pleuropulmonary manifestations and their potential to increase morbidity and mortality. ILD is associated with worse prognosis, mainly the UIP pattern.

CT is an indispensable tool to evaluate the several potential pleuropulmonary manifestations that may occur in patients with RA and often allows the establishment of a diagnosis without the need of histopathological analysis. The widespread use of CT increased the identification of such manifestations, although the differential diagnoses are variable and often challenging, including infections, DILD, and neoplasms.

AUTHOR CONTRIBUTIONS

GPB and MVYS: study design; data collection; data analysis; and drafting and review of the manuscript. MW: data collection; data analysis; and drafting and review of the manuscript. LVSS: data collection; and drafting and review of the manuscript. RAK and LKD: data analysis; and drafting and review of the manuscript. BGB: guarantor of the study; study design; data collection; data analysis; and drafting and review of the manuscript. All authors read and approved the final version of the manuscript.

CONFLICTS OF INTEREST

None declared.

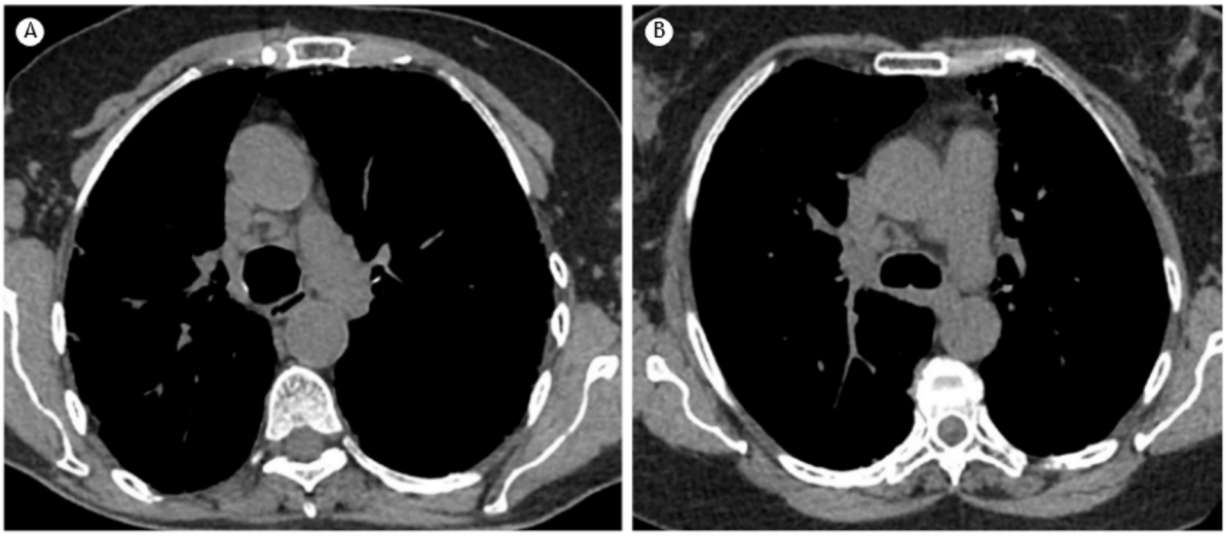

Figure 10. CT scans in axial reconstructions of a 64-year-old female patient with rheumatoid arthritis show mediastinal lymph node enlargement.

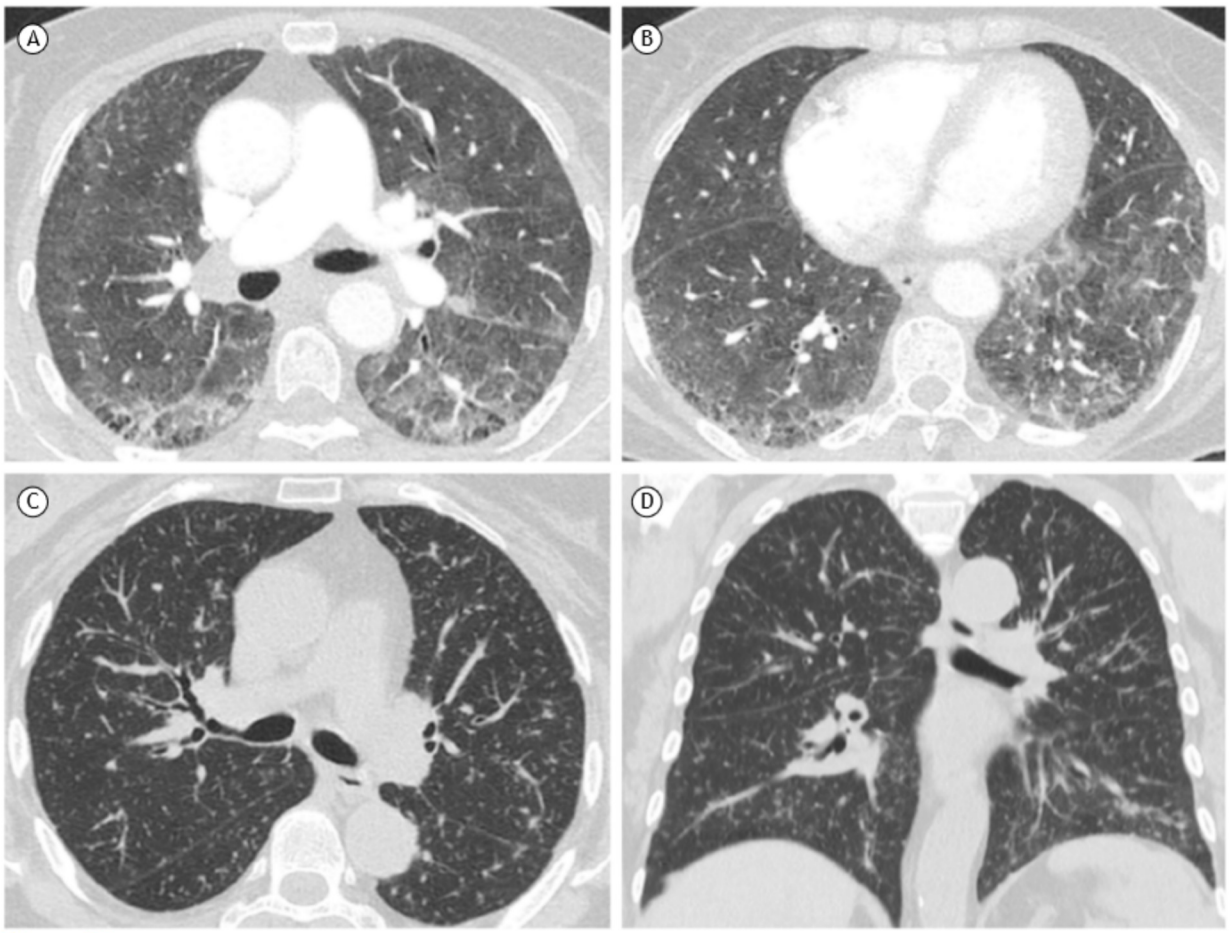

Figure 11. Drug-induced lung disease. In A and B, CT scans in axial reconstructions of a patient with rheumatoid arthritis and lung toxicity associated with the use of methotrexate demonstrate diffuse ground-glass opacities, compatible with hypersensitivity reaction. In C and D, CT scans in axial reconstructions of a patient with rheumatoid arthritis and sarcoid-like reaction associated with the use of TNF-α inhibitor demonstrate diffuse, predominantly perilymphatic, micronodules.

REFERENCES

1. Chansakul T, Dellaripa PF, Doyle TJ, Madan R. Intra-thoracic rheumatoid arthritis: Imaging spectrum of typical findings and treatment related complications. Eur J Radiol. 2015;84(10):1981-1991. https://doi.org/10.1016/j.ejrad.2015.07.008
2. Kadura S, Raghu G. Rheumatoid arthritis-interstitial lung disease: manifestations and current concepts in pathogenesis and management. Eur Respir Rev. 2021;30(160):210011. https://doi.org/10.1183/16000617.0011-2021
3. Esposito AJ, Chu SG, Madan R, Doyle TJ, Dellaripa PF. Thoracic Manifestations of Rheumatoid Arthritis. Clin Chest Med. 2019;40(3):545-560. https://doi.org/10.1016/j.ccm.2019.05.003
4. Groner LK, Green DB, Weisman SV, Legasto AC, Toy D, Gruden JF, et al. Thoracic Manifestations of Rheumatoid Arthritis. Radiographics. 2021;41(1):32-55. https://doi.org/10.1148/rg.2021200091
5. Duarte AC, Porter JC, Leandro MJ. The lung in a cohort of rheumatoid arthritis patients-an overview of different types of involvement and treatment. Rheumatology (Oxford). 2019;58(11):2031-2038. https://doi.org/10.1093/rheumatology/kez177
6. Doyle TJ, Dellaripa PF, Rosas IO. Risk Factors and Biomarkers of RA-ILD. In: Fischer A, Lee JS, editors. Lung disease in rheumatoid arthritis. Cham: Springer International Publishing; 2018. p. 59-72. https://doi.org/10.1007/978-3-319-68888-6_5
7. Marigliano B, Soriano A, Margiotta D, Vadacca M, Afeltra A. Lung involvement in connective tissue diseases: a comprehensive review and a focus on rheumatoid arthritis. Autoimmun Rev. 2013;12(11):1076-1084. https://doi.org/10.1016/j.autrev.2013.05.001
8. Kawano-Dourado L, Bonfiglioli K. Heterogeneity in rheumatoid arthritis-associated interstitial lung disease: time for splitting? J Bras Pneumol. 2022;48(6):e20220426. https://doi.org/10.36416/1806-3756/e20220426
9. Kristen Demoruelle M, Olson AL, Solomon JJ. The epidemiology of rheumatoid arthritis-associated lung disease. In: Fischer A, Lee JS, editors. Lung Disease in Rheumatoid Arthritis. Cham: Springer International Publishing; 2018. p. 45-58. https://doi.org/10.1007/978-3-319-68888-6_4
10. Walsh S. Thoracic imaging in rheumatoid arthritis. In: Fischer A, Lee JS, editors. Lung Disease in Rheumatoid Arthritis. Cham: Springer International Publishing; 2018. p. 73-91. https://doi.org/10.1007/978-3-319-68888-6_6
11. Kusmirek JE, Kanne JP. Thoracic Manifestations of Connective Tissue Diseases. Semin Ultrasound CT MR. 2019;40(3):239-254. https://doi.org/10.1053/j.sult.2018.12.003
12. Chung JH, Cox CW, Montner SM, Adegunsoye A, Oldham JM, Husain AN, et al. Features of the Usual Interstitial Pneumonia Pattern: Differentiating Connective Tissue Disease-Associated Interstitial Lung Disease From Idiopathic Pulmonary Fibrosis. AJR Am J Roentgenol. 2018;210(2):307-313. https://doi.org/10.2214/AJR.17.18384
13. Spagnolo P, Lee JS, Sverzellati N, Rossi G, Cottin V. The Lung in Rheumatoid Arthritis: Focus on Interstitial Lung Disease. Arthritis Rheumatol. 2018;70(10):1544-1554. https://doi.org/10.1002/art.40574
14. Gono T. Comprehensive understanding of interstitial lung disease in rheumatoid arthritis. In: Gono T, Tokuda H, Sakai F, Takemura T, editors. Lung Disease Associated with Rheumatoid Arthritis. Singapore: Springer Singapore; 2018. p. 81-90. https://doi.org/10.1007/978-981-10-6750-1_6
15. Doyle TJ, Dellaripa PF. Lung Manifestations in the Rheumatic Diseases. Chest. 2017;152(6):1283-1295. https://doi.org/10.1016/j.chest.2017.05.015
16. Baldi BG, Carvalho CRR, Dias OM, Marchiori E, Hochhegger B. Diffuse cystic lung diseases: differential diagnosis. J Bras

Pneumol. 2017;43(2):140-149. https://doi.org/10.1590/s1806-37562016000000341

17. Kawano-Dourado L, Doyle TJ, Bonfiglioli K, Sawamura MVY, Nakagawa RH, Arimura FE, et al. Baseline Characteristics and Progression of a Spectrum of Interstitial Lung Abnormalities and Disease in Rheumatoid Arthritis. Chest. 2020;158(4):1546-1554. https://doi.org/10.1016/j.chest.2020.04.061
18. Dong H, Julien PJ, Demoruelle MK, Deane KD, Weisman MH. Interstitial lung abnormalities in patients with early rheumatoid arthritis: A pilot study evaluating prevalence and progression. Eur J Rheumatol. 2018;6(4):193-198. https://doi.org/10.5152/eurjrheum.2019.19044
19. Hatabu H, Hunninghake GM, Richeldi L, Brown KK, Wells AU, Remy-Jardin M, et al. Interstitial lung abnormalities detected incidentally on CT: a Position Paper from the Fleischner Society. Lancet Respir Med. 2020;8(7):726-737. https://doi.org/10.1016/S2213-2600(20)30168-5
20. Hellemons ME, Moor CC, von der Thüsen J, Rossius M, Odink A, Thorgersen LH, et al. Desquamative interstitial pneumonia: a systematic review of its features and outcomes [published correction appears in Eur Respir Rev. 2020 Aug 4;29(157):]. Eur Respir Rev. 2020;29(156):190181. https://doi.org/10.1183/16000617.0181-2019
21. Toyoshima H, Kusaba T, Yamaguchi M. Cause of death in autopsied RA patients [Article in Japanese]. Ryumachi. 1993;33(3):209-214.
22. Baqir M, Ryu JH. The Non-ILD Pulmonary manifestations of RA. In: Fischer A, Lee JS, editors. Lung Disease in Rheumatoid Arthritis. Cham, Switzerland: Humana, 2018; p. 163-173. https://doi.org/10.1007/978-3-319-68888-6_10
23. Koslow M, Young JR, Yi ES, Baqir M, Decker PA, Johnson GB, et al. Rheumatoid pulmonary nodules: clinical and imaging features compared with malignancy. Eur Radiol. 2019;29(4):1684-1692. https://doi.org/10.1007/s00330-018-5755-x
24. Shaw M, Collins BF, Ho LA, Raghu G. Rheumatoid arthritis-associated lung disease. Eur Respir Rev. 2015;24(135):1-16. https://doi.org/10.1183/09059180.00008014
25. CAPLAN A. Certain unusual radiological appearances in the chest of coal-miners suffering from rheumatoid arthritis. Thorax. 1953;8(1):29-37. https://doi.org/10.1136/thx.8.1.29
26. Schreiber J, Koschel D, Kekow J, Waldburg N, Goette A, Merget R. Rheumatoid pneumoconiosis (Caplan's syndrome). Eur J Intern Med. 2010;21(3):168-172. https://doi.org/10.1016/j.ejim.2010.02.004
27. Lieberman-Maran L, Orzano IM, Passero MA, Lally EV. Bronchiectasis in rheumatoid arthritis: report of four cases and a review of the literature–implications for management with biologic response modifiers. Semin Arthritis Rheum. 2006;35(6):379-387. https://doi.org/10.1016/j.semarthrit.2006.02.003
28. Tyker A, Ventura IB, Lee CT, Strykowski R, Garcia N, Guzy R, et al. High-titer rheumatoid factor seropositivity predicts mediastinal lymphadenopathy and mortality in rheumatoid arthritis-related interstitial lung disease. Sci Rep. 2021;11(1):22821. https://doi.org/10.1038/s41598-021-02066-9
29. Adegunsoye A, Oldham JM, Bonham C, Hrusch C, Nolan P, Klejch W, et al. Prognosticating Outcomes in Interstitial Lung Disease by Mediastinal Lymph Node Assessment. An Observational Cohort Study with Independent Validation. Am J Respir Crit Care Med. 2019;199(6):747-759. https://doi.org/10.1164/rccm.201804-0761OC
30. Okabe Y, Aoki T, Terasawa T, Kinoshita S, Nakayamada S, Tanaka Y, et al. Mediastinal and axillar lymphadenopathy in patients with rheumatoid arthritis: prevalence and clinical significance. Clin Imaging. 2019;55:140-143. https://doi.org/10.1016/j.clinimag.2019.02.014
31. Juge PA, Lee JS, Lau J, Kawano-Dourado L, Rojas Serrano J, Sebastiani M, et al. Methotrexate and rheumatoid arthritis associated interstitial lung disease. Eur Respir J. 2021;57(2):2000337. https://doi.org/10.1183/13993003.00337-2020

Revista da Sociedade Brasileira de Medicina Tropical
Journal of the Brazilian Society of Tropical Medicine
Vol.:57 | (e00917-2024) | 2024
https://doi.org/10.1590/0037-8682-0168-2024

Images in Infectious Diseases

Pulmonary mucormycosis in a patient with uncontrolled diabetes

Luciana Volpon Soares Souza[1], *Arthur Soares Souza Jr*[1],[2], *Gláucia Zanetti*[3] and *Edson Marchiori*[3]

[1]. Ultra X, São José do Rio Preto,SP, Brasil.
[2]. Faculdade de Medicina de São José do Rio Preto, SP, Brasil.
[3]. Universidade Federal do Rio de Janeiro, Rio de Janeiro, RJ, Brasil.

A 54-year-old obese woman with uncontrolled diabetes mellitus (glycemia, 644 mg/dL; glycated hemoglobin, 21.7%) presented with a 2-week history of fever and cough. The serological test results for human immunodeficiency virus infection were negative.

Chest radiography performed on admission showed nonhomogeneous consolidations in both lungs (**Figure 1A**). Chest computed tomography revealed multiple reversed halo signs (RHSs) in both lungs, with low attenuation areas inside the halos and thick outer rims of consolidation (**Figure 1B, C**). A pulmonary biopsy revealed yeast and hyphae suggestive of mucormycosis (**Figure 1D**). Therefore, the patient was diagnosed with pulmonary mucormycosis. The patient had a poor prognosis and died 8 days after admission.

Pulmonary mucormycosis, previously known as zygomycosis, is a severe, invasive lung infection caused by filamentous fungi belonging to the order Mucorales. It occurs almost exclusively in diabetic and immunocompromised patients and has a mortality rate exceeding 50%[1,2].

The clinical signs and imaging findings of pulmonary mucormycosis are nonspecific, although the presence of RHS in patients with neutropenia is highly suggestive of the disease. Some morphological characteristics of RHS contribute to diagnostic suspicion. Reticulation inside an RHS with an outer consolidation rim > 1 cm thick, strongly suggests invasive fungal infections, particularly pulmonary mucormycosis[3-5]. Although the definitive diagnosis should be based on a biopsy, with the identification of hyphae in infected tissues, the presence of an RHS with these morphological characteristics should be sufficient for the early initiation of appropriate therapy, thereby improving the outcome.

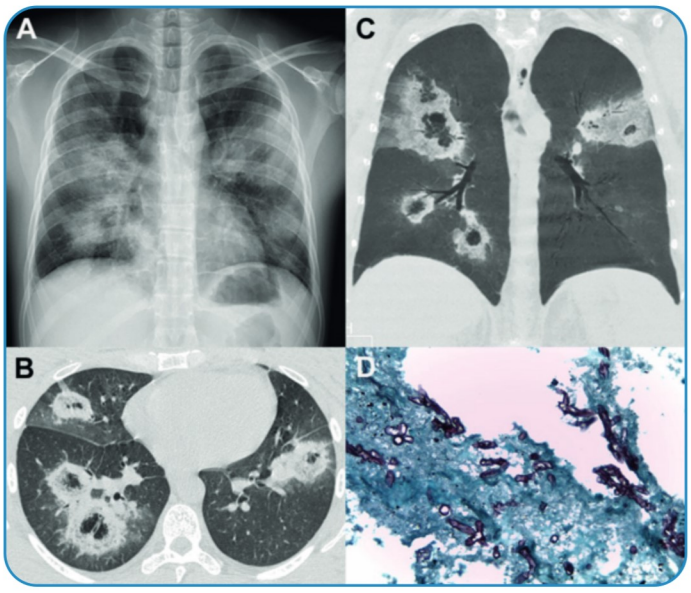

FIGURE 1: (A) Chest radiograph showing rounded focal consolidations with hypertransparent centers in both lungs. Chest computed tomography images with axial **(B)** and coronal reconstruction with minimum intensity projection **(C)**, demonstrating multiple reversed halo signs in both lungs, with low-attenuation areas inside the halos and thick outer rims of consolidation. **(D)** Grocott's special stain identifying the presence of fungal hyphae, confirming the diagnosis of mucormycosis (×100).

Dr. Edson Marchiori. **e-mail:** edmarchiori@gmail.com

Authors' contribution: All authors contributed significantly to the work, and have read the manuscript and approved its submission. ASSJr and GZ took part in conception of the manuscript and data acquisition. LVSS and EM contributed to the analysis and interpretation of data. LVSS drafted the manuscript and reviewed the literature. All authors gave final approval of the version to be published.

Conflic of Interest: The authors declare that they have no conflicts of interest to express.

Financial Support: None.

Received 19 May 2024 - **Accepted** 27 May 2024

REFERENCES

1. Agrawal R, Yeldandi A, Savas H, Parekh ND, Lombardi PJ, Hart EM. Pulmonary Mucormycosis: Risk Factors, Radiologic Findings, and Pathologic Correlation. Radiographics. 2020;40(3):656-66. Available from: https://doi.org/10.1148/rg.2020190156
2. Danion F, Coste A, Le Hyaric C, Melenotte C, Lamoth F, Calandra T, et al. What Is New in Pulmonary Mucormycosis? J Fungi (Basel). 2023;9(3):307. Available from: https://doi.org/10.3390/jof9030307
3. Hammer MM, Madan R, Hatabu H. Pulmonary Mucormycosis: Radiologic Features at Presentation and Over Time. AJR Am J Roentgenol. 2018;210(4):742-7. Available from: https://doi.org/10.2214/AJR.17.18792
4. Marchiori E, Hochhegger B, Zanetti G. Importance of the reversed halo sign for diagnosis of mucormycosis. Lancet Infect Dis. 2020;20(5):538. Available from: https://doi.org/10.1016/S1473-3099(20)30266-8
5. Marchiori E, Marom EM, Zanetti G, Hochhegger B, Irion KL, Godoy MC. Reversed Halo Sign in Invasive Fungal Infections: Criteria for Differentiation from Organizing Pneumonia. Chest 2012; 142(6):1469–73. Available from: https://doi.org/10.1378/chest.12-0114

BJR

https://doi.org/10.1259/bjr.20220235

Received: 25 February 2022 | Revised: 09 August 2022 | Accepted: 30 August 2022 | Published online: 13 October 2022

Cite this article as:
Hochhegger B, Zanon M, Patel PP, Verma N, Eifer DA, Torres PPTeS, et al. The diagnostic value of magnetic resonance imaging compared to computed tomography in the evaluation of fat-containing thoracic lesions. *Br J Radiol* (2022) 10.1259/bjr.20220235.

REVIEW ARTICLE

The diagnostic value of magnetic resonance imaging compared to computed tomography in the evaluation of fat-containing thoracic lesions

[1,2]BRUNO HOCHHEGGER, MD, PhD, [1]MATHEUS ZANON, MD, [2]PRATIK P PATEL, MD, [2]NUPUR VERMA, MD, [1]DIEGO ANDRÉ EIFER, MD, [1]PEDRO PAULO TEIXEIRA E SILVA TORRES, MD, [3]ARTHUR S SOUZA, MD, PhD, [3]LUCIANA VOLPON SOARES SOUZA, MD, [2]TAN-LUCIEN MOHAMMED, MD, [4]EDSON MARCHIORI, MD, PhD and [5]JEANNE B ACKMAN, MD

[1]Department of Radiology, Hospital São Lucas, Pontificia Universidade Catolica do Rio Grande do Sul - Av. Ipiranga, Porto Alegre, Brazil
[2]Department of Radiology, College of Medicine, University of Florida, Gainesville, United States
[3]Department of Radiology, Rio Preto Radiodiagnostic Intitute – R. Cila, São José do Rio Preto, Brazil
[4]Department of Radiology, Federal University of Rio de Janeiro - Av. Carlos Chagas Filho, Rio de Janeiro, Brazil
[5]Department of Radiology, Division of Thoracic Imaging and Intervention, Massachusetts General Hospital and Harvard Medical School - Founders House, Boston, United States

Address correspondence to: Mr Matheus Zanon
E-mail: *mhgzanon@hotmail.com*

ABSTRACT

Intrathoracic fat-containing lesions may arise in the mediastinum, lungs, pleura, or chest wall. While CT can be helpful in the detection and diagnosis of these lesions, it can only do so if the lesions contain *macro*scopic fat. Furthermore, because CT cannot demonstrate microscopic or intravoxel fat, it can fail to identify and diagnose microscopic fat-containing lesions. MRI, employing spectral and chemical shift fat suppression techniques, can identify both macroscopic and microscopic fat, with resultant enhanced capability to diagnose these intrathoracic lesions non-invasively and without ionizing radiation. This paper aims to review the CT and MRI findings of fat-containing lesions of the chest and describes the fat-suppression techniques utilized in their assessment.

INTRODUCTION

Intrathoracic fat-containing lesions may arise in the mediastinum, lungs, pleura, or chest wall. CT can be helpful in the detection and diagnosis of these lesions.[1] However, CT is solely able to identify *macroscopic* fat-containing lesions that contain tissue similar in attenuation to the subcutaneous fat of the chest wall.[1] Because CT cannot demonstrate microscopic or intravoxel fat, it can fail to identify and diagnose microscopic fat-containing lesions. Such lesions may exhibit water attenuation or higher attenuation values on CT, confounding interpretation. MRI, employing spectral and chemical shift fat suppression techniques, can identify macroscopic fat and microscopic fat, respectively, with resultant enhanced capability to diagnose these intrathoracic lesions non-invasively.[2] An additional advantage of MRI over CT in depicting fat is its ability to do so without ionizing radiation. Several MRI techniques have been developed over the past few decades to handle the challenges posed by cardiorespiratory motion. In addition, inflation-adjusted MRI costs have dropped considerably over the last few decades.[3,4] MRI's primary remaining disadvantage compared with CT is its significantly longer image acquisition time.[3]

Magnetic resonance fat suppression can be achieved by two primary means and for two different purposes[1]: spectral fat suppression or "fat saturation" to identify the presence of macroscopic fat, and[2] fat suppression by chemical shift gradient-echo imaging for identification of microscopic fat.[5,6] On MRI, macroscopic fat within a lesion appears hyperintense on T_1- and T_2 weighted fast spin-echo images and on in-phase T_1 weighted images. When spectral fat suppression is utilized, the macroscopic fat signal is suppressed, an occurrence often referred to as "fat-saturation." Spectral fat suppression can also be employed to enhance the soft tissue contrast of non-macroscopic fat-containing tissues, highlighting the T2-hyperintensity of non-fatty lesions and magnifying the enhancement of lesions on post-contrast T_1 weighted imaging. When in- and opposed-phase chemical shift MRI is employed, areas within a lesion

containing intravoxel fat and water that are imperceptible by CT, so-called "microscopic fat," suppress on opposed-phase imaging. The term "fat-suppression" is correct terminology for both scenarios, though it is more commonly used in the latter context, with "fat-saturation" used more commonly in the context of spectral fat suppression.[5–8]

This paper aims to review the CT and MRI findings of various fat-containing lesions of the chest and describe the fat-suppression techniques used in their assessment.

FAT SUPPRESSION TECHNIQUES

Fat suppression is achieved via several techniques, each with specific capabilities.[5–8] Fat suppression techniques take advantage of the difference in resonance frequency between protons in fat and water milieus. Fat–water separation methods are based on: (1) the water–fat chemical shift (resonance frequency difference); (2) the short T1 of fat; or (3) both (hybrid techniques).

Chemical-shift techniques

Two-dimensional in- and opposed-phase chemical shift MRI. There are two forms of chemical shift artifact: Type 1 and Type 2. Type 1 occurs along the axis of the frequency-encoding gradient on an MR image.[6] As spatial encoding by MRI depends on inferring the spatial position from the precession frequency, a water proton and a fat proton located at the same physical position will be mildly shifted within an image due to their different precession frequencies. This spatial misregistration creates a shift in the spatial location in the frequency-encoding direction and can occur not only with gradient echo imaging but also with spin echo imaging.[6,9] This artifact appears as a dark and/or white bands at the interface between water-containing soft tissue and fat. Type 2 chemical shift artifact, also known as phase cancellation, occurs only with gradient echo sequences and is related to the phase shift between water and lipid protons. It solely occurs in the phase-encoding direction.

In- and opposed-phase MRI takes advantage of Type 2 chemical shift artifact to identify the presence of intravoxel fat (so-called microscopic fat) and water within tissue. Images are acquired using T_1 weighted gradient-recalled echo (GRE) sequences. By selecting the appropriate time-to-echo (TE), the signal from water and fat protons in the same voxel can be made to interact constructively (in-phase TE) or destructively (opposed-phase TE). Destructive interference yields nulling of the signal within voxels containing both fat and water. By its very nature, opposed-phase imaging will not suppress or null signal within voxels containing primarily adipocytes. Therefore, this technique will not suppress the signal from adipose tissue or macroscopic fat,[6] though it will null signal at the interface between macroscopic fat-containing and water-containing structures to yield a chemical shift artifact known as "India ink artifact." In the context of chest imaging, chemical shift MRI is performed during $a \leq 20$ s breath-hold, to freeze respiratory motion and help ensure good imaging quality. Depending on the MRI scanner, MRI software package, and craniocaudal length of the patient's chest, axial coverage ranging from one-third to nearly all of the chest can be achieved in a single 20 s breath-hold. The diagnostic utility of this technique lies in its sensitivity for detection of small amounts of fat in a lesion or organ, imperceptible to the eye on CT and non-chemical shift MRI, including that in adrenal adenomas, hepatic steatosis, normal thymus, thymic hyperplasia, and microscopic fat-containing pulmonary hamartomas.[6,10–12]

The Dixon technique. The Dixon method is a three-dimensional (3D) volume acquisition technique for acquisition of in- and out-of-phase imaging. In a single breath-hold acquisition, it acquires 3D in- and opposed-phase images, and then, upon post-processing, yields water-only images which suppress all macroscopic fat on the image and fat-only images which suppress all water-containing structures in the image. This technique therefore enables detection of microscopic fat via the initially acquired in- and opposed-phase T_1 weighted images and detection of macroscopic fat via the subsequent, mathematically derived water-only images. Water-only images amplify the signal of water-containing structures while suppressing macroscopic fat. The appearance of the water-only images resembles that of spectrally fat-suppressed T_1 weighted imaging. The Dixon method achieves both forms of fat suppression upon post-processing by *summing* the in-phase (water + fat) and opposed-phase (water - fat) images to produce a pure water-only image:

(water + fat) + (water - fat) = pure water-only

image and by *subtracting* the in- and opposed-phase images to produce a pure fat-only image:

[(water + fat) - (water - fat) = pure fat-only image[5–8] (Figure 1).

Fat quantification is also possible.[13] The in- and opposed-phase images and fat- and water-only images acquired by the Dixon technique are obtained during a single, typically 20 s, breath-hold acquisition, allowing image co-registration and shortening of body MR imaging protocols. The Dixon technique has been used broadly for imaging of the abdomen, limbs, extremities, and spine as well. DIXON is preferred to 2D-chemical shift MR imaging for 3T MRI to ensure proper TE selection and accurate quantification of percentage signal dropout.

Disadvantages of the Dixon technique include: (1) its occasional unpredictable and inconsistent flip of water-only and fat-only post-processing within a given water-only or fat-only series of images. This water-only/fat-only post-processing swap can occur just over the lesion itself, with the remainder of the image exhibiting the appropriate, expected water or fat suppression. It is essential to be aware of this potential mishap to avert image misinterpretation/errors in tissue characterization; (2) occasionally, it too does not yield satisfactory, homogeneous macroscopic fat suppression; and

Figure 1. 43-year-old male with pulmonary hypertension. Axial T_1 weighted Dixon sequence with in-phase (a), opposed-phase (b), and water-only (c) images. Axial T_2 weighted sequence with CHESS (d),STIR (e), and SPAIR (f) images showing variable degrees of fat saturation in the same patient at similar levels. In this example, the SPAIR sequence (f) yields the most selective fat-suppression due to its relative insensitivity to magnetic field inhomogeneity. CHESS, chemical shift selective; SPAIR, spectral attenuated inversion recovery; STIR, short tau inversion recovery.

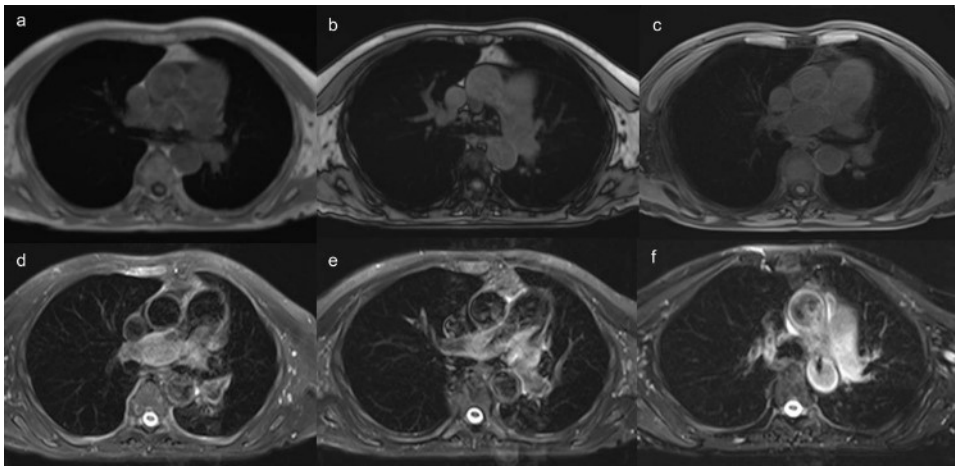

(3) the image quality may be of lesser quality than standard 2D in- and opposed-phase imaging.

Spectral fat saturation (Fat-sat)/Chemical shift selective (CHESS)

Fat saturation imaging helps increase soft tissue contrast. It highlights edema and blood products on T_1- and T_2 weighted images and gadolinium-enhanced tissue on T_1 weighted images by eliminating the high-intensity signal of fat; in doing so, the full spectrum of contrast gradations available at the display workstation can be applied to a narrower spectrum of contrast gradations in the acquired image data set. Macroscopic fatty tissue is extremely water-poor. Spectral fat suppression is achieved by tuning a narrow radiofrequency (RF) pulse to the resonance frequency of protons in a fatty milieu and rotating their magnetization into the transverse plane. A spoiler gradient is then applied to the transversely magnetized fat protons to dephase them. The resultant nulling of fat signal primarily leaves protons in water milieus to produce signal, highlighting non-fatty tissues, most of which contain varying amounts of water[5–8] (Figure 1). This technique is very versatile and can be appended to any T_1- or T_2 weighted pulse sequence. It requires a homogeneous magnetic field to work correctly and thus may fail around metallic hardware, imaging far from isocenter, or in anatomic regions with susceptibility distortions (sinuses, head, and neck, and in some areas of the mediastinum, including the thymus and distal esophageal region). The term "CHESS" refers to "CHEmical Shift *Selective*" suppression in the context of *spectrally* selective suppression of water or fat, not in- and opposed-phase chemical shift MRI imaging. The term "fat saturation" or "fat-sat" refers specifically to spectrally selected suppression of the fat peak. The selective fat suppression version of CHESS is commonly used for T_1 weighted contrast-enhanced MR imaging. Unlike short *tau* inversion recovery (STIR) imaging, another form of fat suppression to be discussed below, it is not affected by the tissue T1 value, which is shortened using intravenous contrast material. It is also employed with T_2 weighted imaging, when increased conspicuity of the T2 signal of a lesion or soft tissue edema is desired.

Fat suppression based on the short T1 of fat

Short tau inversion recovery (STIR) imaging. STIR is another widely used sequence and is applicable at all MRI field strengths. Because fat has a shorter T1 than nearly all other tissues in the body, its signal can be selectively nulled using a magnitude-reconstructed inversion recovery sequence with short time-to-inversion (TI) values (150–180 ms at 1.5T)[5–8] (Figure 1). This spin echo, as opposed to gradient echo, method is relatively insensitive to field inhomogeneities and can be used near metal and over large fields of view. STIR imaging has its limitations, however. The signal intensity in inversion-recovery sequences is related to the absolute value of the longitudinal magnetization (*i.e.* regardless of whether it has passed the null point). Therefore, tissue with a short T1 and tissue with a long T1 may produce the same signal intensity.[5–8] The most misleading and disadvantageous aspect of STIR imaging is that fat is not the only tissue type that can be suppressed. The signal from tissue or fluid with a T1 similar to that of fat will also be suppressed, including mucus, hemorrhage, proteinaceous fluid, melanin, and gadolinium. Thus, STIR should not be used for demonstration of contrast enhancement upon intravenous gadolinium administration. Furthermore, STIR should not be used in concert with diffusion-weighted imaging (DWI) (STIR-DWI) after i.v. contrast administration.[5–8] Lack of awareness of STIR's disadvantages or pitfalls can lead to diagnostic error.

Hybrid techniques

SPIR and SPAIR. These techniques combine a greater-than-90° CHESS pulse with an inversion delay and spoiling

Table 1. Additional imaging features of fat-containing mediastinal, lung, pleural, and chest wall lesions which contribute to diagnostic specificity

Lesion	Typical imaging findings
Mediastinal lipomatosis	Abundant, symmetrically distributed, mature, macroscopic adipose tissue in the mediastinum, without significant displacement of or mass effect on vital structures.
Thymic hyperplasia	Excess thymic tissue for age, without aggressive or invasive appearance; may contain macroscopic or microscopic fat and occasionally no CT- or MR-detectable fat.
Thymolipoma	An often large, malleable, well-defined, macroscopically fatty mass in the anterior or prevascular mediastinum, which drapes along the heart.
Mature teratomas/dermoid cysts	Mass usually in the prevascular mediastinum, that may contain calcifications (latter usually T1/T2-hypointense on MRI) and fat (macro- and/or microscopic). Presence of fat-fluid level may be diagnostic.
Lipomatous hypertrophy of the interatrial septum	Non-encapsulated, well-circumscribed fatty tissue involving the interatrial septum; fat is macroscopic.
Arrhythmogenic right ventricular dysplasia	Late gadolinium enhancement on MRI and dysmotility of anterior right ventricular wall, on MRI, gated CT, or echocardiography. In MR imaging, detection of intramyocardial fat within the RV wall as signal voids employs using spectrally selective fat suppression with the black blood sequences.
Post-myocardial infarction lipomatous metaplasia	Thinned myocardial wall that presents with contraction abnormalities and macroscopic fat-containing areas within the myocardium
Extramedullary hematopoiesis	Paraspinal soft tissue mass(es), sometimes with associated rib expansion; fat may be macroscopic or microscopic
Pulmonary hamartoma	Pulmonary nodule of variable CT attenuation and MRI signal depending upon lesion content, whether fatty, cartilaginous, mixed fatty-cartilaginous, or other; fat content may be macroscopic or microscopic
Lipoid pneumonia	Chronic, fat-containing consolidative lesion with gravitational distribution; fat may be macroscopic or microscopic
Lipoma	Well-defined margins; homogeneous CT isoattenuation and MRI isointensity to subcutaneous macroscopic fat
Liposarcoma	Usually contains macroscopic fat, with or without soft tissue components; often >10 cm, with thickened septa, and nodular soft tissue, mass effect, and displacement of adjacent structures; enhancement of soft tissue component is more readily discernible by MRI than CT
Lipoblastoma	Large mediastinal lesion with septations, non-fatty and macroscopic fatty components, contrast enhancement of non-fatty component, and compartmental invasion, typically presenting in children under the age of 3 years.

to null the signal from fat. The main difference between SPIR (spectral presaturation with inversion recovery) and SPAIR (spectral attenuated inversion recovery) is that the latter uses a full 180° adiabatic inverting pulse insensitive to B0 inhomogeneity.[14] As a result, both SPIR and SPAIR are less sensitive to B0 field inhomogeneity and selectively suppress fat, in contrast to STIR that suppresses all tissues with short T1 values including fat. Also, SPIR/SPAIR sequences have higher signal-to-noise than STIR.[14] These advantages explain the increasing use of these sequences for fat suppression at MR imaging with high-field-strength magnets which are prone to greater magnetic susceptibility artifact (Figure 1).

CLINICAL APPLICATIONS IN THE CHEST

Mediastinum

Mediastinal lipomatosis and hernias involving the mediastinum

Both CT and MRI readily depict and facilitate the diagnosis of mediastinal lipomatosis and hernias involving the mediastinum, because these entities contain macroscopic fat. Mediastinal lipomatosis is a benign excessive deposition of mature adipose tissue in the mediastinum.[15] It is a benign cause of mediastinal widening on chest radiographs. Both imaging modalities will demonstrate abundant, fairly symmetrically distributed, mature, macroscopic adipose tissue in the mediastinum, without significant displacement of or mass effect on vital structures.[16]

Hiatal hernias often carry perigastric fat into the mediastinum, along with adjacent stomach and occasionally other abdominal content, sometimes with a disproportionate amount of fat to bowel. Bochdalek and Morgagni hernias manifest as fatty mediastinal masses as a result of herniation of fatty intra-abdominal content through congenital defects in the posterior and anteromedial aspects of the diaphragm, respectively.[17] Retroperitoneal fat and occasionally a portion of the kidney herniate into the chest via a Bochdalek hernia. Morgagni hernias mimic paracardiac fatty masses to some extent, however the anterior abdominal fat and associated normal mesenteric vascular branches which supply it can be tracked upward through the anteromedial diaphragmatic defect into the chest along the heart, differentiating it, *e.g.* from a thymolipoma and a liposarcoma. Thymolipomas are not associated with a diaphragmatic defect and a liposarcoma tracking from abdomen to chest would displace normally arborizing mesenteric vessels. When the presence of a diaphragmatic defect is in question on CT, however, most commonly when overlying the isoattenuating liver or spleen in the context of traumatic diaphragmatic rupture, the higher soft

Figure 2. 37-year-old male undergoing therapy for lymphoma. Axial CT image (a) shows excess thymic soft tissue for age. Axial in-phase T_1 weighted MR image (b) demonstrates partially fatty-intercalated T1-isointense soft tissue in the prevascular mediastinum, without compression or invasion of adjacent structures. Axial out-of-phase MR image (c) shows qualitative loss of signal intensity of this tissue, indicating the presence of microscopic fat and thereby proving the tissue to represent thymic hyperplasia.

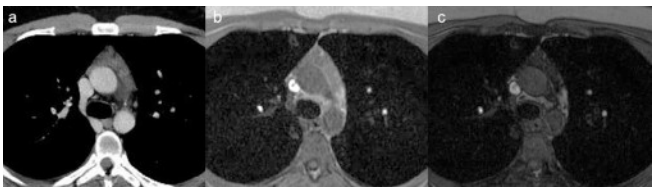

tissue contrast of T_2 weighted MRI can be employed to prove or exclude the presence of a diaphragmatic defect. On CT, the diaphragm is isoattenuating to the underlying liver and spleen.[1] On MRI, because the skeletal muscle of the diaphragm is T2-hypointense and the liver and spleen are of intermediate T2 signal, the diaphragm is more easily discernible from these organs, as is any discontinuity of the diaphragm (Table 1).

Normal thymus and thymic hyperplasia

As patients age, the normal thymus is progressively replaced by fat, a process with a variable time course per individual and within the thymus itself. As fatty atrophy occurs, the thymus becomes microscopically fatty before it becomes macroscopically fatty. In patients who have a delayed time course of fatty atrophy of the thymus or who have true or lymphoid thymic hyperplasia, thymic soft tissue may be present or reappear in adulthood[18,19] and risks misinterpretation as thymoma and lymphoma.[20] Because chemical-shift MR imaging can detect microscopic fat, it can detect earlier fatty change than CT and has been used to distinguish normal thymus and thymic hyperplasia from thymic tumors (Figure 2) in most adults, but not in children and young adults whose thymuses have not yet begun to atrophy. Ascertaining the percentage signal dropout with the signal intensity index (SII) ([(lesion in-phase signal intensity - lesion out-phase signal intensity) / lesion in-phase signal intensity] * 100%) has been used to distinguish normal thymus and thymic hyperplasia from thymic tumors using a SII cut-off greater than 8.92%, with sensitivity of 100% and specificity of 100%.[18] There should be no signal dropout within thymic epithelial tumors (TETs) and lymphoma. In contrast, there is signal dropout in the normal thymus and thymic hyperplasia in most adults. Use of the SII calculation requires that the in/opposed-phase MRI acquisition be by dual echo technique. If not, the chemical shift ratio (CSR) calculation must be used, with careful ROI placement not only over the thymic tissue of interest, but also over a non-fatty chest wall muscle in the same image and avoidance of associated pitfalls.[21] It is important to remember that normal thymus and thymic hyperplasia in children would not be expected to suppress on opposed-phase imaging on account of insufficient fatty atrophy. Occasionally, normal and hyperplastic thymus does not suppress in adults as well. An adjunctive tool in such cases is to employ diffusion-weighted MR imaging with apparent diffusion coefficient (ADC) mapping. TETs and lymphomas will restrict water diffusion, whereas normal thymic tissue and hyperplasia will not.[22,23]

Thymolipoma

Thymolipoma is a rare benign tumor of the thymus, histologically composed of normal thymic tissue and mature adipose tissue, with the highest incidence in young adults. Patients may be asymptomatic, present with compression symptoms, or present extremely rarely with myasthenia gravis.[24] On CT, macroscopic fat and soft tissue attenuation material are demonstrated within these masses. Like CT, MRI will demonstrate the macroscopic fat within the mass (Figure 3).

Germ cell tumors

Germ cell tumors (GCTs) arise along the midline craniocaudally, from the pineal gland down to the presacral region.[25] They form due to the incomplete migration of primitive germ cells during the early stage of embryonic development.[25] Most GCTs arise in a gonadal tissue; however, 50–70% of extragonadal GCTs occur in the mediastinum.[25] GCTs are broadly classified as teratomatous and non-teratomatous.[25]

Teratomas are composed of various internal constituents including fat, soft tissue, calcification, and fluid. These are easily identifiable on MRI, with the exception of calcification, which CT more reliably and definitively identifies. Intralesional macroscopic fat has high signal intensity on T_1- and T_2 weighted images, which is suppressed by spectral fat-suppression (Figure 4).[25] When present, a fat-fluid level may be diagnostic.[25] Occasionally, these tumors may contain only microscopic fat in its fluid and/or soft tissue component, which CT will fail to detect, but chemical shift MRI will demonstrate.

Intracardiac fatty lesions

Ectopic intracardiac fat is a common finding in thoracic imaging in both healthy and diseased patients. Physiologic ectopic cardiac adipose tissue may be present without clinical consequence.[26] It has been observed during routine chest and cardiac CT and MR imaging and is more frequent in the right ventricle (RV) than in the left ventricle (LV), with an overall prevalence of RV ectopic intramyocardial fat of 16–43%.[26] In the elderly, physiologic RV myocardial fat can be found, with linear or patchy morphology in the free wall, in the subepicardial layers of anterolateral or apical segments, and along the RV outflow tract (RVOT), in concert with preserved or increased myocardial thickness. Fat in the LV wall can indicate an old myocardial infarct.

Lipomatous hypertrophy of the interatrial septum (LHIS) is a benign non-encapsulated mass of fatty tissue infiltrating the atrial septum and was first described in 1964.[27,28] It is typically detected in patients older than 50 years and is more common in females. It is characterized by the excessive deposition of fat in the interatrial septum, with a thickness greater than 2 cm. Although histologically benign, LHIS has been associated with adverse clinical sequelae including supraventricular arrhythmias, syncope, and sudden death.[29,30] On imaging, it is typically dumbbell-shaped, spanning the interatrial septum but sparing the fossa ovalis.[27,28]

Figure 3. 23-year-old male with thymolipoma. Coronal (a) and axial (b) double inversion recovery T_1 weighted MR images and fat spin-echo T_2 weighted axial image (c) demonstrate a large heterogeneous signal lesion in the anterior half of the chest, with predominantly high signal intensity areas representing macroscopic fat within the lesion and small scattered areas of relatively hypointense signal representing thymic tissue. On the coronal (d) and axial (e) fat-saturated T_2 weighted images, the areas of high signal intensity completely suppress, indicating adipose tissue. The signal characteristics and draping, apparently pliable nature of this large lesion favor a thymolipoma over a liposarcoma.

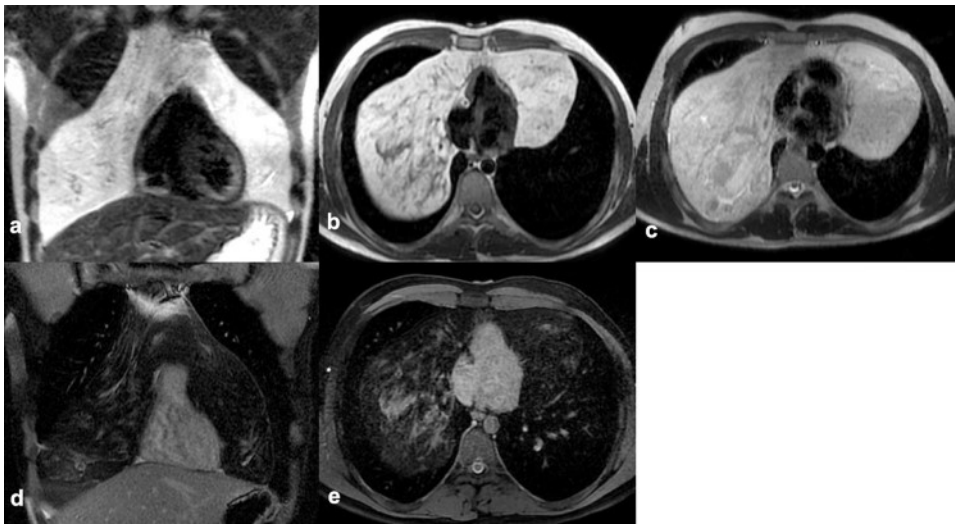

Figure 4. 33-year-old male with a paravertebral mediastinal teratoma. (a) Axial in-phase T_1 weighted image demonstrates a large heterogeneous signal mass in the left paravertebral space with areas isointense to chest wall subcutaneous fat and with chemical shift India ink artifact on the (b) out-of-phase sequence delineating intralesional macroscopic fat from water-containing soft tissue. The intralesional macroscopic fat is isointense to the macroscopic fat in the chest wall on (c) the single-shot spin echo T_2 weighted sequence and (d) the spectral fat-saturated T_1 weighted sequence.

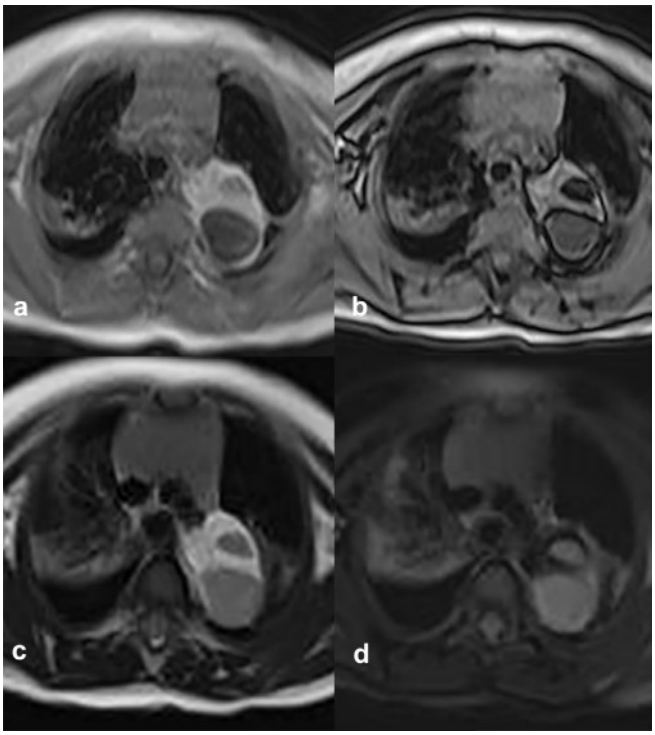

Arrhythmogenic right ventricular dysplasia (ARVD) is defined by fatty or fibrofatty replacement of the normal right ventricular myocardium.[31] The fatty replacement characteristically involves the right ventricle; however, it is occasionally present in the left ventricle. The typical patient is a young adult presenting with ventricular arrhythmia. MRI helps evaluate these patients, as it depicts right ventricular enlargement, poor right ventricular function, wall motion abnormalities, and the presence and extent of fatty or fibrofatty myocardial replacement (Figure 5).[31] MRI with single shot fast spin echo T_1 weighted black blood sequences, with and without fat saturation, can facilitate the differentiation of pathological fatty infiltration from normal epicardial adipose tissue.[31] Late gadolinium enhancement (LGE) technique can help detect myocardial fibrous degeneration. However, it can be occasionally challenging to distinguish enhancement from intramyocardial fat in a thinned RV myocardium because both are T1-hyperintense in conventional LGE.[32] By using a multiecho Dixon fat and water separation method in LGE, distinction between fibrosis and fat is feasible.[33] CT imaging is also used to evaluate ARVD, as it can demonstrate morphologic abnormalities such as RV enlargement, excessive trabeculations, fatty infiltration, and marked RV hypokinesis. Although cardiac CT imaging may yield high radiation doses and suboptimal volumetric assessment of the RV, it is usually used for claustrophobic patients and often used for those that receive implantable cardiac defibrillators (ICDs), though, increasingly, performance of MRI on patients with ICDs is possible if appropriate vetting of devices and other precautions are taken.[34]

Post-myocardial infarction lipomatous metaplasia (PILM) is a tissue transformation process that may occur within the scar of healed myocardial infarction (MI). The prevalence of PILM at histology in the LV reached values of 68–84% in excised hearts undergoing transplantation for ischemic heart disease.[35] PILM is

Figure 5. 42-year-old male with ARVD and fatty infiltration of both the RV and LV. (a) Non-contrast axial CT image demonstrates areas of fatty infiltration of the myocardium in the interventricular septum. Axial cine SSFP images at diastole (b) and systole (c) demonstrate foci of fatty infiltration in the biventricular myocardium. Focal areas of wall motion abnormality (dyskinesia) are also noted (arrow). (d) Axial black blood single shot fast spin echo T_2 weighted image shows correspondent areas of fatty infiltration (arrowheads). SAO LGE images (e, f) show patchy areas of T1 hyperintensity in the RV free wall and LV myocardium, corresponding to areas of fibrofatty infiltration. ARVD, arrhythmogenic right ventricular dysplasia; LGE, late gadolinium enhancement; LV, left ventricle; RV, right ventricle; SAO, short axis oblique; SSFP, steady-state free precession.

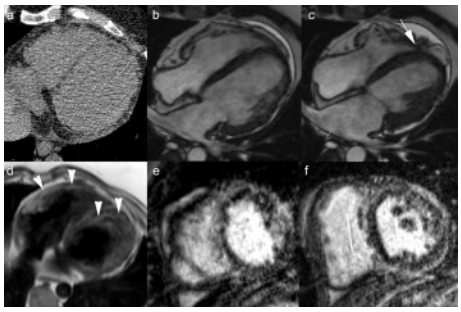

Figure 6. 62-year-old female with PILM. (a) Mid-ventricle short-axis CT shows thinning of the septum with lipomatous metaplasia. (b) Four-chamber late gadolinium enhancement and (c) cine SSFP images demonstrate fat within the myocardial wall of both the right and left ventricle, with chemical shift artifacts (arrows) and hyperintense T1 signal, as well as apical transmural enhancement (arrowhead). (d) Mid-ventricle short-axis late gadolinium enhancement image demonstrates transmural enhancement of the anterior wall (asterisk). Finally, two-chamber cine (e) and black-blood single shot fast spin echo T_2 weighted imaging (f) show chemical shift artifacts (arrow) and hyperintense T2 signal within the inferior apical wall (arrowhead), respectively. PILM, post-myocardial infarction lipomatous metaplasia; SSFP, steady-state free precession.

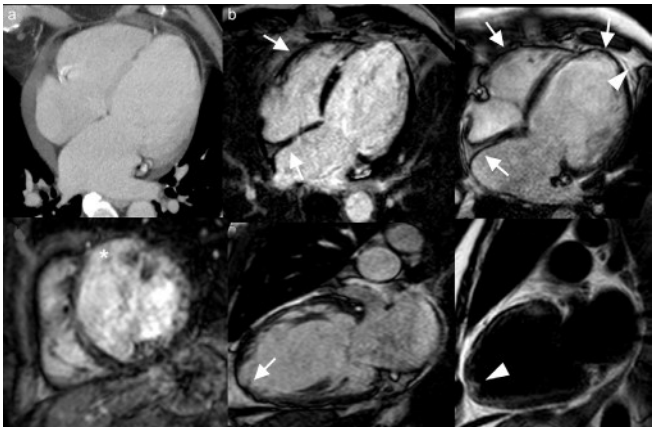

Figure 7. 83-year-old male with right paraspinal thoracic mass and biopsy-proven extramedullary hematopoiesis. MRI demonstrates a heterogeneous signal intensity lesion on all pulse sequences: (a) fat-saturated T_1 weighted image without IV contrast; (b) fat-saturated T_1 weighted image with IV contrast; (c) T_1 weighted in-phase and (d) out-of-phase sequences show qualitative signal dropout or suppression on the opposed-phase image, indicating the presence of microscopic fat, and strongly favoring a diagnosis of extramedullary hematopoiesis over a lymphoproliferative process. (e) T_2 weighted coronal image of this right paraspinal mass.

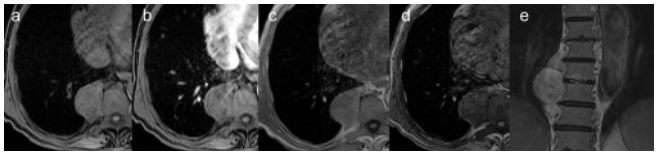

usually found in a thinned necrotic myocardial wall that demonstrates contraction abnormalities, such as dyskinesia and hypokinesia (Figure 6).[35] In cardiac MRI, PILM is generally detectable as subendocardial hyperintense stripes on EKG-gated T_1- and T_2 weighted black blood pulse sequences and on bright blood balanced gradient echo sequences, like cine steady-state free precession (SSFP), and on fat suppression sequences, signal will be nulled.

Extramedullary hematopoiesis

Extramedullary hematopoiesis (EMH) is the production of blood elements outside of the bone marrow. EMH generally occurs in patients with deficient bone marrow hematopoiesis secondary to either peripheral red cell destruction or marrow replacement. It derives from the escape of progenitor cells from marrow which lodge in other organs.[36] EMH is most often seen in the reticuloendothelial system (liver, spleen, and lymph nodes) and rarely occurs in other organs. It is often microscopic and asymptomatic, but it can sometimes yield tumor-like masses. In the thorax, it most commonly manifests on CT and MRI as paravertebral, macroscopic fat-containing masses, with occasionally expanded ribs. When no macroscopic fat is present within a paravertebral mass, the differential diagnosis broadens to include neurogenic tumors, IgG4-related disease, and lymphoproliferative lesions such as lymphoma. Chemical shift MRI, unlike CT, can help to differentiate microscopically fatty EMH tumor-like masses from the above-mentioned non-fat-containing paravertebral masses (Figure 7).

Lung

Pulmonary hamartoma

Pulmonary hamartoma is the third most frequent type of solitary pulmonary nodule and is the most common benign pulmonary neoplasm.[2,37] Some, but not all, contain macroscopic or microscopic fat and cartilage. The radiologic diagnosis of a fat-containing pulmonary hamartoma is often made by CT detection of characteristic popcorn calcification and/or macroscopic fat within the lesion.[2] Nevertheless, 50% of pulmonary hamartomas may not contain detectable fat or calcification by CT.[2,29] MRI with thin-slice collimation (typically 3–4 mm, depending upon the size of the lesion) of a pulmonary hamartoma can not

Figure 8. 50-year-old male with pulmonary hamartoma. (a) Axial CT image demonstrate a heterogenous attenuation lesion containing small areas of fatty attenuation. The lesion is of heterogeneous signal on (b) fat-saturated T_2 weighted imaging and show marked qualitative suppression of some areas between the (c) in-phase and (d) opposed-phase images, indicating the presence of microscopic fat and proving the lesion to represent a hamartoma (provided there is no history of metastatic fat-containing renal cell carcinoma, hepatocellular carcinoma, or liposarcoma).

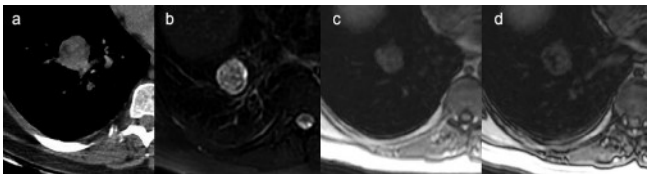

only identify macroscopic fat-containing hamartomas, which CT can do, but also identify microscopic fat-containing hamartomas. The percentage decrease in signal intensity is calculated by the SII as follows: $[(SI_{IP} - SI_{OP}) / SI_{IP}] \times 100$, where SI_{IP} and SI_{OP} are the signal intensities of the nodule measured on in- and opposed-phase images. An SII greater than 17% is considered an appropriate cut-off value for lipid-rich lesions.[2] Calcifications will generally manifest as low T1/T2 signal foci.[30] Spectral fat suppression will allow for detection of macroscopic fat in the nodule on MRI (Figure 8).[38] Cartilage within a hamartoma will demonstrate the MRI signal characteristics of water (T1-hypointense, T2-hyperintense, non-enhancing).[39] On dynamic contrast-enhanced (DCE) imaging, both fat- and cartilage-containing pulmonary hamartomas typically demonstrate peripheral enhancement and enhancement of any internal clefts or septae, with little-to-no enhancement of the interstices of the lesion, because water-rich cartilage and fat do not discernibly enhance. Post-processed subtraction DCE imaging can highlight the hypoenhancement or lack of enhancement of both fat- and cartilage-containing pulmonary hamartomas, which might otherwise be less discernible, and should therefore be referenced during imaging interpretation.

Lipoid pneumonia

Lipoid pneumonia results from the pulmonary accumulation of endogenous or exogenous lipids. Host tissue reactions to the inhaled substances differ according to their chemical characteristics. Therefore, symptoms can vary significantly among individuals, ranging from asymptomatic to severe, life-threatening disease.[40] Possible complications include superinfection by non-tuberculous mycobacteria, pulmonary fibrosis, respiratory insufficiency, and *cor pulmonale*. The disease presents with variable patterns and distribution. The finding of macroscopic fat within lung consolidation on CT (or MRI) is diagnostic of this entity. When macroscopic fat is not present within these lesions on CT, the CT findings are non-specific and can mimic many other forms of pneumonia, in addition to pulmonary neoplasms.[40] Exogenous and endogenous lipoid pneumonia manifests as an adipose-containing mass. On CT, lipoid pneumonia may demonstrate similar attenuation values to macroscopic fat, but occasionally it contains insufficient fat to detect by CT. In addition

Figure 9. 43-year-old female with lipoid pneumonia due to chronic aspiration of mineral oil. Axial CT images (a, b) demonstrate areas of bilateral lower lobe consolidation, with adjacent ground-glass and superimposed interlobular septal thickening, the latter forming the so-called "crazy paving" pattern. No definite fat is discernable within this consolidation on CT, allowing for possible overlying artifact. On MRI, microscopic fat-containing areas within the consolidation demonstrate loss of signal between the in-phase (c) and opposed-phase (d) sequences, indicating the presence of lipid within the consolidation and thereby a specific diagnosis of lipoid pneumonia.

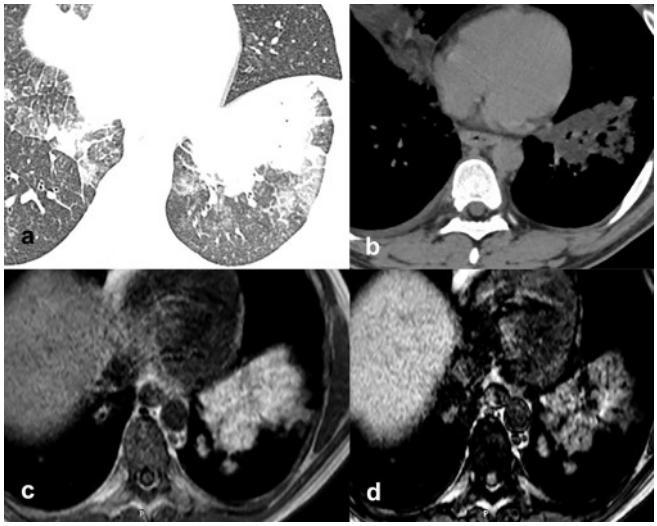

to demonstrating fat saturation of macroscopically fatty lipoid pneumonia, MRI can demonstrate CT-occult, microscopic fat-containing lipoid pneumonia. On MRI, lesions present with high signal on T_1 weighted images and signal loss on the spectral fat-saturated image if macroscopic fat is present and with signal loss on the opposed-phase chemical shift GRE T_1 weighted sequence if microscopic fat is present (Figure 9).

Extrapulmonary (pleura, chest wall, mediastinum)

Lipoma, liposarcoma and lipoblastoma

Lipoma is the most frequently encountered benign soft tissue tumor and originates from adipose cells.[41,42] Lipomas can arise in the pleura. In the chest wall, they are categorized according to their location as superficial, *e.g.* subcutaneous, or deep-seated, *e.g.* intramuscular.[41,42] The latter can be encapsulated or infiltrative and, if infiltrative, may resemble a liposarcoma. For this reason, early radiological detection and characterization are necessary to obtain a complete wide resection and histopathological evaluation to differentiate benign from malignant lesions. CT is adequate to demonstrate the macroscopic fat in these lesions and provide a preliminary diagnosis, though arguably exposing the patient to unnecessary ionizing radiation. MRI is an excellent imaging modality to distinguish lipomas from liposarcoma, without ionizing radiation exposure. The fatty tissue in the lipomas demonstrates high signal intensity on both T_1- and T_2 weighted images (Figure 10). Spectral fat suppression and STIR imaging will show signal suppression of the macroscopic fat within the tumor. Lipomas can be homogeneous in signal and

Figure 10. 44-year-old female with a lipoma in the left serratus anterior muscle. (a) Axial T_2 weighted image demonstrates a homogenously T2-hyperintense lesion in the left serratus anterior muscle (arrow) that is isointense to subcutaneous adipose tissue and completely suppresses on the fat-saturated T_2 weighted sequence (b). The lesion is T1-hyperintense to muscle and isointense to subcutaneous fat (c). It suppresses on the spectrally fat-saturated T_1 weighted sequence (d). The homogeneous, macroscopic fatty content of this lesion is compatible with a lipoma.

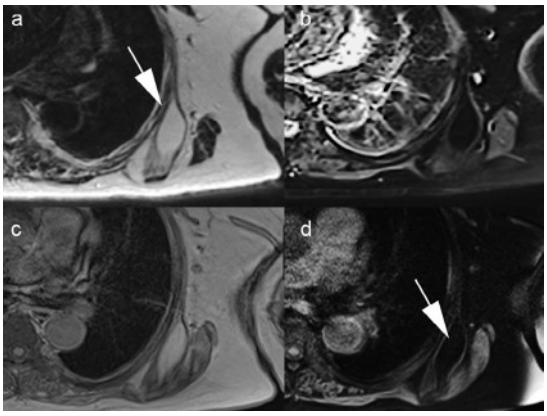

isointense to subcutaneous fat or heterogeneous in signal, on account of intermingled muscle fibers.[41,42]

Primary intrathoracic liposarcomas are rare, accounting for only 2.7% of liposarcomas.[43] Mediastinal liposarcomas comprise only 0.1–0.8% of all mediastinal tumors.[44] Morphology and signal characteristics can help distinguish an infiltrative intramuscular lipoma from well-differentiated liposarcoma. For example, well-differentiated liposarcoma may show tumor tissue heterogeneity, with nodular non-adipose soft tissue, thickened, irregular, and/or nodular septa, and heterogeneous fat suppression (Figure 11). To date, the differentiation of lipomas from low-grade liposarcomas cannot be achieved exclusively by imaging CT or MRI.[45] To our knowledge, there are no studies comparing the accuracy of CT *vs* MRI for this purpose. However, these imaging methods can be complimentary in the evaluation of these lesions and helpful in differential diagnostic weighting. In a series that included both CT and MRI, presence of the following imaging features favored the diagnosis of liposarcoma *vs* lipoma: lesion size >10 cm, percentage of fat <75%, thickened septa, presence of nodular areas, and associated non-adipose mass.[46] In another study, MRI was 100% sensitive, 83% specific, and 84% accurate for identifying well-differentiated liposarcomas from other fatty masses.[47] For the diagnosis of a simple lipoma, MRI was 100% specific.[47] MRI is more sensitive than CT in detecting soft tissue enhancement within liposarcomas, on account of its higher soft tissue contrast (Figure 11).

Lipoblastoma is a rare benign neoplasm of embryonal fat cells that usually presents in children. Most are diagnosed before age 3.[48] It appears that these tumors result from the clonal expansion of mesenchymal pre-adipocytes from alterations in the pleomorphic adenoma gene 1 (PLAG1) on Chromosome 8, causing transcriptional upregulation that promotes lipoblast proliferation.[48]

Figure 11. 43-year-old male with pleural liposarcoma. Axial (a) and coronal (b) CT images demonstrate a large mass of heterogeneous, although primarily fatty attenuation in the posteroinferior right hemithorax, which compresses the adjacent lung. On the axial T_2 weighted MR image (c), the lesion exhibits heterogeneous high signal intensity; its macroscopically fatty component suppresses upon spectral fat-saturation (d). On the in-phase T_1 weighted sequence (e), the lesion demonstrates predominantly high signal intensity, with areas of suppression on the opposed-phase sequence (f) because of the presence of microscopic fat. On the axial (g) and coronal (h) fat-saturated post-contrast T_1 weighted sequence, the lesion shows enhancement of the septae, beyond that which would be expected for enhancing muscle fibers, favoring a liposarcoma over a lipoma.

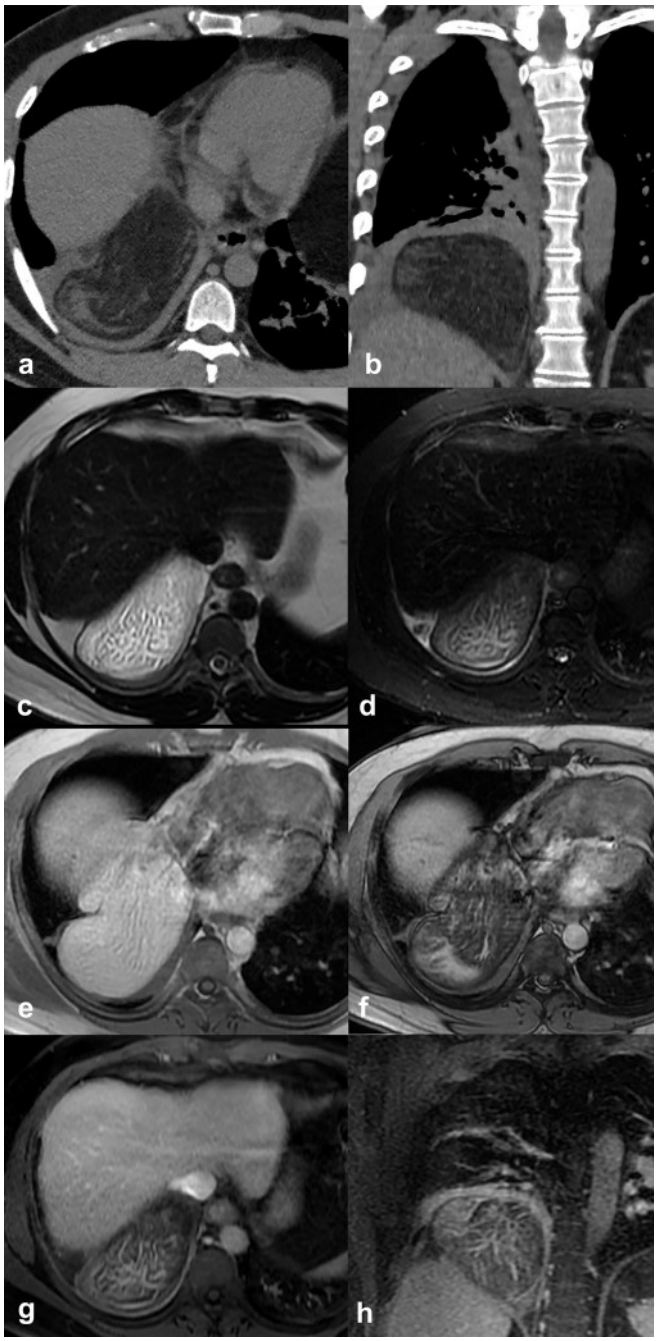

Lipoblastoma most commonly occurs at sites with large amounts of immature fat in the neonate, with cases reported in the subcutaneous tissues of the extremities and the cervical, mediastinal, and peritoneal regions.[48] Moderate complexity is frequent in lipoblastoma on MRI, with septations, non-adipose components, contrast enhancement, and compartmental invasion commonly encountered. Lipoblastoma and liposarcoma may be indistinguishable by imaging, but consideration of patient age is helpful because liposarcomas are extremely rare in children.[49]

CONCLUSION

MRI is a valuable tool for the evaluation of both macroscopic and microscopic fat-containing thoracic lesions without ionizing radiation exposure. The distinctive ability of MRI to detect CT-occult microscopic fat can refine the differential diagnosis and add diagnostic specificity to a broader spectrum of fat-containing lesions in the chest. Fundamental knowledge about MRI techniques, findings, and pathology can help radiologists and other healthcare providers with non-invasive diagnosis and clinical management of fat-containing intrathoracic lesions.

HIGHLIGHTS

- MRI of chest can identify both macroscopic fat and microscopic fat by employing spectral and chemical shift fat suppression techniques, respectively.
- *Macro*scopic fat-containing thoracic lesions can be diagnosed by both CT and MRI, with the latter via spectral fat suppression.
- Microscopic fat-containing thoracic lesions, including some forms of thymic hyperplasia, pulmonary hamartoma, lipoid pneumonia, and extramedullary hematopoiesis, can be more challenging to diagnose by CT, but can be specifically diagnosed by chemical shift MRI.

REFERENCES

1. Gaerte SC, Meyer CA, Winer-Muram HT, Tarver RD, Conces DJ. Fat-containing lesions of the chest. *Radiographics* 2002; **22 Spec No**: S61–78. https://doi.org/10.1148/radiographics.22.suppl_1.g02oc08s61
2. Hochhegger B, Marchiori E, dos Reis DQ, Souza AS Jr, Souza LS, Brum T, et al. Chemical-shift MRI of pulmonary hamartomas: initial experience using a modified technique to assess nodule fat. *AJR Am J Roentgenol* 2012; **199**: W331–4. https://doi.org/10.2214/AJR.11.8056
3. Ackman JB, Wu CC, Halpern EF, Abbott GF, Shepard J-AO. Nonvascular thoracic magnetic resonance imaging: the current state of training, utilization, and perceived value: survey of the Society of thoracic radiology membership. *J Thorac Imaging* 2014; **29**: 252–57. https://doi.org/10.1097/RTI.0000000000000072
4. Wild JM, Marshall H, Bock M, Schad LR, Jakob PM, Puderbach M, et al. Mri of the lung (1/3): methods. *Insights Imaging* 2012; **3**: 345–53. https://doi.org/10.1007/s13244-012-0176-x
5. Bley TA, Wieben O, François CJ, Brittain JH, Reeder SB. Fat and water magnetic resonance imaging. *J Magn Reson Imaging* 2010; **31**: 4–18. https://doi.org/10.1002/jmri.21895
6. Delfaut EM, Beltran J, Johnson G, Rousseau J, Marchandise X, Cotten A. Fat suppression in MR imaging: techniques and pitfalls. *Radiographics* 1999; **19**: 373–82. https://doi.org/10.1148/radiographics.19.2.g99mr03373
7. Bitar R, Leung G, Perng R, Tadros S, Moody AR, Sarrazin J, et al. Mr pulse sequences: what every radiologist wants to know but is afraid to ask. *Radiographics* 2006; **26**: 513–37. https://doi.org/10.1148/rg.262055063
8. Erturk SM, Alberich-Bayarri A, Herrmann KA, Marti-Bonmati L, Ros PR. Use of 3.0-T MR imaging for evaluation of the abdomen. *Radiographics* 2009; **29**: 1547–63. https://doi.org/10.1148/rg.296095516
9. Huang SY, Seethamraju RT, Patel P, Hahn PF, Kirsch JE, Guimaraes AR. Body MR imaging: artifacts, k-space, and solutions. *Radiographics* 2015; **35**: 1439–60. https://doi.org/10.1148/rg.2015140289
10. Pokharel SS, Macura KJ, Kamel IR, Zaheer A. Current MR imaging lipid detection techniques for diagnosis of lesions in the abdomen and pelvis. *Radiographics* 2013; **33**: 681–702. https://doi.org/10.1148/rg.333125068
11. Cho CS, Curran S, Schwartz LH, Kooby DA, Klimstra DS, Shia J, et al. Preoperative radiographic assessment of hepatic steatosis with histologic correlation. *J Am Coll Surg* 2008; **206**: 480–88. https://doi.org/10.1016/j.jamcollsurg.2007.08.020
12. Inaoka T, Takahashi K, Mineta M, Yamada T, Shuke N, Okizaki A, et al. Thymic hyperplasia and thymus gland tumors: differentiation with chemical shift MR imaging. *Radiology* 2007; **243**: 869–76. https://doi.org/10.1148/radiol.2433060797
13. Dixon WT. Simple proton spectroscopic imaging. *Radiology* 1984; **153**: 189–94. https://doi.org/10.1148/radiology.153.1.6089263
14. Del Grande F, Santini F, Herzka DA, Aro MR, Dean CW, Gold GE, et al. Fat-suppression techniques for 3-T MR imaging of the musculoskeletal system. *Radiographics* 2014; **34**: 217–33. https://doi.org/10.1148/rg.341135130
15. Mohapatra PR, Janmeja AK. Asymptomatic mediastinal lipomatosis. *N Engl J Med* 2010; **363**: 1265. https://doi.org/10.1056/NEJMicm1000714
16. Kashikar S, Gulkari AJ, Singhania PK. Ct to the rescue in benign, symmetrical mediastinal lipomatosis. *Thorax* 2012; **67**(8): 758. https://doi.org/10.1136/thoraxjnl-2012-201911
17. Eren S, Ciriş F. Diaphragmatic hernia: diagnostic approaches with review of the literature. *Eur J Radiol* 2005; **54**: 448–59. https://doi.org/10.1016/j.ejrad.2004.09.008
18. Raptis CA, McWilliams SR, Ratkowski KL, Broncano J, Green DB, Bhalla S. Mediastinal and pleural MR imaging: practical approach for daily practice. *Radiographics* 2018; **38**: 37–55. https://doi.org/10.1148/rg.2018170091
19. Ackman JB. Invited commentary on " mediastinal and pleural MR imaging: practical approach for daily practice. " *Radiographics* 2018; **38**: 55–57. https://doi.org/10.1148/rg.2018170198
20. Ackman JB, Verzosa S, Kovach AE, Louissaint A Jr, Lanuti M, Wright CD, et al. High rate of unnecessary thymectomy and its cause. can computed tomography distinguish thymoma, lymphoma, thymic hyperplasia, and thymic cysts? *Eur J Radiol* 2015; **84**: S0720-048X(14)00571-3: 524–33: . https://doi.org/10.1016/j.ejrad.2014.11.042
21. McInnis MC, Flores EJ, Shepard J-AO, Ackman JB. Pitfalls in the imaging and interpretation of benign thymic lesions: how thymic MRI can help. *AJR Am J Roentgenol* 2016; **206**: W1–8. https://doi.org/10.2214/AJR.15.15303

22. Ackman JB, Mino-Kenudson M, Morse CR. Nonsuppressing normal thymus on chemical shift magnetic resonance imaging in a young woman. *J Thorac Imaging* 2012; **27**: W196–8. https://doi.org/10.1097/RTI.0b013e318249936a
23. Priola AM, Priola SM, Gned D, Giraudo MT, Veltri A. Nonsuppressing normal thymus on chemical-shift MR imaging and anterior mediastinal lymphoma: differentiation with diffusion-weighted MR imaging by using the apparent diffusion coefficient. *Eur Radiol* 2018; **28**: 1427–37. https://doi.org/10.1007/s00330-017-5142-z
24. Calandriello L, Larici AR, Sica G, Ciliberto M, Manfredi R. The added value of chemical shift MRI in the preoperative diagnosis of thymolipoma. *Tumori* 2018; **104**: 57–60. https://doi.org/10.1177/0300891618763204
25. Park JW, Jeong WG, Lee JE, Lee HJ, Ki SY, Lee BC, et al. Pictorial review of mediastinal masses with an emphasis on magnetic resonance imaging. *Korean J Radiol* 2021; **22**: 139–54. https://doi.org/10.3348/kjr.2019.0897
26. Jacobi AH, Gohari A, Zalta B, Stein MW, Haramati LB. Ventricular myocardial fat: CT findings and clinical correlates. *J Thorac Imaging* 2007; **22**: 130–35. https://doi.org/10.1097/01.rti.0000213576.39774.68
27. Meaney JF, Kazerooni EA, Jamadar DA, Korobkin M. Ct appearance of lipomatous hypertrophy of the interatrial septum. *AJR Am J Roentgenol* 1997; **168**: 1081–84. https://doi.org/10.2214/ajr.168.4.9124119
28. Heyer CM, Kagel T, Lemburg SP, Bauer TT, Nicolas V. Lipomatous hypertrophy of the interatrial septum: a prospective study of incidence, imaging findings, and clinical symptoms. *Chest* 2003; **124**: 2068–73. https://doi.org/10.1378/chest.124.6.2068
29. Siegelman SS, Khouri NF, Scott WW Jr, Leo FP, Hamper UM, Fishman EK, et al. Pulmonary hamartoma: CT findings. *Radiology* 1986; **160**: 313–17. https://doi.org/10.1148/radiology.160.2.3726106
30. Zampieri JF, Pacini GS, Zanon M, Altmayer SPL, Watte G, Barros M, et al. Thoracic calcifications on magnetic resonance imaging: correlations with computed tomography. *J Bras Pneumol* 2019; **45**: e2018 0168S1806-37132019000400203. https://doi.org/10.1590/1806-3713/e20180168
31. Castillo E, Tandri H, Rodriguez ER, Nasir K, Rutberg J, Calkins H, et al. Arrhythmogenic right ventricular dysplasia: ex vivo and in vivo fat detection with black-blood MR imaging. *Radiology* 2004; **232**: 38–48. https://doi.org/10.1148/radiol.2321030688
32. Kellman P, Hernando D, Arai AE. Myocardial fat imaging. *Curr Cardiovasc Imaging Rep* 2010; **3**: 83–91. https://doi.org/10.1007/s12410-010-9012-1
33. Kellman P, Hernando D, Shah S, Zuehlsdorff S, Jerecic R, Mancini C, et al. Multiecho Dixon fat and water separation method for detecting fibrofatty infiltration in the myocardium. *Magn Reson Med* 2009; **61**: 215–21. https://doi.org/10.1002/mrm.21657
34. Tandri H, Calkins H. Magnetic resonance and computed tomographic imaging in arrhythmogenic cardiomyopathy. *Card Electrophysiol Clin* 2011; **3**: 269–80. https://doi.org/10.1016/j.ccep.2011.02.002
35. Ichikawa A, Morita M, Kuba K, Imai Y. In vivo imaging of damage associated molecular patterns (DAMPs) DNA in mouse lungs with ARDS. *Am J Respir Crit Care Med* 2012; **185**: A6380.
36. Hashmi MA, Guha S, Sengupta P, Basu D, Baboo S. Thoracic cord compression by extramedullary hematopoiesis in thalassemia. *Asian J Neurosurg* 2014; **9**: 102–4. https://doi.org/10.4103/1793-5482.136726
37. Snoeckx A, Reyntiens P, Desbuquoit D, Spinhoven MJ, Van Schil PE, van Meerbeeck JP, et al. Evaluation of the solitary pulmonary nodule: size matters, but do not ignore the power of morphology. *Insights Imaging* 2018; **9**: 73–86. https://doi.org/10.1007/s13244-017-0581-2
38. Hochhegger B, Nin CS, Alves GRT, Hochhegger DR, de Souza VVS, Watte G, et al. Multidetector computed tomography findings in pulmonary hamartomas: a new fat detection threshold. *J Thorac Imaging* 2016; **31**: 11–14. https://doi.org/10.1097/RTI.0000000000000180
39. Leiter Herrán F, Restrepo CS, Alvarez Gómez DI, Suby-Long T, Ocazionez D, Vargas D. Hamartomas from head to toe: an imaging overview. *Br J Radiol* 2017; **90**(1071): 20160607. https://doi.org/10.1259/bjr.20160607
40. Marchiori E, Zanetti G, Mano CM, Hochhegger B. Exogenous lipoid pneumonia clinical and radiological manifestations. *Respir Med X* 2011; **105**: 659–66.
41. Nishida J, Morita T, Ogose A, Okada K, Kakizaki H, Tajino T, et al. Imaging characteristics of deep-seated lipomatous tumors: intramuscular lipoma, intermuscular lipoma, and lipoma-like liposarcoma. *J Orthop Sci* 2007; **12**: 533–41. https://doi.org/10.1007/s00776-007-1177-3
42. Matsumoto K, Hukuda S, Ishizawa M, Chano T, Okabe H. Mri findings in intramuscular lipomas. *Skeletal Radiol* 1999; **28**: 145–52. https://doi.org/10.1007/s002560050491
43. O'Regan KN, Jagannathan J, Krajewski K, Zukotynski K, Souza F, Wagner AJ, et al. Imaging of liposarcoma: classification, patterns of tumor recurrence, and response to treatment. *AJR Am J Roentgenol* 2011; **197**: W37–43. https://doi.org/10.2214/AJR.10.5824
44. Chen M, Yang J, Zhu L, Zhou C, Zhao H. Primary intrathoracic liposarcoma: a clinicopathologic study and prognostic analysis of 23 cases. *J Cardiothorac Surg* 2014; **9**: 119: 1–8: . https://doi.org/10.1186/1749-8090-9-119
45. Shin N, Kim M-J, Chung J-J, Chung Y-E, Choi J-Y, Park Y-N. The differential imaging features of fat-containing tumors in the peritoneal cavity and retroperitoneum: the radiologic-pathologic correlation. *Korean J Radiol* 2010; **11**: 333–45. https://doi.org/10.3348/kjr.2010.11.3.333
46. Kransdorf MJ, Bancroft LW, Peterson JJ, Murphey MD, Foster WC, Temple HT. Imaging of fatty tumors: distinction of lipoma and well-differentiated liposarcoma. *Radiology* 2002; **224**: 99–104. https://doi.org/10.1148/radiol.2241011113
47. Gaskin CM, Helms CA. Lipomas, lipoma variants, and well-differentiated liposarcomas (atypical lipomas): results of MRI evaluations of 126 consecutive fatty masses. *AJR Am J Roentgenol* 2004; **182**: 733–39. https://doi.org/10.2214/ajr.182.3.1820733
48. Degnan AJ, Jelinek JS, Murphey MD. Lipoblastoma: computed tomographic and magnetic resonance imaging features correlate with tumor behavior and pathology. *Pediatr Radiol* 2021; **51**: 614–21. https://doi.org/10.1007/s00247-020-04882-z
49. Kransdorf MJ, Moser RP Jr, Meis JM, Meyer CA. Fat-containing soft-tissue masses of the extremities. *Radiographics* 1991; **11**: 81–106. https://doi.org/10.1148/radiographics.11.1.1996399